The University Of Sheffield.

Study of Fluid Penetration and Lubrication in a Threaded Contact

By

Parhaam Parikhaah

A thesis submitted for the degree of
Doctor of Philosophy

Department of Mechanical Engineering

June 2018

Summary

Penetrating oil producers consider the loosening rate of seized bolted joints as the key performance indicator of their products. Penetrating oils are low viscosity lubricants, which are used to loosen rusted and seized mechanical parts, i.e., bolted joints. The oil penetrates by moving through narrow spaces between the bolt and nut threads and reduces the coefficient of friction. To improve the effectiveness of a penetrating oil product, their penetration and lubrication performance need to be understood. Both of these issues are investigated in this thesis.

In the first phase of the research, a non-intrusive ultrasonic method was developed to measure the penetration time of various fluid samples in fasteners. This technique, utilizing piezo-electric crystals and ultrasonic physics, detects the presence of penetrant in a threaded contact based on the portion of the ultrasound waves reflected, which is different at a dry and lubricated contact. An experimental rig was built and a signal processing procedure was used to obtain the ultrasonic data. The findings shows that for lower viscosity fluid samples, penetration time decreases.

The second phase of the project involved modelling the penetration process based on the principles of laminar fluid flow in capillary tubes. Equation for fluid flow under capillary forces in micro channels of the threaded contact was derived, which is essentially the Washburn equation but with a slight difference due to the geometry of the channel. Viscosity and surface tension of the fluid and the geometrical characteristic of the threaded contact were the data input into the model. Two assumed fluid flow paths were modelled based on the interpretation of the ultrasonic data. The theoretical model was then compared with the experimental data.

The last phase of work focused on studying the lubrication behaviour of the penetrants. An experimental set up was prepared, whereby the tightening torque was first measured and then the loosening torque was measured at different stages of fluid penetration. It was found that different penetrants show different rate of lubrication as they progressed along further threads. However, there was not much difference in the loosening torque after complete fluid penetration. Furthermore, the tension force was measured using a load cell which allowed the calculation of coefficient of friction at the threads. The coefficient of friction before and after fluid penetration was found to be within 0.24 to 0.26 and 0.17 to 0.18 respectively. The lubrication behaviour was also modelled analytically and a good

agreement was found between the coefficient of friction obtained experimentally and analytically. The findings of the work will be used to formulate penetrants with enhanced penetration and lubrication performance.

Acknowledgements

I would like to offer my sincerest gratitude to my supervisor Prof Rob Dwyer-Joyce, for all his support, guidance and friendship during all the phases of my studies.

Special thanks to Dr Robin Mills for his continuous support during all these years. I have certainly learnt a lot from him. I am also grateful to Dr Jennifer Vail for her help and advice during the initial phase of the project. I would also like to thank Dave Butcher and John at the workshop for all their hard work and valuable input.

Thanks to all the people at the Leonardo centre for Tribology, especially Dr Tom Howard for his helpful advice during the project. I had a great time working in such a vibrant research group.

Many thanks to WD-40 company, especially Mike Counts and Ernie Bernarducci for providing funding and fluid samples. I have enjoyed our discussions and am truly grateful for all the advice and recommendations given throughout the project.

Special mention to all my friends, who made the experience more joyful. Thanks to Claire Maxwell for the friendship and kindness especially during the difficult times. Special mention to Hamza Al-Tameemi and Dlair Ramadan for all their helpful comments and support. To my housemates, Thomas Holmes and Adam Samuel, thank you Sirs!

Last but not least, thanks to my wonderful mother and brother for everything. I appreciate all the unconditional love, especially for putting up with me during the write up time.

Nomenclature

B	Bulk Modulus, Pa
c	Acoustic velocity, m/s
D	Diameter of the piezo-electric crystal, m
D_a	Bolt major diameter, m
D_b	Bolt pitch diameter, m
D_c	Bolt minor diameter, m
D_h	Hydraulic diameter, m
E	Elastic (Young's) Modulus, Pa
F	Fastener Tension Force, N
f	Frequency of ultrasound, Hz
f_c	Resonant frequency of ultrasound, Hz
h	gap size, m
h_{film}	Lubricant film thickness, m
K	Nut factor, dimensionless
K_l	Lubricant film stiffness, GPa/micron
K_s	Interfacial stiffness, GPa/micron
l	Length, m
N	Near field distance, m
n	Number of threads
p	Pressure, Pa
p_{nom}	Nominal contact pressure, Pa
P	Pitch, m

q	Volumetric flow rate, m^3/s
R_i	Normal reaction force, N
Re	Reynold number, dimensionless
T	Torque, Nm
t	Time, s
u	Fluid velocity, m/s
V	Volume, m^3
W	Axial load, N
z	Acoustic impedance, $kgm^2s \times 10^6$

Greek Symbols

β	Half of the thread profile angle, °
γ	Surface tension, dynes/cm
θ	Contact angle, °
μ	Dynamic viscosity, Pa.s
μ_t	Coefficient of friction at thread
μ_b	Coefficient of friction at bolt under head
ρ	Density, kg/m^3
τ	Shear stress, Pa
ω	Angular frequency of pulse, radians

List of figures

Contents

1

Introduction

1.1 Threaded fasteners

Fasteners play a critical role in the functionality of machines. They are used to serve two main purposes:

- Facilitating disassembly of a machine, so that inspection and repair can be carried out.
- Improving modularity, whereby a machine can be designed to consist of several sub-assemblies.

Different types of fasteners are used depending on the application. Bolt and nut, screw and stud are some of the common fasteners (Figure 1.1). The primary function of bolt and nut is to hold a component together and provide a clamping force, i.e., bolted joints. Bolted joints are used in various applications from household appliances to pipe flanges, automotive engines and chemical reactors. A typical hexagonal bolt used in a bolted joint configuration is shown in Figure 1.2. Screws can be used as fasteners without a nut, for instance it can be inserted into a tapped hole and tightened up using the heads. Studs, on the other hand, do not have any head and their full length is threaded. One end of it is inside a tapped hole whilst the other end is where the nut is fitted.

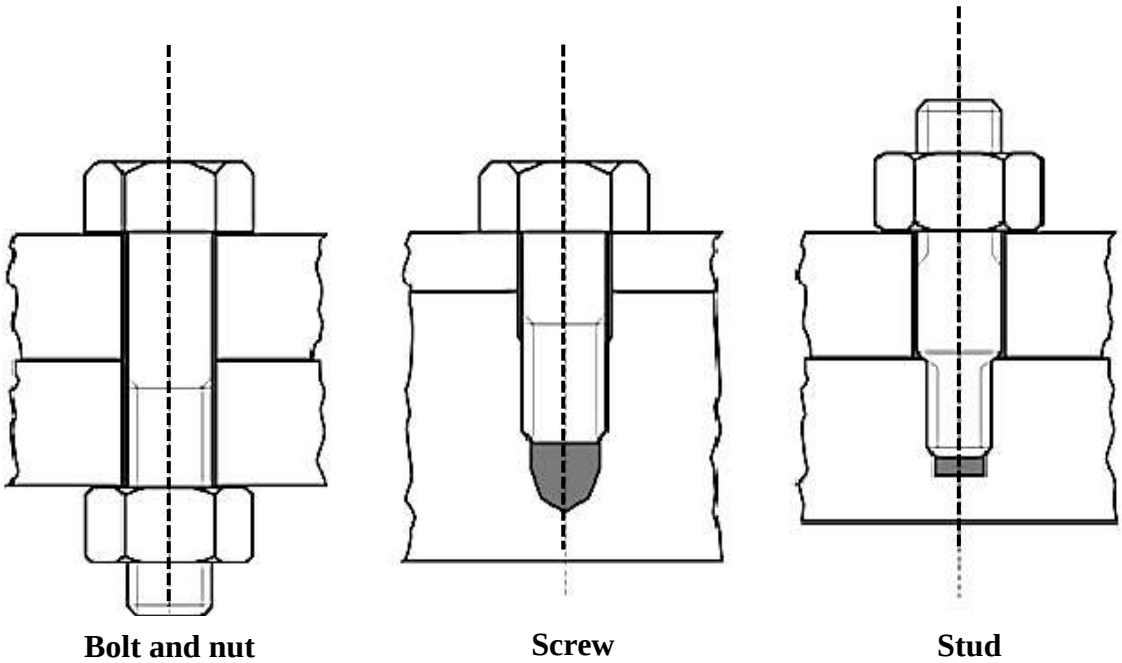

Figure 1.1 Different types of threaded fasteners

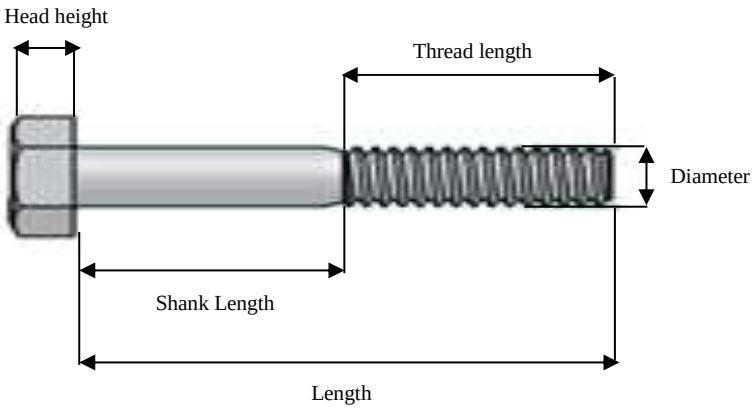

Figure 1.2 A typical hexagonal bolt

There has been a rise in demand for fasteners worldwide due to continued industrialization efforts and healthy economic growth. It is forecasted that the sales will reach $93.8 billion by 2018 (“Fastener Industry News”, 2015).

1.2 Thread terminology

A bolt or nut thread can be considered as a ridge of uniform section in a helical form on either the external or internal surface of a cylinder. Figure 1.3 shows a bolt thread profile, comprises of crest, root and flanks. Crests are at the top of the threads and roots are at the bottom of the threads. Flanks join crests and roots together. The distance between two consecutive crests parallel to thread axis is the thread pitch. For the external thread, major diameter is at crests whilst the minor diameter occurs at roots. The pitch diameter is about halfway between the major and minor diameters.

Threaded fasteners are categorised in different Classes based on their mechanical properties, for instance, a higher Class means a stronger fastener. In addition, thread tolerance Classification specifies the amount of tolerance allowed as well as the installation fit desired.

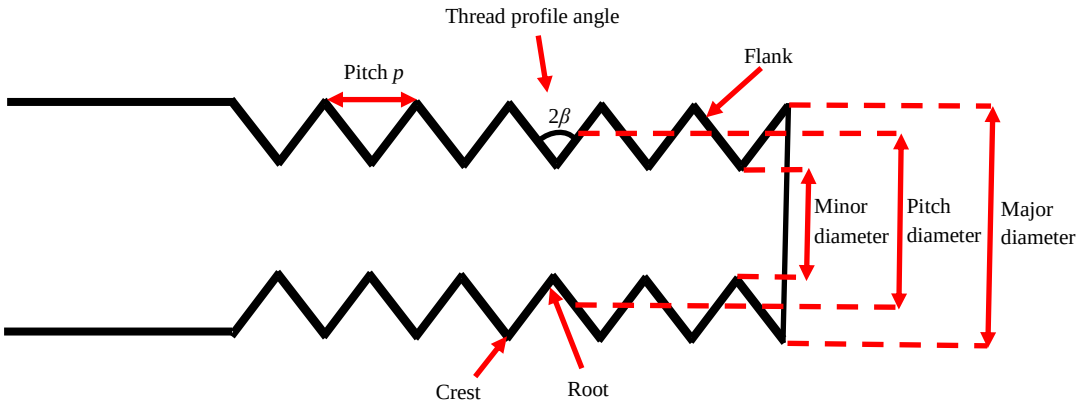

Figure 1.3 Characteristics of a bolt

1.3 Seizure of a thread

Although threaded fasteners are considered a well-developed technology, many problems may arise from using them. One of the root causes of failures in threaded joints is seizure, which is defined as stopping of relative motion between contacting surfaces due to interfacial friction ("Friction, Wear and Lubrication Glossary", 1969).

During the tightening process of a threaded fastener, pressure builds up between the sliding bolt and nut threads and under heavy loads, the tips of asperities make contact with one another and deform resulting in cold welding (Ling & Saibel, 1957). In the absence of lubricants, adhesive wear is severe and is noted as galling (Williams, 1994), which can cause thread seizure.

The likelihood of thread seizure increases when bolt and nut are similar in metallurgy. Hardness of the interacting materials plays an important factor when considering the surface damage. For instance, similar hard metals wear each other equally as noted by Bowden (1944). In addition, Bowden and Tabor (1964) stated that severe wear arose only by shearing of strong metallic bonds and that difference in behaviour between different metal pairs could be identified in terms of the interfacial strength. The strength of an interface quantifies the maximum amount of mechanical work required to be transferred across the interface before separation of the materials takes place (Hertzberg, 1989). If the interface is stronger than the strength of either metals, marked hardening and damage of both surfaces (steel/steel) can be observed (Bowden & Tabor, 1964).

Exposure to environment can also play a role in failure of fasteners. The reason for this is the natural tendency of metals to restore back to their original state by interacting with environment. Roberge (1999) defines corrosion as the destructive attack of a material due to its reaction with environment. The most common form of corrosion in steel fasteners is metallic oxidation (rust).

Adhesive wear in threaded contacts can break the protective oxide layers ("Review of the Wear and Galling", 1978) and accelerate the rate of corrosion. Therefore, when stainless steel is under attack by corrosion and wear, stainless steel performs as ineffective as ordinary carbon steel. Rust leads to loss of metal, increase in surface roughness and frictional resistance, Therefore formation of oxidation products in a threaded contact can result in its seizure.

1.4 Penetrating oils

One effective way of loosening seized bolts due to rusting is to use oil penetrants. The penetrating oil is usually a mixture of a lubricant and a highly volatile low viscosity solvent. Some of them may have additional solid materials inside them. When penetrating oil products are applied to rusted fasteners they flow between the narrow spaces and break down the rust. A thin lubricant film is formed and coefficient of friction is reduced, hence facilitating the removal process. Therefore, in a threaded fastener where the threads are seized because of both cold-welding and rusting at the contact asperities (Figure 1.4), a penetrant product will only tackle the rust by forming a thin lubricant film and reducing the overall coefficient of friction, hence facilitating the removal process.

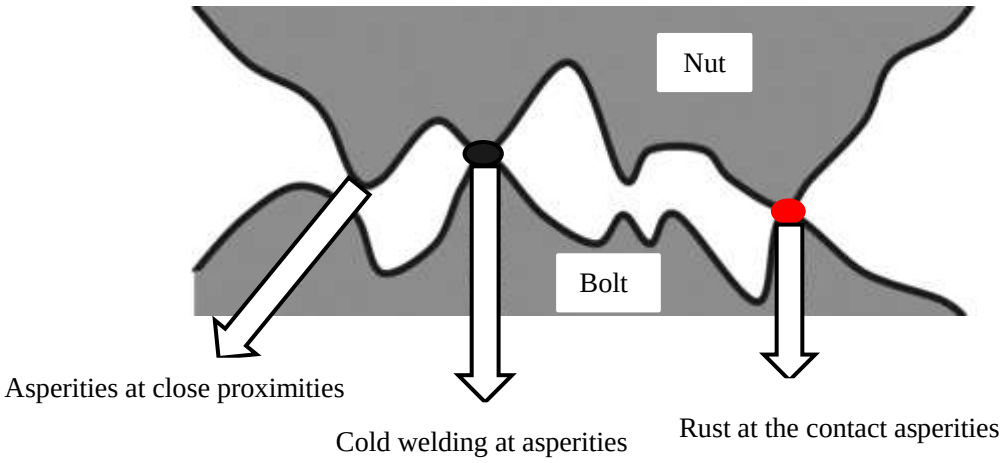

Figure 1.4 A schematic of the possible causes of bolt and nut thread seizure at the asperities level

There are a range of penetrant products. For instance, a common product such as WD-40 Multi-Purpose contains lubricating ingredients and protects metals with corrosion resistant ingredients. There are also products for more specific applications such as WD-40 Specialist Rust Release Penetrant, which is designed to tackle rust more effectively. It acts faster, penetrates rust and loosens the rusted and corroded bolts. In addition, a protective layer is left behind to prevent rust and corrosion from re-forming.

1.5 Problem statement

Companies such as WD-40 are interested in improving their products. The key to formulate better penetrants is to understand how they perform when they are inside a threaded contact. An ideal product would penetrate at a fast rate and provide a good

lubrication. Thus it is important to investigate both penetration and lubrication performance.

When a penetrant is sprayed onto a fastener, it is drawn into the threaded contact by capillary forces and fluid penetration initiates (Vail et al., 2013). Key fluid properties such as viscosity and surface tension as well as the geometrical properties of the bolt and nut threads affect the penetration process in the capillary channels (Washburn, 1921). The performance of a penetrant can be assessed by measuring the penetration time. Conventional methods such as nail climb test is used in industry to measure the time a penetrant climbs a vertical nail. However, this method cannot provide an accurate assessment of fluid penetration in a threaded contact.

The main research problem in this work is the requirement for a non-intrusive technique to study the penetration performance of penetrant samples with different viscosity and surface tension in a threaded contact. Therefore, initially the challenge is to establish a direct non-invasive technique that is capable of detecting the oil films in a threaded fastener. Although, the rusted condition is not studied in this work, the potential of this technique to investigate such conditions is discussed.

Ultrasonic reflectometry was initially used by Dwyer-Joyce et al. (2003) to measure lubricant films and since then numerous studies have been carried out. This technique is based on principles of ultrasonic wave reflection from the interface of interest and will be used in this study to obtain the penetration time.

To investigate the lubricating performance of the penetrants, the loosening torque will be measured as a function of the penetration time to give an indication of the rate at which the fastener is lubricated.

1.6 Aims and objectives

This research has two main aims. The first aim is to develop an experimental technique to measure the fluid penetration time in-situ and compare it with fluid properties and a theoretical framework to gain a better understanding of penetration performance. The second aim is to investigate the rate at which the penetrants loosen the threaded fasteners and provide information about the lubrication performance. The findings of this research can then help with improving the formulation of oil penetrants.

The project objectives are:

1. Development of a non-invasive ultrasonic method to measure penetration time of fluids inside a threaded contact.
2. Investigate the penetration performance of various fluid samples with a range of viscosities.
3. Develop an analytical method to model fluid penetration based on viscosity and surface tension as well as the geometrical characteristics of the threaded contact and compare it with the data obtained from the experimental technique.
4. Investigate the lubrication performance of some of the fluids (commercial products) by measuring the loosening rate of the bolt and calculating the coefficient of friction at the bolt and nut threads.

1.7 Outline of thesis

This thesis is divided into the following chapters:

Chapter 1 - In this chapter, the project is introduced and the motivation for research is given. In addition the aims and objectives are laid out.

Chapter 2 - In this chapter, a review of the work carried out on tribology of threaded fasteners, fluid penetration science and oil film monitoring techniques will be given. There will also be an emphasis on studies using an ultrasonic technique when applied to bolted joint as well as the oil film measurements.

Chapter 3 - In this chapter, the principles of ultrasound is given. It is explained how ultrasound waves are generated and detected by making use of transducers and ultrasonic apparatus. Different modes of wave propagation is discussed. In addition, reflection of ultrasound waves at a boundary is described.

Chapter 4 - In this chapter, the detail of the concept for measurement of fluid penetration in threaded fasteners is given. The design and preparation of the ultrasonic rig is discussed. In addition, it is explained how raw data obtained from a typical measurement.

Chapter 5 - In this chapter, results obtained from fluid penetration technique are given and discussed. In addition, the penetration time of different samples are compared with each other.

Chapter 6 - A theoretical model for the penetration process is given. The results of the model is then compared with the data from the experimental technique.

Chapter 7 - In this chapter, the lubrication performance of some of the fluid samples are studied by firstly measuring the loosening torque as fluid penetrates into the threaded contact. In addition, the coefficient of friction at the threads is deduced.

Chapter 8 - In this chapter, the contributions and limitations of the work are highlighted. Some recommendations for future work are also given.

2

Literature Review

This chapter provides a review of the literature discussing various works covering friction and lubrication in threaded fasteners, principles of fluid penetration in capillary tubes and techniques to measure oil films. Some applications of the ultrasonic technique are also highlighted. The basic principles of ultrasonic reflection are then given in Chapter 3.

2.1 Introduction

The aim of this chapter is to consider the research conducted in areas relevant to the work done in this thesis. The following three topics are considered in this chapter:

- Threaded fasteners

  The survey will consider some of the important work completed to date especially from a tribological point of view. Friction and lubrication will be the main subjects to evaluate.

- Science of fluid penetration

  Particularly looking into the work, considering the mechanism of fluid penetration in capillaries and micro tubes. Geometrical effects of the channel and fluid properties will be also considered.

- Oil film measurement techniques

  An overview of oil film monitoring techniques will be given with advantages and disadvantages of each technique. The latest work on the measurement of fluid penetration in the threaded fasteners is discussed and the limitations are highlighted to form the basis for the work carried out in this thesis.

2.2 Threaded fasteners – A historical perspective

The history of threads goes back to around 400 BC. Although there is no clear documentations about the exact origin, according to Eccles, Archytas of Tarentum (400BC) is known to be the inventor of screw (Eccles). Archimedes (287BC– 212BC) then applied the mechanical principles of screw to build screw pumps for lifting water from river for irrigation purposes.

Although threads have been around for quite a while, fasteners have been available for the last couple of centuries. German Johannes Gutenburg used screws in fasteners in his invention of a printing press in the 15th century (Eames, 2012).

The industrial revolution marked a new era, when novel manufacturing processes were introduced (Eames, 2012). Until than fastener screws were produced by hands, however, as there was a rise in demand, the production process had to be stepped up. In Britain in 1760, J and W Wyatt started a factory making screw threads in mass (Eames, 2012). Other companies also started to produce their own bolt and nuts. And a challenge was the

absence of a standard system for threads, which caused problems for machinery manufacturers.

Figure 2.1 Archimedes Screw Pump (Eames, 2012)

In 1841, Joseph Whitworth proposed a solution for a standard system by setting the thread angle profile at 55˚ (Figure 2.2) and defining the number of threads per inch for various diameter ("British tools & fasteners - BSW thread profile", no date).

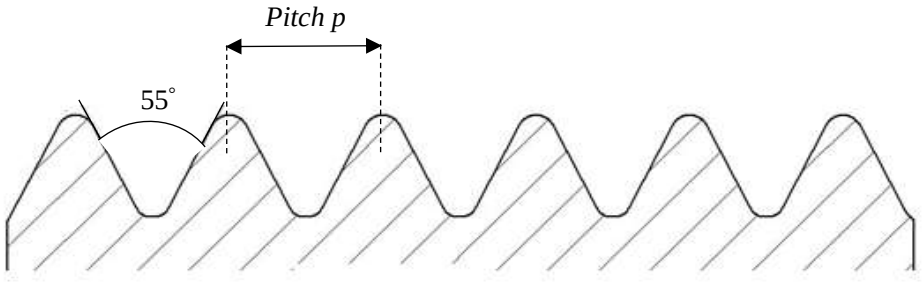

Figure 2.2 Whitworth thread (British tools & fasteners - BSW thread profile, no date)

In 1948, the International Organisation for Standardization (ISO) started work on a standard screw thread system (Figure 2.3) for worldwide application and an agreement was finalized on a standard thread system in 1964 (Shih, 2014).

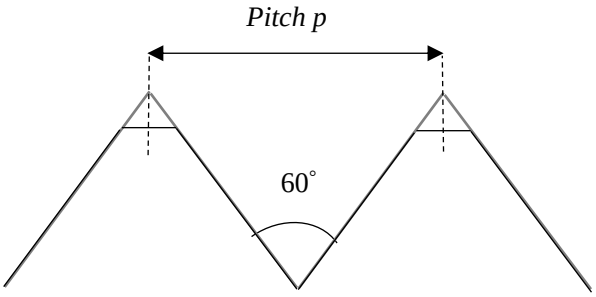

Figure 2.3 ISO Metric Thread Profile

Over the last few decades, with the most recent updates in fine-tuning of the bolts, there has been rapid improvement in bolt's strength and properties. Over the years, bolt technology has become more sophisticated, with a variety of materials available to meet the needs of industry.

2.3 Tribology of threaded fasteners

2.3.1 Torque-tension relationship

As a fastener is tightened up, a preload is created, which provides the clamping force, responsible for the safety and reliability of the bolted assemblies (Nasser et al., 2005). Tribological aspects of the threaded fasteners are significant, as these control the torque-tension relationship (Eccles, 2014).

In a bolted assembly, the torque is applied on the bolt or the nut (Figure 2.4). Most of the tightening torque, however, is consumed in overcoming the friction present in the fastener (Nasser et al., 2005). There are two main frictional components, the under head friction and the thread friction. The remaining torque, about 10% of the input torque, is used to produce the tension force (Juvinall et al., 2000).

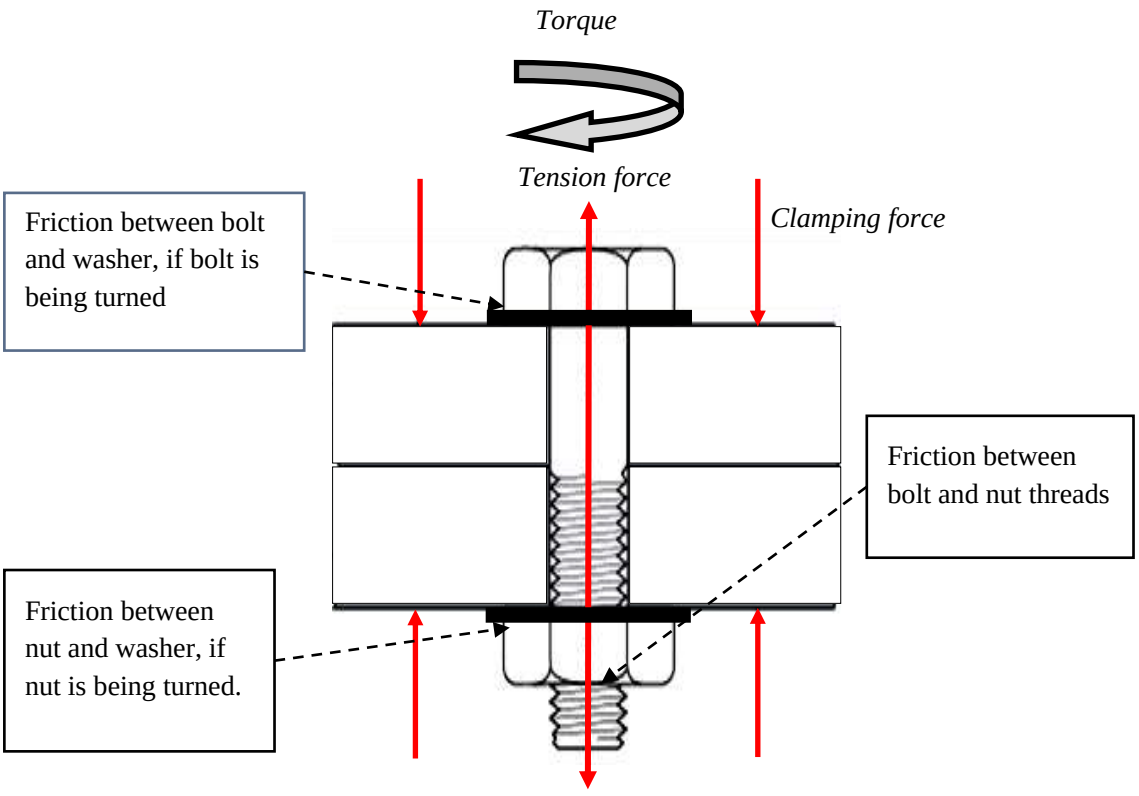

Figure 2.1 Schematic of a bolted assembly showing the tension force and sources of friction present

When using a torque-tension relationship, if the friction-torque components are not determined accurately, the fastener tension will not be estimated correctly. Underestimation of the fastener tension will result in the failure of the threaded fastener by over stressing the assembly. An overestimation of the tension force, on the other hand, could lead to fastener loosening, joint separation and fatigue (Nasser et al., 2004).

The torque-tension relationship (Bickford, 1977), which is in common use by most practicing engineers and scientists is given as:

$$T = KDF \tag{2.1}$$

where T is the tightening torque, D is the nominal diameter and F is the fastener tension and K is the nut factor. The Nut factor is influenced by many parameters such as thread and under head friction, fastener geometry, contact areas, surface conditions, materials and contact pressure distribution.

Juvinall et al. (2000) provided a rough guide for nut factor (K=0.2) for static applications, however, this is not a true representation of a complex system. Bolted joints have different design and characteristics; therefore, a more accurate value of the nut factor is required. The best approach is to find the nut factor experimentally from measurement of the torque and tension force for any given bolted assembly.

2.3.2 Friction in fasteners

When the bolt or nut is tightened, its motion can be considered as a body moving up an inclined plane (Eccles, 2010), as shown in Figure 2.5, where a horizontal force P, applied at the mean thread radius (half of the bolt pitch diameter d_b). The development of a thread is an inclined plane with pitch p indicating the height and the base is the circumference at the pitch diameter d_b. The fastener tension force F is at an angle α (helix angle of thread) and reaction force R is at angle φ normal to the plane. Analysing the forces shown in Figure 2.5 (Eccles, 2010),

$$P = Ftan(\alpha + \varphi) \tag{2.2}$$

The torque acting on thread is:

$$T = P \times \frac{d_b}{2} \tag{2.3}$$

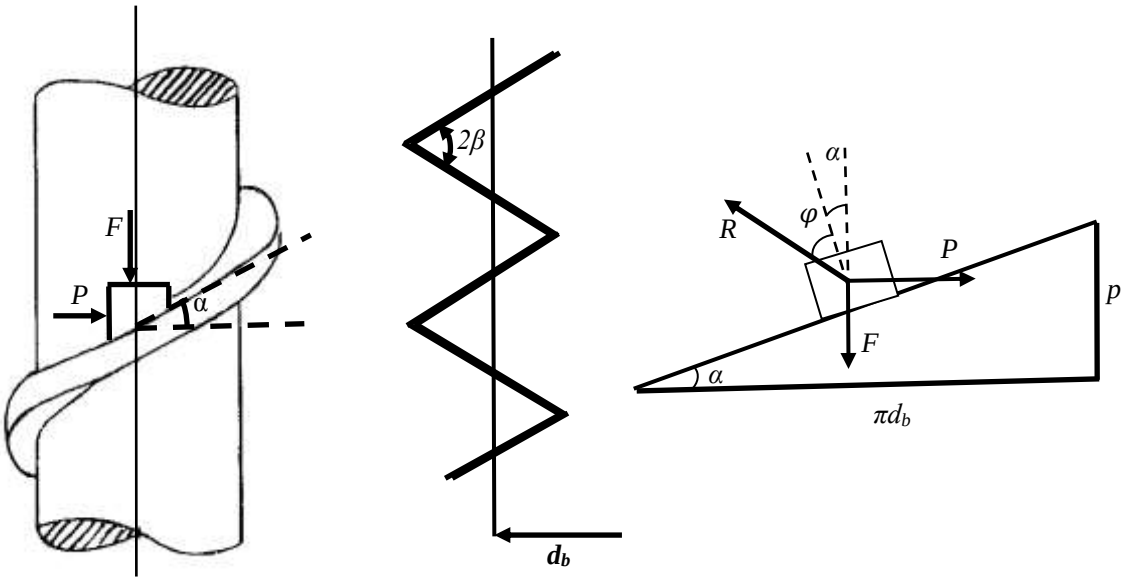

Figure 2.2 Schematics showing the tightening process modelled as a load moving up an inclined plane

Hence:

$$T = F\frac{d_b}{2}tan(\alpha + \varphi) \tag{2.4}$$

In the case of V threads such as bolt and nuts, which are used for clamping parts together, F acts at an angle β, which is half the thread profile angle 2β.

Therefore the normal reaction force, as shown in Figure 2.6, is given as:

$$R_N = \frac{F}{cos\beta} \tag{2.5}$$

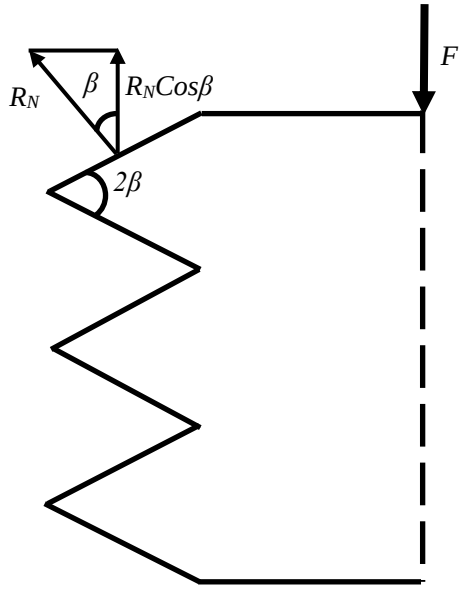

Figure 2.3 Schematics showing the V-thread and the reaction force

The friction force acting tangentially to the thread surface is given as:

$$\mu_t R_N = \mu_t \frac{F}{cos\beta} = \frac{\mu_t}{cos\beta} F = \mu' F \tag{2.6}$$

$$\mu' = \frac{\mu_t}{cos\beta} \tag{2.7}$$

where $\mu_t$the coefficient of friction between the bolt and nut is thread surfaces and μ' is known as the effective coefficient of friction. Expanding equation (2.4) gives:

$$T = F \frac{d_b}{2} \left[\frac{tan\alpha + tan\varphi}{1 - tan\alpha tan\varphi} \right] \tag{2.8}$$

where:

$$tan\alpha = \frac{p}{\pi d_b} \tag{2.9}$$

φ is known as the friction angle, hence:

$$tan\varphi = \mu' = \frac{\mu_t}{cos\beta} \tag{2.10}$$

Therefore equation (2.8) can be arranged as:

$$T = F \frac{d_b}{2} \left[\frac{\frac{p}{\pi d_b} + \frac{\mu_t}{cos\beta}}{1 - \frac{p}{\pi d_b} \frac{\mu_t}{cos\beta}} \right] \tag{2.11}$$

Because the denominator is small, equation (2.11) reduces to:

$$T = F \frac{d_b}{2} \left[\frac{p}{\pi d_b} + \frac{\mu_t}{cos\beta} \right] \tag{2.12}$$

The other friction torque component is due to the bolt or nut head. In here, the bolt is considered to be tightened. Hence the friction torque at the bolt head, is given as:

$$T_{bolt} = F \mu_n \frac{D_e}{2} \tag{2.13}$$

$$D_e = \frac{d_0 + d_i}{2} \tag{2.14}$$

where d_0 the outer diameter of the bolt is head and d_i is the inner diameter of the bolt head. Where μ_n is the coefficient of friction at the bolt under head and D_e is the effective diameter of the circle, where the friction is acting.

Combining the torque components results in equation (2.15), given as:

$$T = F \left[\frac{P}{2\pi} + \frac{d_2}{2} \frac{\mu_t}{cos\beta} + \mu_n \frac{D_e}{2} \right] \tag{2.15}$$

This equation was introduced by Motosh (1976), which provided a more accurate torque-tension relationship, which contains the friction torque components, thread extension torque, fastener geometry and thread angle profile.

2.3.3 Experimental studies on friction

There have been many works investigating the friction in a bolted assembly. Sakai (1978) conducted some experiments investigating different factors that affect the torque-tension relationship. The effect of lubrication, surface treatment and different bolt and nut materials were investigated. Another significant factor was the tightening speed, which was varied from 0.8 rpm to 12 rpm. In his work, the variation of tightening speed was plotted against the total coefficient of friction, as shown in Figure 2.7. The main finding was the fact that at very slow fastening, the friction coefficient is higher. This appears to be the case for all the conditions. At very slow fastening speed, metal-to-metal contact occurs at the threads, hence a higher coefficient of friction were obtained. The other finding of this work was that the coefficient of friction measured at the threads was higher than the one at the bolt under head bearing.

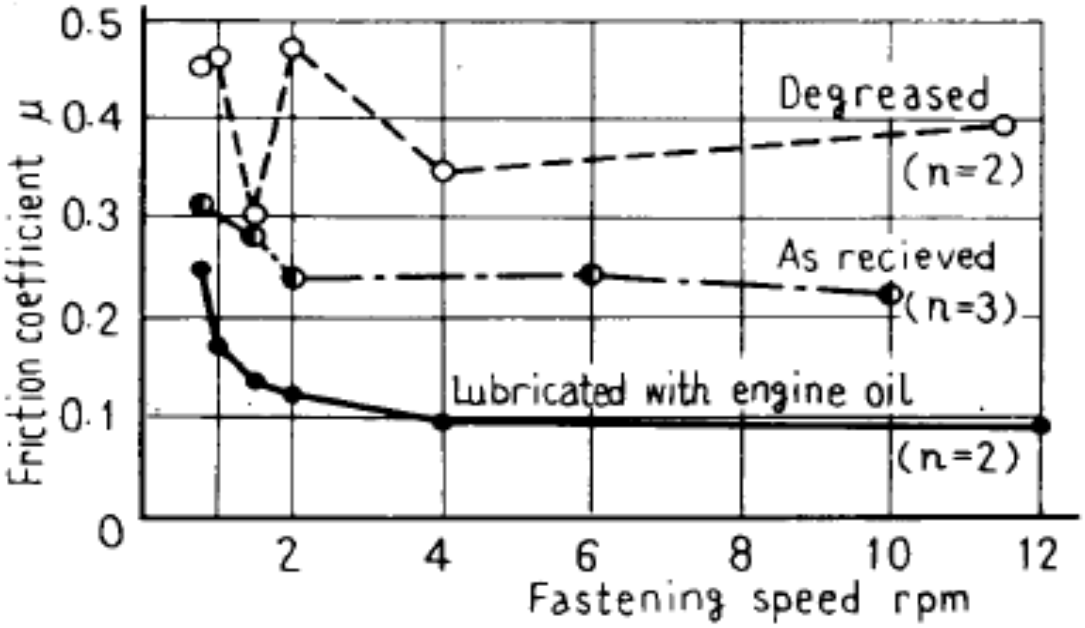

Figure 2.4 Effect of fastening speed on friction coefficient (Sakai, 1978)

In another study carried out by Nasser et al. (2005) the effect of thread and fastener geometry on the friction torque component in the torque-tension relationship was explored. The experimental results showed that the class of the material fastener has a notable effect on the thread coefficient of friction. In order, this was followed by the significance of the fastener size and thread classification.

Zou et al. (2007) investigated the effect of lubrication on friction and torque-tension relationship on M12 coarse and fine fasteners. A series of experiments were conducted to study the effects of different types of lubricants such as oil, grease and solid films whilst varying the tightening speed from 1 rpm to 100 rpm. Two types of fasteners with coarse and fine threads were tested. When solid film lubricants were applied, the lowest values of friction coefficient for thread and under head bearing were obtained, implying that a higher clamping force was generated. With the case of grease and oil, there was not much difference in their frictional behaviour. Figure 2.8 shows the coefficient of friction at the threads for the low viscosity oil samples for both the fine and coarse threads.

The coefficient of friction is significantly higher when the tightening speed is less than 5rpm. This is because at such a low tightening speed and a low viscosity oil sample, the sliding surfaces are most likely working in the boundary or mixed lubrication regime, hence the higher friction. But as the tightening speed increases, it is likely that a hydrodynamic lubrication regime forms and therefore a lower coefficient of friction.

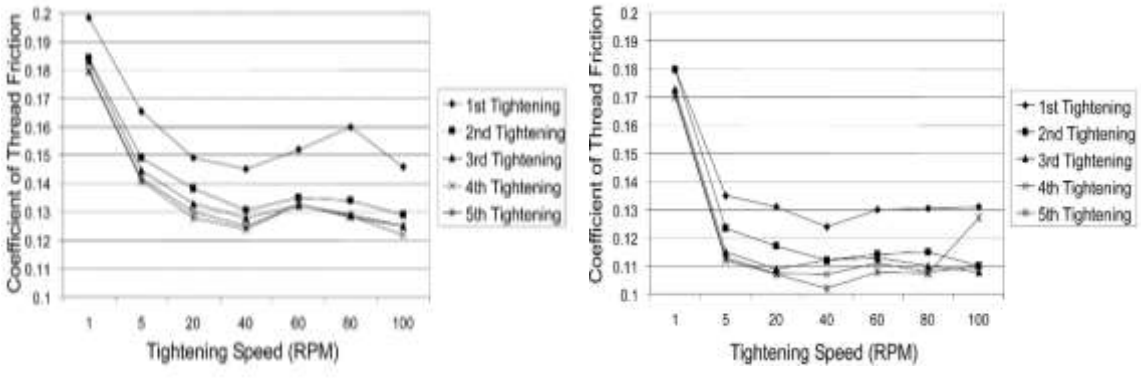

Figure 2.5 Thread coefficient of friction with low viscosity oil (Zou et al., 2007)

In another work by Nassar et al. (2007), the effect of the number of tightening and loosening events on M12 Class 8.8 bolt with and without zinc coating was studied against both the nut factor and thread coefficient of friction. For unlubricated zinc coated fasteners, as the tightening speed increases a significant decrease in nut factor can be observed and the same trend is true for coefficient of friction. In addition to this, the repeated tightening and loosening cycles showed a notable increase in the coefficient of friction. For plain fasteners in dry condition, no measurements were recorded due to amount of heat generated during the tests. For the lubricated condition, however, there was no major change in the nut factor or coefficient of friction, as the tightening speed increases, the same trend is true for the coefficient of friction.

2.3.3.1 Non-rotational loosening

Once a fastener is tightened, the clamp load may decrease without any rotation of the nut in the assembly. This process is referred to as non-rotational loosening (Eccles, 2011). Non-rotational loosening can happen due to several factors, some of them are listed below:

- Stress relaxation

  It is a form of creep and occurs when a high stress in a material is relieved (Sachs and Evans, 1973). Over time, the stress is relaxed with a subsequent reduction in bolt preload.

- Embedding

  Embedding is localized plastic deformation that occurs under the nut face, in the joint faces and in the threads and contributes towards the loss of clamp force acting on the joint (Eccles, 2011). This happens even when the loading is below the yield point of the bolt resulting in asperities flattening and increasing the real contact area.

2.3.3.2 Self-loosening

Threaded fasteners are used in various machines and functioning structure. Thus they are subjected to dynamic loads. A fastener can unintentionally loosen, which can result in catastrophic failures. This process was first noticed in the middle of 19th century and initial efforts were made to improve the design of bolt and nuts to prevent loosening in railway joints due to vibration (Ibbotson et al., 1880).

However, it was not until Goodier and Sweeney (1945), when an in-depth study of the self-loosening in bolted joints commenced. They investigated the effect of dynamic loading, when applied to the bolted joints in the axial direction. They concluded that under the influence of axial loads, the nut and bolt radially expand and contract respectively, causing small movements between bolt and nut threads, hence causing the loosening.

In a later work by Sauer et al. (1950), the work of Goodier and Sweeney (1945) was examined. The experimental work involved using a fatigue testing machine by firstly subjecting bolts to static loads and then adding a dynamic load. The vibration frequency was set at 30 Hz. It was found that the loosening rate was at its highest (maximum loosening of nut being less than 6 degrees) during the initial cycles of vibrations. However, as the number of cycles increased, the rate of loosening dropped. In addition, it was observed that an increase in dynamic to static load ratio intensified the loosening

rate. Furthermore, it was concluded that an increase in preload decreased the rate of loosening.

In a later work carried out by Gambrell (1968), effects of axial loading and lubrication condition on the loosening of fine and coarse fasteners were investigated. The dynamic to static ratio (DSR), initial preload and the frequency of loading were varied. For DSR greater than 1, fine threads loosened less than coarse threads. Lubrication condition was found to influence the loosening of coarse threads, but not the fine ones. Furthermore, he revealed that as the number of load cycles increased, the rate of loosening decreased. Also when the tests were run within a frequency range of 3.3 Hz to 20 Hz, no effect on the loosening was observed.

Up until 1969, the main cause of self-loosening was thought to be due to the axial loading and vibrations, however, Junker (1969) in his significant contribution found that transverse dynamic loads (Figure 2.9) generate a far more severe condition than dynamic axial loads. He reasoned that radial movement under axial loading is considerably less than that which is produced under transverse loading. The transverse loading first overcome the frictional forces and then cause the movements between bolt and nut threads.

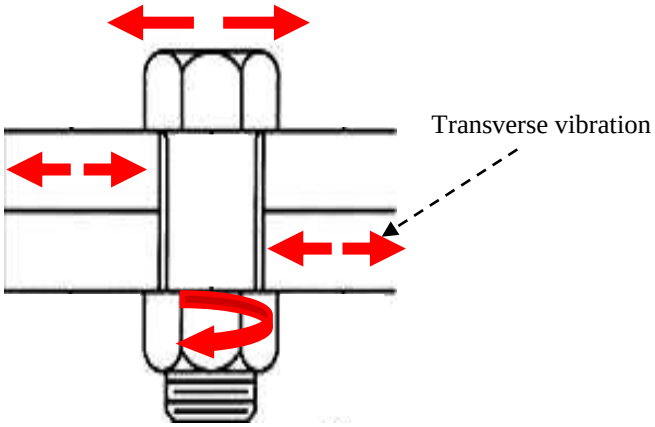

Figure 2.9 Fasteners when subjected to transverse vibration

2.3.4 Tightness check of fasteners

Considering the significance of the tightness of the fastener and accordingly the clamping force generated, for fasteners used in assemblies, Eccles (2014) introduced a new means of measuring the load present. By tightening up a bolt and immediately loosening it, it is possible to find the load. This can be introduced by the torque-tension relationship, where

the torque-tension relationship, Equation (2.2), for the tightening process was given before and the equation for the loosening process is:

$$T_l = \left[-\frac{P}{2\pi} + \frac{\mu_t r_t}{cos\beta} + \mu_b r_b\right]\mathrm{F} \tag{2.16}$$

When the bolt is being untightened, less torque is required, since the thread extension torque $\left(-\frac{P}{2\pi}\right) F$, helps with the process. Considering the total input tightening torque as T_t and the torque to loosen the bolt as T_l, the difference in the tightening and loosening torque was found in Eccles work (Eccles, 2014) as:

$$T_t - T_l = F\left[\frac{p}{\pi}\right] \tag{2.17}$$

To derive equation (2.17), there was an assumption that the frictional components in the tightening and loosening process are equal.

2.3.5 Thread overload

If excessive torque is applied during fastener tightening, pressure increases between the contacting and sliding thread surfaces. Under high contact sliding forces, the first phase of adhesive wear initiates, which is when the protective oxides are worn away, hence, exposing the material ("Fastener + Fixing Magazine", 2015). Due to intimate contact at the high points of both metal contact, the asperities are sheared and locked, and cold-welding occurs at the micro joint ("Review of the Wear and Galling", 1978). Under further sliding the rupture of the welded asperities and material transfer will result in severe adhesive wear. This is known as galling, which is common in stainless steel (Summers, 2011). In extreme cases, galling in fasteners can lead to seizure and ultimately failure by ripping out the threads.

There are several measures that can be taken to avoid thread galling, which are summarized as follows:

- Installation torque: It is critical to ensure that correct tightening torque is applied. Since any additional torque implies generation of more heat, which increases the chance of thread galling.
- Material choice: Using different grades of stainless alloy for the internal and external threads can reduce the chance of galling. The main point is to have different hardness for the bolt and nut materials.

- Lubrication: Lubrication is a very effective way to tackle any future galling. This can be solid or fluid and can be applied before or at the point of assembly. The lubrication regimes are discussed in the next section.

2.3.6 Load distribution in threads

The load distribution in the threads of a threaded fasteners is not uniform. In early works by Den Hartog (1929) pointed out that when a bolt and nut of similar pitch are loaded, the bolt and nut is under tension and compression forces respectively, which causes the elongation of the bolt and contraction of the nut. As a result, the pitch of the mating threads are no longer the same, hence the non-uniform load distribution along the thread. He solved the problem theoretically and took into accounts factors such as axial extension of the bolt, nut compression and bending of the threads. The result of his research was a theoretical load distribution with a parabolic shape, indicating that 45% of the total load is taken by the first two threads. Sopwidth (1948) developed Hartog's work further and considered the radial displacement of the bolt and nut thread when predicting the load distribution. His analysis gained acceptance and to this date is used by many to assess load distribution in threads. In one of the works (Wang et al. 1995), the load distribution for 8 engaged threads in a threaded connection was analysed applying an adapted spring model based on the work of Miller (1983). The load applied on each thread is given in Table 2.1.

Thread Number	***Loading distribution (%)***
1	30
2	20
3	16
4	11
5	9
6	7
7	5
8	2

Table 2.1 Loading distribution of 8 engaged threaded in a threaded connection (Wang et al., 1995)

2.4 Fluid penetration into small channels

In section 2.3.3, a survey of some of the key studies regarding the effects of lubrication in threaded fasteners was given, bearing in mind that samples were lubricated before tightening up. As in this thesis, the effect of lubrication of fluid penetration in the threads are considered once the fasteners is tightened up, it is important to have an understanding of the fundamentals of fluid penetration science.

2.4.1 Contact angle and the Laplace-Young Equation

In liquids, there are strong cohesive forces acting between the molecules. The strength of these cohesive forces dictates the surface tension of different liquids and hence the liquid-gas interfaces. Molecules of a liquid also have attraction to the solid surfaces and this is normally defined by wettability. Wettability is measured by contact angle θ. Figure 2.10 shows different types of fluid-solid interaction.

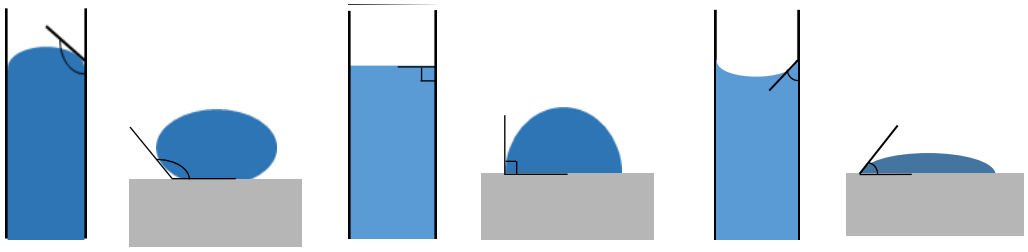

a) $\theta > 90°$ b) $\theta = 90°$ c) $\theta < 90^{\circ}$

Figure 2.10 Formation of contact angle θ

It can be observed that there are three main cases. From left to right, when $\theta > 90°$, wettability is low and liquid-gas interface in the capillary tube is convex from the liquid side. At $\theta = 90°$, wettability is neutral, however, for contact angles less than 90°, fluid wettability improves and as it reaches 0°, it fully spreads. In this condition, the interface in the capillary tube is concave from the liquid side.

The curved interface is due to the surface tension of the fluid, which introduces a pressure difference across the liquid-gas interface, hence drives the fluid forward. The pressure difference is also known as the capillary pressure. The rise of liquid through a capillary tube is shown in Figure 2.11. The liquid rises to an equilibrium height, h. The radius of the capillary is r_c.

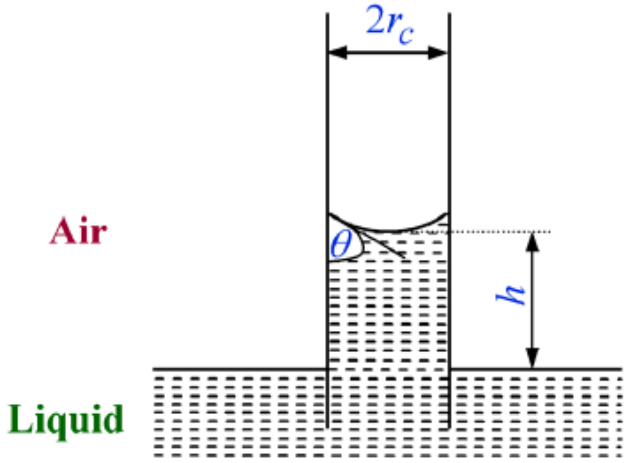

Figure 2.11 Capillary rise (Ghosh, 2014)

Some of the very early works on capillary pressure was carried out by Young (1805) and Laplace (1806), which led to the introduction of the Laplace-Young Equation. This equation states that the pressure drop across the liquid-gas interface from the concave to the convex side is inversely proportional to the curvature of the interface:

$$\Delta P = \gamma \left(\frac{1}{r_1} + \frac{1}{r_2}\right) \tag{2.18}$$

where γ is the surface tension of the fluid, and r_1 and r_2 is the radius of curvature. Since the capillary has circular cross-section and its radius r_c is small, the meniscus can be approximated by a cap of a hemisphere of radius, $\frac{r_c}{cos\theta}$ (Ghosh, 2014).

Therefore, $r_1 = r_2 = r_c/cos\theta$. From Young-Laplace equation, the pressure drop is given as:

$$\Delta P = \left(\frac{2\gamma cos\theta}{r_c}\right) \tag{2.19}$$

For rectangular channel, however, r_c is replaced by h, the gap between two walls, therefore the pressure drop across the interface is given as:

$$\Delta P = \left(\frac{2\gamma cos\theta}{h}\right) \tag{2.20}$$

The Laplace-Young Equation is fundamental to derivation of Washburn equation (Washburn, 1921).

2.4.2 Capillary flow

Washburn (1921) studied the rate of fluid penetration in cylindrical capillary tubes by treating the phenomena as a balance of forces between viscous and capillary forces.

Washburn derived the equation for fluid flow in both vertical and horizontal cylindrical tubes. The equations were derived from Poiseuille's law for viscous flow, assuming the pressure drop across the liquid-gas interface given as equation (2.20). In his derivation of the equation for fluid flow in cylindrical horizontal capillary tubes, he did not take into account gravitation and other effects. He found that the distance of fluid penetration was proportional to the square root of the time.

The equation that he derived is given as:

$$l^2 = \left(\frac{\gamma}{\eta}\right)\left(\frac{cos\theta}{2}\right) r_c t \tag{2.21}$$

where l is the length of fluid penetration, γ is surface tension, η is viscosity, θ is contact angle, r_c is the capillary radius and t is the time of penetration. The concept of penetrativity of liquid or the coefficient of penetrance $\left(\frac{\gamma cos\theta}{2\eta}\right)$ was introduced, which he defined it as the distance which the liquid will penetrate a capillary tube of unit radius in unit time, when flowing under its own capillary pressure.

Washburn can be also applied to fluid penetration in porous media (Good, 1973 ; Dang-vu, 2005), since the porous media can be assumed as a bundle of horizontal or vertical circular capillaries tubes depending on the application of interest.

Expanding on Washburn's work, Rideal (1922) took into account the inertia force of the liquid in the tube. However, for small values of capillary radius, the derived equation is simplified to the original Washburn one. Bosanquet (1923) developed it further by understanding the effect of inlet acceleration of the liquid into the horizontal capillary. But in later research, Letelier (1979) did not consider the effects from the inlet acceleration.

Experimental work was carried out in later years to compare with the theoretical work. Fisher and Lark (1979) studied the flow of water and cyclohexane in glass capillaries both theoretically and experimentally. The results obtained for the experiments at capillary radius of 3 to 400 micron agreed with the Washburn model. However, the flow rate of water decreased for smaller capillaries and bubbles were observed in the liquid. They explained that bubble formation could be the main cause of reduction in the water flow rate.

Ichikawa and Satoda (1994) provided a detailed analysis of interface dynamics of horizontal capillaries for several test liquids in Pyrex glass, quartz, and Teflon tubes with

capillary radius ranging from 0.5-4 mm. The dimensionless analysis was carried out and the theoretical work agreed well with the experimental data.

Capillary action has been of interest to many engineering application during the recent years. Schwiebert and Leong built a model to understand the flow of epoxy under fill in a flip-chip interconnect (Schwiebert et al., 1996). Flip-chip interconnect is popular because of its high electrical performance. However, the epoxy under fill is required in order to improve the reliability of the flip-chip interconnect. For manufacturing purposes the flow rate of the under fill material needs to be understood. The difference of this work to the previous ones discussed is that the fluid flows between the parallel plates.

In another piece of work, Ballerini et al. (2011) investigated the fluid flow mechanism in thread-based microfluidic devices. Understanding the penetration behaviour and fluid velocity in these devices can help with the development of more advanced and functional thread-based sensor designs with application to both medical and environmental monitoring. In this paper, however, the capillary rise was against gravity**,** therefore Washburn equation was used for the vertical capillaries. It was observed that the fluid penetration slowed down in all the thread samples used. It was argued that the main reason for this was the loss of capillary force due to gravity as well as the possibility of fluid evaporation causing fluid starvation in the capillary channels.

2.4.3 Measurement of contact angle

Another method to assess the penetration ability is to find out how well the fluid spreads. This can be done by measuring the contact angle of the fluid as described in section 2.4.1. Lower contact angles mean better wettability, hence better fluid penetration.

Although this method provides some indication of fluid penetration, it does not give a direct measurement of fluid penetration performance into a threaded contact. There are various direct measurement methods for lubricants in engineering contacts, which will be reviewed in section 2.7.

2.5 Measurement of pressure in bolted joints

Ultrasonic testing techniques have been applied to a wide range of bolted joint problems. In one of the earliest work carried out by Ito et al. (1979), ultrasonic waves were used to measure the interface pressure distribution of a bolted-flange assembly. Various factors such as the surface topography, joint material and upper flange thickness were considered

and the findings suggested that these factors had a significant effect on the interface pressure distribution curve.

In a later work by Marshall et al. (2006), the contact-pressure distribution in bolted joints was studied by means of an ultrasonic technique. An ultrasound wave, generated by a 10 MHz transducer, was focused on the clamping interface and the reflection signals were recorded (Figure 2.12).

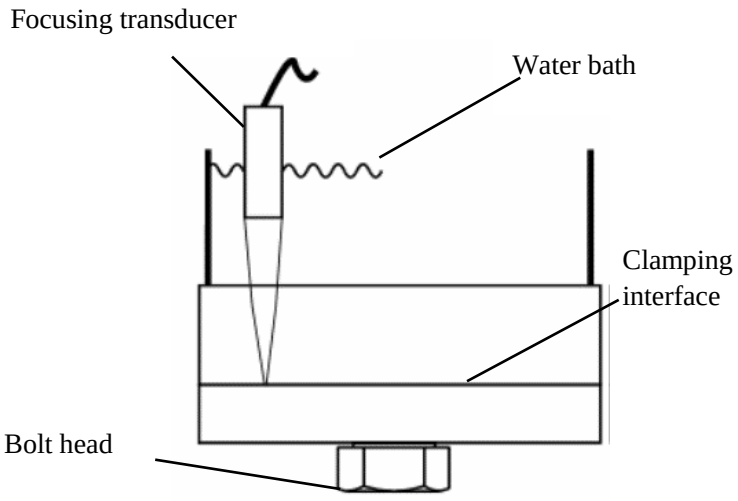

Figure 2.12 Measurement of contact pressure at the clamping interface by the focusing transducer (Marshall et al., 2006).

Different ground surfaces as well as the effect of a washer at different values of torque were investigated. The results showed that as the bolt is tightened, the joint is loaded. Furthermore, the spread of the contact pressure distribution found to be in good agreement with results obtained from previous works.

In another work carried out by Pau et al. (2007), an ultrasound method was used to analyse different joints, considering different factors such as plate thickness and applied load. The accuracy of the results were compared with experimental data obtained from pressure-sensitive film experiments as well as the results of a finite element model (FEM) and good agreement was found. Further investigation was carried out by Stephen et al. (2014), where the effect of plate thickness on the interfacial contact pressure in the bolted joints were measured ultrasonically. The findings suggested that the plate thickness had an important role in the position of the peak value of the contact pressure distribution at the interface. He also found out that for any plate thickness, an increase in the applied load results in an increase in the contact pressure.

2.6 Study of dry contacts

An ultrasonic technique has also been applied to dry contacts to study the interaction of ultrasound waves with rough interfaces (Kendall et al., 1971, Drinkwater et al., 1997, Dwyer-Joyce et al., 2001).

In an early work carried out by Kendall et al. (1971), they developed a novel ultrasonic technique to study contact between stationary and sliding contacts. Materials tested were metals, smooth and rough glasses, rubber and polymers. The findings showed that the transmitted pulse depended on the elastic stiffness of the contact. The main contribution of this work at that time was the fact that it provided a direct measurement of the contact condition, something that the previous electrical and optical methods did not offer.

In later work, carried out by Drinkwater et al. (1997), the proportion of the ultrasonic wave reflected was measured at an aluminium-aluminium interface. The measurements were recorded over a range of transducer frequency. Three different contact conditions were considered, no contact, partial contact and perfect contact. When there is no contact between the two aluminium specimens, the reflection coefficient (defined in section 3.8.1) is at unity, and when there is perfect contact, it approaches zero. However, reflection coefficient was found to be dependent on the range of frequencies tested, when there was partial contact and this was confirmed by the spring model of the interface. Moreover, the interfacial stiffness obtained from the experimental data was compared with plastic and elastic contact models and there was a qualitative agreement.

Following up, in one of the studies, Dwyer-Joyce et al. (2001) investigated rough surface interfaces using low frequency ultrasound waves. The first part of the study involved measuring the reflection coefficient at the interface between a rough nominally flat aluminium specimen and a rough hardened steel punch specimen. Various degrees of roughness and loads were applied. The interfacial stiffness was then measured from the reflection coefficient using the spring model. Furthermore, analysis was carried out to find out how sensitive ultrasonic technique is to small gaps at the interface. Gaps were modelled as cracks and stiffness was predicted and it was found that the technique was sensitive to gaps of around 2 μm at 10 MHz. The effect of roughness was considered and it was found that as the roughness increases, the stiffness at a given contact pressure decreases. The second part of study involved modelling the contact roughness to predict

the stiffness and comparing it with the measured data from the experimental data. However, only qualitative agreement was found.

2.7 Measurement of thin oil film in contacts

2.7.1 Electrical methods

Existing techniques for measuring lubricant films at engineering contacts were limited to electrical resistance and optical method for a couple of decades. Initial works (El-Sisi & Shawki, 1960) employed a technique based on electrical resistance to measure oil film thickness. In later works (Astridge & Longfield, 1967; Hamilton & Moore 1967) an electrical capacitance technique provided a relatively easy way of measuring the oil film thickness. However, the main limitation of this technique is measuring oil films, which are of the same order as the surface roughness of the contact, as in this lubrication regime, contact of the central electrode with the opposite component is possible.

2.7.2 Optical methods

Optical techniques brought a new concept, which measured oil film thickness in the elasto hydrodynamic regime (Cameron & Gohar, 1966) and boundary lubrication regime (Johnston et al., 1991). This method is a non-invasive technique and involves reflecting light from the oil film. The main disadvantage of this method is the requirement for a transparent window. Considering all the techniques discussed above, they all introduce some limitation and complexity especially for studying lubrication in a threaded contact of a bolted fastener systems.

2.7.3 Ultrasonic methods

Lubricant film measurement by means of ultrasonic has been researched in-depth, a selection of the work carried out, is briefly discussed (Dwyer-Joyce et al., 2003; Dwyer-Joyce et al., 2004; Zhang et al., 2006; Reddyhoff et al., 2008; Mills et al., 2012).

In an initial study carried out by Dwyer-Joyce et al. (2003), an ultrasonic technique was developed to measure the thickness of lubricants in bearings. The measurement principle involved using an ultrasonic transducer outside the bearing shell, which transmitted the ultrasound waves onto the lubricant film at the contact and then received the reflected portions. The reflection coefficient was then measured, from which the lubricant film thickness was found from either the layer stiffness or resonant frequency. Film thickness

data obtained were in the range of 50-500 nm. The experimental data was then compared with the theoretical film prediction and good agreement was observed.

In another work by Dwyer-Joyce et al. (2004) an ultrasonic technique was implemented to measure oil film thickness in hydrodynamic journal bearings. Lubricant film thickness within the range of 4-20 µm was measured. In addition it was possible to observe the fluctuations in film thickness, when different speed and load were applied.

Some other applications of ultrasonic technique for fluid film thickness measurement has been in ball bearing contacts (2006), in liquid face seals (2008) and at piston-cylinder contacts in a fired engine (2011).

In a very recent work by Vail et al. (2013), a non-invasive ultrasonic technique was developed to detect an oil film in the threads of a bolted connection, and hence quantified the rate at which fluid penetrated into the threads.

The measurement concept in this work is based on sending and receiving ultrasonic waves from the threaded contact. As shown in Figure 2.13, two piezo-electric elements were placed at 30° to the axis of an M10 bolt thread to transmit an ultrasonic pulse to a section of the threaded contact and receive the reflected waves.

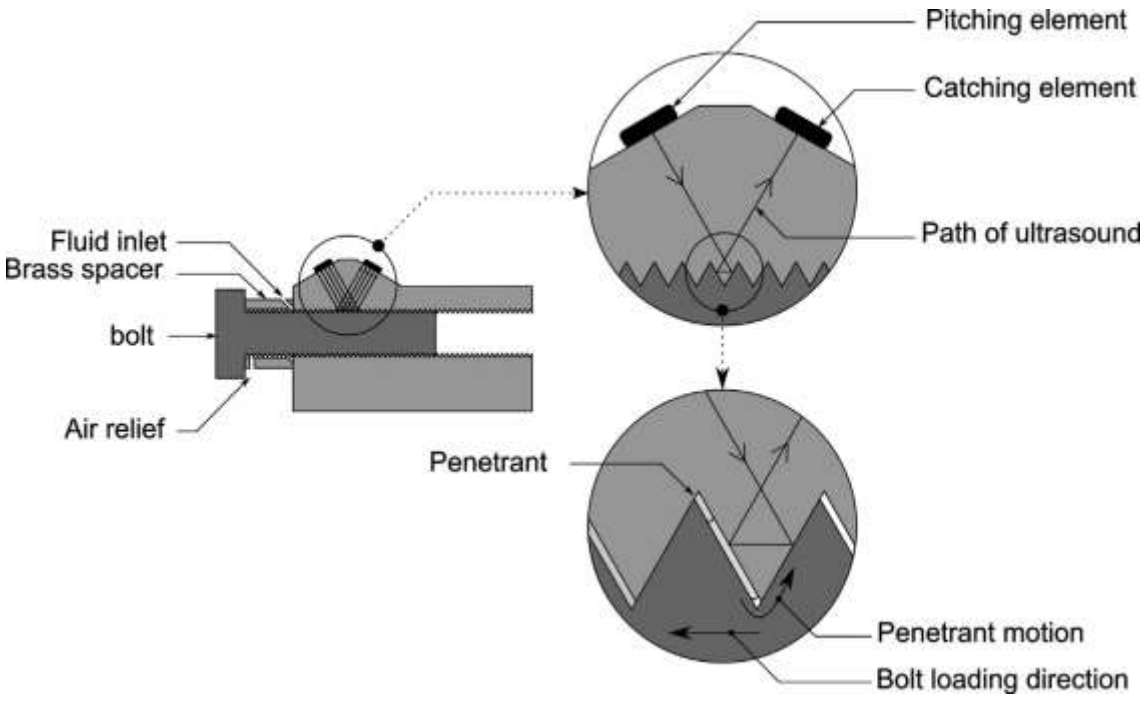

Figure 2.13 Schematic diagram showing ultrasound path for thread geometry (Vail et al., 2013)

By monitoring the reflected ultrasonic energy it was possible to infer what was occurring at the interface. As fluid penetrates into the ultrasonically monitored section of the threaded contact, a drop in signal amplitude occurs. Using this information the penetration time of fluid into threads were found. The details of the measurement concept is given in Chapter 4.

The experimental rig in this work (Vail et al., 2013) utilized 6 pair of ultrasonic piezo-electric elements equally spaced circumferentially around the apparatus. These sensors monitor multiple threads around the bolt. A sectioned schematic of the apparatus is given in Figure 2.14.

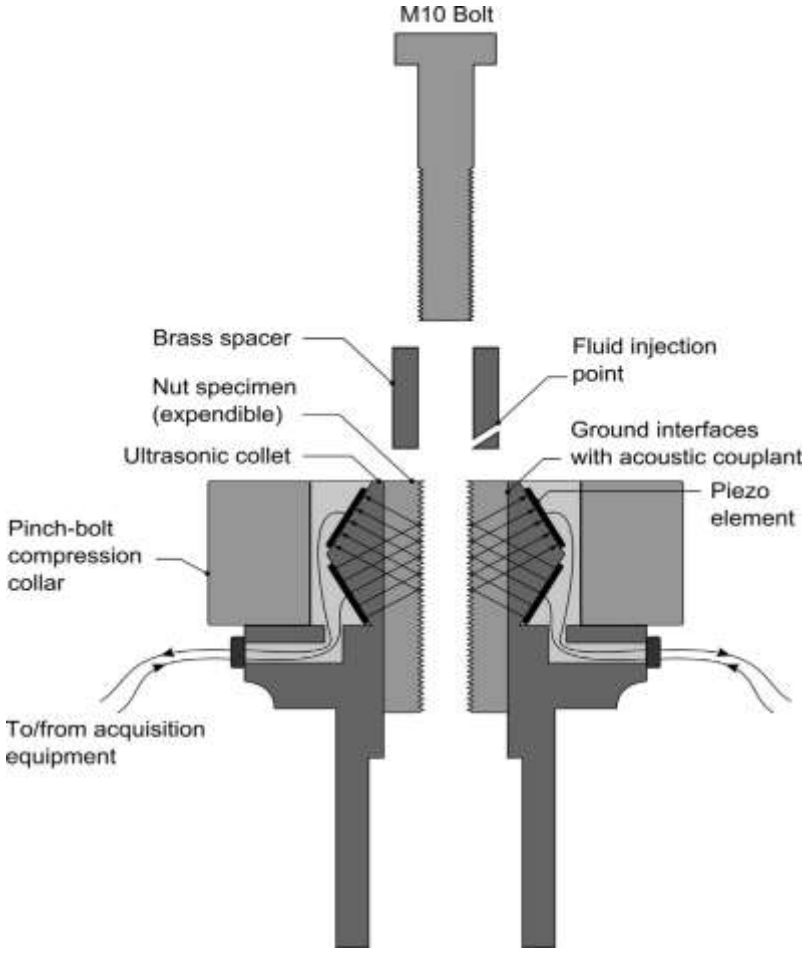

Figure 2.14 Sectioned schematic of test rig (Vail et al., 2013)

To validate the method, three penetrant samples were tested in this work and penetration time was measured. To quantify this, a parameter, τ, was defined to represent the total time for the fluid to penetrate into 4 consecutive threads. The mean fluid penetration time is given in Table 2.2. The two commercially available penetrating fluid samples were referred to as A and B and the solvent was known as C.

Fluid Sample	*Average , τ (s)*
A	40.81±4
B	54.15±6
C	43.81±2.78

Figure 2.2 Table of total penetration time into four consecutive threads (Vail et al. 2013)

The finding of this work suggests that the ultrasonic technique has the potential to measure the penetration time of fluid in a threaded fastener. Having said that, study of the number of fluid samples in this work was limited and it also did not include the lower viscosity ones (less than 2.40 mPa.s). Therefore, it was not possible to complete a comprehensive research on the penetration performance of all the fluid samples.

2.8 Conclusions

The literature survey carried out in this chapter addressed three main topics. Firstly, the work on torque-tension relationship was studied and the effect of thread geometry and lubrication were investigated. However, the lubrication behaviour needs to be understood after the penetrant is injected into the threaded contact, which is something not studied in literature.

Secondly, fluid penetration in capillary tubes was discussed and some applications of it to microfluidic systems were considered. These principles will be applied to model the fluid penetration in threaded fasteners.

Thirdly, a review of the oil film monitoring techniques was carried out. In addition to this, applications of ultrasonic techniques to bolted joints was discussed and development of various ultrasonic technique for dry and lubrication contacts were considered. The latest work on application of an ultrasonic to measure fluid penetration was highlighted (Vail et al., 2013). Although this work had some limitations, especially when measuring lower viscosity fluids. It is hypothesized that with further work, this ultrasonic technique can measure samples with a range of viscosities.

3

Principles of Ultrasound

In chapter 2, a literature survey was carried out listing some of the key studies including some of the works employing the ultrasonic technique. In this chapter, an overview of relevant ultrasound principles in this thesis is given. In Chapter 4, these principles are applied in developing a method and apparatus for measurement of penetration time.

3.1 Background

When sound waves are generated by a source, they propagate in the host medium, where the efficiency of wave propagation is dependent on the elastic and inertial properties of the material. There are three categories of sound waves differentiated by frequency of the waveforms: Infrasonic are (below 20 Hz), Sonic (20 Hz – 20 kHz), Ultrasonic (Above 20 kHz, which is the limit of human hearing).

Depending on the frequency of ultrasonic waves, they can be applied to different applications. For instance, ultrasound wave in the range of 20 to 100 kHz is used in chemically important systems, in which chemical and physical changes are desired (Pilli et al., 2011), whilst at a higher range of frequencies, i.e., 1-50 MHz, ultrasound can be employed for medical diagnosis, non-destructive testing of materials to find flaws and various other applications of mechanical testing.

As ultrasound waves are introduced into mechanical components by ultrasonic sensors, their behaviour become important especially when a change in material occurs or when they strike a dry or lubricated interface between two contacts. For all these cases, investigating the relationship between the transmitted and reflected waves led to meaningful information.

3.2 Modes of ultrasound waves propagation

As the sound waves propagate, particles of the host medium move back and forth from their equilibrium positions. The motion of these particles is caused by two main factors: the wave pressure, which makes the particles move at the first place and the restoring force of the molecules also referred to as the elasticity of the medium. There are two main modes of wave propagation, longitudinal and shear waves.

3.2.1 Longitudinal waves

Figure 3.1(a) shows how longitudinal acoustic waves travel. Wave propagation happens from left to right, displacing the particles around their equilibrium position. These displacements results in two zones of high (compression) and low (rarefaction) density in the material that relates to high and low amplitude in the acoustic wave respectively (Figure 3.1(b)).

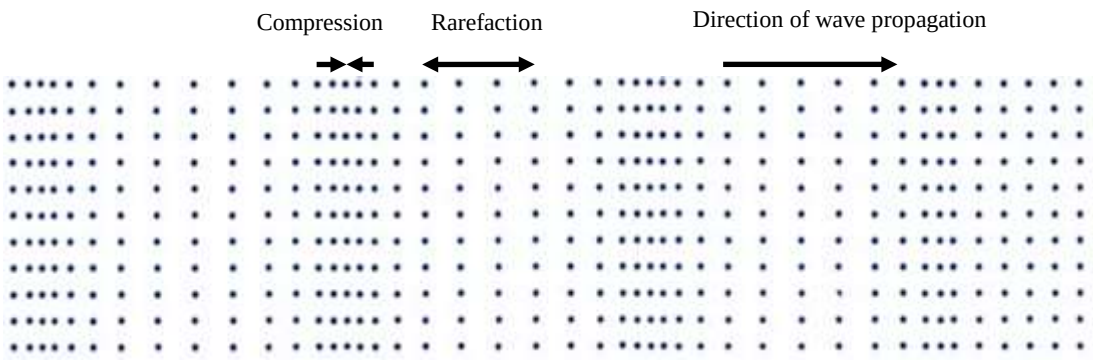

(a)

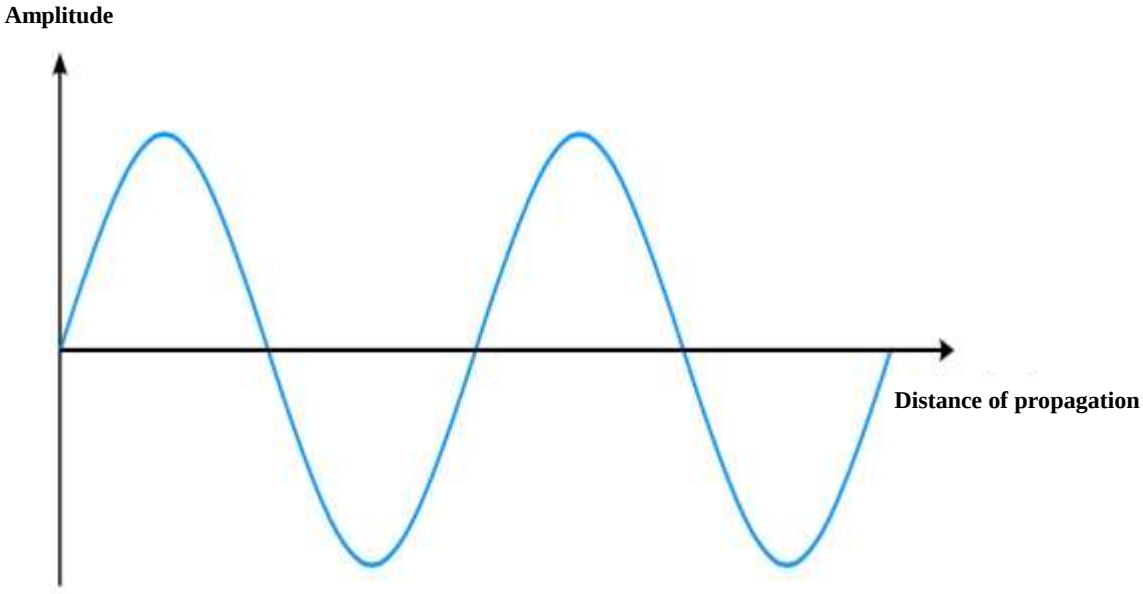

(b)

Figure 3.1 (a) Schematic of longitudinal wave propagation. (b)The compression and rarefaction zones relate to high and low amplitude of the wave

3.2.2 Shear waves

Shear or transverse waves are mainly generated by ultrasonic shear sensors. In this mode of wave propagation, the particles of the host medium vibrate around their equilibrium positions perpendicular to direction of wave propagation, as shown in Figure 3.2.

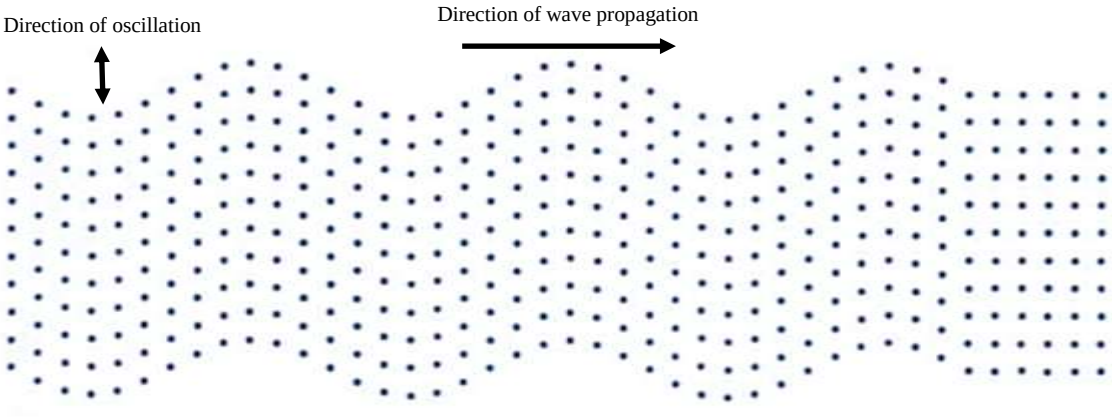

Figure 3.2 Diagram showing the shear wave propagation

3.3 Speed of sound

The rate at which sound waves propagate through solid and fluids varies. Speed of sound is dependent on two main factors:

- The elastic and bulk modulus for solids and fluids respectively
- Density

Considering different materials from a particle point of view, bond strength between these particles are critical to how waves travel though the host medium. When mechanical waves are introduced, the forces between particles act like springs, thus when subjected to oscillatory movements, those ones of a material that can return to their equilibrium positions faster, are ready to move again in a shorter time. Thus, sound can travel faster through steel than rubber because of having higher elastic modulus. Speed of longitudinal waves in a solid medium is given as equation (3.1):

$$c = \sqrt{\frac{E}{\rho}} \tag{3.1}$$

where E is the elastic modulus, and ρ is the density of the material. Speed of sound is also defined in terms of the frequency f and wavelength λ, as given in equation (3.2):

$$c = f\lambda \tag{3.2}$$

3.4 Acoustic Impedance

Acoustic impedance is a measure of the opposition that ultrasound waves are faced with, when they propagate through their host medium. Acoustic impedance is defined as the product of density ρ and speed of sound in the material, as given in equation (3.3):

$$z = \rho c \tag{3.3}$$

Knowledge of acoustic impedance is essential for determination of the portion of ultrasound waves, transmitted and reflected at an interface between two materials.

3.5 Ultrasonic field

When ultrasound waves are generated, they come from the entire surface of the piezo-electric element and not just a single point. This phenomenon will be explained by the Huygens principle in section 3.7. Close to the transducer face, multiple constructive and destructive wave interference happen, hence significant fluctuation in amplitude takes place. This region, is referred to as the near-field zone, where the beam is converging. Just beyond this point is where the maximum intensity is seen, as shown in Figure 3.3, and is known as the natural focus of a flat or unfocused transducer. From the transition point and into the far field, the wave propagation is stabilised, however, the wave intensity starts to decrease with distance from the face of the transducer.

The near field zone of the transducer is a function of the diameter *D* of the piezo-electric crystal, frequency *f* and velocity of sound in the host medium *c* (NDT Resource Centre):

$$N = \frac{D^2 f}{4c} \tag{3.4}$$

The material used in this thesis is steel. Hence, the near-field for a 10 MHz piezo-electric element with 7mm diameter is 20mm.

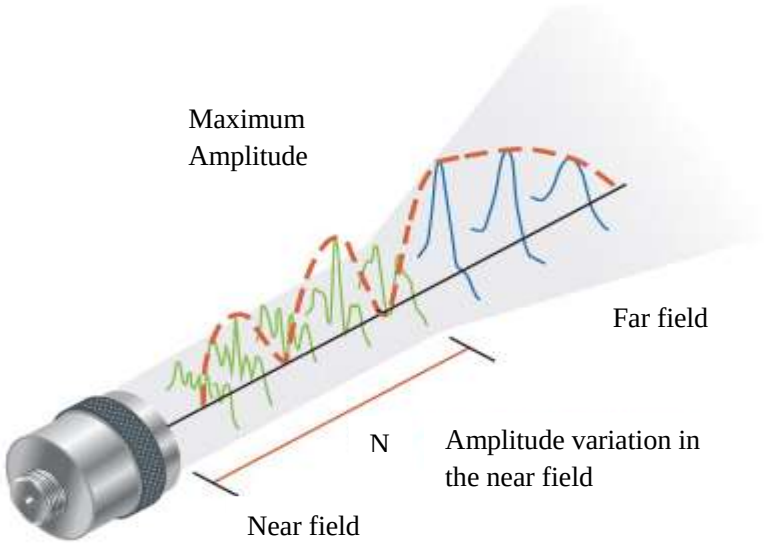

Figure 3.3 Ultrasound field of a transducer (Courtesy of NDT Resource Centre)

3.6 Huygens principle

Based on Huygens principle, the surface of a transducer can be considered to consist of an infinite number of point sources of energy, where each of these points generate a wavelet of the same frequency and phase. Figure 3.4 shows the front of an ultrasonic transducer, divided to eight energy sources and three stages of wavelet generation has been shown. Increasing the number of energy sources will result in a flat wave front, tangential to forward-propagating wavelets. This wave front is equal to the sensor size.

Direction of wave propagation is shown by the arrows. The energy transmitted on the sides of the sensor, are reflected outside the measurement and may not be detectable.

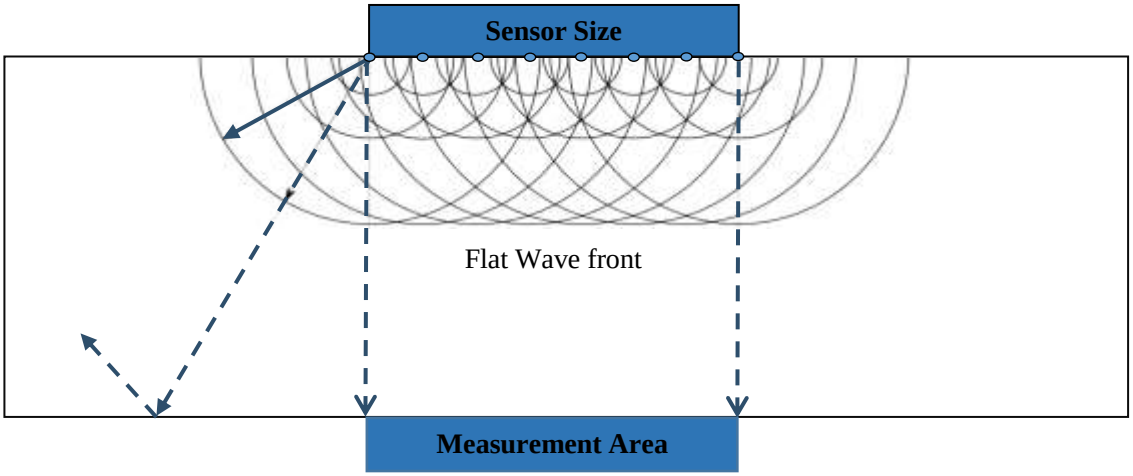

Figure 3.4 The 2D ultrasonic wave propagation in a solid body (Brunskill, 2013)

3.7 Reflection of ultrasound at a boundary

3.7.1 Normal incidence

When two engineering surfaces are lightly pressed against each other, assuming that they are both perfect and smooth, the proportion of ultrasound waves reflected at the interface can be given as reflection coefficient *R*:

$$R = \frac{z_1 - z_2}{z_1 + z_2} \tag{3.4}$$

where z_1 and z_2 is the acoustic impedance of the two materials.

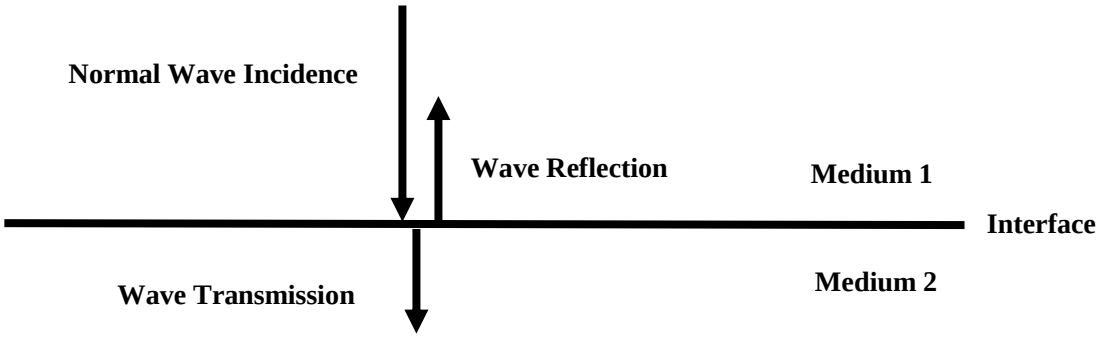

Figure 3.5 Reflection and transmission of ultrasound wave normal incidence at an interface

3.7.2 Oblique incidence

When a longitudinal ultrasound wave strikes a perfectly bonded interface at an oblique angle, the transmitted and reflected waves will travel at specific directions depending on the incidence angle and the acoustic velocities of the media. In addition to longitudinal waves, shear waves are also generated. This is explained by the phenomena of mode conversion.

Mode conversion can be defines as transformation of wave energy from one form to another. As longitudinal waves hits an interface at an angle, some of the energy can cause particle movement in the transverse direction to start a shear (transverse) wave (NDT Resource Centre).

Snell's law relates the angle of the incident wave with the angle of the transmitted wave at the interface of two mediums. For the waves shown in Figure 3.6, Snell's law is expressed as:

$$\frac{sin\theta_1}{V_{L_1}} = \frac{sin\theta_2}{V_{S_1}} = \frac{sin\theta_3}{V_{L_2}} = \frac{sin\theta_4}{V_{S_2}} \tag{3.5}$$

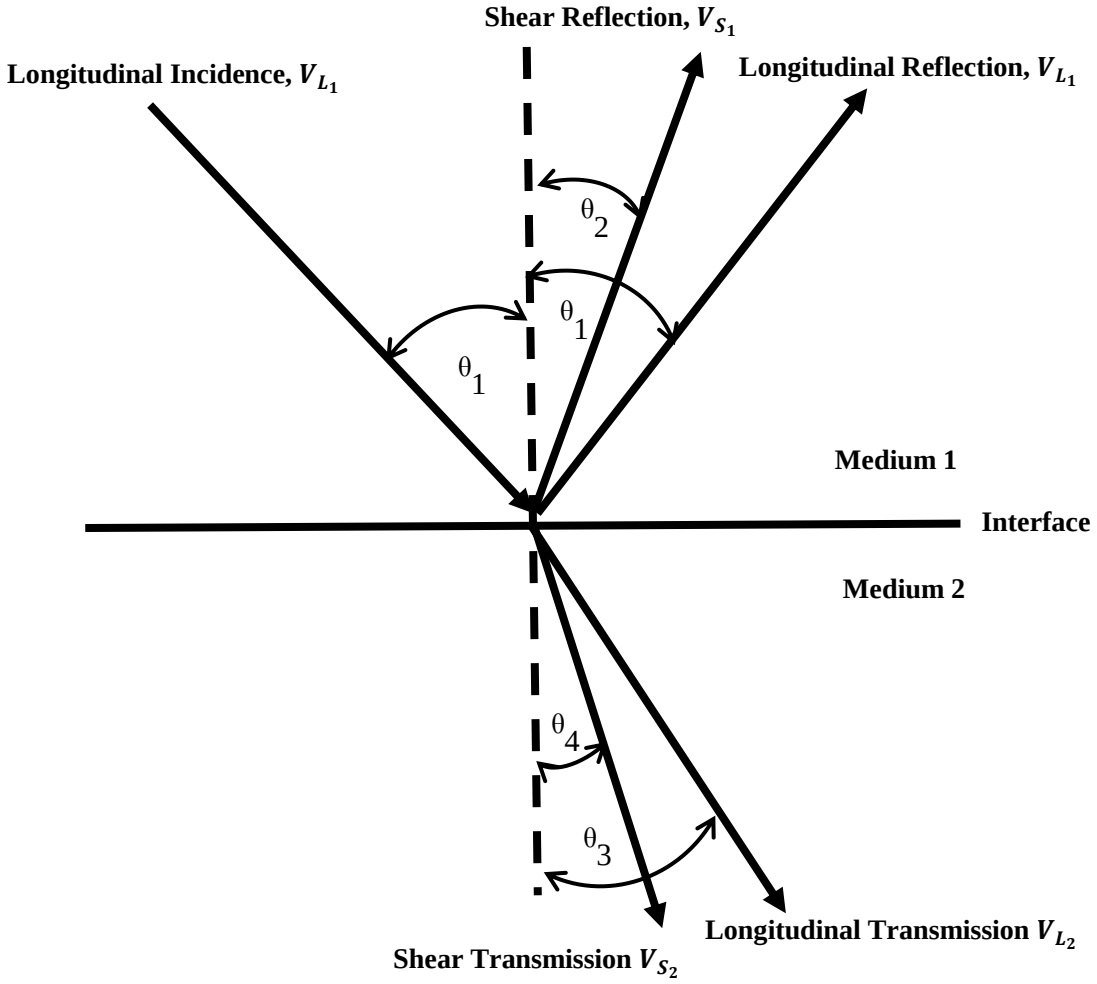

Figure 3.6 Reflection and transmission of longitudinal oblique incidence at a single interface

3.7.3 Partial interface

When two engineering surfaces are lightly pressed against each other, the true area of contact is different to the apparent area of contact. The true area at the interface, when considered from a microscopic point of view, consist of asperities touching as well as air gaps. Therefore, the true area of the contact is smaller than the apparent area of contact. When ultrasound waves strike such interface, some of the waves are transmitted through asperities, however, a considerable proportion of the waves are reflected back. This is due to the large presence of air gaps around asperities, which essentially work as acoustic reflectors (shown in Figure 3.7).

As load is applied, asperities deform and the true area of contact increases. As a result more ultrasound waves are transmitted through to the adjacent component. To quantify the reflected portion of the ultrasound waves, Tattersall (1973) built a model to obtain reflection coefficient, *R*, considering the interface at the two contacts as a series of springs with stiffness *K* per unit area. However, for the model to be valid, the amplitude of surface roughness should be much smaller than the wavelength of the ultrasound waves propagating normal to the surface. *R* is is given as:

$$R = \frac{z_1 - z_2 + \frac{i\omega z_1 z_2}{K}}{z_1 + z_2 + \frac{i\omega z_1 z_2}{K}} \tag{3.6}$$

where, ω is the angular frequency of the ultrasound wave and *K* is equivalent spring stiffness. For a dry contact, interfacial stiffness is only dependent on the stiffness of the asperities at the contact, given as K_s. Thomas et al. (1977) defined the interfacial stiffness K_s as equation 3.7:

$$K_s = -\frac{dp_{nom}}{du} \tag{3.7}$$

where p_{nom} the nominal contact pressure and *u* is the separation of the mean lines of the two contact surfaces.

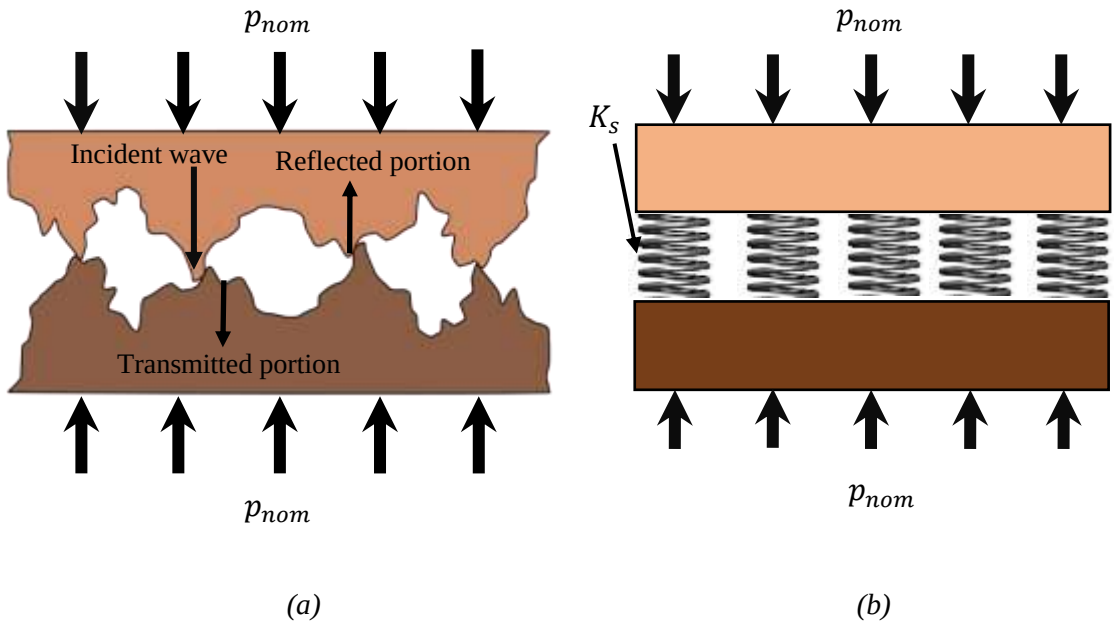

Figure 3.7(a) Schematic of a dry interface, showing the ultrasound interaction at asperities level (b) Modelling of the contact as a series of springs K_s

3.7.4 Mixed lubricant and solid interface

If a lubricant is then introduced into the contact between the two solid surfaces, the portion of the ultrasound wave reflected, is decreased, which is due to the change in the total contact stiffness. In a work carried out by Dwyer-Joyce et al. (2004), it was shown that the oil formed in hydrodynamic and elasto hydrodynamic regimes are governed by the spring model and it is in fact the liquid layer that controls the ultrasonic reflection. The stiffness of an interfacial layer was defined as:

$$K_l = \frac{B}{h} \tag{3.8}$$

where *B is* the bulk modulus of the fluid and *h* is the lubricant film thickness.

In very slow speed or static lubricated contacts under high loads, both the asperities and lubricant stiffness become significant. Dwyer-Joyce et al. (2011) showed that such contact can be modelled with K_s and K_l in parallel, as shown in Figure 3.8. Therefore, the total contact stiffness is given as:

$$K = K_s + K_l \tag{3.9}$$

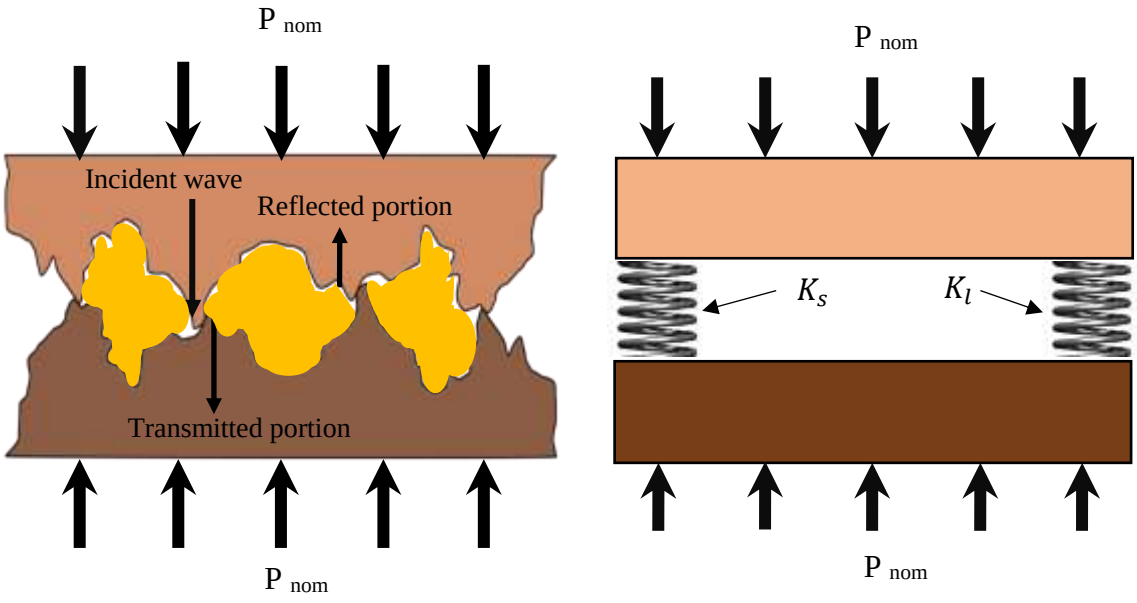

(a) *(b)*

Figure 3.8 (a) Schematic of a lubricated interface, showing the ultrasound waves interaction at a lubricated contact (b) Spring model representation of the contact

3.8 Generation and detection of ultrasound waves

3.8.1 Piezo-electric effect in ultrasonic transducers

Ultrasonic transducers can be used to both generate and detect ultrasound waves. Electrical energy is converted to mechanical energy for generation, and the vice-versa takes place for detection purposes. Different types and configurations of transducers are available, however, the functionality of all is dependent on the piezo-electric effect, which occurs at their active element. A cross-section of a typical commercial transducer is shown in Figure 3.9.

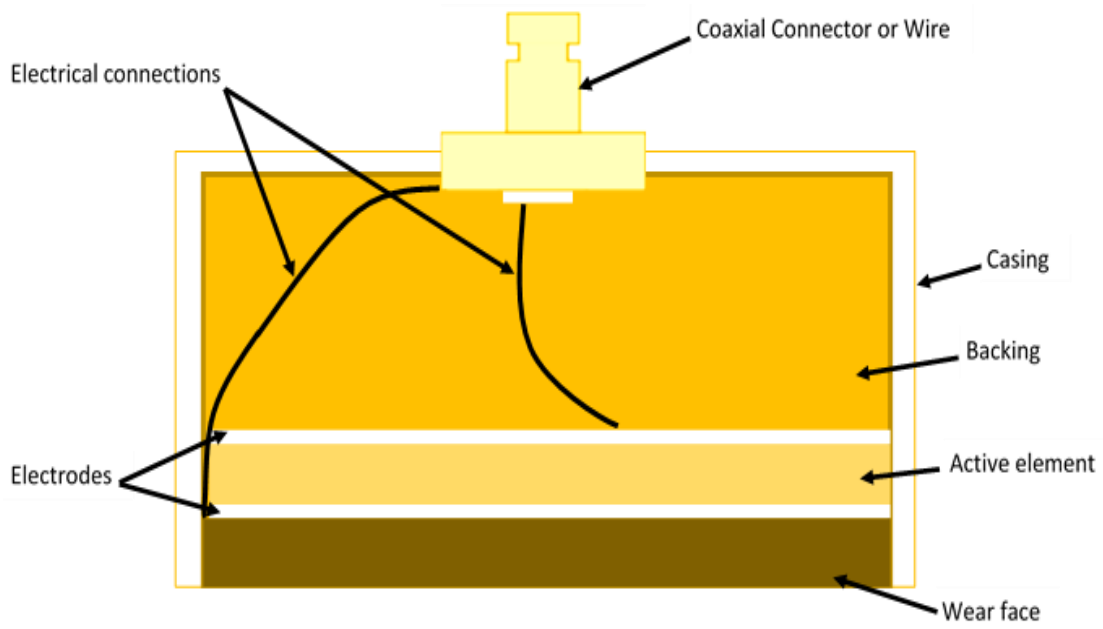

Figure 3.9 Cross section of a typical commercial NDT Transducer

The piezo-electric effect is exhibited by crystalline materials such as quartz and lead zirconate-titanate (PZT). When an electrical field is applied across a standard piezo-electric element, as shown by Figure 3.10(a), it causes a through thickness vibration of the plate resulting in production of mechanical pressure waves. This phenomena is called the inverse piezo-electric effect. Conversely, when the active element is mechanically deformed by the reflected sound waves, an electrical voltage is generated. This process is referred to as the direct piezo-electric effect.

Although, standard piezo-electric elements are widely common in commercial transducers such as the contact and focusing ones. In this thesis, the piezo-electric elements used are the bare element with wrap-around electrodes, as shown in Figure

3.10(b), where only one surface is used and the other surface is bonded to the component. The electrodes are pre-sputtered by the manufacturer.

These off-the shelf products can be obtained at low cost whilst providing stable and strong piezo-electric characteristics. In addition, these disk-shaped crystals can be shaped to the desired size based on the application.

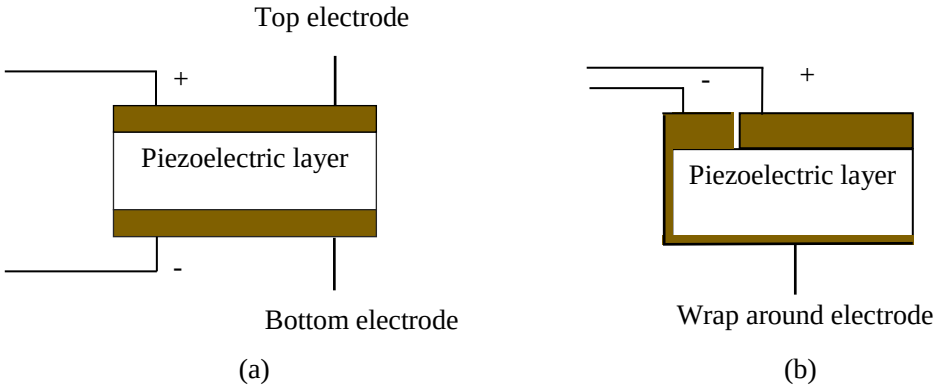

Figure 3.10 Schematic of two piezo-electric elements with (a) standard electrodes (b) Wrap-around electrodes

3.8.2 Ultrasonic apparatus

To employ an ultrasonic technique, it is essential to firstly have the appropriate apparatus capable of generating, receiving and digitising the data and secondly to have the means of controlling the process and storing the data. Figure 3.11 shows the schematic of an integrated hardware system (Tribosonics Ltd. FMS100), which houses the pulser/receiver and digitiser PCI Cards allowing 8 channels for 8 transducers.

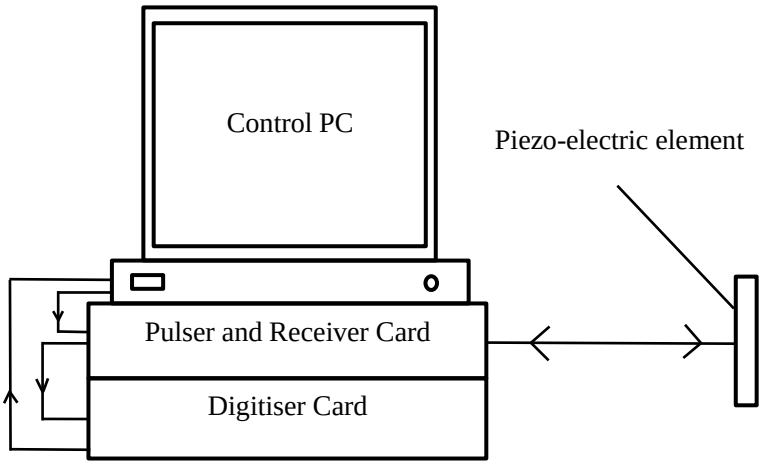

Figure 3.11 Schematic of the ultrasonic apparatus

The configuration enables both pulsing and receiving from the same transducer (pulse-echo) or pulsing one transducer and receiving on the other one (pulse-catch). A pulse-echo configuration is shown in Figure 3.11. The pulser produces a high frequency voltage pulse, which excites the piezo-electric element resulting in conversion of electrical signals to mechanical waves. The reflected waves from the contact of interest then strike the piezo-electric element where the mechanical waves are converted back to electrical signals by direct piezo-electric effect (Section 3.9.1). The total pulse rate can be adjusted up to 80,000 pulse/s, dividing over 8 channels makes it 10,000 pulse/s per channel.

The electrical signals received from the transducers are sent from the receiving unit to the digitiser. The analogue signal is sampled at a resolution of 12 bits at the rate of 100 million samples/s.

A National Instrument Labview software, written by Dr Robin Mills for the Leonardo Centre, is used for controlling the pulsing, receiving, displaying and recording an ultrasonic signal. The number of active channels are switched on depending on the number of transducers in use in the measurement process. Some important features of the software, which needs tuning are listed as follows:

Voltage and gain

The transducers are excited with a spike voltage. The recommended driving voltage is related to transducer thickness, and hence the operating frequency. For instance, lower frequency commercial transducers (5MHz or less) can be driven up to 500-600V, therefore for higher frequencies, i.e., 10 MHz commercial transducer with thinner piezo element, it is not uncommon to use a voltage of up to 300V. However, for the piezo-electric crystals, which are directly bonded to the component the recommended voltage is between 30V to 50V. For additional amplification, the gain feature may be used to achieve the desirable amplitude, although the only issue is the amplification of noise present in the signal.

Pulse repetition rate

This is the number of pulses transmitted per second. The thickness of the host medium is important when tuning the pulse rate, since the reflected pulse needs to be received before another pulse is sent out.

Delay and Range

Each of the channels display an ultrasonic response, where the waveform of interest needs to be recognised. Delay and range help with choosing the waveform of interest to be the only one displayed and stored for later processing.

3.8.3 Resonant frequency and element size

The resonant frequency of a piezo-electric crystals is governed by its thickness. To satisfy the resonance conditions, thickness should be equal to one half of the wavelength. The relationship between resonant frequency, f_c, thickness, l, and speed of sound, c, in the crystal is given as equation 3.10:

$$f_c = \frac{c}{2l} \tag{3.10}$$

3.9 Acoustic coupling

Acoustic couplants are commonly used when using ultrasonic transducers to make the transmission of ultrasound waves through testing specimens easier. For instance, When a probe is attached to the surface of a specimen, there are air gaps at the contact between the two surfaces, which act as acoustic reflector due to the large impedance mismatch between the probe and air, thus by applying a couplant, the objective is to minimise the air gaps between the two surfaces, hence facilitating the transmission of ultrasound waves. Some of the couplants that are common to use are oil and gel.

3.10 Summary

In this chapter, the basic principles of ultrasound were covered. The piezo-electric effect of ultrasonic transducers was explained and the propagation of wave in a solid media was discussed. Furthermore, the interaction of ultrasound waves with both dry and lubricated contacts has been discussed. The proportion of ultrasound waves reflected was said to be dependent on the contact stiffness of the interface at the contacts and the interfacial stiffness as the contact changes, when it is loaded and when lubricant is added to the contact. These principles will be used to understand the interaction of ultrasound waves at a threaded contact and to detect the lubricant presence when the contact is loaded.

4

Development of a Fluid Penetration Measurement Instrument

Building on the discussion of the basic ultrasonic principles in Chapter 3, this chapter describes the experimental apparatus and procedure for obtaining penetration time. The measurement steps are explained from capturing the ultrasonic reflection waves to providing the final penetration time. The experimental results are then presented in Chapter 5.

4.1 Introduction

Penetration performance of the oil penetrant relies heavily on how it is formulated. A typical penetrant oil is composed of around less than 25% mineral oil, which is diluted by a volatile hydrocarbon to give a low viscosity fluid suitable to be sprayed. Oil penetrant producers would like to investigate different formulations of penetrant oil product. Moreover, a further understanding of the components of each product (mineral oil or solvents) is required for an improved formulation.

Some of the current techniques used in industry to measure the effectiveness of penetration are the nail climb test, surface tension measurement and contact angle measurement. Although these techniques give some indication of the penetrant ability, they do not provide any direct information of penetrant performance when it is inside the threaded contact.

There have been various studies on bolted joints considering self-loosening (Eccles 2010, Jiang et al. 2004), thread and bearing friction (Nassar et al., 2005), and lubrication effects (Zou et al. 2006; Hemmati Vand et al., 2008). But none of these studies assess the effectiveness of fluid penetration in a threaded contact.

In a recent work at the University of Sheffield (Vail et al., 2013), a measurement concept was introduced and an ultrasonic test rig was built to obtain penetration time. This technique was used to measure a few fluid samples, however, it could not measure the higher volatility low viscosity samples.

This chapter describes the design and development of a new rig. The redesign included improvement of the clamping mechanism in order to maximise the transmission of ultrasound waves. In addition, the rig was designed to be more robust by making it shorter to lower the centre of mass. Moreover, the signal processing steps were modified and a different approach was taken to obtain the penetration time. The rig design and signal processing will be discussed in more detail in section 4.3 and 4.5 respectively.

4.2 Measurement concept

Figure 4.1 shows the ultrasound wave path over the threaded contact. A pair of piezo-electric crystals are arranged in a pitch-catch mode such that the transmitting ultrasound waves, shown by the green arrow, first strike the threaded contact at 30° to normal. This

results in a first reflection (the same angle to the incident angle) to the opposite side of thread contact and a subsequent reflection is caught by the catching element.

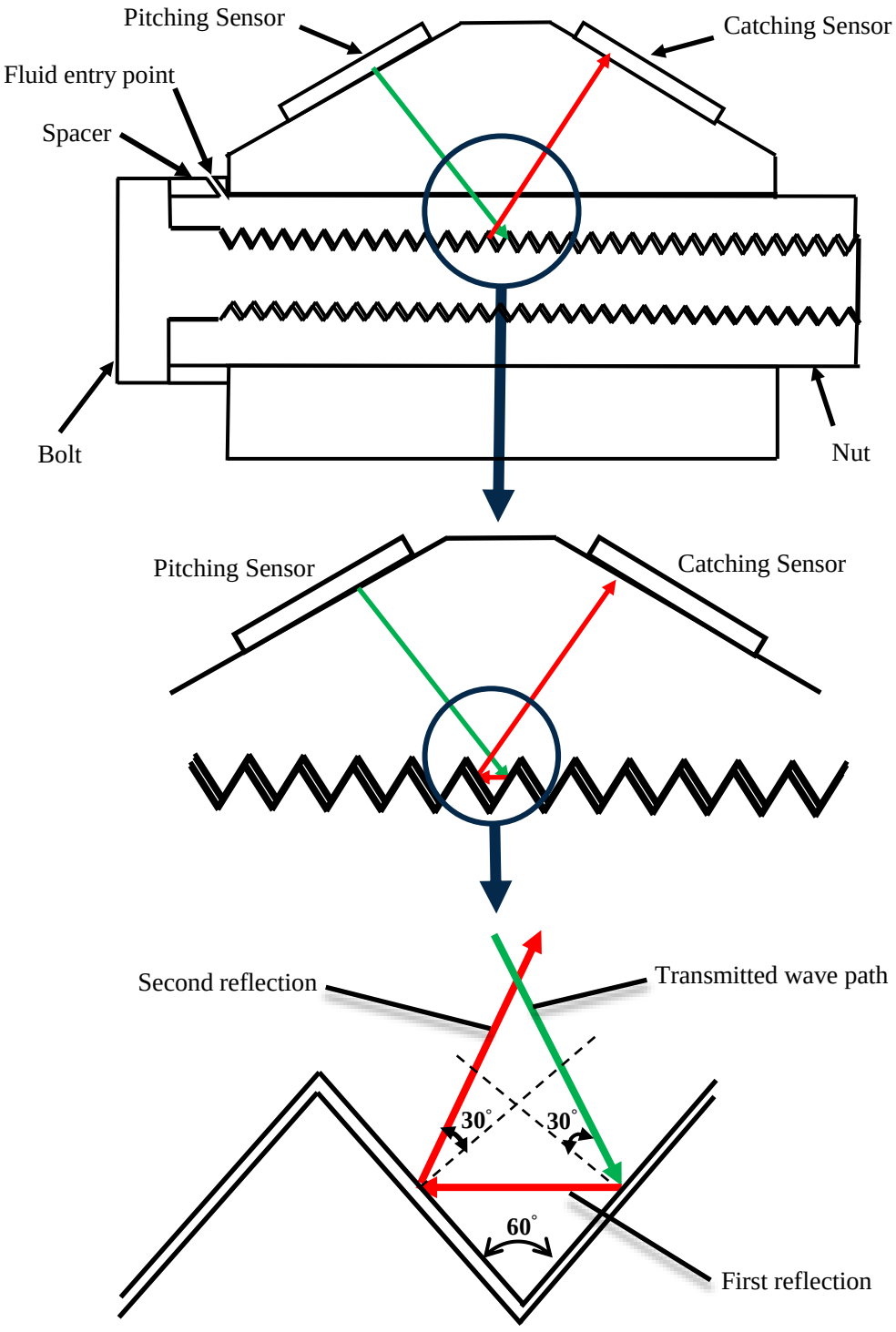

Figure 4.1 Schematics showing the paths of ultrasound at M10 bolt and nut threads

The reflected ultrasonic waves are affected by the loading and lubrication of the contact by the fluid injected. As explained in Chapter 3, the stiffness of the contact affects the

proportion of the ultrasound waves reflected. In the case of a loaded and lubricated threaded contact, a mixed lubrication regime exists where the combined stiffness of the asperities and lubricant influence the reflected waves. Figure 4.2 shows three conditions of unloaded (a), loaded (b) and loaded and lubricated (c).

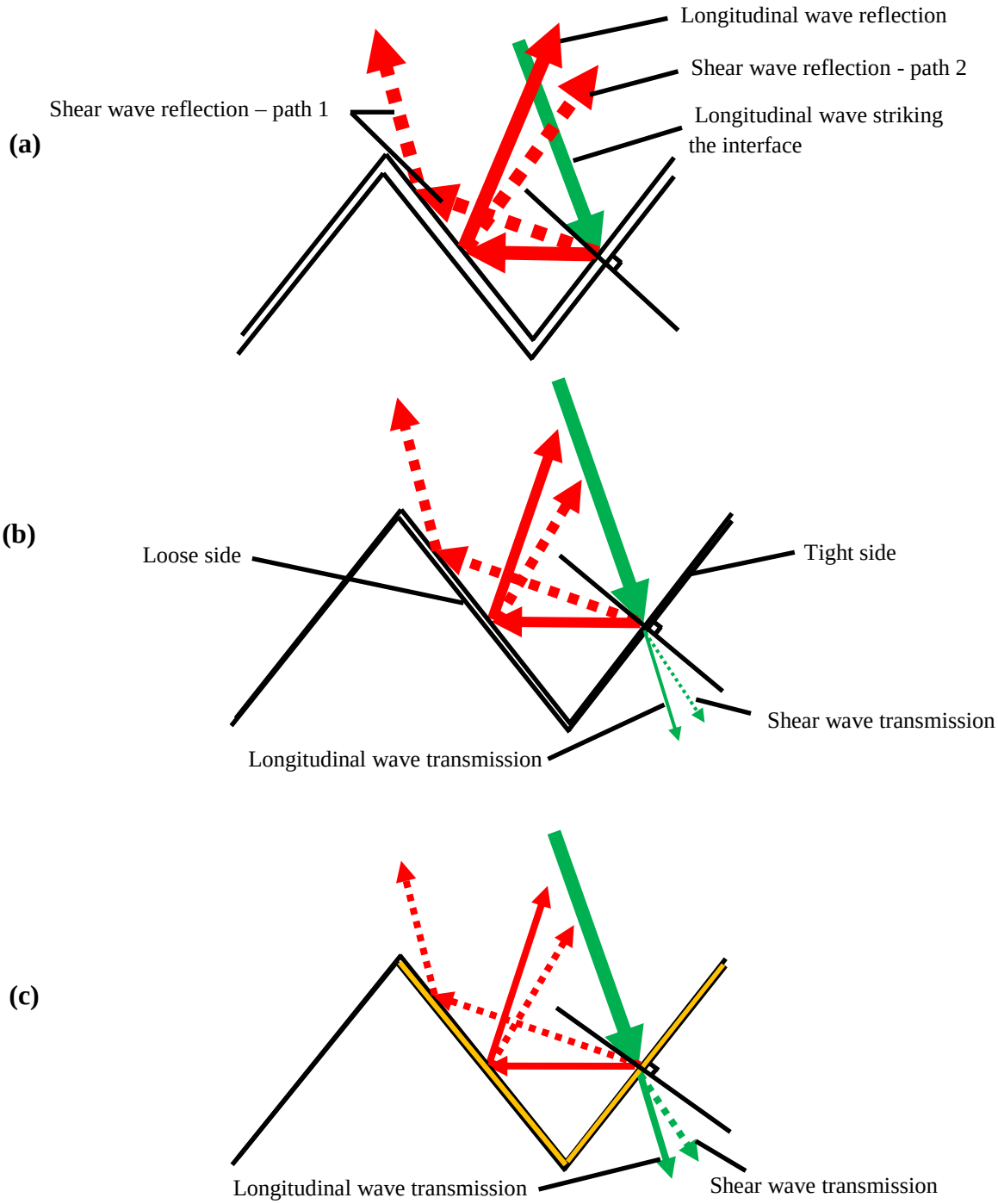

Figure 4.2 Schematic showing the transmission and reflection of ultrasound waves by green and red arrows respectively. The ultrasound wave modes are indicated by solid lines for longitudinal and dotted lines for shear. The changes in the amplitude as the wave hits an interface is illustrated by the thickness of the arrow. (a) Unloaded, (b) Loaded, (c) Loaded and lubricated

Figure 4.2(a) shows the ultrasound waves strike the unloaded contact (indicated by a green arrow), where the bolt and nut threads are engaged, but unloaded, ultrasound waves are reflected back due to the large presence of air pockets. In addition a mode conversion occurs at an oblique angle, as explained in chapter 3, which results in generation of shear waves (dotted arrows). There are two paths for the reflected shear wave: the first path is reflected outside the coverage of the receiving sensor, hence stays undetected. The second path goes towards the receiving sensor, however, a shear sensor is required to obtain a powerful signal. Although shear waves may still be received using the longitudinal piezo-electric crystals, their amplitude is too small to be detectable. In the loaded case (Figure 4.2(b)), as the bolted joint is tightened up, two threaded contacts with different gap size will form, which is referred to as the "tight side" and the "loose side". On the tight side of the contact, bolt and nut threads are pressed against each other resulting in an increase in the actual area of contact, which results in some transmission of waves both in longitudinal and shear modes. Therefore, a reduction in the size of the reflected waves occurs due to the contacting asperity stiffness. In addition, as penetrant is introduced into the contact, a lubricant film will form (Figure 4.2(c)), which will further decrease the amplitude of the reflected ultrasonic wave since more transmission takes place. This is due to the added effect of lubricant stiffness. Hence, this measurement technique only detects the oil film in the tight side of the thread.

The ultrasonic wave paths strike multiple threads outside the near field of the sensors. Figure 4.3 shows the measurement zone over which the ultrasonic beam is projected.

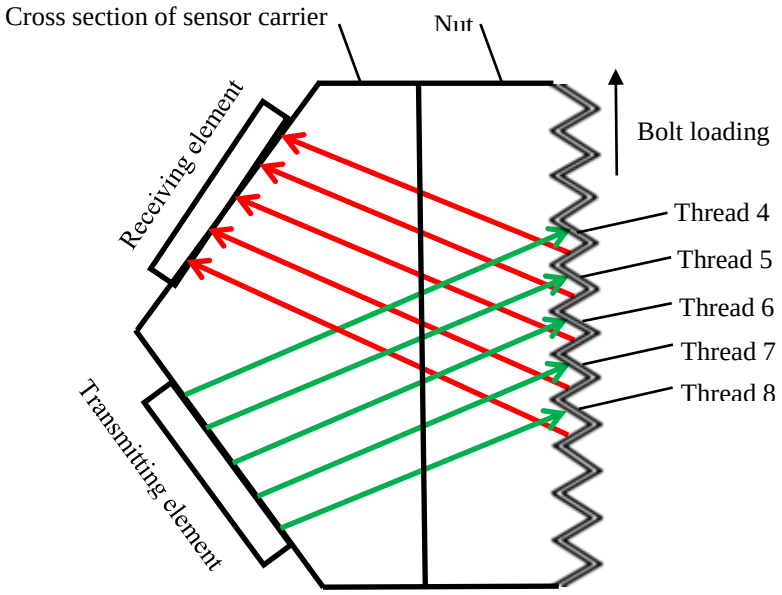

Figure 4.3 Schematic showing the threads within the range of transmitting and receiving sensors

The measurement zone is dependent on the active elements of the piezo-electric crystals as well as their arrangement. The active area of each of the elements was 7mm by 1mm, placed at 30° to the axis of the threaded fastener, covering 5 threads with a pitch of 1.5, and thread 4 being the starting one.

4.3 Experimental approach and instrumentation

4.3.1 Bolt loading assembly

In the previous work carried out on measuring the penetration time (Vail et al., 2013), an apparatus was designed and built. An image and a sectioned schematic of the previous test rig are given in Figure 4.4.

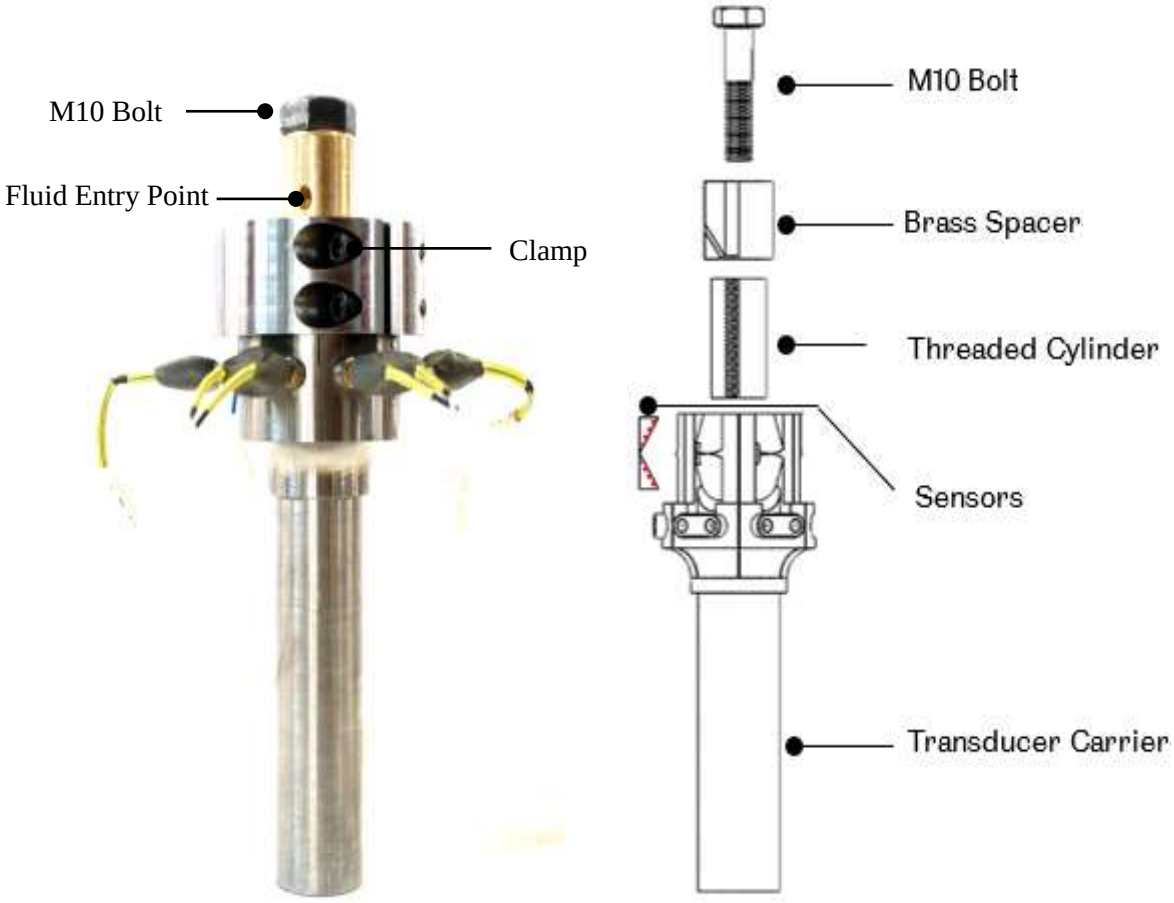

Figure 4.4 Image and schematic of the apparatus used for the previous work ((Vail et al., 2013)

Although the previous apparatus was functional for the work carried out before, trial tests of the new lower viscosity test samples on the previous test set up indicated erratic results. In addition, the amplitude of the reflected signals were quite low. Another issue was the robustness of the test apparatus due to its narrow base, as any accidental drop of the apparatus could break off sensors or knock them out of alignment.

Therefore, to rectify the limitations above, a new test apparatus was designed and built for the work carried out in this thesis. A schematic of the new design is shown in Figure 4.5. The rig was designed to be shorter to lower the centre of mass. Fastener testing samples are held in the bore. Bearing in mind that there is an interface between the ultrasound collet and the nut of the threaded fastener, it is important to maximise the transmission and reflection of the ultrasound waves at the interface to obtain signals with higher amplitudes. Therefore, in the new rig, the bore diameter was adjusted to have an improved fit with the nut. A clamping mechanism was then permitted at the base of the rig for tightening up the assembly. To improve the clamping further, some additional slots were also provided as marked on the diagram (Figure 4.5 and Figure 4.6), which allowed further tightening of the rig.

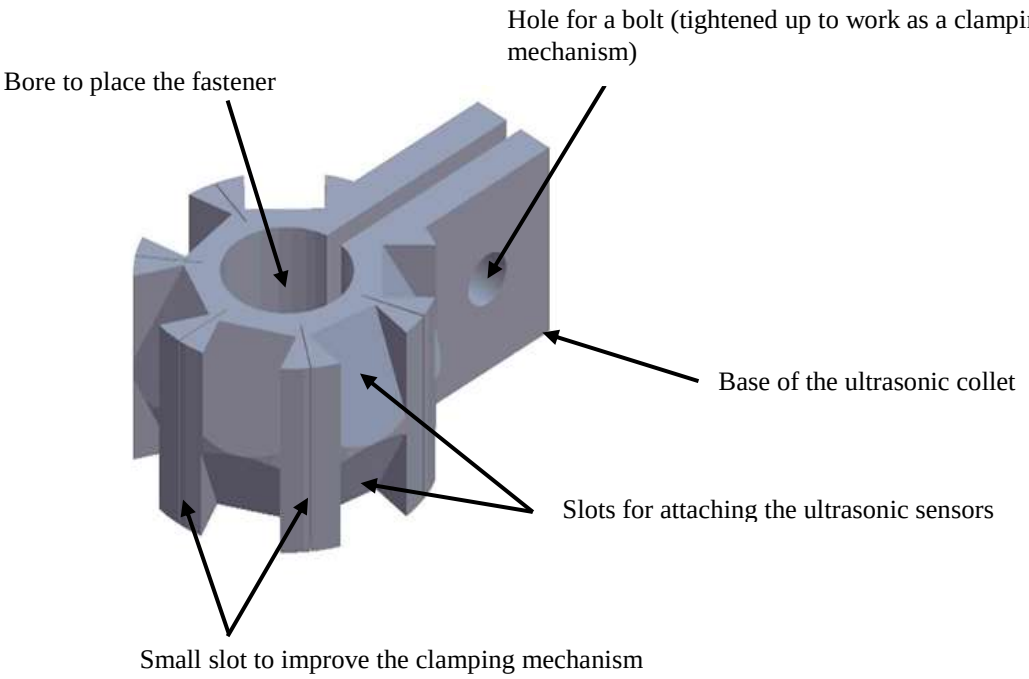

Figure 4.5 Schematic showing the collet

There are twelve slots positioned circumferentially around the rig, to accommodate 6 pairs of transmitting and receiving piezo-electric sensors (described in section 4.3.2). This is the same number of slots as the previous apparatus.

The locations where each pair of transmitting and receiving elements were bonded is shown in Figure 4.6.

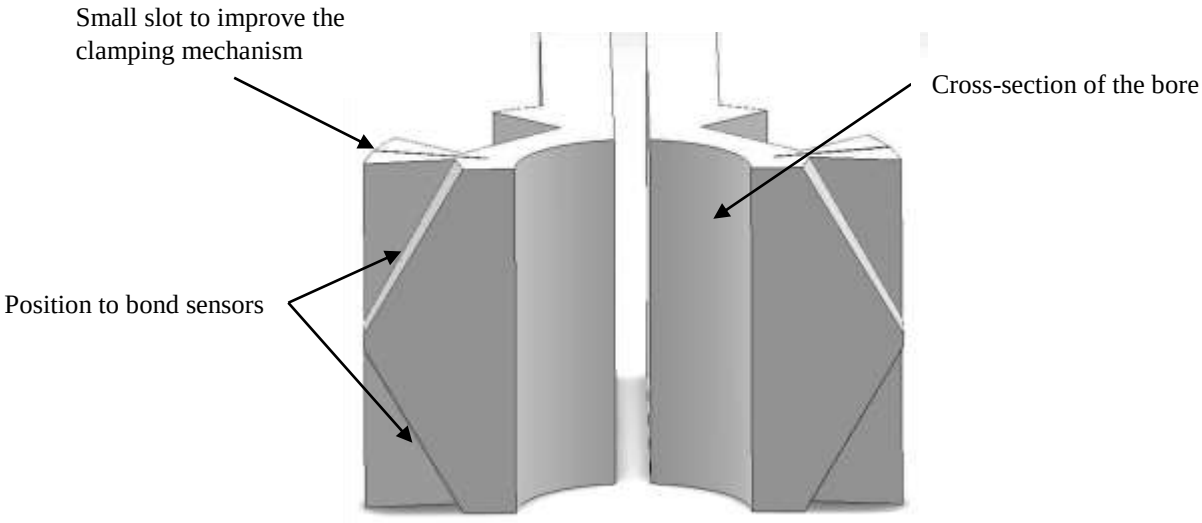

Figure 4.6 Schematic showing the bore and locations for bonding the piezo-electric elements

4.3.2 Sensor preparation

The centre frequency of the sensor was decided taking into account the contact studied in this work. To avoid complex scattering phenomena occurring, the wavelength needs to be large enough so that the proportion of the transmitted and reflected waves are no longer dependent on the exact shape and size of each air gap but on the stiffness (Drinkwater, 1997). Considering the air gaps to be around 50 μm at the interface of bolt and nut threads, the wavelength needs to be at least 500 μm. Velocity of the longitudinal wave propagation in steel is around 5900 m/s, giving a frequency of just below 12 MHz. The available piezo-electric crystal used for this work has a centre frequency of 10 MHz, which is within the right range to study the contact.

The piezo-electric crystal has a diameter of 7 mm, but the active size element was cut to 7mm by 1mm using a blade. The reason for shaping the crystal to a width of 1mm is for better focusing of ultrasonic beam onto the measurement area. After preparing the sensors, they were attached in position in their designated slots. The sensors were glued to the surface using a high temperature adhesive (M-Bond 610) with a maximum temperature limit of 230°C and then placed in the oven for temperature curing. Once all the sensors were bonded, their signals were tested to ensure that the signal to noise ratio was acceptable. A coaxial cable was prepared for each of the sensors. Each of the cables

has two wires, the core and the secondary ones, which are connected to the sensor in two stages. Firstly a stress relief tab is placed next to the sensor, where the wires are soldered. A pair of copper wires would then make the connection to the positive and negative electrodes of the sensor (Figure 4.7).

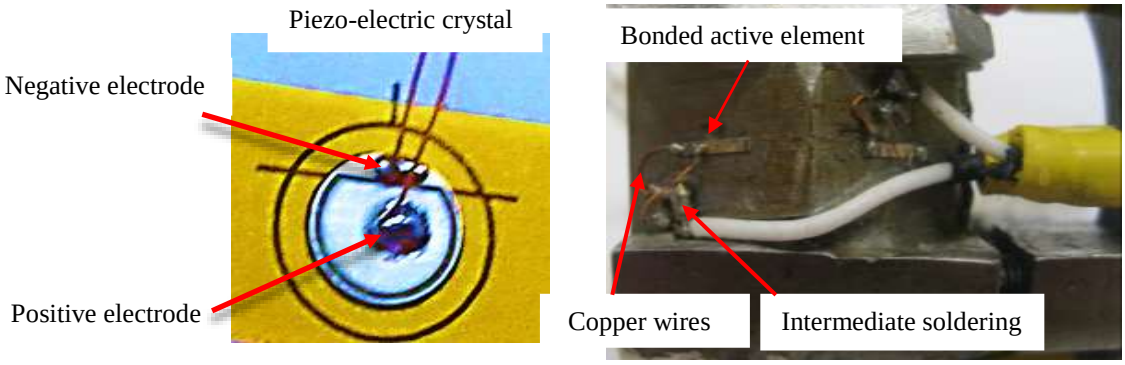

Figure 4.7 Bonding and position of the transmitting and receiving elements

The arrangement of the six sensors is shown in Figure 4.8.

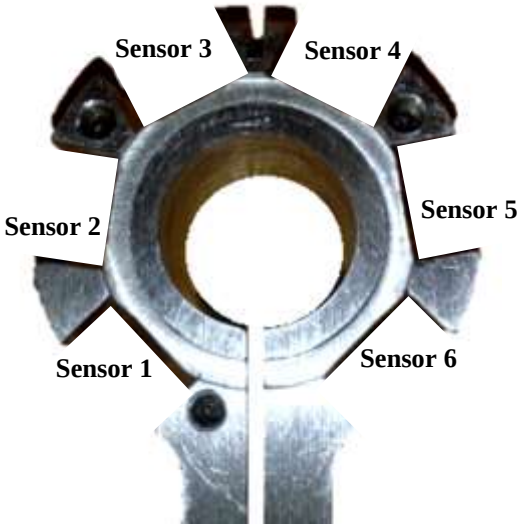

Figure 4.8 Arrangement of sensors

Once all the wires were soldered, they were connected to a series of male and female SMA connectors (Figure 4.9) fixed into a plate tightened to the top of the ultrasonic collet, as shown in Figure 4.10. These wires are then connected via the SMB connectors to the ultrasonic pulsing and receiving hardware unit.

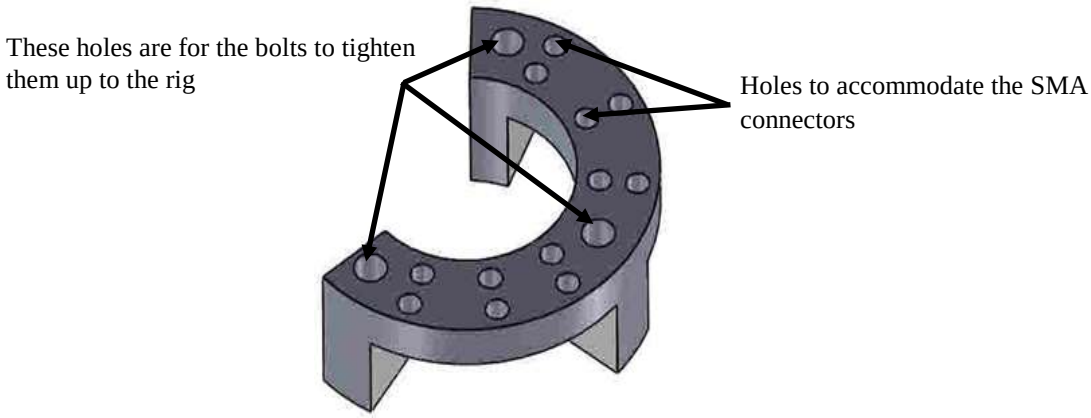

Figure 4.9 Schematic of the component for holding the connectors

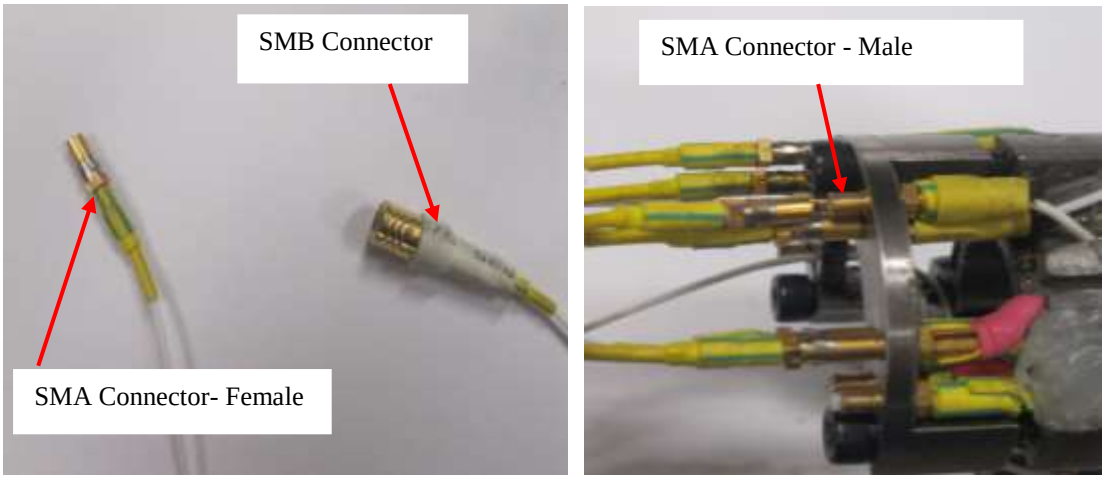

Figure 4.10 Schematics of the cabling system

4.3.3 Pulsing and receiving instrumentation

Production and detection of ultrasound waves by the pitching and catching piezo-electric crystals was carried out by a high performance Pulser, Receiver and Digitiser, as shown schematically by Figure 4.11. This unit (FMS100 PC System) contains all the necessary components and show the received ultrasound signals. The unit contains PCI Cards with 8 channels for both the pulser and receiver allowing up to 8 transducers to be used simultaneously. Pulsing voltage can be varied from 5 V to 300 V.

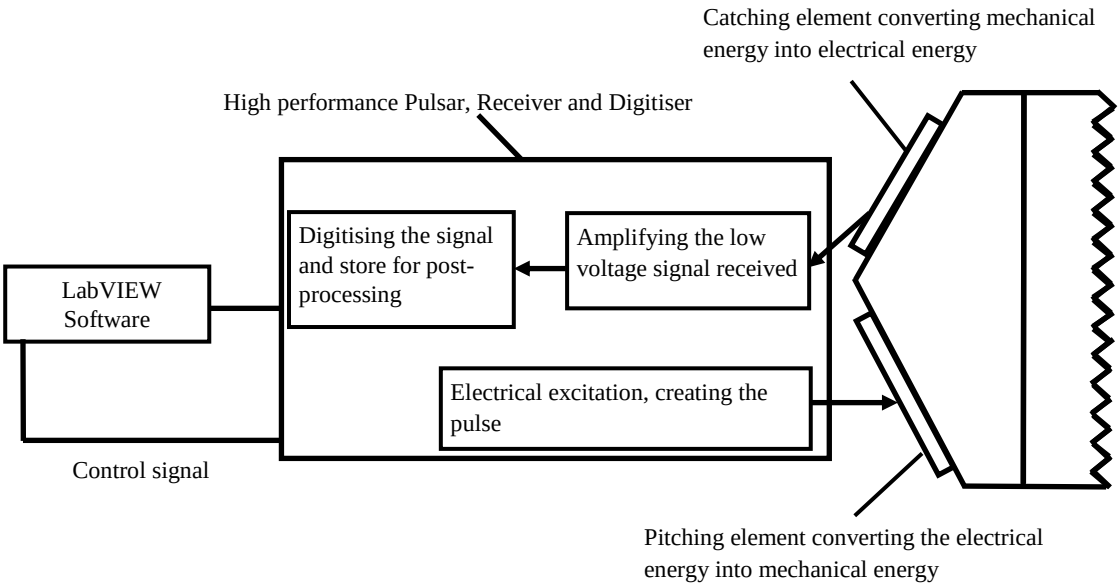

Figure 4.11 Schematic diagram of pulsing and receiving equipment

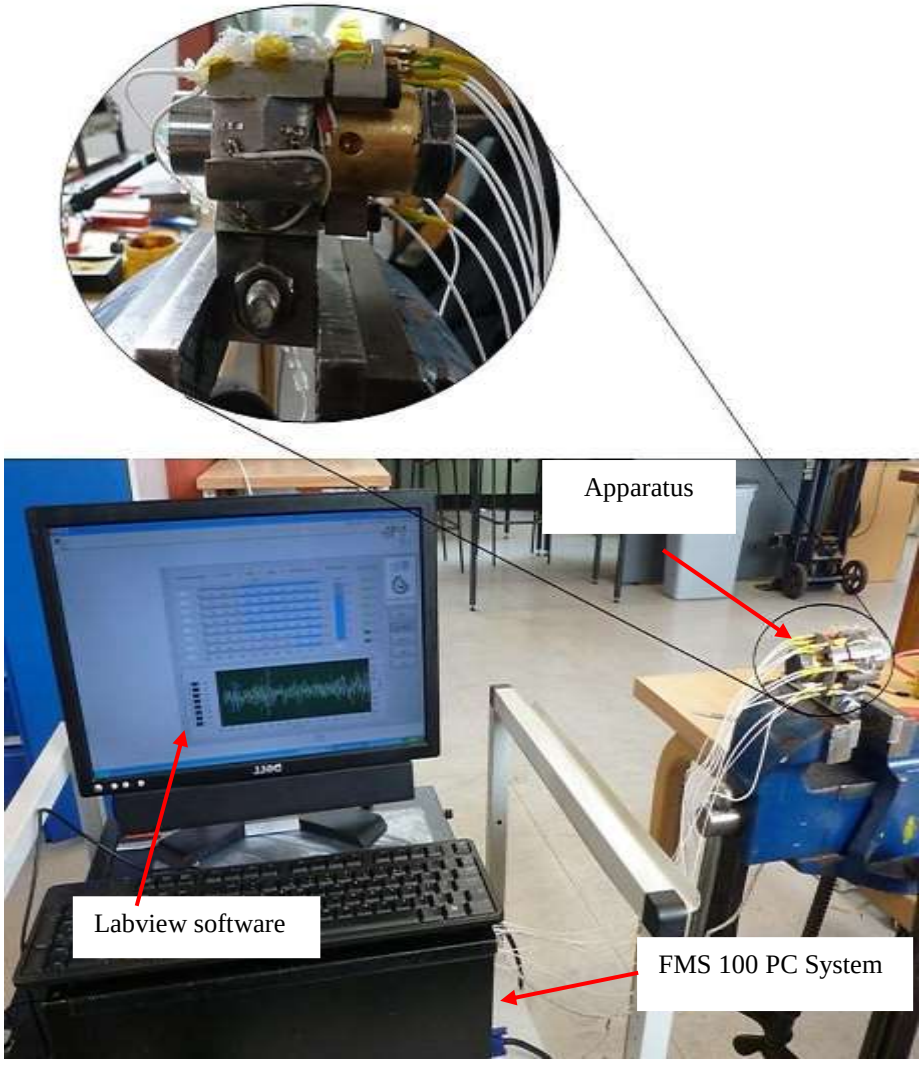

Figure 4.12 Photograph of the apparatus and instrumentation

The in-built hardware unit is controlled by a Labview software (Figure 4.12). The pulser is triggered by a control signal, which results in generation of a pulse with high frequency. The pulse then electrically excite the transducer, which then transmit ultrasound waves to the contact of interest. Once the reflected ultrasound waves return to the piezo-electric plate, the mechanical vibration is converted to voltage. The voltage was then digitised at a sampling rate of 100 MSamples per second, which is ten time the centre frequency (10 MHz) of the transducer. The six transducers, operating in pitch-catch mode, were pulsed at a rate of 500 Pulse/s to 600 Pulse/s, where the best signals were obtained and did not overlap. Higher pulse rates was not necessary as it would only consume more memory. An excitation voltage of 50 V was applied and further amplification was carried out on the signals.

4.3.4 Materials and specimens

From the earlier tests, it was found that the off-the shelf M10 bolts are very irregular in thread geometry, therefore, bolt specimens were re-machined and turned from M14 to M10 using a CNC lathe to enhance geometric tolerance and uniformity. The nut specimens were prepared by tapping silver steel cylinders (Figure 4.13). A brass spacer was used between the bolt head and nut. A hole was provided on the spacer for fluid entry, which provides a route for fluid entry into thread, as otherwise the bolt head would have restricted the fluid flow.

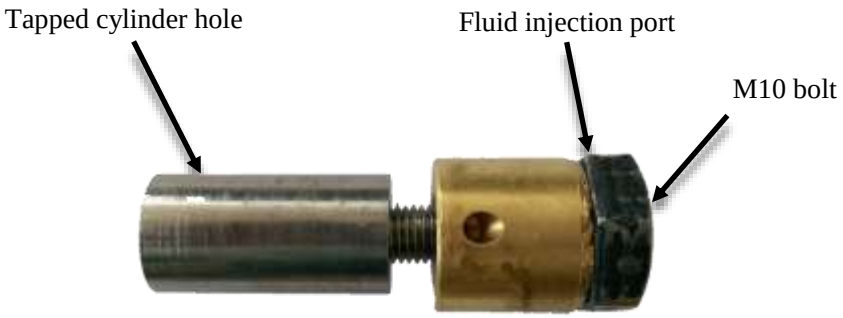

Figure 4.13 Bolt and nut specimen used in the experiments

As shown in Figure 4.14, for injecting fluid into the threads a pipette was used with a tip that can hold 100 µl of each fluid sample. The tip was changed after each test. When the fluid is injected, it fills up the reservoir between the brass spacer and bolt threads and then

fluid penetration is initiated by capillary forces, driving the fluid into the channels created by the threads. The full process will be explained in detail in Chapter 5.

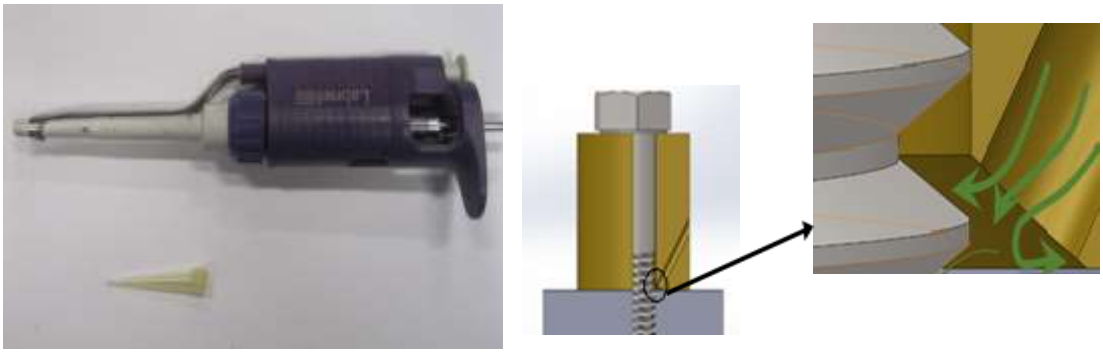

Figure 4.14 Pipette used for fluid injection into the threads

4.4 Experimental procedure

- Before each test, the bolt, nut and the fluid injection port were all cleaned in an ultrasonic bath for 10 minutes, and then they were dried.
- The bolt was tightened up to a torque of 45 Nm. This is the value found by the general torque-tension relationship (Bickford, 1977) given in Chapter 2, where the nut factor and tension force values are obtained from the guidelines (Technical Reference Guide, 2005).
- A layer of acoustic couplant was applied at the interface of the nut and the bore of the ultrasonic collet. This was to maximise the transmission and reflection of the ultrasound waves. The fastener is then clamped using the mechanism, shown in Figure 4.5.
- The six pairs of cables were then connected to the FMS, in the pitch (transmitting) and catch (receiving) mode.
- The tests were carried out at the room temperature. The room temperature was checked by a digital thermometer with the accuracy specified by the manufacturer as ±0.5% of reading (±1°C). As not all the tests were run at the same day, but overall the temperature recorded during all the testing were within ±4°C.
- The measurement began as 10 µl of fluid was injected into the threaded contact using a pippete. The ultrasonic data was recorded for 5 minutes.

4.5 Signal processing procedure

For a typical measurement, the pulse of interest was extracted from the measurement window in the time domain, as shown in Figure 4.15.

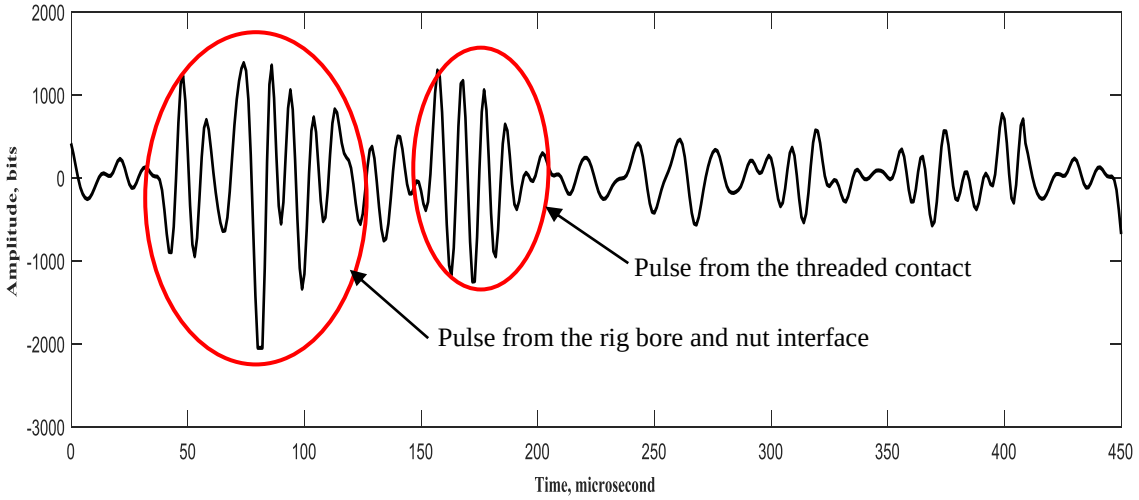

Figure 4.15 The measurement window of the ultrasound response in time domain

The pulse from the threaded contact is shown in Figure 4.16 in the time domain. The pulse was transformed to frequency domain, as shown in Figure 4.17, using Fast Fourier Transform.

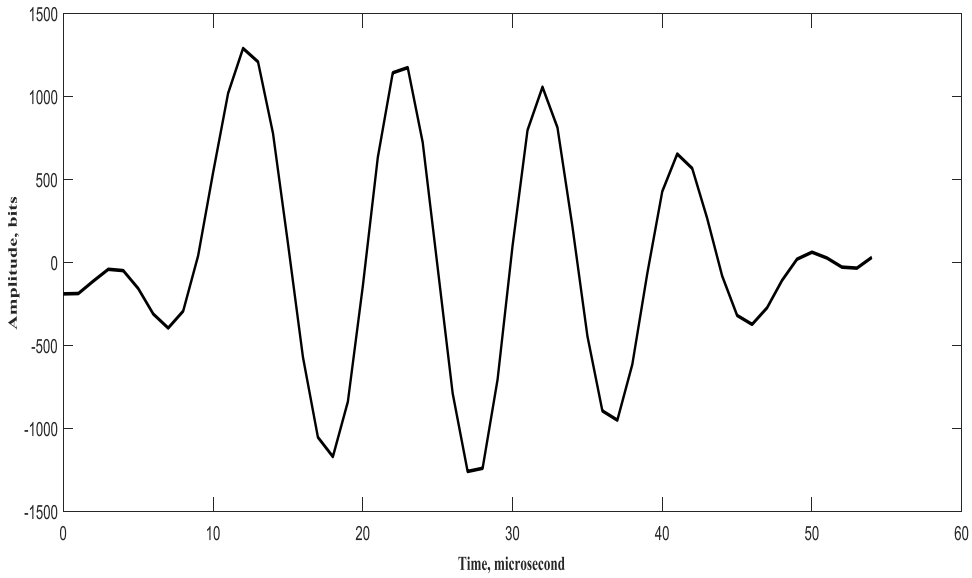

Figure 4.16 Pulse from the threaded contact in time-domain

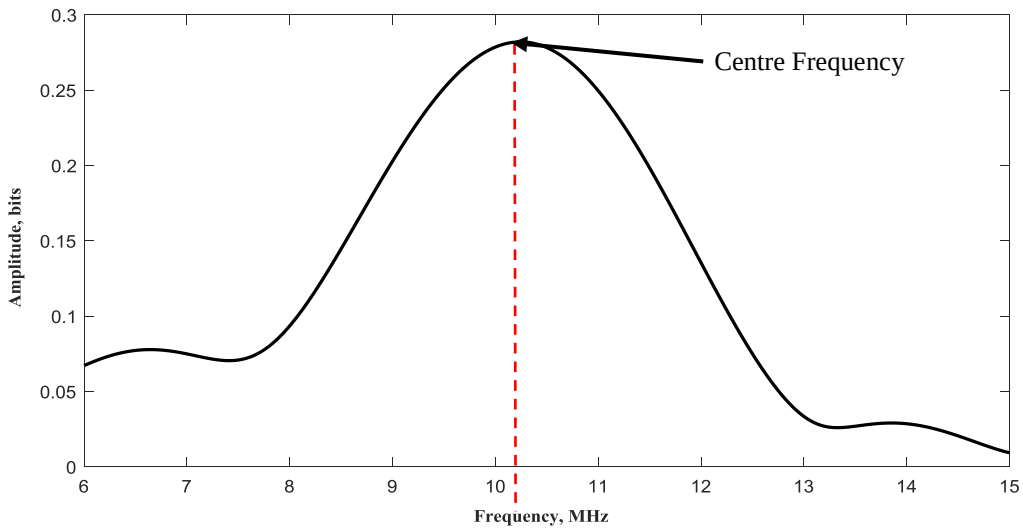

Figure 4.17 Fast Fourier Transform (FFT) of the pulse from the threaded contact

As explained in section 4.9, prior to taking any measurements the bolt is tightened up, therefore loading the threaded contact. The pulse shown in Figure 4.16 is for a loaded contact. The peak amplitude of the FFT response was monitored over an entire test to observe changes when a contact is lubricated. The effect of loading and lubricating the threaded contact is shown in Figure 4.18 and 4.19 on the pulse in both time and frequency domains respectively. The unloaded condition refers to when the fastener was clamped in the bore with the bolt and nut just engaged but not tightened up. The dry loaded condition is when the fastener was tightened up by a torque of 45Nm before being clamped in the bore. The lubricated condition is when fluid was injected and lubricated the threaded contact.

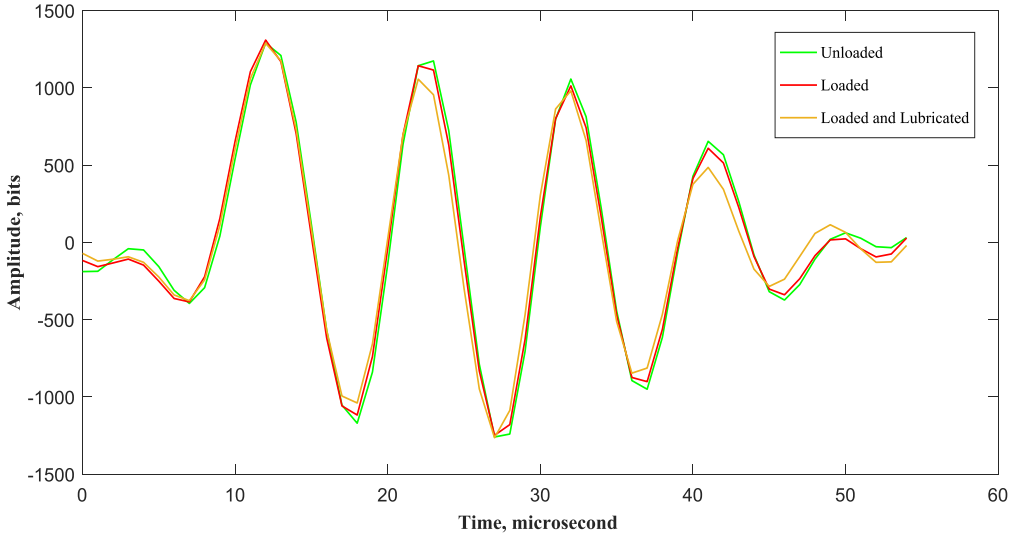

Figure 4.18 Time-domain ultrasound response in unloaded, loaded and lubricated conditions

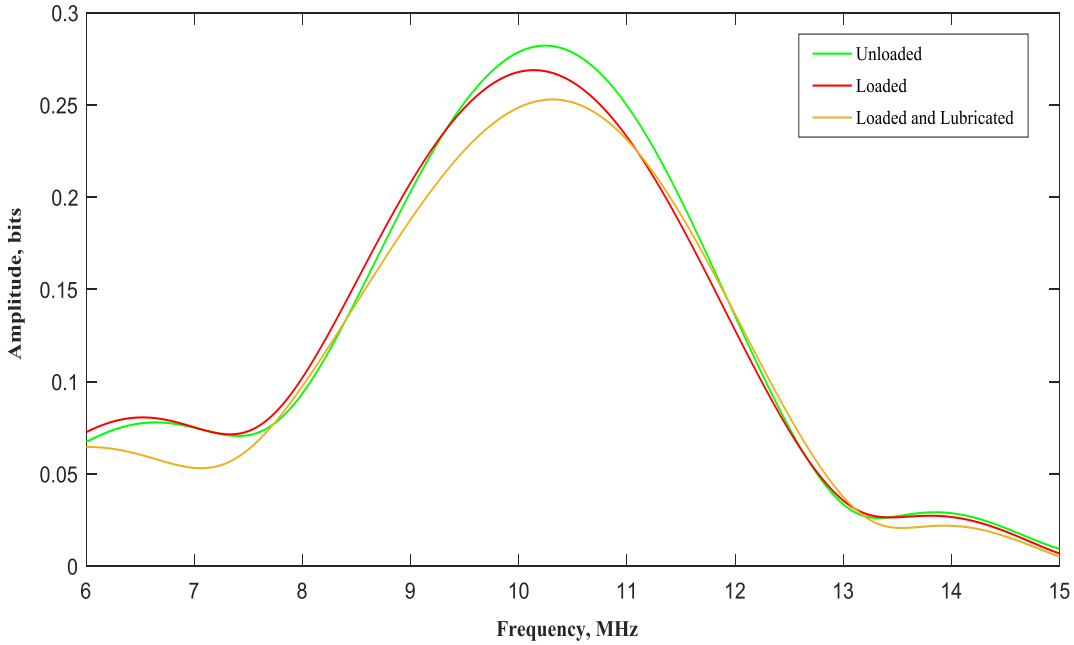

Figure 4.19 Frequency domain ultrasound response in unloaded, loaded and lubricated conditions

It is shown that there is a decrease in signal amplitude, once the bolt is loaded. There is a further decrease in the amplitude when fluid penetrates the contact. As discussed in section 4.2, once the fluid is injected and lubricates the contacts, the increase in contact stiffness at the ultrasonic detectable thread contact (tight side) results in reduction of the reflection signal amplitude. The comparison is clearer, when observed in the frequency domain (Figure 4.19). The raw data obtained from monitoring the FFT response of the six sensors for a fluid sample (PB Blaster Penetrating Catalyst) is shown in Figure 4.20.

The pattern in Figure 4.20 indicates a step-by-step drop in normalised amplitude. The normalised amplitude was obtained by dividing the amplitude response of each of the sensors by the initial value of the amplitude before fluid penetration.

The ultrasonic data shows that there is no change in amplitude for the initial 24 seconds. This is due to the fact that fluid is travelling though the first three threads before it reaches thread 4. And as discussed previously, the first three threads are not within the monitoring range of ultrasonic sensors. In addition, fluid flow in the voids created by the edges of the loose side is expected to take longer before it reaches the ultrasonically detectable region of the thread 4 (tight side).

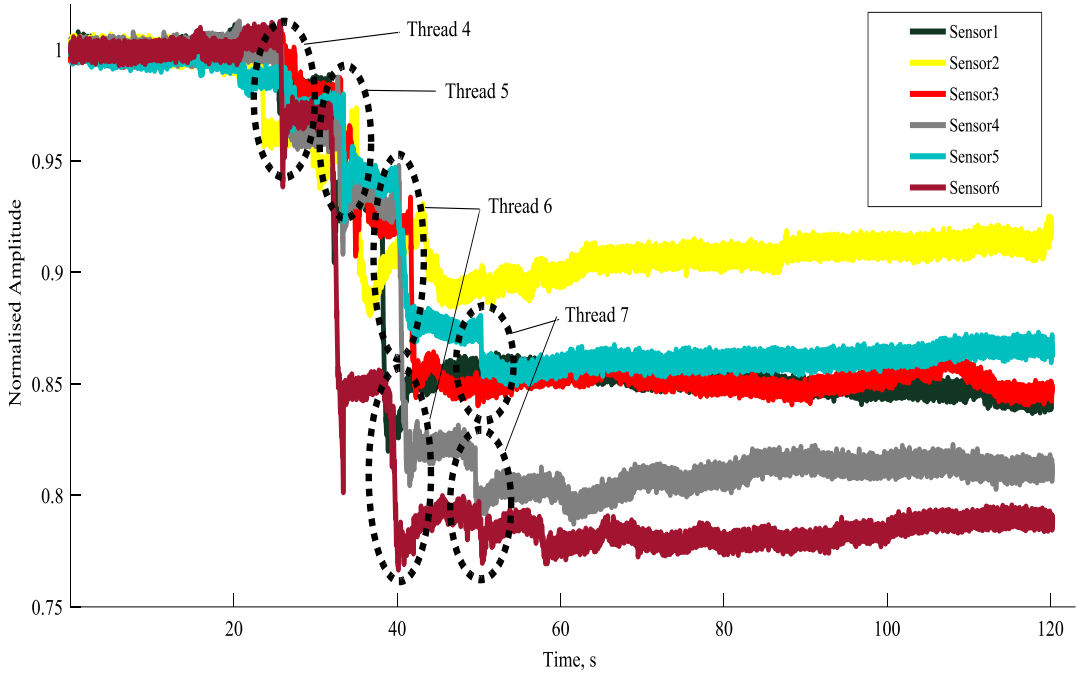

Figure 4.20 A typical measurement from the six sensors for PB Blaster Penetrating Catalyst

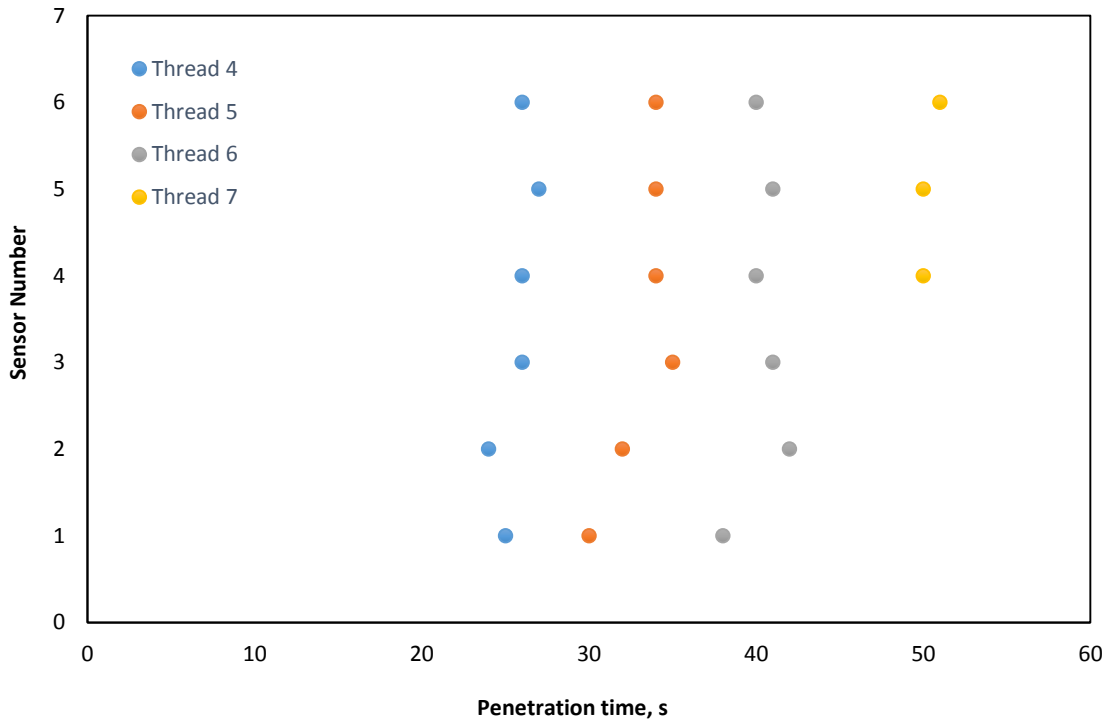

Figure 4.21 Penetration time of fluid into threads

The mechanism of fluid penetration from the loose to the tight side is very complex, and there could be various fluid flow paths that happens at the same time. For instance, data from all the sensors for thread 4 indicate that the vertical drops occur at almost the same time regardless of the circumferential position of sensors. This implies that fluid fills in

the tight side of the thread at the same time, suggesting a more or less simultaneous downward flow of penetrant from the loose to the tight side of the threads.

Another possible fluid flow path can be observed from sensors 1 to 3 for thread 5, where fluid penetration from the loose to the tight side occurs in a sequential manner at 30, 32 and 35 seconds respectively. This could mean as fluid progressively fills in the voids created by the edges of the loose side of the thread, side flows into the tight side of the thread take place.

In addition to different fluid flow paths, penetrant reaches certain locations of the thread at a slightly faster or slower rate. For instance, this was the case for sensor 3, when detecting fluid in threads 4 and 5. Moreover, as mentioned, the depth of fluid penetration is as far as thread 7, although even thread 7 is only partially penetrated, since no fluid presence was detected by sensors 1, 2 and 3. There are several factors, which could explain the observations mentioned above, such as the variation in surface roughness, bubble formation in the microchannel, multi-phase properties of the sample, etc. These will be discussed in Chapter 5, when the penetration time of all the fluid samples will be given and results are discussed.

4.6 Conclusions

In this chapter, an ultrasonic apparatus and measurement technique has been developed to determine the penetration time of fluids into threaded fasteners. In this work, whilst using the same measurement concept as Vail et al. (2013), the new apparatus was developed with the aim of improving measurement sensitivity and repeatability, particularly when dealing with lower viscosity fluids, which was the main limitation of the previous apparatus.

To improve the signal obtained, the bore size was adjusted to have a better fit with the nut. The clamping mechanism was also improved to maximise the transmission of the ultrasound waves at the bore and nut interface.

The new test rig was also made to be more robust by lowering the centre of mass. This was to avoid any accidental drop of the rig, which could cause damage to the sensors or knock them out of alignment.

Similar to the previous rig, twelve piezo-electric crystals were prepared and cured onto the rig, arranged as 6 pairs of transmitting and receiving sensors. The sensors were positioned circumferentially to track the fluid at different locations of the thread, and providing an ultrasonic coverage of 5 threads, starting from thread 4 to thread 8.

The raw data for a typical measurement on a fluid sample (PB Blaster) was shown. The post processing of the acquired data was carried out, converting the time domain signal to frequency domain. The amplitude of the frequency domain signal was then monitored, and a drop in amplitude was associated with the presence of fluid in the tight side of the thread.

Analysis of the data suggested the complexity of fluid penetration mechanism in a threaded fastener. In one fluid mechanism, fluid fills in the tight side of the thread at the same time, indicating a more or less simultaneous downward flow of penetrant from the loose to the tight side of the thread. Whilst another possibility is that as the fluid progressively fills in the voids created by the edges of the loose side of the thread; side flows into the tight side of the thread take place.

There are other factors that could affect the fluid penetration mechanism. In this work, the bolt and nut were re-machined and turned from M14 to M10 for a more regular geometry. A more consistent thread gap particularly on the tight side of the thread is important, as the oil film is detected in this section. Therefore the enhanced tolerance and geometry help with obtaining a strong reflection signal from this region at a loaded condition.

Furthermore, it was found from the earlier trial tests using off-the-shelf products that the irregular thread geometry affects the practicality of the ultrasonic measurement due to signal scattering being too great. Considering the pitch and catch configuration of the set-up, with a more regular thread geometry, it is more likely for the sound waves to bounce off at the thread interfaces at the desired angles.

5

Measurement of Fluid Penetration

In this chapter, the method described in Chapter 4 was used to determine the rate of penetration of fluids into bolted joints. It was found that the data from this method was reproducible and several fluid samples with different viscosities and surface tension were measured. Results are then compared to an analytical model for fluid penetration process in Chapter 6.

5.1 Introduction

The effectiveness of a penetrant product mainly depends on the penetration time and penetrant producers use this information to improve their formulations. There are several factors that affect the penetration time. Physical properties such as viscosity and surface tension are thought to be the main ones. In addition to this, chemical composition, multiphase effects and volatility may play a role.

The nail climb test, as explained in Chapter 2, has been the main method of measuring penetration time. However, it is a very crude test and does not offer any direct information about how the fluid performs when it is inside threads. The ultrasonic technique, developed in Chapter 4, provides a direct method of measuring penetration time of fluid inside the contact.

This chapter focuses on three main objectives:

- Demonstrating that the ultrasonic technique is a robust method for measurement of penetration time of several fluids with different properties.
- Investigating the effects of surface tension and viscosity on the penetration mechanism of fluid tested.
- Exploring the effect of volatile organic compound (VOC%) content on penetration performance

5.2 Test samples

In Table 5.1, a list of samples with their fluid properties is presented. Viscosity and surface tension data were measured using a viscometer and tensiometer. The density of most of the fluid samples was provided from data sheets. A few of them were measured in the laboratory. The measurement process of fluid properties is provided in Appendix.

Fluid samples chosen for testing consisted of three main categories:

- Commercial Penetrant Products: This is the first category shown in Table 5.1. These are the samples which are normally available off the shelf. For instance, WD-40 product is one of these commonly used products. The exact fluid composition is a trade secret, however, WD-40 alongside other commercial penetrants are normally made of base oil and a solvent. The base oil is responsible

for lubrication whilst the solvent's function is to dilute the oil. Understanding how these samples perform will help to formulate better products.

- Volatile Organic Compound (VOC %): The second category considers the amount of VOC in WD-40 penetrant. Four fluids with different percentage of VOC is tested to find out if the variation of high vapour pressure organic chemical affects the penetration time.
- Solvents: The third category includes the solvents. The reason for choosing to test solvents is their key role in the formulation of a penetrant. The solvent makes the penetrant suitable for spraying it into a fastener. Another possibly important factor, which is worth considering is their chemical composition (Fluid Samples Technical Sheets). For instance, it will be interesting to see the additional effect of sulphur and Bromine content or Naphthenes and Paraffins on the penetration performance.

Fluid Category	Fluid Sample	Fluid Composition	Fluid Properties		
			Viscosity [mPa.s]	Surface Tension [Dynes/cm]	Density [kg/m^3]
Commercial Products	**Kano Aerokroil**		4.35	25	800
	WD-40 (UK Sample)		4.20	25	820
	PB Penetrating Catalyst		3.43	27	910
	WD-40 Specialist Penetrant		2.40	28	800
	3 In One Penetrant		2.10	25	800
WD-40 (VOC %) Content	**WD-40 (VOC 10%)**		4.82	28	800
	WD-40 (VOC 25%)		4.30	27	800
	WD-40 (VOC 50%)		4.18	25	800
	WD-40 (VOC 67%)		3.10	27	800
Solvents	**D60**	Aromatics and Benzene	2.30	24	800
	D95	Aromatics	2.30	27	803
	ISOPAR E	Aromatics, Bromine And Sulphur	2.30	22	720
	ISOPAR tm M	Aromatics, Bromine and some Sulphur	1.50	23	784
	D100	Aromatics and Sulphur	1.30	23	803
	D40	Aromatics, Naphthenes, Paraffins	1.10	25	774

Table 5.1 Table of fluid samples, VOC % refers to the amount of Volatile Organic Compound

5.3 Example penetration results

In this section, an example of raw data obtained from one sensor is shown for three fluids (Figure 5.1, 5.3 and 5.5):

- Kano AeroKroil (Slow penetration)
- D60 (Medium speed penetration)
- Isopar E (Fast penetration)

The speed of fluid penetration is based on comparison with other fluids tested. A flow velocity analysis is described in section 5.4.4. The amplitude data obtained from the raw data is then shown for all six sensors in Figure 5.2, 5.4 and 5.6.

Example 1: Kano AeroKroil (Slow penetration)

Figure 5.1 shows the amplitude of the reflected signal from sensor 2 (see Figure 4.7) as it varies with time. For the period 0 to 40 seconds, the fluid is travelling from the injection port to thread 4. At 40 s, the fluid penetrates into thread 4, at the location of sensor 2. As described in Chapter 4, the loose region of the thread is filled up first, then side flow occurs into the tight region. The mechanism of fluid penetration is explained in greater detail in section 5.3.1. This penetration occurs at around 40 s for thread 4, 50 s for thread 5 and 60 s for thread 6. At 80 s, there seems to be a change in amplitude, this is thought to be due to the presence of bubbles in the threads (anomalies measurements are described in detail in section 5.3.1 to 5.3.4). Since, the drop is not very clear, there may be a lack of fluid penetration into thread 7.

From 80 s to 120 s, amplitude seems to be stabilised, and no more fluid penetration can be observed. Considering the nature of drops that occurred and the consistency, Kano AeroKroil does not appear to penetrate further than thread 6.

Three measurements were carried out and the penetration time in each of the threads was recorded and the mean and standard deviation obtained for each of the thread locations, as shown in Figure 5.2.

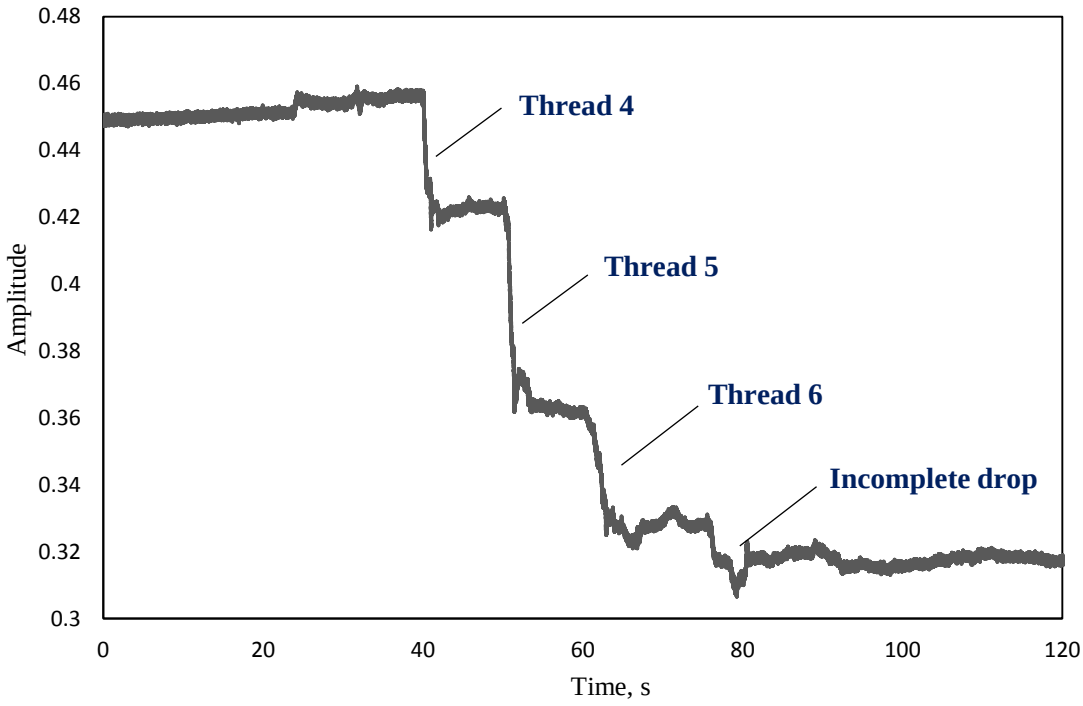

Figure 5.1 Ultrasound amplitude data received from sensor 2

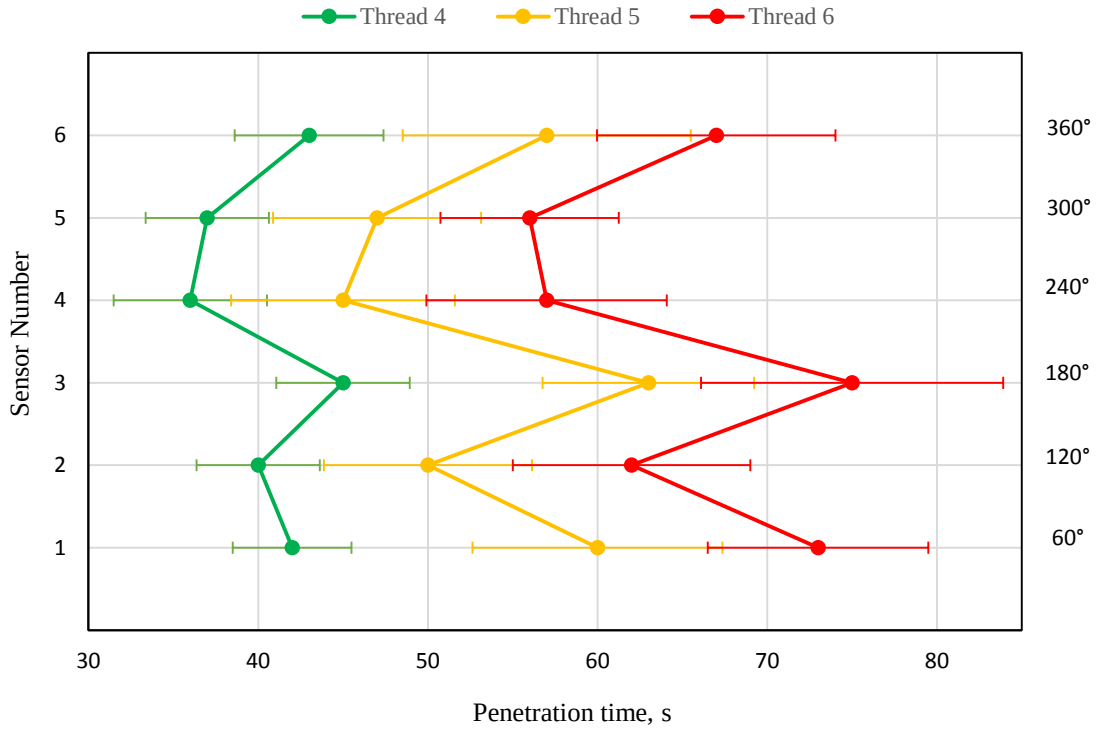

Figure 5.2 Averaged penetration time obtained from all the sensors

It is shown that fluid penetrates up to thread 6 and the total penetration time takes around 75 seconds. Kano AeroKroil is one of the slowest samples tested as compared with others and this can be explained by the viscosity data provided in Table 5.1.

Fluid penetration pattern is shown in Figure 5.2 by connecting the data points for all the threads. It is observed that fluid presence in different thread locations is noticed at different times. For instance, it can be seen that the fluid reaches the location monitored by sensor 2 earlier than sensor 1, but sensor 3 seems to be the slowest. In addition, fluid penetration is fastest into thread locations monitored by sensors 4 and 5.

Fluid flow velocity at those thread locations monitored by the sensors are calculated as fluid flows from thread 4 to 5 and then from thread 5 to 6 (Figure 5.3). The length of fluid penetration is worked out considering the downward flow of penetrant from one thread to the next one as discussed in section 4.5. More details regarding the calculation of the penetration length for this fluid mechanism is given in section 5.4.2.1.

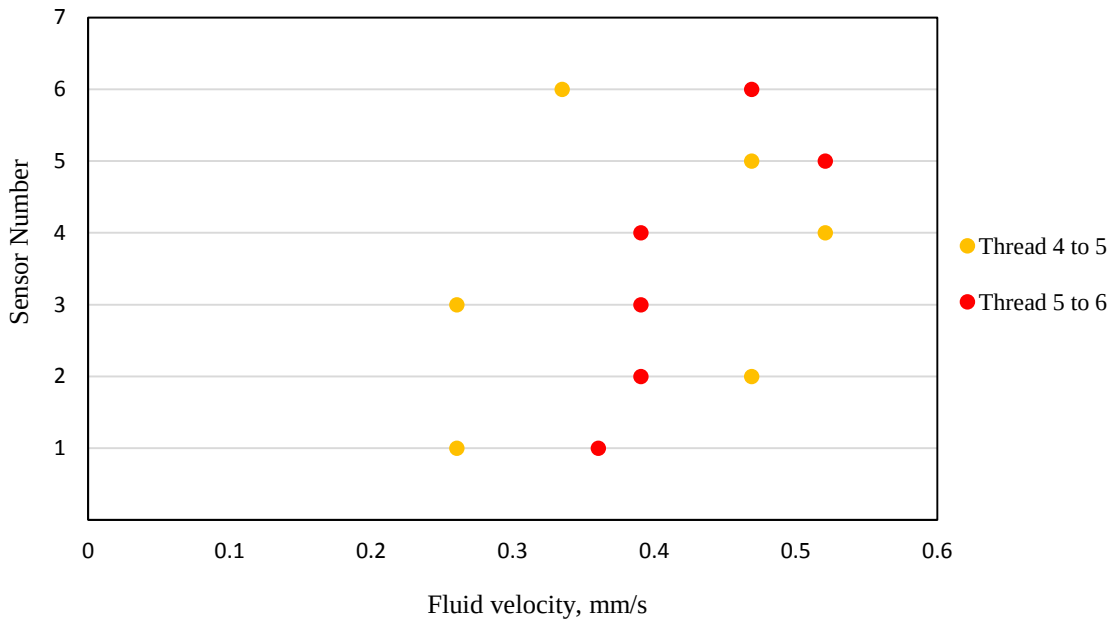

Figure 5.3 Fluid velocity calculations at thread locations monitored by sensors

There seems to be some variation in fluid velocity across different thread locations. It is thought that this could be due to a change of surface roughness at the thread contact. This will be discussed further in section 5.3.2.

Example 2: D60 (Medium speed penetration)

D60 has a faster penetration time mainly due to the fact that it is a low viscosity solvent (Table 1). Figure 5.4 shows the amplitude of the reflected signal from sensor 6 (Figure 4.7) as it varies with time for a test of duration of 70 s. For the period 0 to 11 s, the fluid is travelling from the injection port to thread 4. However, at around 12 s, there is an initial small decrease in amplitude (as labelled on Figure 5.4). This could be due to the presence of some oil residual very close to the monitoring range of the sensor, which is moved forward into the monitoring range of the sensor momentarily (around 2 seconds) due to some pressure build up between the advancing fluid in the contact and the thin oil film. However, as the fluid advances, the pressure may not be enough to move the film completely out of the monitoring range of the sensor, and at around 14 s, the fluid goes over the residual film and fluid penetration into thread 4 occurs as identified by a full amplitude drop. This issue of residual oil films will be explored more in section 5.3.4. Following this, the fluid penetration continues into thread 5 and thread 6 at around 20 s and 24 s respectively. After this, there is no further clear amplitude drop that can be associated with a thread, and at around 37 s the amplitude is stabilised.

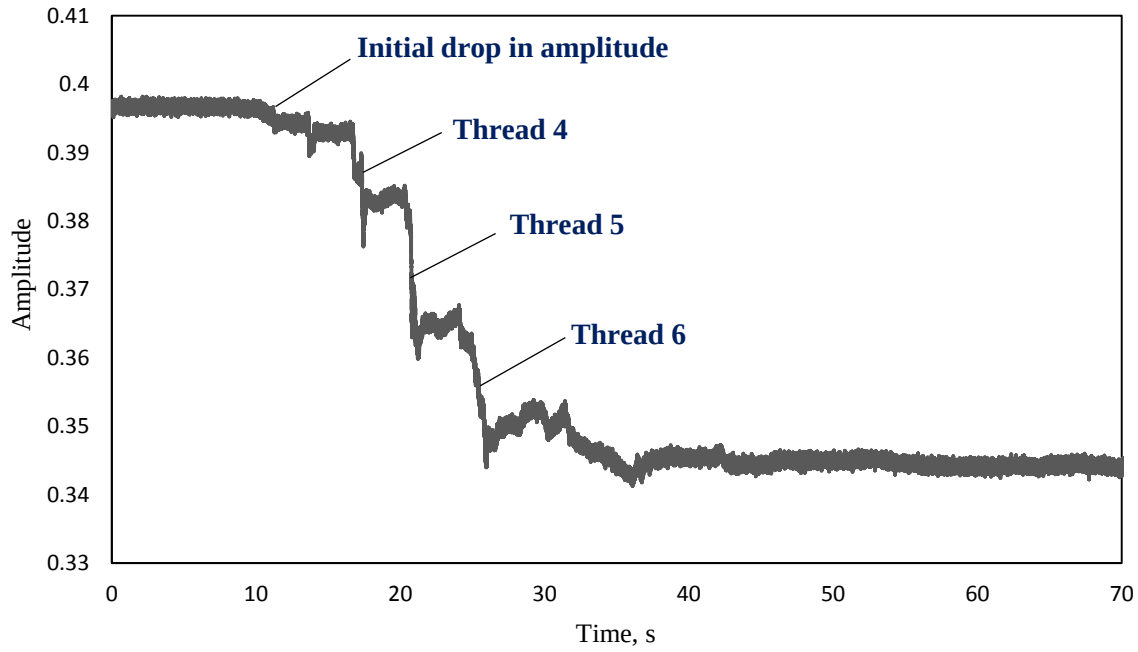

Figure 5.4 Ultrasound amplitude data as obtained for sensor 6

The penetration time of the fluid into each of the thread locations was recorded and averaged. Figure 5.5 shows the data received from all the six sensors and Figure 5.6 shows the fluid flow velocity at different thread locations.

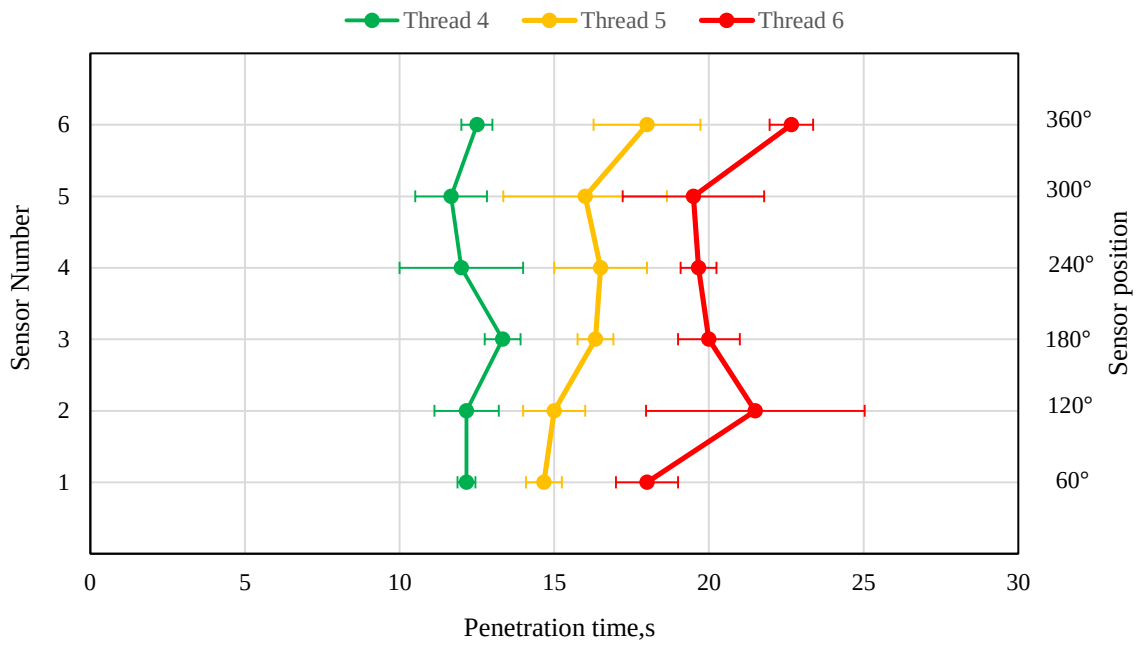

Figure 5.5 Averaged penetration time obtained from all the six sensors

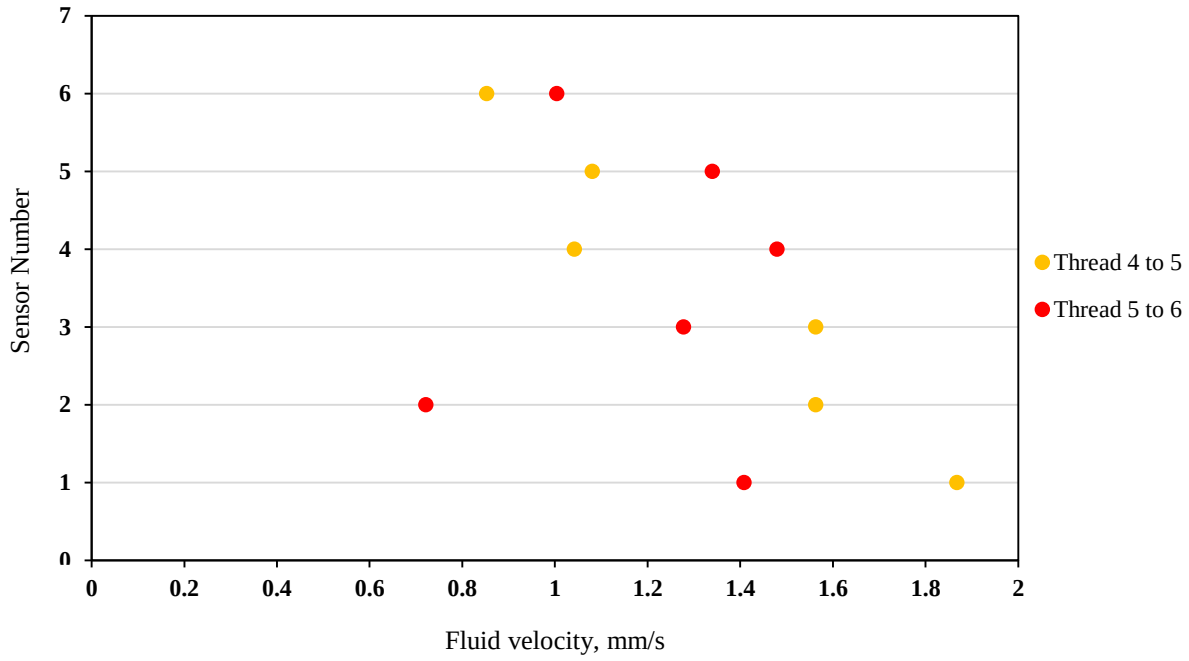

Figure 5.6 Fluid velocity calculations at thread locations monitored by sensors

According to Figure 5.5, it can be observed that for thread 4, sensors 1, 2, 3 and 6 detect the fluid slightly later than sensors 4 and 5. However, for threads 5 and 6, the pattern is different. For both threads 5 and 6, from sensors 1 to 3, there is a general decrease in penetration time, but for thread 6, fluid reaches the location monitored by sensor 3, later than the one monitored by sensor 2 by 2 seconds as compared to thread 5, which is 1 second. Fluid penetration into thread locations, monitored by sensors 4 and 5, starts to get faster but sensor 6 detect the fluid the latest in both threads 5 and 6.

Comparing Figure 5.6 with Figure 5.3 shows that the fluid penetration velocity profile is different. There are various factors that affect the fluid movement inside the threaded contact, which will be discussed in depth in section 5.3.2.

Example 3: Isopar E (Fast speed penetration)

Isopar E was seen to be one of the fastest penetrants tested and it can penetrate up to thread 7 as shown by rapid amplitude drops in Figure 5.7. Similar to D60, this fluid is a pure solvent. Figure 5.7 shows the amplitude of the reflected signal from sensor 1, as it varies with time for a test of duration of 30 s. For the period 0 to 7 s, the fluid is travelling from the injection port to thread 4. The fluid starts to fill in the loose side and from there it penetrates into the tight side, which is the ultrasound detectable region by sensor 1. The fluid then continues the penetration process into thread 5 at 9 s, thread 6 at 11 s and thread 7 at 13 s.

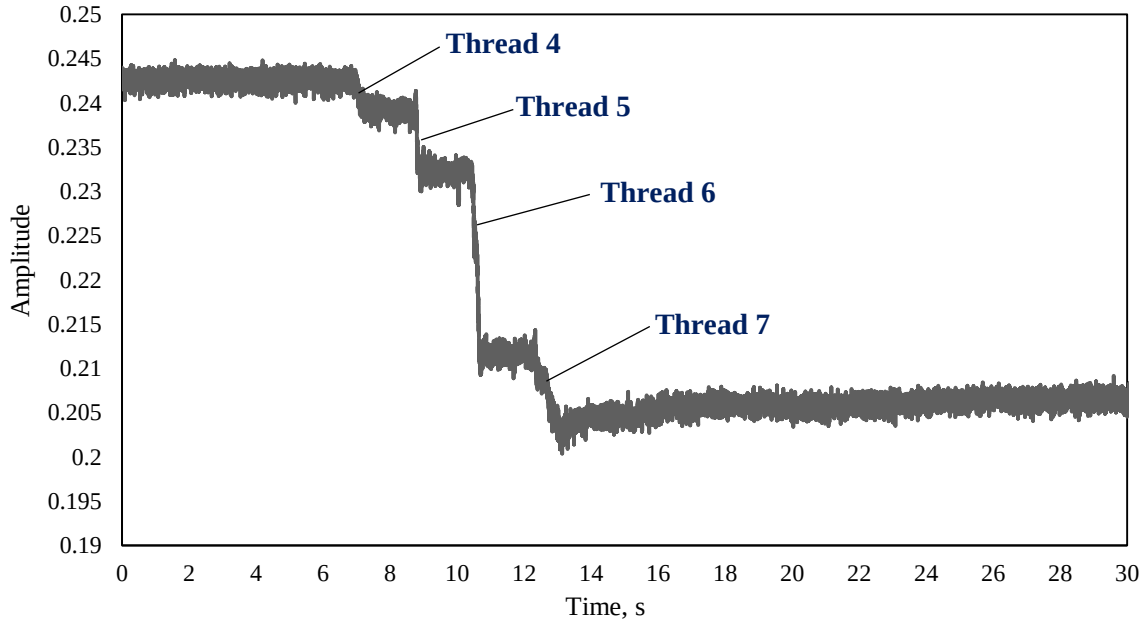

Figure 5.7 Ultrasound amplitude data as obtained for sensor 1

The penetration time of the fluid into each of the thread's locations is then obtained similarly to previous examples and is shown in Figure 5.8.

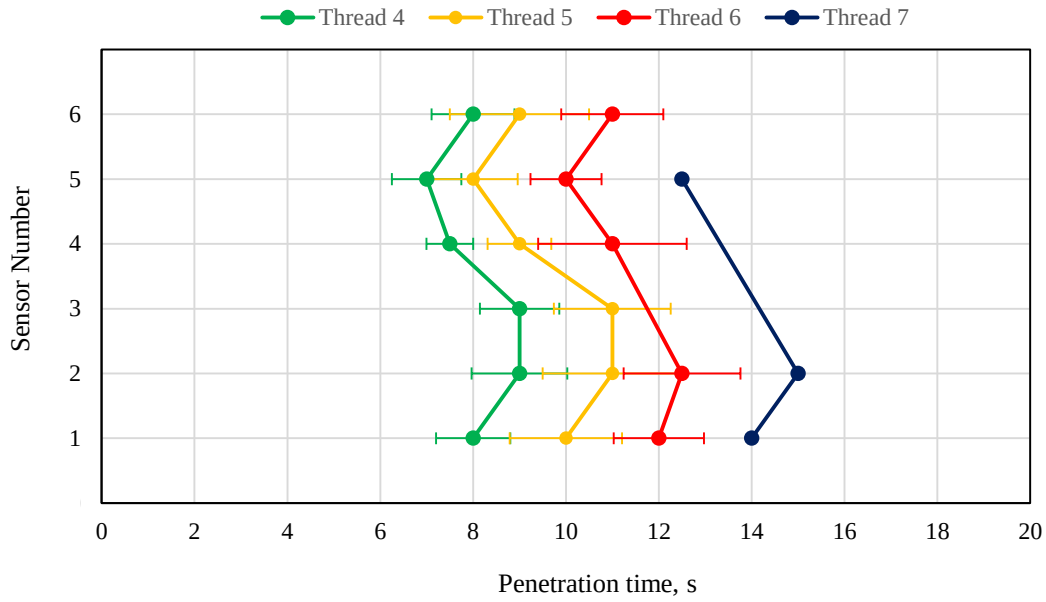

Figure 5.8 Averaged penetration time obtained from all the six sensor for threads 4, 5 and 6 and one set of measurement for thread 7

As it can be observed, sensor 1 detects the fluid presence in thread 4 at 7 s, and then there is a delay in the fluid penetration to reach locations monitored by sensors 2 and 3. Sensors 4, 5 and 6 detect the fluid within 1 second of each other. For threads 5 and 6, the same pattern repeats for sensors 2 and 3, but sensors 4, 5 and 6 detect the fluid presence faster than sensor 1. However, sensor 3 does not record any fluid presence in thread 6. Velocity of fluid flow into threads is given in Figure 5.9.

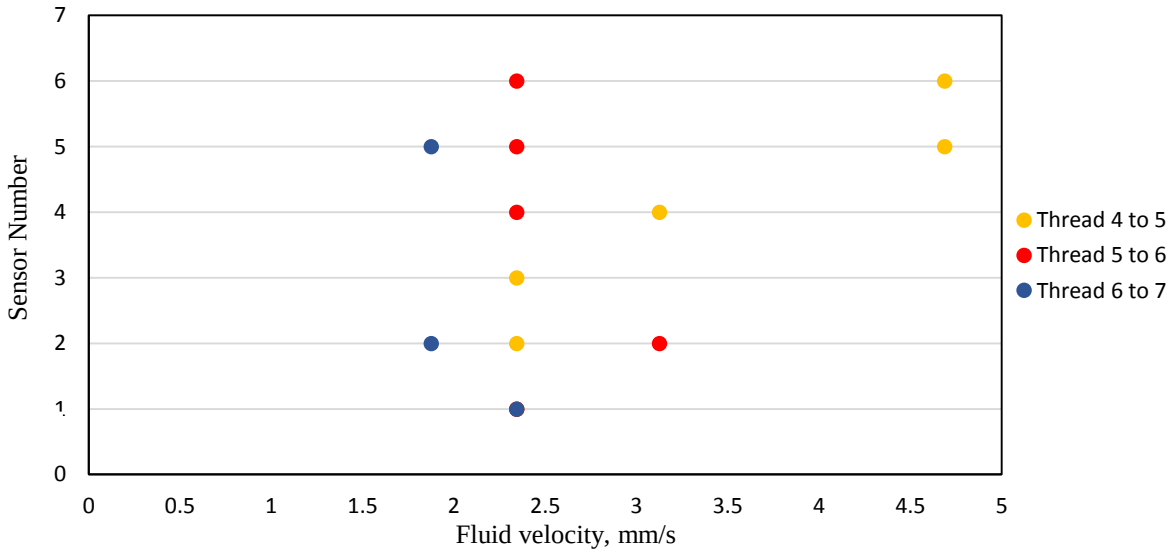

Figure 5.9 Fluid velocity calculations at thread locations monitored by sensors

ISOPAR E has been shown to penetrate into thread 7 at three locations monitored by sensors 1, 2 and 5. It is worth noticing that fluid does not penetrate into thread 7 locations monitored by sensors 3, 4 and 6.

However, this penetration profile for thread 7 varies across different measurements implying that whilst fluid flow into thread 7 occurs, some locations of the thread are not filled with penetrant in one measurement. But in another measurement fluid presence is detected at these locations.

It is thought that variation of surface roughness at different regions of thread 7 could result in blocking the channels and stopping the fluid penetration. In addition, the highly volatile nature of the solvents such as ISOPAR E means faster evaporation, hence it might struggle to fully penetrate into a later thread, i.e., thread 7.

5.4 Features of fluid penetration

5.4.1 Fluid penetration process

As discussed in Chapter 4, interpretation of ultrasonic data suggests two main fluid flow mechanisms, although it is possible that one of them is more dominant. It is predicted that a combination of both mechanisms could take place in a threaded contact. Figure 5.10 and 5.11 show the schematics of both mechanisms. The diagrams represent an unwrapped array of two threads. The region monitored by each of the sensors is marked by the ovals.

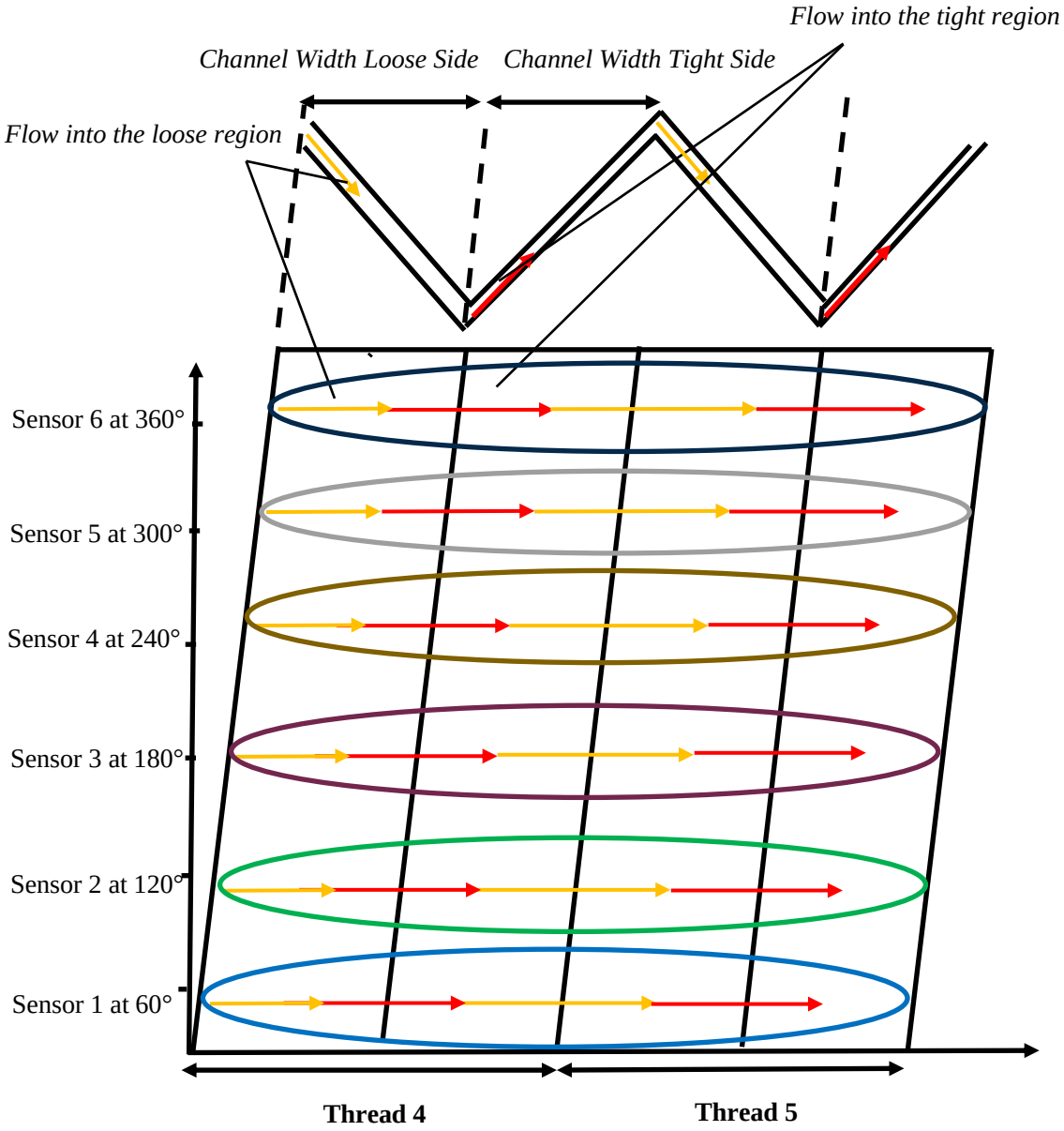

Figure 5.10 Fluid penetration occurs in a downward direction from loose into the tight side and into the loose side again.

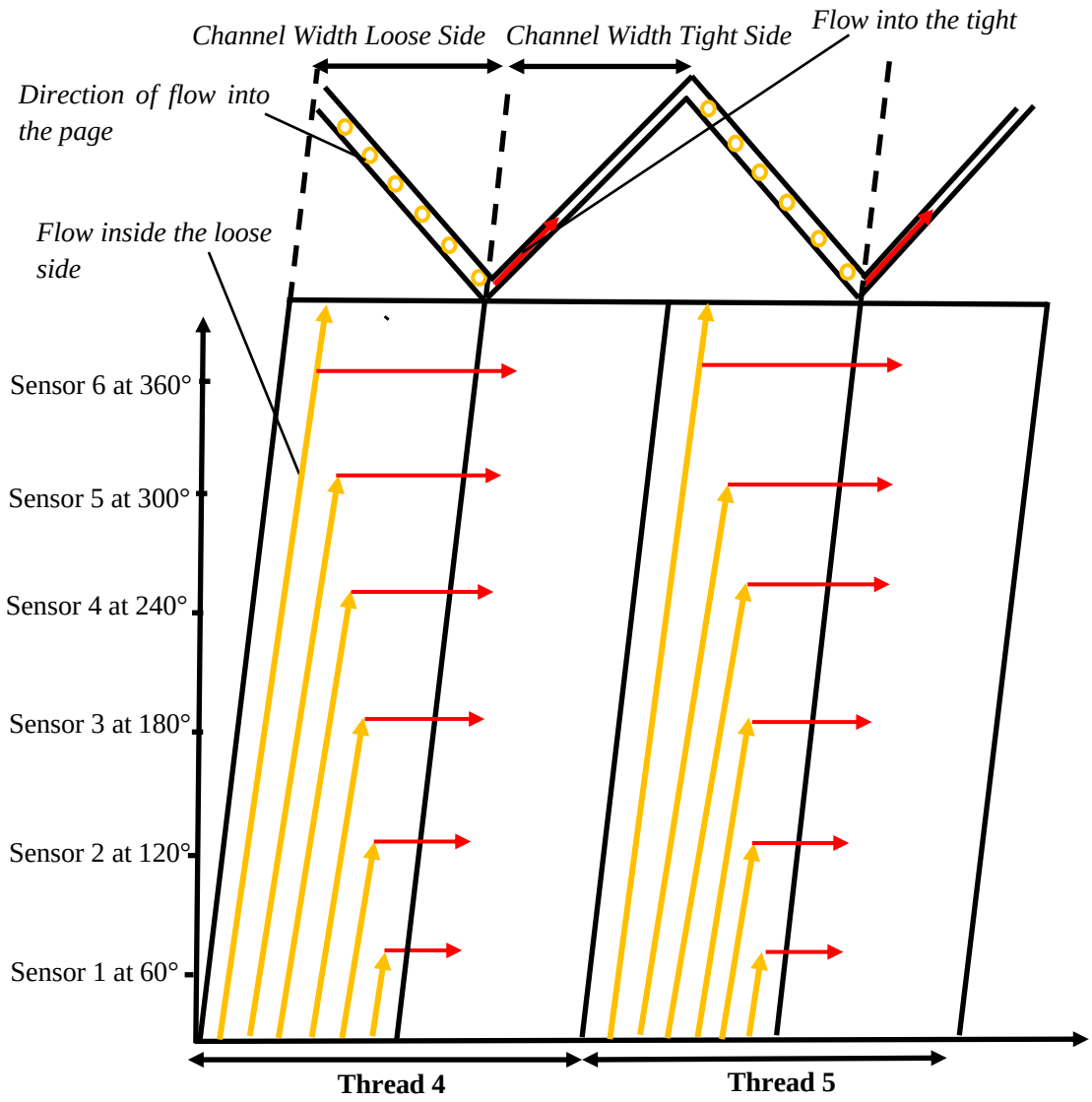

Figure 5.11 Fluid penetration into the tight side takes place as fluid fill the loose side

As the fastener is tightened and bolt and nut threads are fully engaged, two different gaps are created. The side with the smaller gap is referred to as the tight side and the side with the bigger gap is referred to as the loose side. The main fluid flow mechanism occurs downwards and directly from the loose to the tight side. But there is also a possibility that it could penetrate into the rectangular channel created by the loose side of the thread and side flows into the tight side occur as the loose side is being filled.

5.4.2 Delayed fluid penetration

Referring back to Figure 5.2, as mentioned briefly sometimes there is a delay in fluid penetration and this seems to repeat for other fluids too. For Kano AeroKroil, for instance, sensors 1, 3 and 6 detect the fluid presence later than the other sensors. Figure 5.12 shows the main penetration mechanism, where the fluid penetrate downwards across the loose region of the thread and pass though the tight region. The delayed fluid flow is shown by the dotted lines, where the orange and red colours indicate the fluid flow into the loose and tight side of the thread respectively.

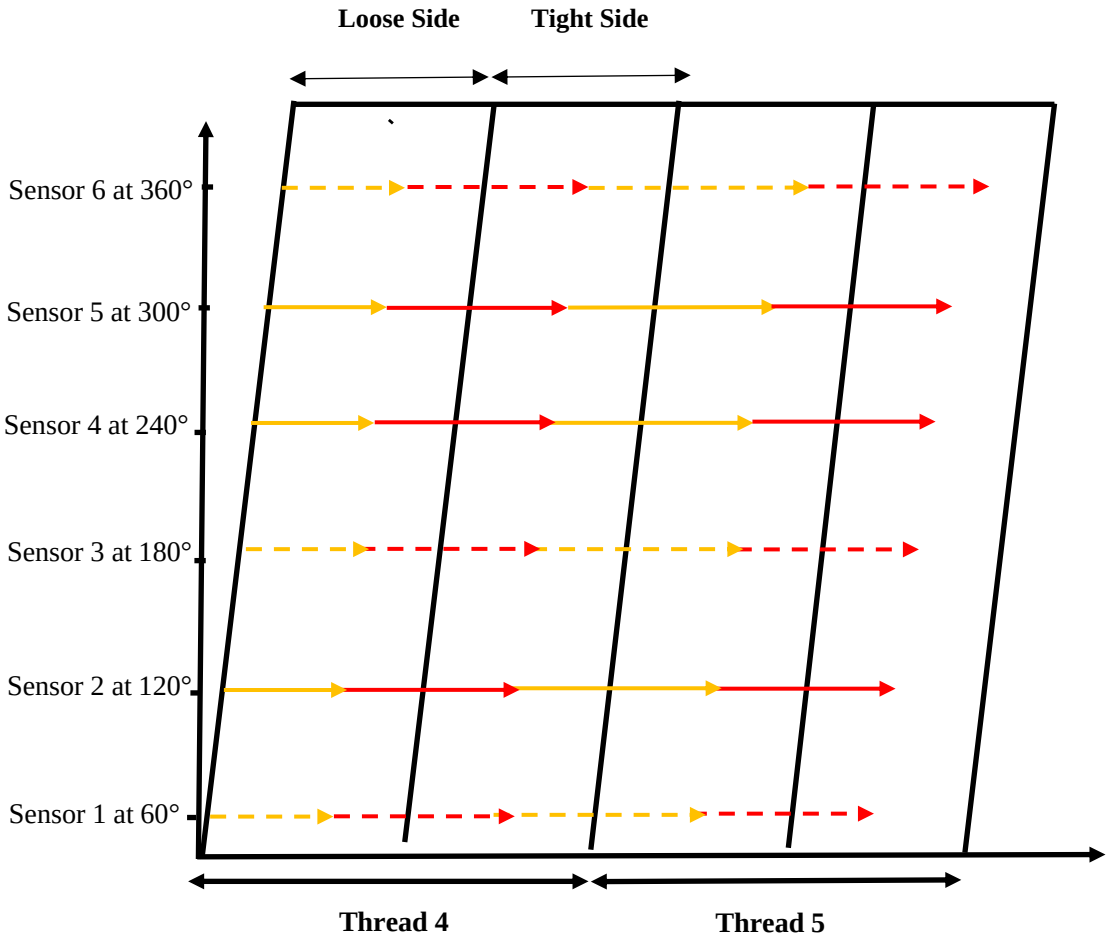

Figure 5.12 Schematics of delayed fluid penetration

The delay in fluid penetration could be due to change of surface roughness at different thread locations. Figure 5.13 shows the threads of a bolt specimen where no test has been carried out. It can be observed that although there are a few regions which have slightly different roughness, the roughness profile is quite uniform. Figure 5.14 shows an SEM

image of the second bolt specimen, which was used for all the tests. It can be seen that damage to the thread surface has occurred during tightening and loosening. There are certain locations, which are marked by the circles, where the roughness seems to be significant. Taking into account the location of these rougher regions and the fact that they are monitored by the same sensor in this case, it is possible that fluid penetration could be delayed at these locations of the thread contact due to the change in roughness.

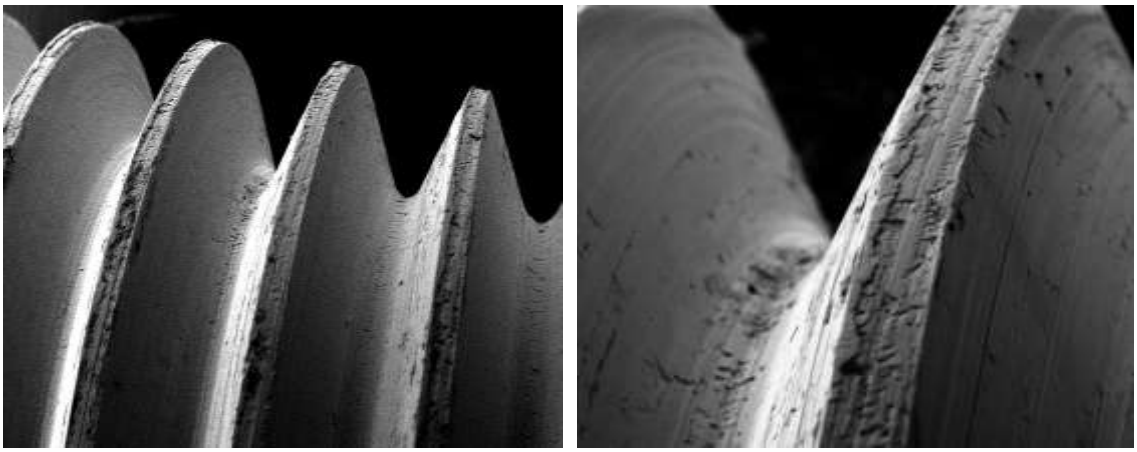

Figure 5.13 Scanning Electron Microscopy (SEM image of the first bolt specimen)

Variation in the roughness profile could largely affect the capillary forces responsible for fluid penetration into micro channels, therefore slight changes in the thread contact can affect the fluid flow implying that fluid may be delayed in reaching a thread location or indeed does not manage to penetrate at all.

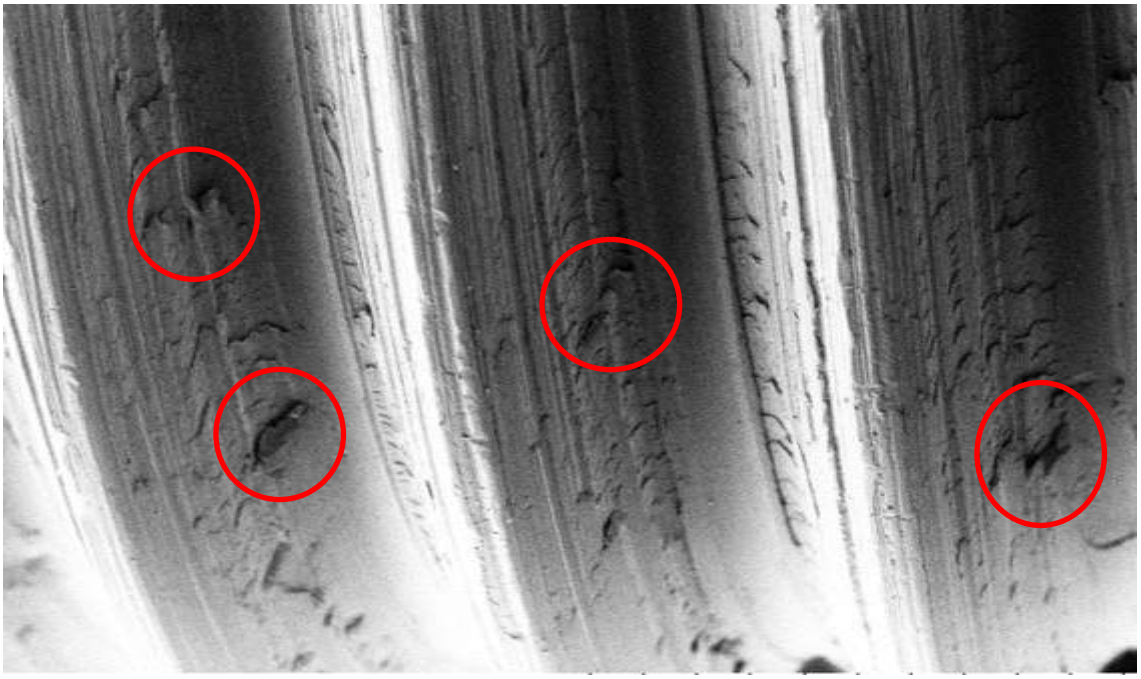

Figure 5.14 SEM image of the second bolt specimen after all the tests were carried out

5.4.3 Presence of bubbles

Figure 5.15 and 5.16 show some of the raw data from the D100 fluid sample. A normal full amplitude response occurs once fluid is detected in the thread contact (Thread 4), however, once fluid reached thread 5, a two stage amplitude drop was observed. For Figure 5.16, the remaining threads are identified by the full amplitude drop, but for Figure 5.15, another two stage amplitude drop is seen for thread 6.

It is suggested that the change in amplitude response is due to the presence of bubbles in the thread. There are several reasons why bubbles may form:

- Air trapped in threads can generate bubbles. Presence of bubbles in microfluidic tubes due to air pockets has been considered previously (Lochovsky, 2012).
- Surface roughness and geometrical irregularities at thread contact could result in sudden expansion and contraction of the microchannel, which could generate bubbles. The geometrical effect of hydrophilic microfluidic channels on generation of the bubbles has been investigated (Jensen et al, 2002). They studied the effect of change in channel size, from a wide one to a narrower one, on the clogging behaviour. Their main findings suggest that for larger bubbles, the tendency for clogging increases.
- Introduction of gas in the fluid at the time of fluid injection due to the use of a pipette could be another reason. The presence of gas in the fluid when it reaches the threaded contact can generate bubbles. The bubble size created is dependent on the surface tension of the fluid.

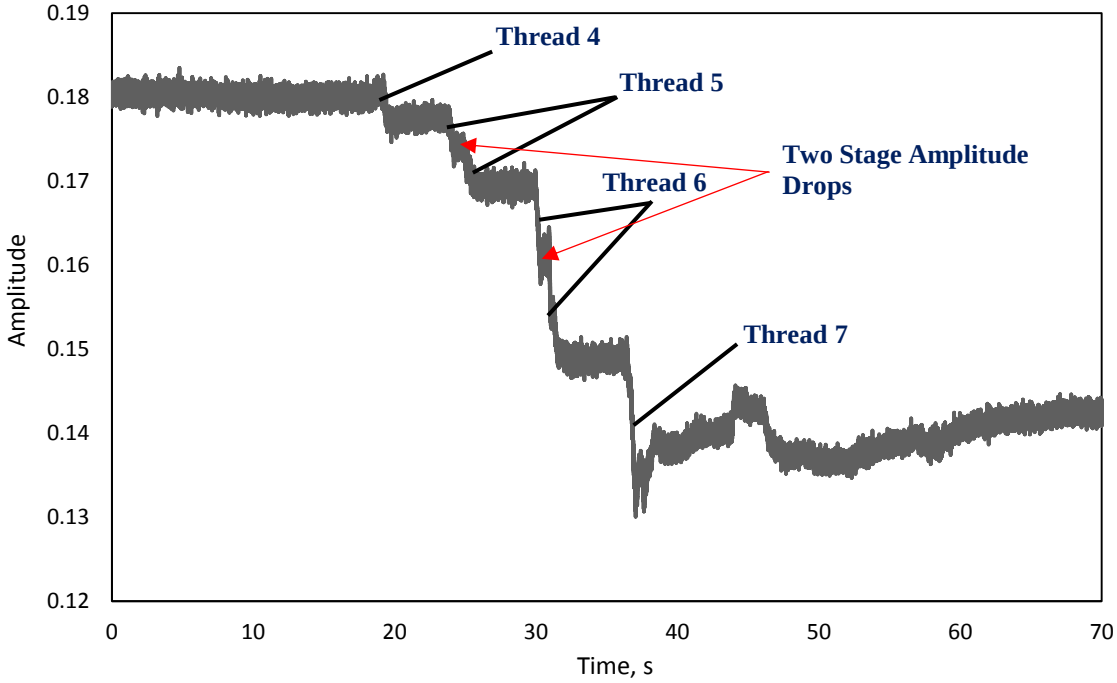

Figure 5.15 Two stage amplitude drop at threads 5 and 6 (D100 fluid sample)

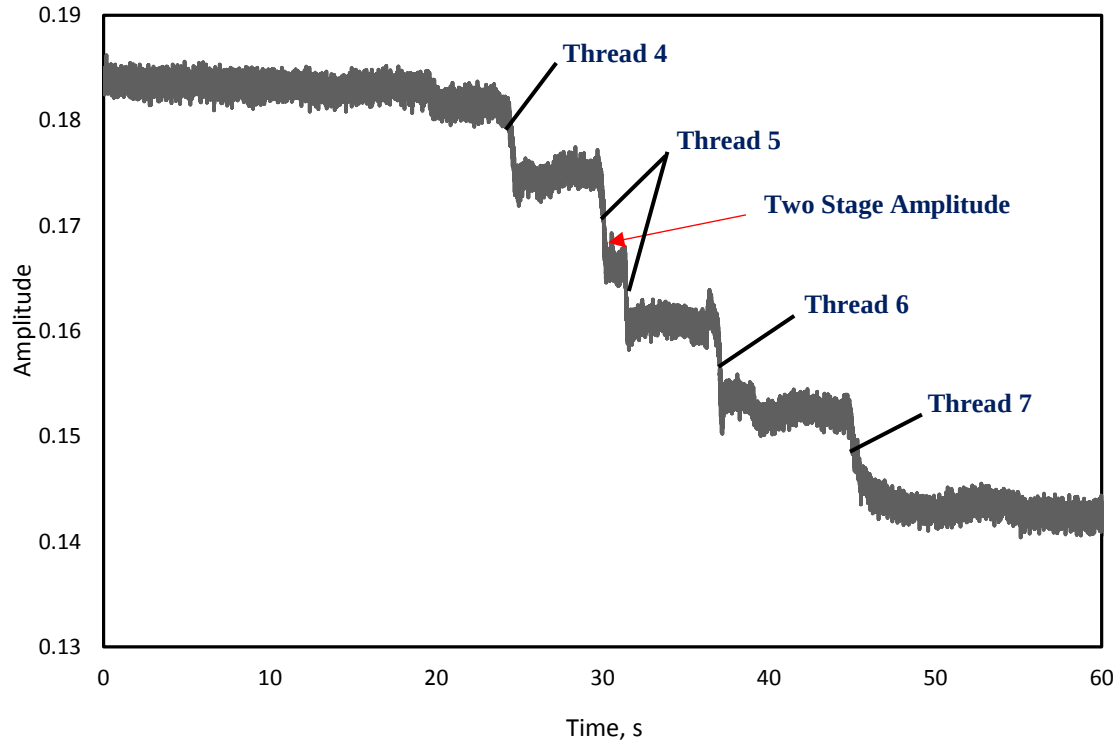

Figure 5.16 Two stage amplitude drop at threads 5 and 6 (D100 fluid sample)

Regardless of how the bubbles are formed, they are seen to be able to slow down the fluid penetration in the threads. The two-stage drop mentioned can be understood by considering how an amplitude drop occurs. Figure 5.17(a) shows that as the fluid fills in the ultrasound detectable region (tight side), the amplitude drop initiates, but as the bubble is formed and observed by the sensor (Figure 5.17(b)), amplitude is stabilised, however, as the bubble goes outside the monitoring range of sensor i.e., leaving the thread, the decrease in amplitude continues till a full drop is achieved (Figure 5.17(c)).

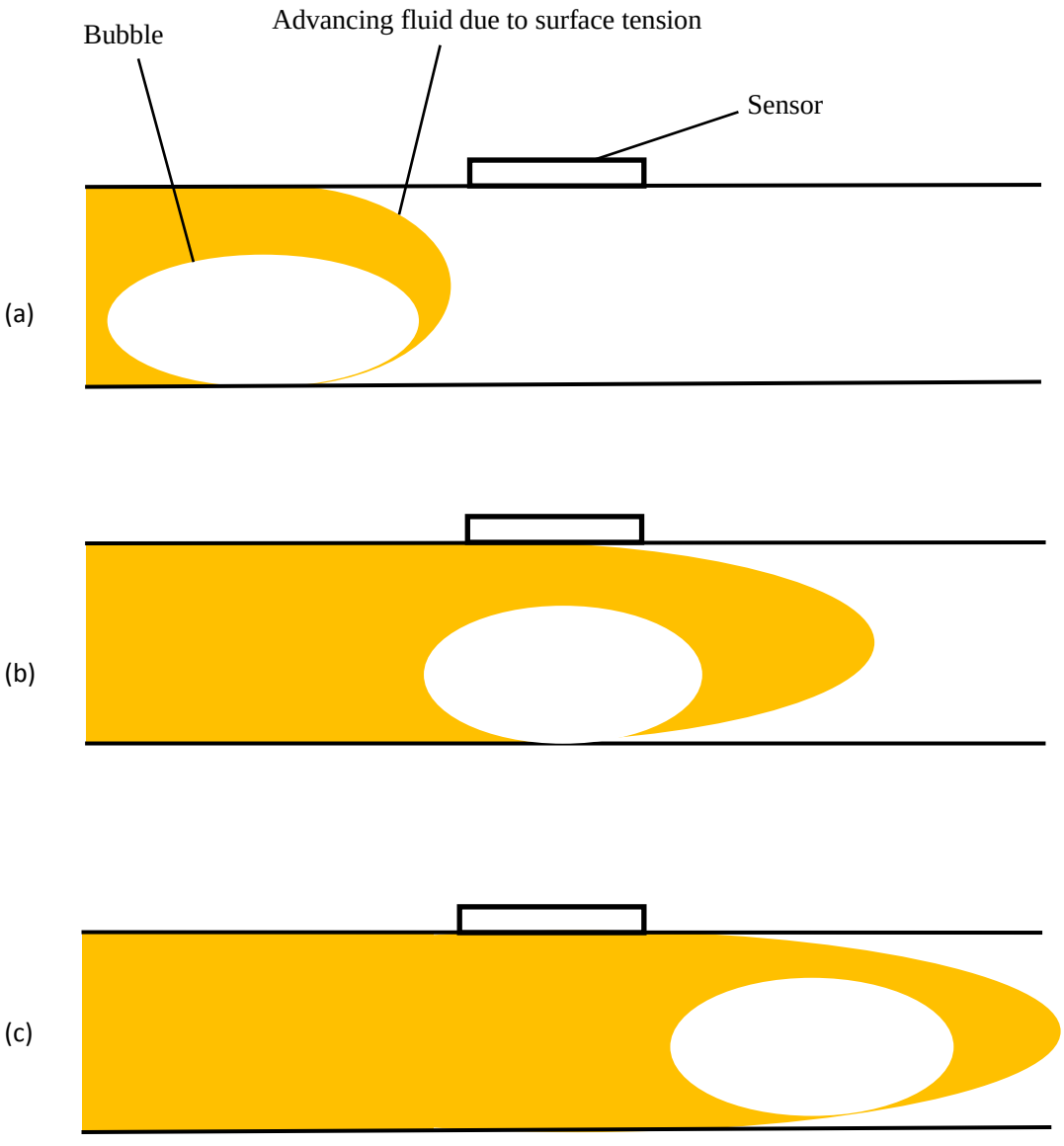

Figure 5.17 Schematic of presence of bubbles in the tight side of the thread (Here a capillary tube is used to simplify the diagram)

5.4.4 Escape of fluid from the tight contact

Figure 5.18 and 5.19 show two plots of amplitude data where an increase in amplitude occurs towards the end of the measurement. As it can be seen, amplitude can increase in one step (Figure 5.18) or it can occur in a step-wise manner (Figure 5.19). This is opposed to a normal measurement, where after all the amplitude drops happen (completion of fluid penetration process), no more major changes can be observed.

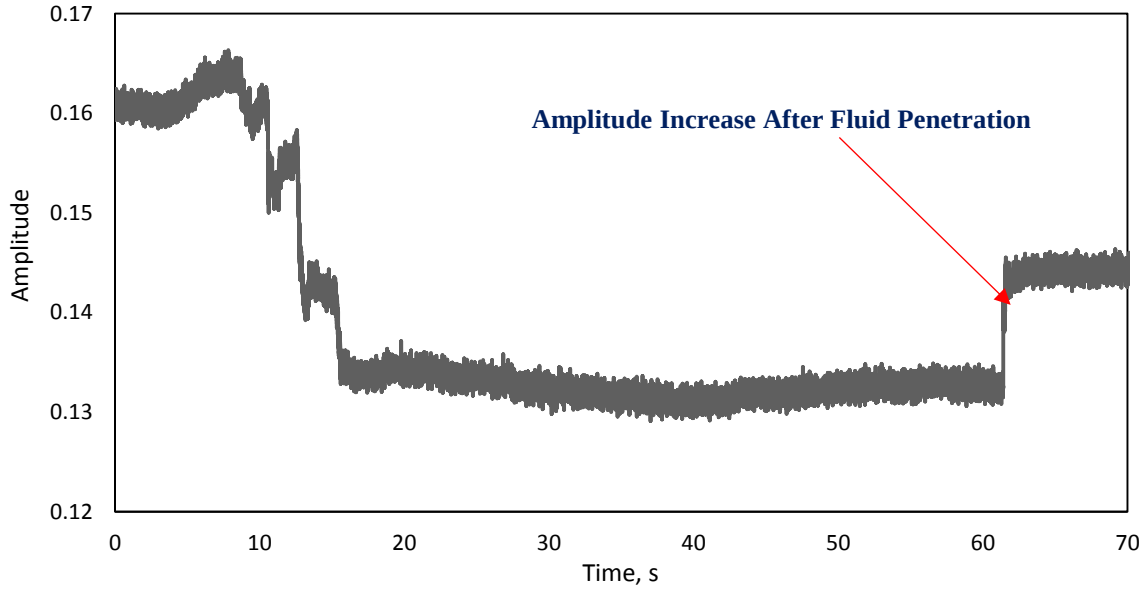

Figure 5.18 Increase in amplitude after fluid penetration (D40 fluid Sample)

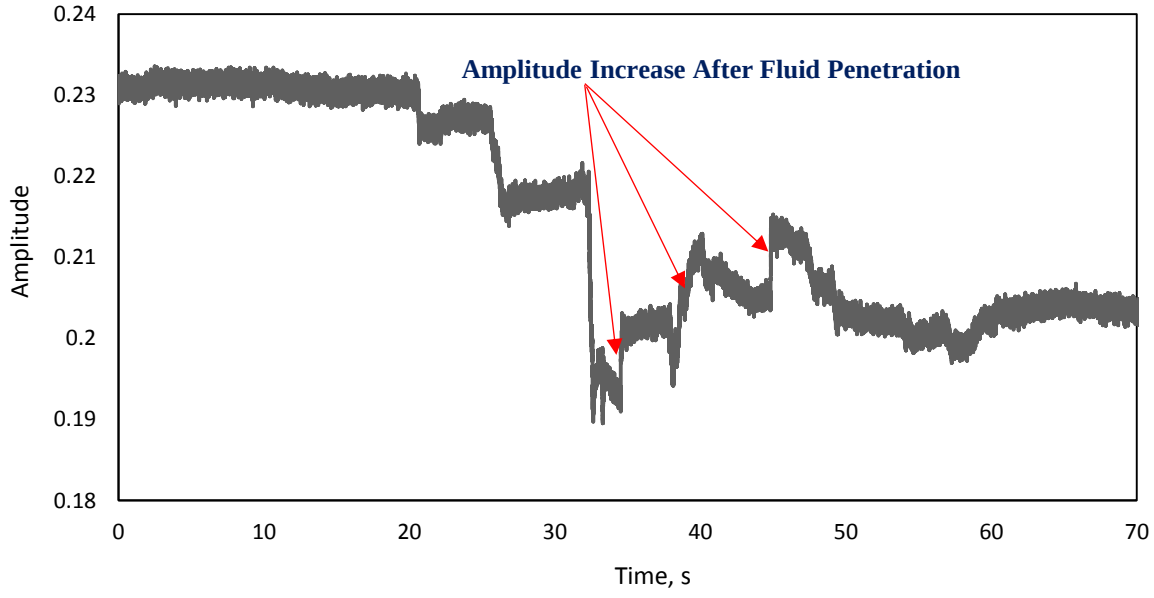

Figure 5.19 Step wise increase in amplitude (ISOPAR tm fluid Sample)

As the thread contacts being monitored are filled with fluid, there are cases where fluid could leak from the tight thread contact into the loose side of the next thread, therefore emptying the contact from any fluid film. In which case, the amplitude start to rise as no more film is detected.

The reason for this phenomena could be due to absent material at the thread, or more specifically the thread crest region, hence increasing the size of the channel and allowing more fluid flow i.e. leakage from the tight side of one thread to the loose region of the next thread.

To investigate this further, some SEM images of the bolt specimen, used for testing, was considered. Figure 5.20 and 5.21 show some of the thread, which are engaged when tightened in the nut and monitored by ultrasound during the fluid penetration process. Referring to Figure 5.20, it can be observed that some materials at the thread crest has been removed, which could be due to adhesive wear resulting from the sliding motion of the bolt and nut threads. Furthermore, in figure 5.21, some cracks on the threads can be observed, which could be due to high contact pressures considering that the first few thread take most of the load. It is very likely that type of damages can affect the fluid behaviour. Further tests were carried out using a new bolt specimen and no more increase in amplitude after fluid penetration was observed.

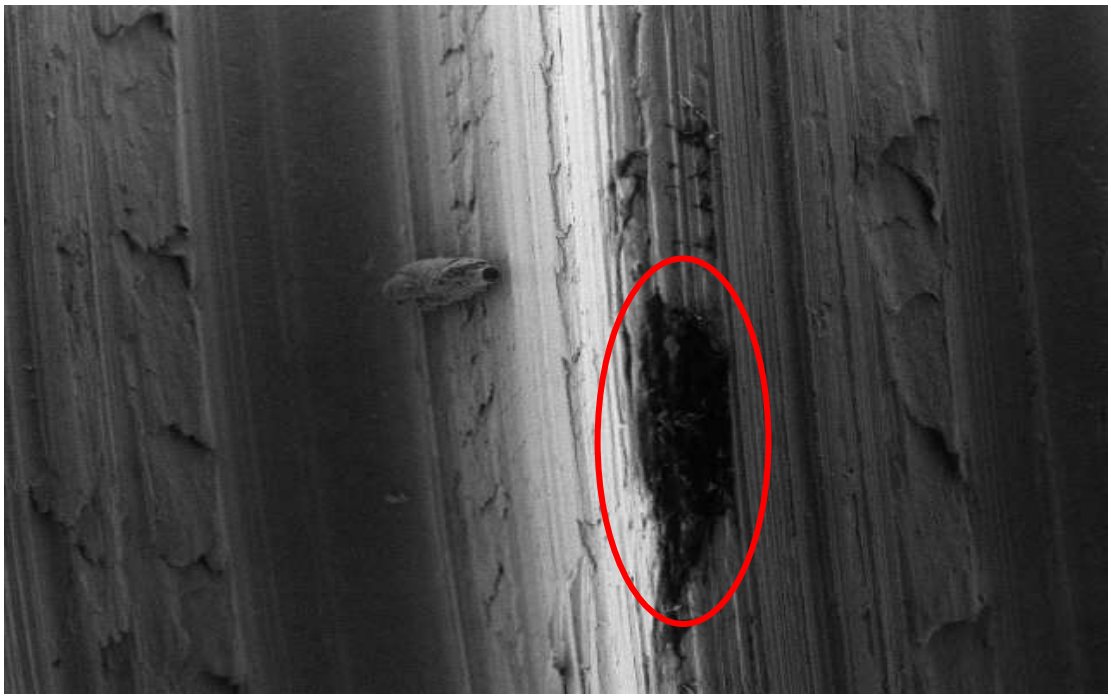

Figure 5.20 The region marked by the red oval, showing material removed from the thread crest

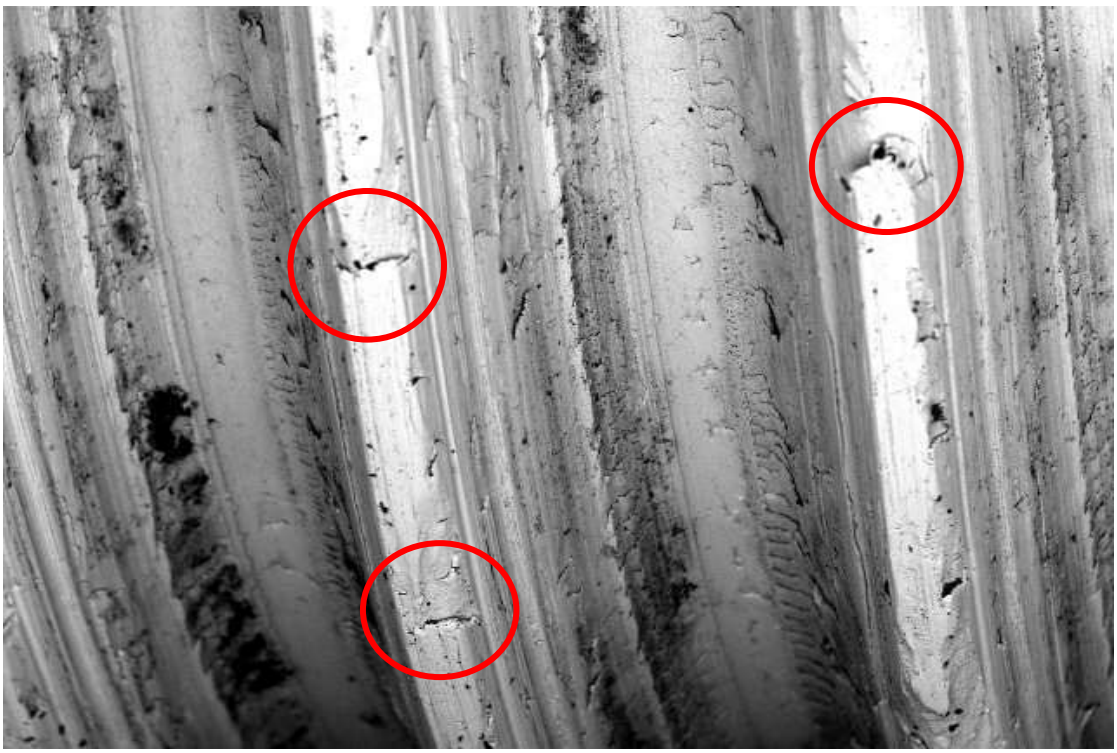

Figure 5.21 The regions marked by the red oval, showing cracks on multiple threads

5.4.5 Residual oil film

Another interesting phenomena seems to take place inside thread contact. By considering Figures 5.22 and 5.23, it is clear that the shape of the amplitude drop initiation is different. At the beginning of the measurement, amplitude is stable but then it seems to increase slightly before actually making the drop. Bearing in mind that this phenomena happened only occasionally during the all testing process, this could be due to presence of some oil residual or a thin oil film deposit. In normal practice, when bolt and nut specimens are fully cleaned using acetone in the ultrasonic bath and dried in the oven, no oil residual would be left behind. To improve on this, both the time of cleaning of the specimens and the drying time in the oven were increased to 10 minutes for each of them and the tests were repeated and a normal response was observed. However, for further work, a better set of experiments could be designed where a controlled amount of residual oil film can be applied at one of the threads and a series of tests carried out to determine whether or not the suggested observation is the main reason or not.

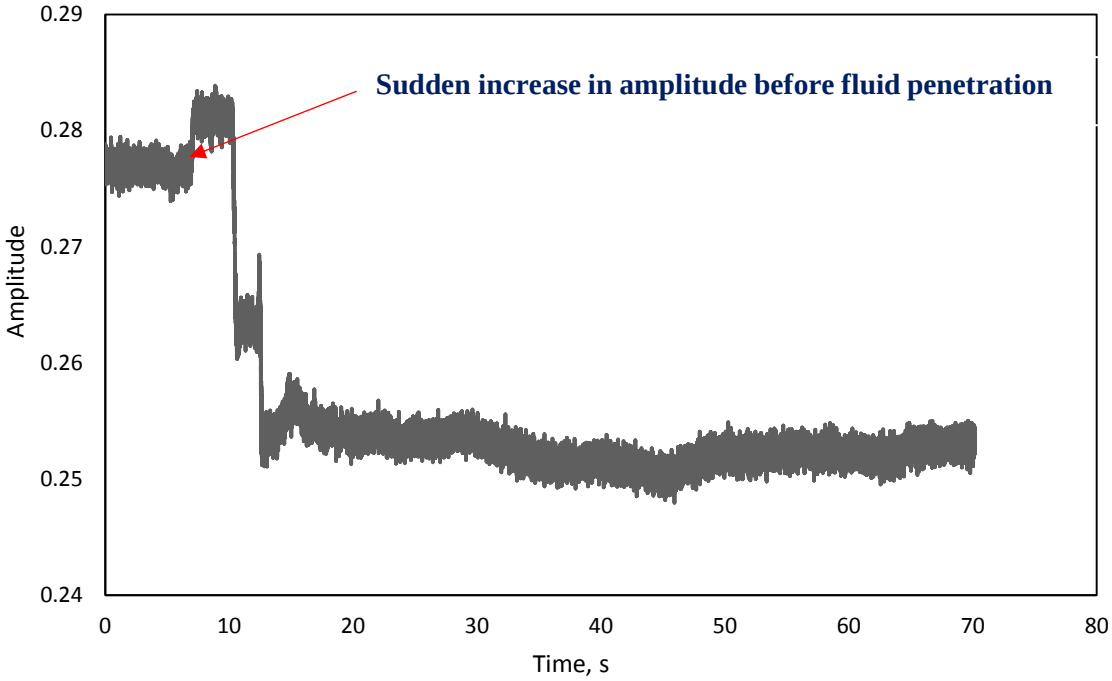

Figure 5.22 Amplitude increase before fluid penetration (ISOPAR E fluid sample)

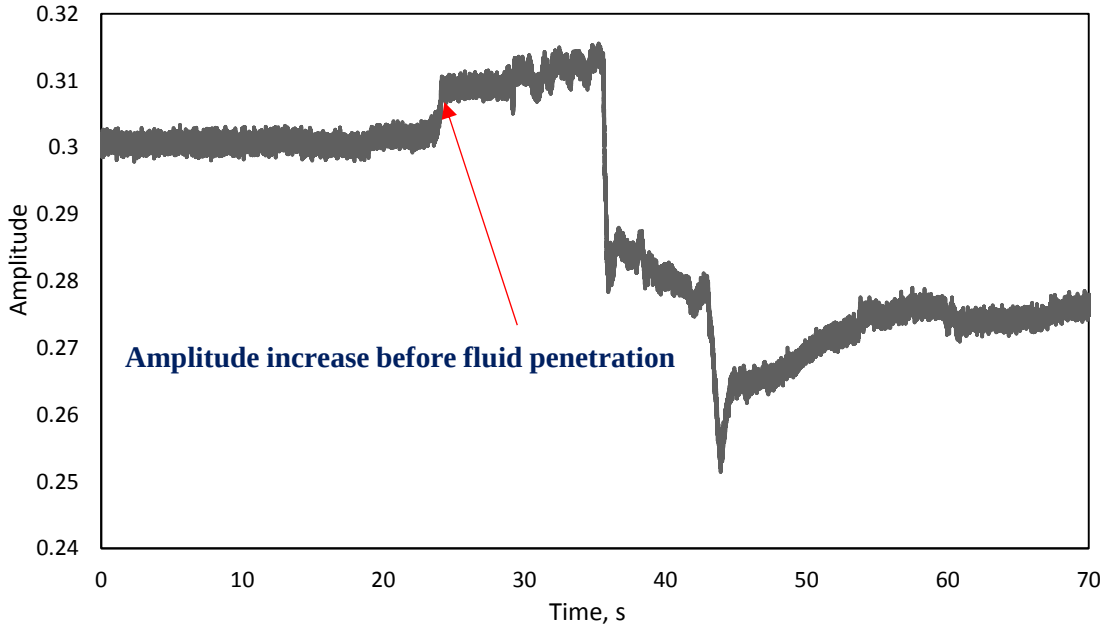

Figure 5.23 Amplitude increase before fluid penetration (WD-40 VOC 50% fluid sample)

Referring back to presence of residual oil in the thread and its effect on the shape of the amplitude, a simplified case of what could be happening is presented in Figure 5.24. Assuming a thin oil film had deposited previously in the contact, the starting signal amplitude is lower than what it should be, since only some of the ultrasound wave

transmitted will be reflected back. Reflected amplitude value will be higher for a metal/air interface than a metal/oil interface. As the penetrant is drawn into the contact, there is also presence of air pockets between the fluid and the residual oil film (Figure 5.24a). The penetrant advances with the capillary action and pressure is built up, moving the thin oil film out of the monitoring range of the sensor and creating a metal/air interface before the arrival of the penetrant (Figure 5.24b). This process may happen for a short time (Figure 5.22), or it may last longer (Figure 5.23).

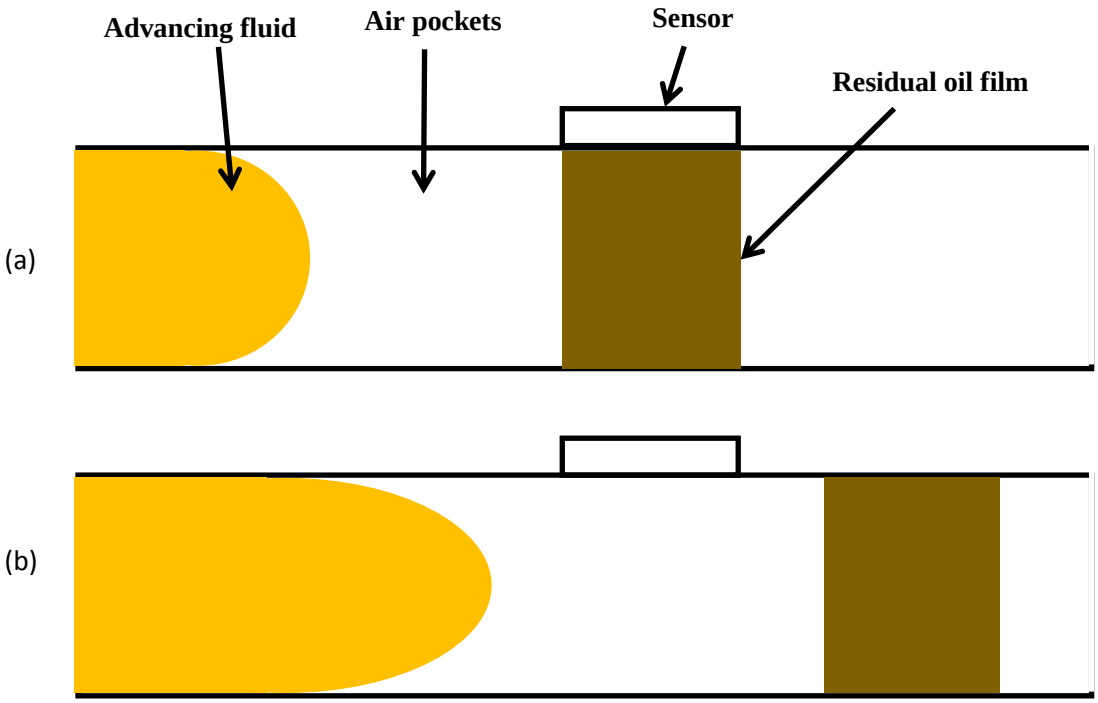

Figure 5.24 Presence of residual oil film in the tight contact

To summarize section 5.3, although some data that has been affected by the factors discussed. The most repeated feature was the delayed fluid penetration. Otherwise, most of the results obtained have a normal response and multiple measurements are carried out for each of the fluid samples to ensure consistency in results.

5.5 Relative penetrant performance

5.5.1 Comparison of penetration time of fluids

In this section, firstly the penetration time obtained from all the fluids are compared with each other. Secondly, the penetration data obtained from some of the samples will be compared against the nail climb data provided by WD-40. In addition to this, the effect of VOC content on penetration time will be investigated.

Figure 5.25 presents the penetration time of the fluids listed. The commercial products are circled red, WD-40 with VOC in green and the solvents in yellow. WD-40 (UK Sample) is the slowest with the mean total penetration time of 94 s and a standard deviation of $\pm$2.5 seconds, and ISOPAR E is the fastest with the mean total penetration time of 14 s and a standard deviation of $\pm$2. This gives a good indication of the ability of the ultrasonic technique to measure the penetration time of a range of fluids.

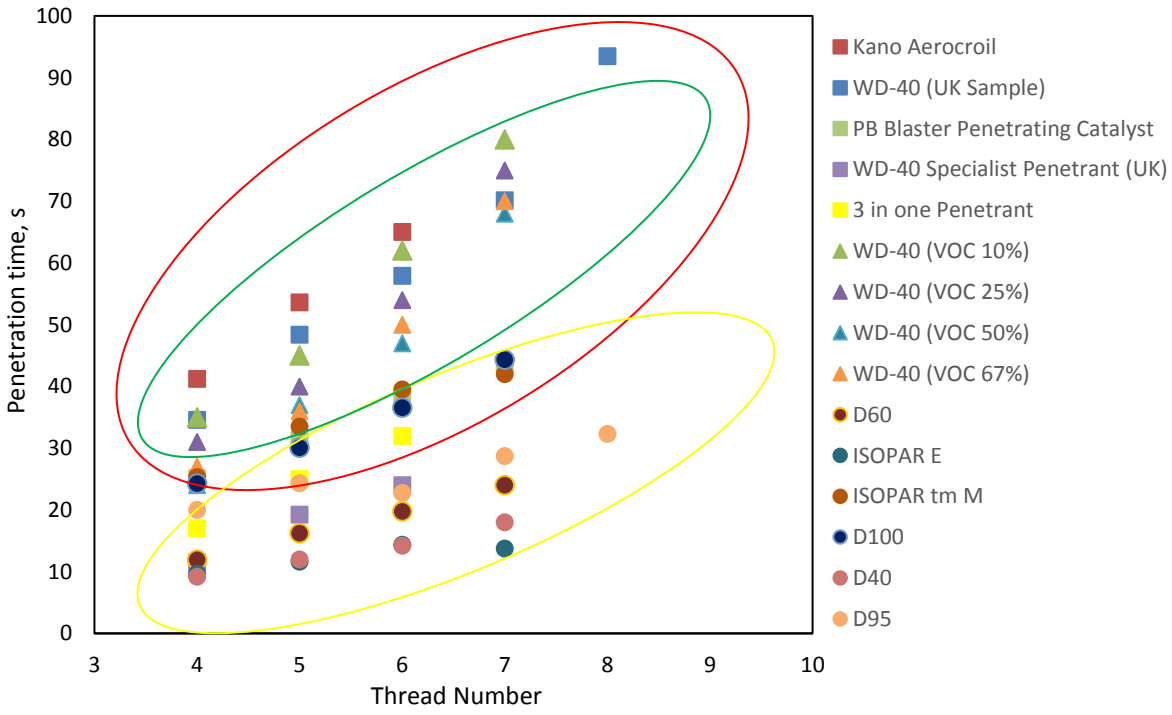

Figure 5.25 Penetration performance of all fluid samples. Red, green and yellow ovals indicate commercial products, WD-40 fluid with VOC and solvents respectively

The three main categories of fluid samples in Figure 5.25 are presented as subplots in Figures 5.26, 5.27 and 5.28.

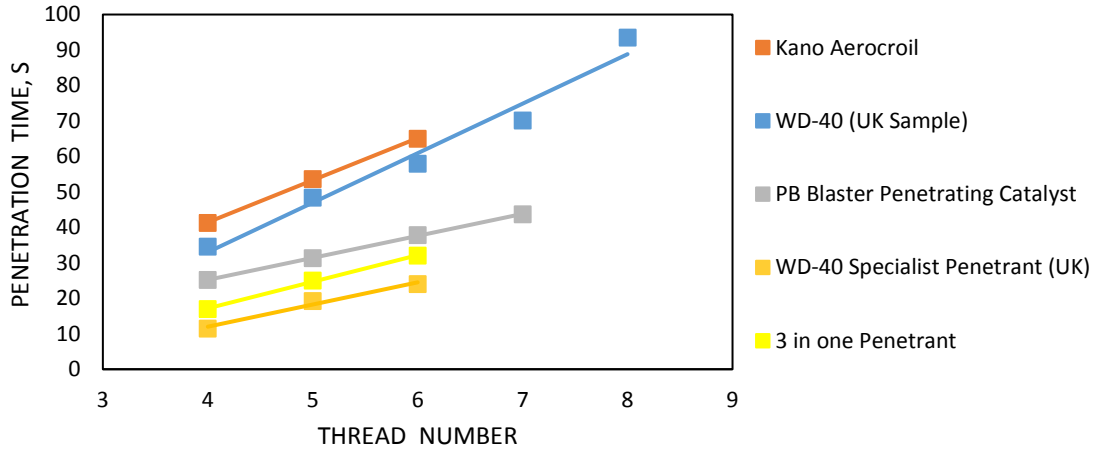

Figure 5.26 Commercial penetrant products

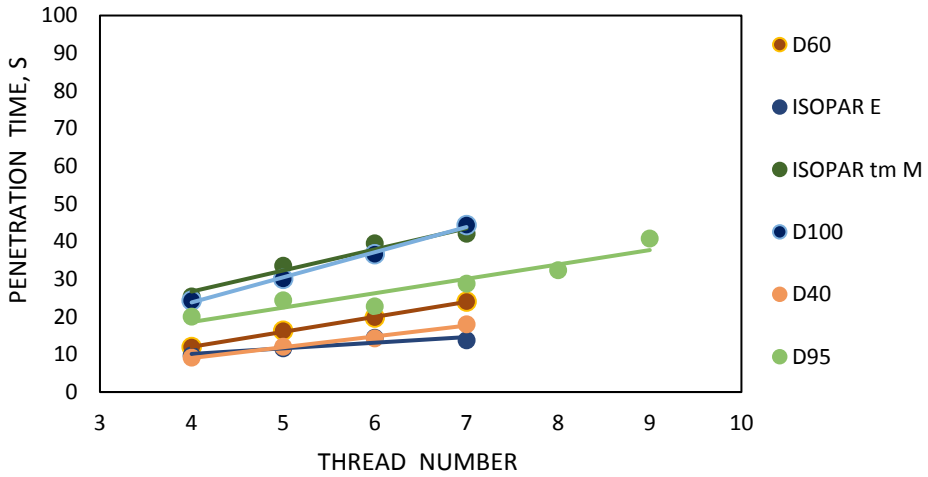

Figure 5.27 Solvent samples

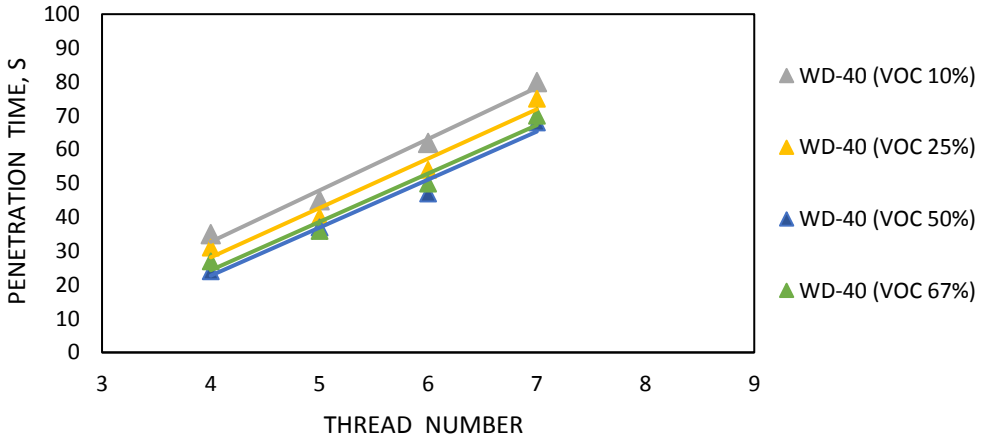

Figure 5.28 WD-40 penetrant product with different VOC content

There could be a relationship between the solvent content and the commercial product. Commercial products such as 3 in one Penetrant and WD-40 Specialist are the fastest penetrants and considering that there are solvents such as D40 and D100 within the same range of penetration time, it is very likely that there is a higher solvent content in WD-40 Specialist or 3 in one Penetrant compared to the rest of commercial products.

Straight lines are drawn through the data for each of the fluid samples in Figures 5.26, 5.27 and 5.28. The gradient of line gives penetration time per thread (Figure 5.29).

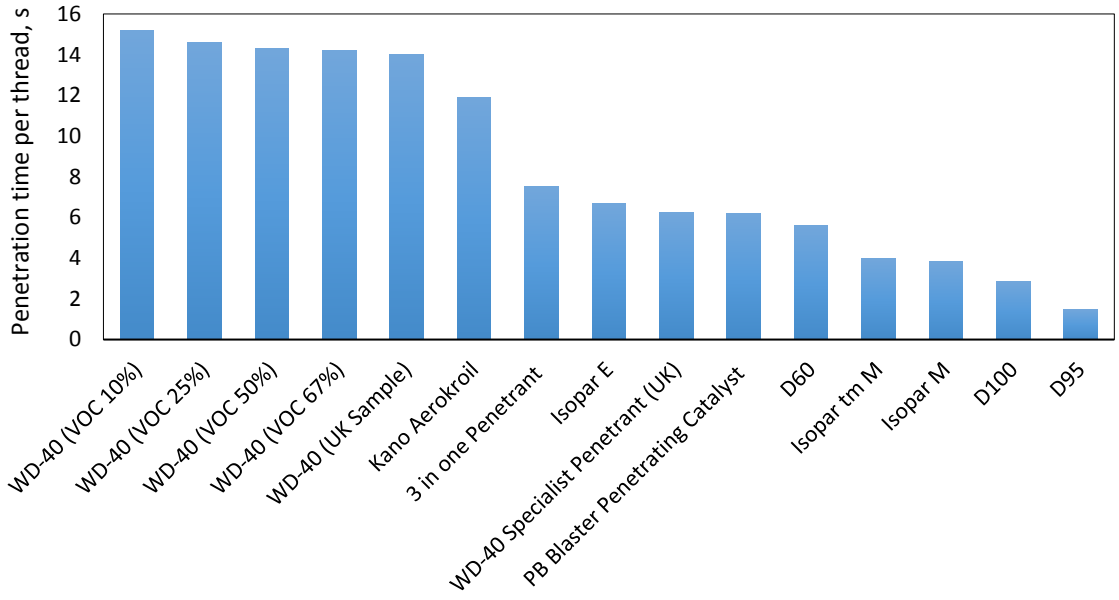

Figure 5.29 Penetration time per thread

Nail Climb Test Data

The data obtained for PB Blaster Penetrating Catalyst and WD-40 Specialist Penetrant using the ultrasonic technique can be compared against the penetration time provided from the nail climb.

As seen in Figure 5.30, WD-40 Specialist Penetrant is almost twice as fast as PB Blaster Penetrating Catalyst according to measurements taken using the ultrasonic technique. The data obtained from the nail climb test, shown in Figure 5.30, also supports this. The climbing distance of the penetrants are given as 1 cm and 2 cm. It is clear that WD-40 Specialist Rust Release Penetrant is two times faster than PB Blaster for climbing 1 cm and just less than 2 times faster for climbing 2 cm.

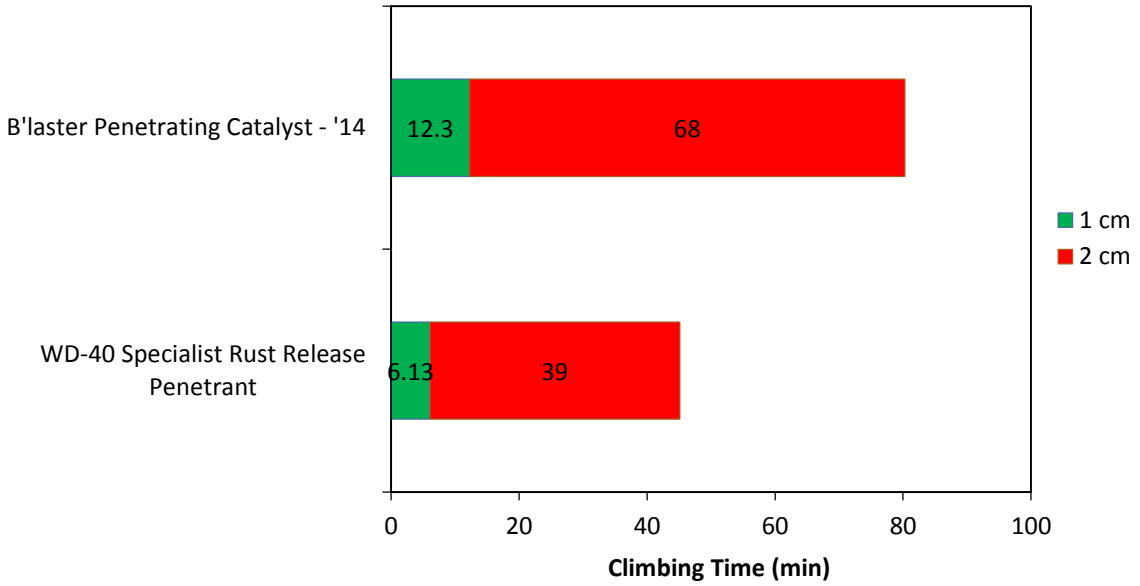

Figure 5.30 Nail Climb Test Data for PB Blaster Penetrating Catalyst sample and WD-40 Specialist Rust Release Penetrant (Data provided by WD-40 Company)

Effect of VOC content on penetration time

It is expected that an increase in volatility decreases the viscosity of the fluid. This is due to fact that that a high viscosity fluid has longer hydrocarbon chains, hence more work is required to disentangle them when heated, therefore they are less volatile. But a low viscosity fluid have short hydrocarbon chain, hence more volatile. This can partly explain the decrease in penetration time of WD-40 as a result of an increase in VOC content (Figure 5.31).

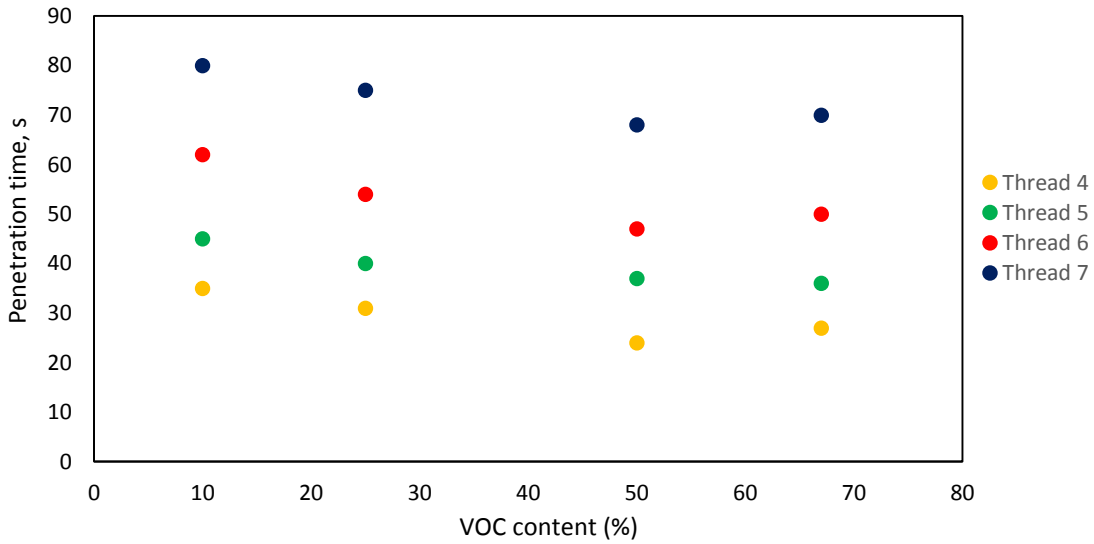

Figure 5.31 Effect of VOC content (%) on the penetration time of WD-40 fluid sample

5.5.2 Fluid flow velocity

In this section, velocity of fluid flow is determined based on the two main fluid flow mechanisms discussed.

5.5.2.1 Directly downwards fluid flow

In this fluid mechanism, length of fluid penetration as it moves from the tight side of one thread to the next one is approximately $2l$ as shown in Figure 5.32.

l is calculated using the maximum diameter D_a and minimum diameter D_c for the bolt (Figure 5.32).

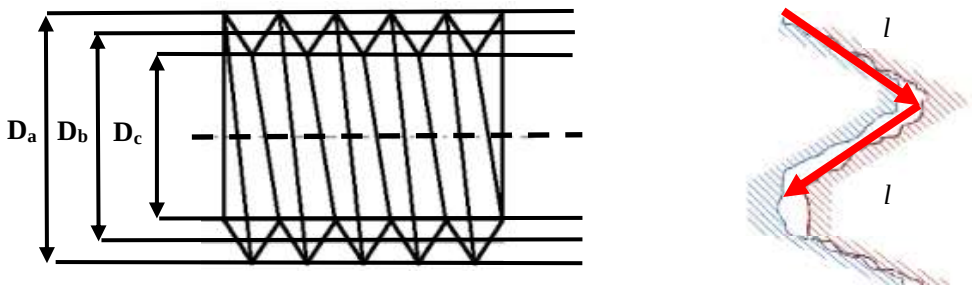

Figure 5.32 Length of fluid penetration from one thread to the next one

Penetration speed per thread can be found by dividing penetration length by penetration time per thread (Figure 5.29)**:**

$$penetration\ speed\ u = \frac{2l}{penetration\ time\ per\ thread}$$

The penetration speed of the samples is given in Figure 5.33.

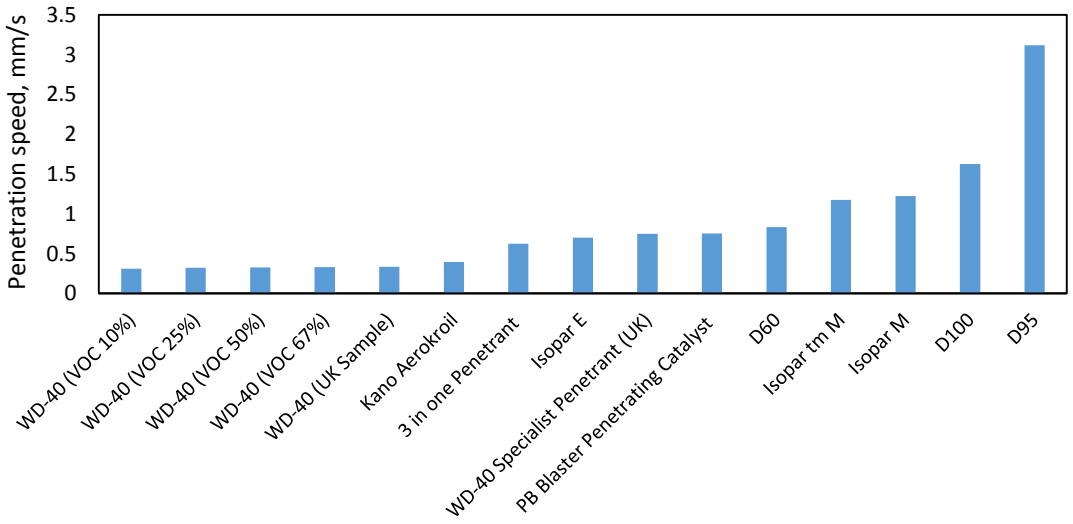

Figure 5.33 Penetration speed of fluid samples

5.5.2.2 Spiral revolution of fluid flow

In this section, the fluid flow mechanism is assumed to spirally fill in the loose section of the thread, where at the same time flow occurs into the tight side of the thread.

For the purpose of calculation, the total penetration time of the fluid to fill in the loose section is added to the time taken for the fluid to penetrate into the tight side. In here, the length of fluid penetration in both loose and tight region is given as l_1 and l_2 and shown on Figure 5.34.

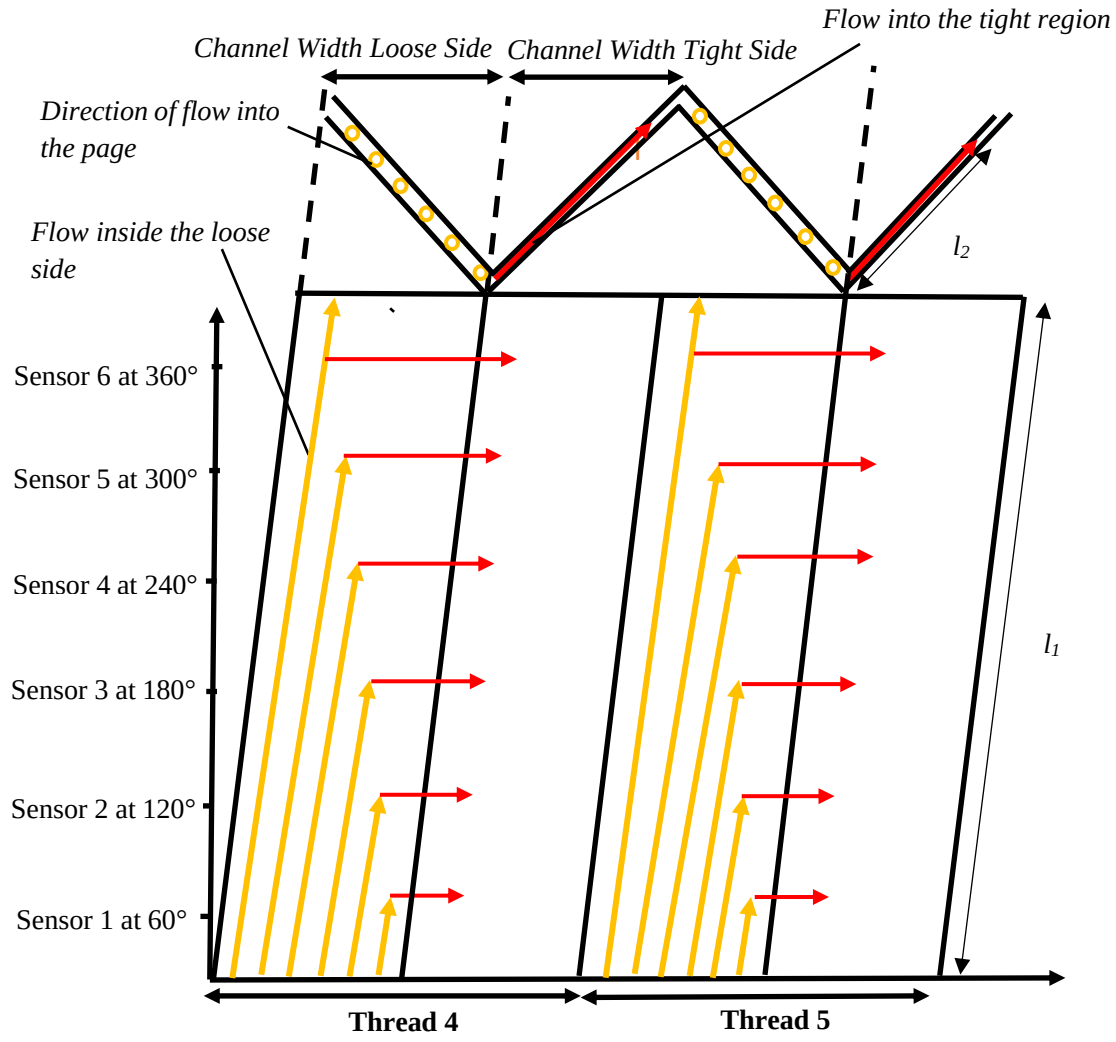

Figure 5.34 Spiral fluid flow in thread, with the length of fluid penetration shown for the loose and tight channel

l_1 and l_2 are determined from the thread geometry. After the fluid is injected, it is assumed that the main fluid flow follows a spiral pattern, hence to reach thread 4 (First thread in the ultrasonic coverage), four helical channels is filled. The secondary fluid flow will then occur into the tight contact, where the gap size is estimated to be around 60 µm smaller

than the one in the loose contact (See Chapter 6 for estimation of the gap size in the loose and tight contact). The main flow path in one thread follows the length of a helix. Figure 5.35 shows an unwrapped helix.

The main flow path in one thread follows the length of a helix. Figure 5.35 shows an unwrapped helix.

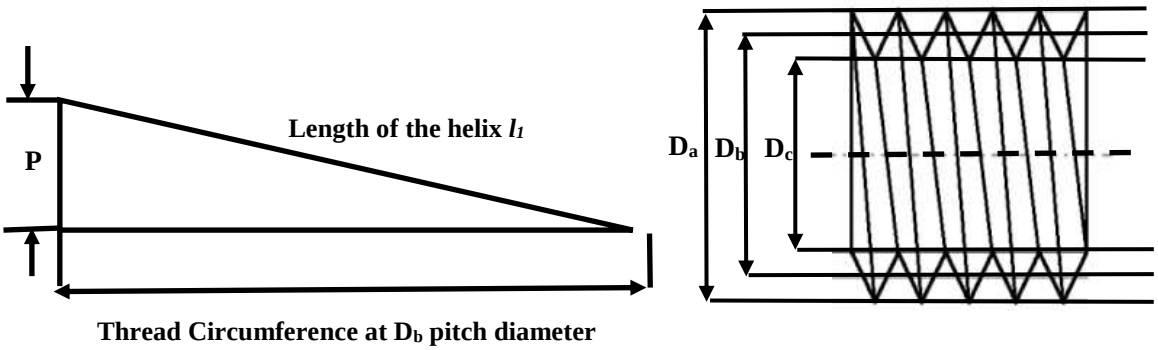

Figure 5.35 Unwrapping of one thread to find the length of the helix

Major diameter, pitch diameter and minor diameter are labelled as D_a, D_b and D_c. To find the thread circumference D_b is used as most of the fluid flow is expected to be happening at his point of the thread. The pitch diameter for an M10 bolt thread with a pitch of 1.5mm is 8.334mm. Therefore the length of the helix for one thread is:

$l_1 = \sqrt{(\pi D_b)^2 + p^2}$ = 26.225mm

l_2, as labelled on Figure 5.34, is calculated using D_a and D_b and gives around 4.60 mm.

Fluid velocity in the loose region u_1 and fluid velocity in the tight region u_2 is analysed separately and given as equations (5.1) and (5.2):

$$u_1 = \frac{nl_1}{c_{n1}t_n} \tag{5.1}$$

$$u_2 = \frac{l_2}{c_{n2}t_n} \tag{5.2}$$

where n is the number of threads and t_n is the penetration time at thread n. c_{n1} and c_{n2} are the constants indicating the proportion of penetration time spent in the loose and tight channels respectively. Penetration time of the fluid is mostly spent in the helical channel, which is created by the loose side of one or more threads, whilst a smaller proportion of it is used in the tight region. Theoretical analysis of fluid penetration based on the

Washburn equation is given in Chapter 6 (section 6.6), which suggests that for thread 4, the breakdown of the time spent in the helical and tight channels is 96% and 4% respectively, whilst for the following threads 5,6 and 7, it is 98% and 2%. These values are used for the constants in equations (5.1) and (5.2).

Figure 5.36 shows the fluid flow velocity in the tight and loose regions of the threads for all the fluid samples.

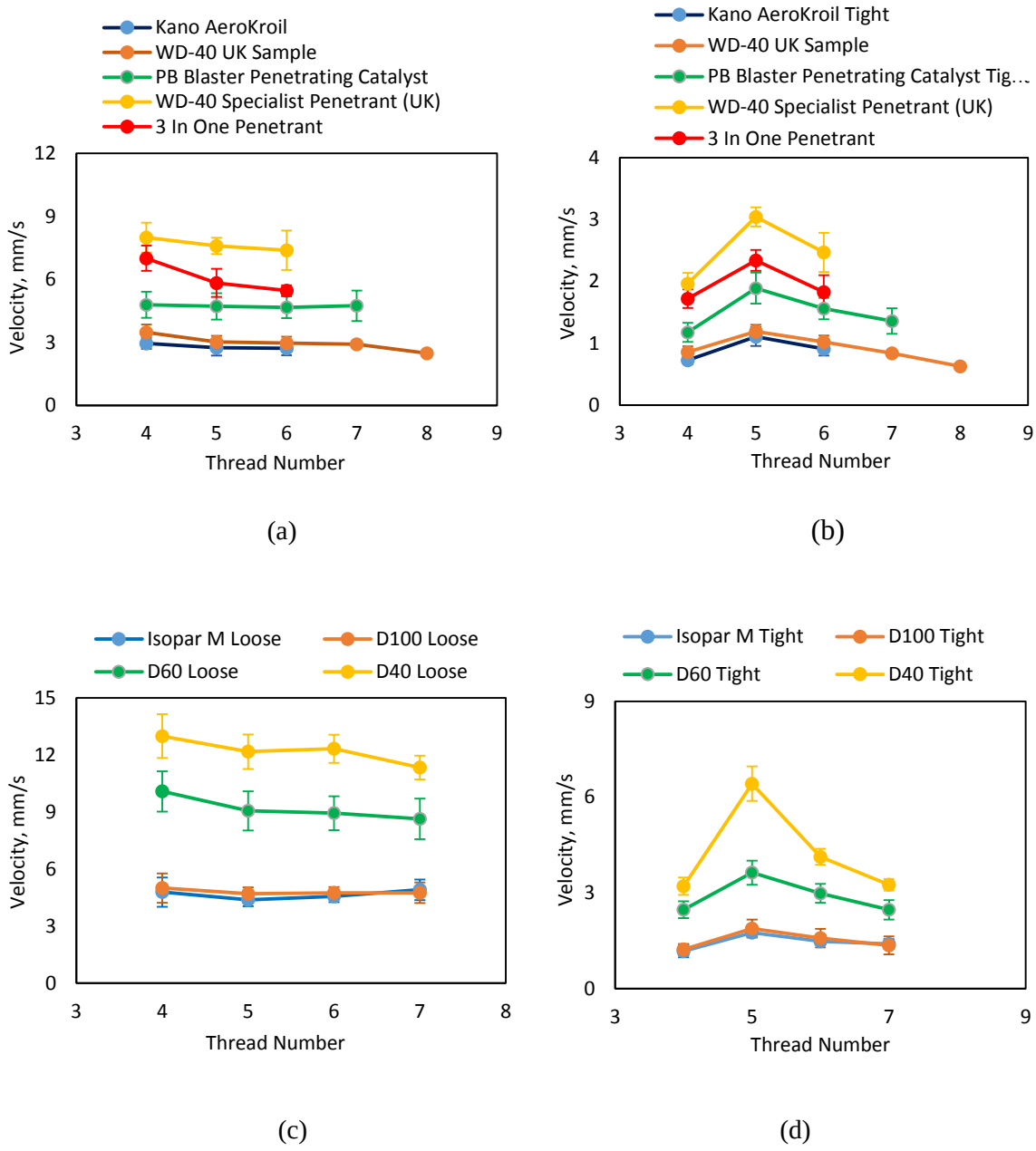

Figure 5.36 (a), (c), fluid velocity in the loose region. (b), (d), fluid velocity in the tight region

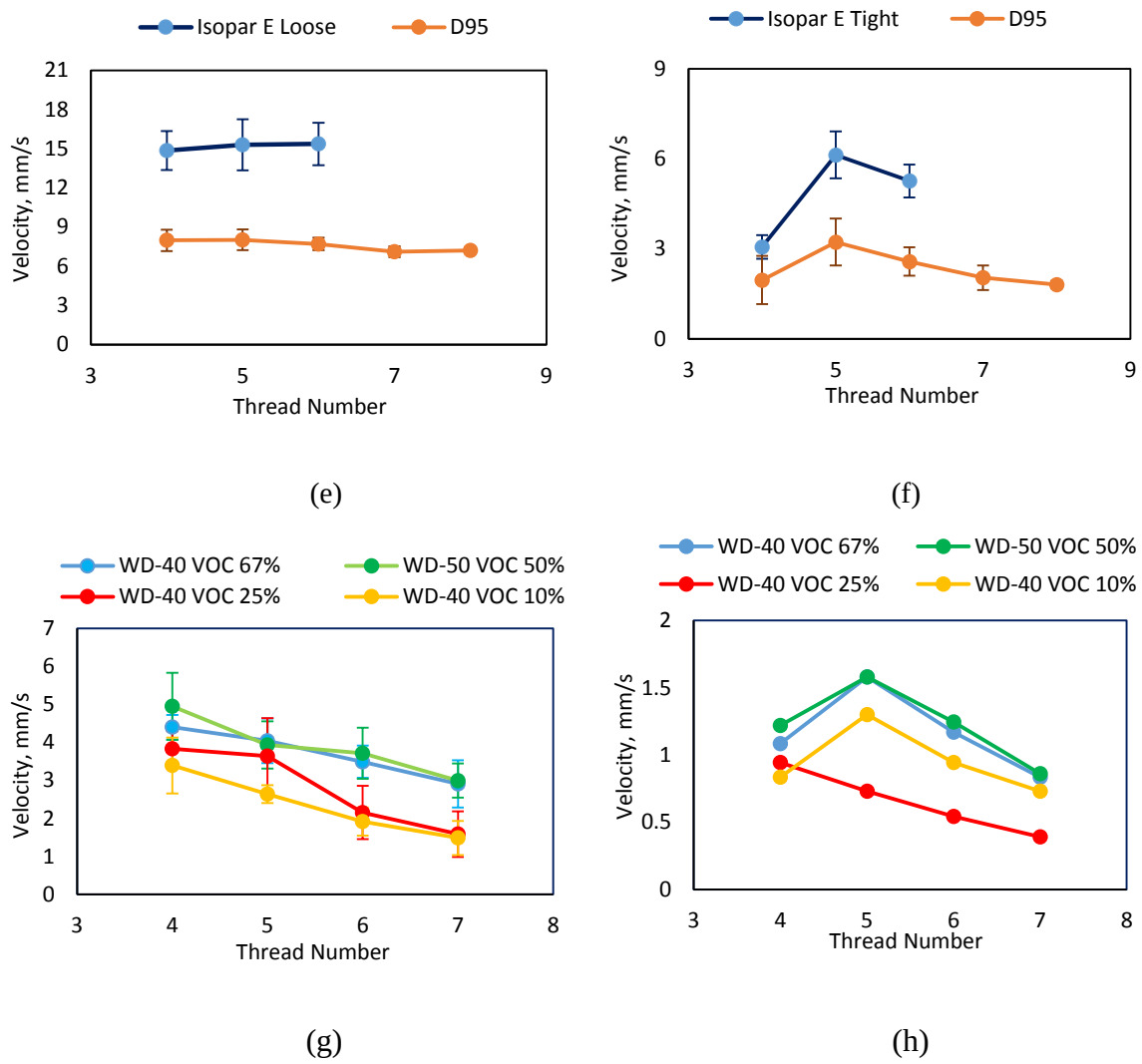

Figure 5.36 (e), (g) fluid velocity in the loose region. (f) and (h) fluid velocity in the tight region

There are a few patterns that can be observed in the data:

- For the loose region, the overall velocity of the fluid reduces as it reaches further threads, this is due to the fact that fluid movement at this scale is mostly viscous dominant. This is true for microfluidic systems with a channel size of less than 100 µm.
- For the tight region, the main observation is the increase in velocity at thread 5 for most of the fluids before the fluid slows down again. This could be due to an increase in the size of gap at these threads. In a threaded fastener system, the first 4 threads take most of the load, however, the threads further down the bolt carry less load (Kenny & Patterson, 1989). It is possible that with the sudden change of load, from a higher load to a lower load, the gap at the thread contact face a sudden increase as well. This could result in a faster fluid penetration.

To sum up the velocity analysis, due to the complex geometry of the contact, there could be multiple fluid flow happening at the same time, so the velocity of the fluid might fluctuate. The presented data are the mean values and the error bars show the standard deviation obtained from the penetration time of all the sensors.

5.5.3 Effect of fluid properties on penetration time

It is expected that lower viscosity fluids have a higher penetration speed compared to the higher viscosity ones. With regard to surface tension (surface energy per unit area), since all the fluid samples have a low surface energy, a lot lower than the surface energy of the steel contact, they fully wet (contact angle $\theta = 0°$) the steel surface. But as the fluid flow occurs in a micro channel under capillary action, surface tension is thought to provide the driving force, therefore, it is expected that a higher surface tension fluid with $\theta = 0°$, would enhance the speed of penetration. This is supported by Washburn (1921), who studied the fluid flow in capillary tubes. Further analysis is included in Chapter 6, where an analytical model is developed. Figure 5.37 shows the viscosity of all the samples plotted against the penetration time. A line of best fit is drawn to find the relationship, and it is clear that as viscosity increases, it takes longer for fluids to penetrate into each of the threads. It should be noted that the line of best fit for thread 8 has a different slope, which is due to the fact that there are only three data points available.

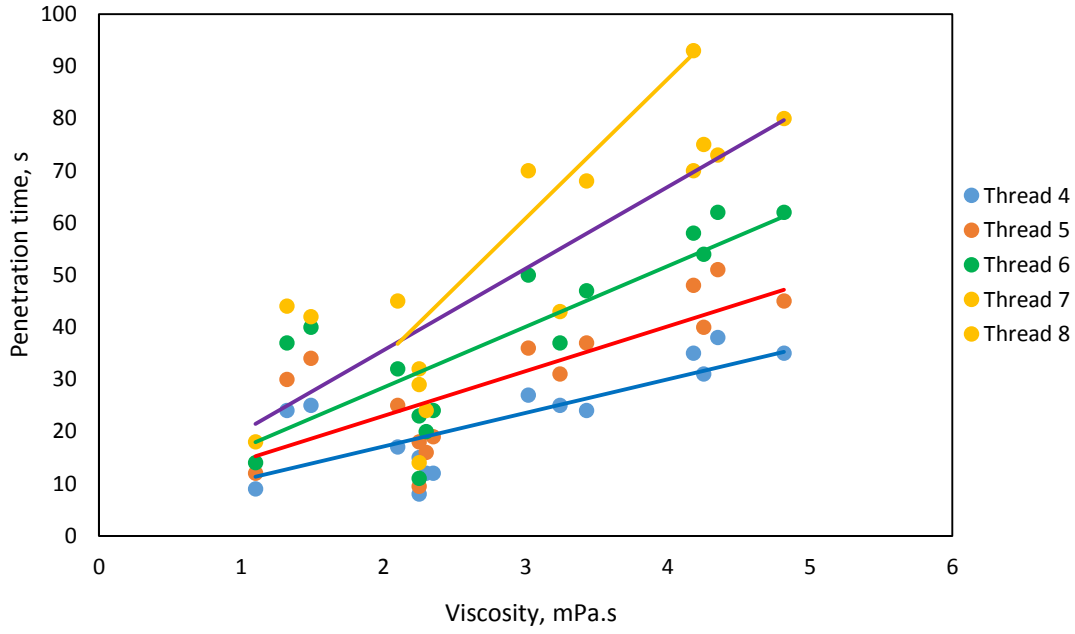

Figure 5.37 Penetration time of fluids plotted against viscosity for 5 threads

5.5.4 Effect of fluid properties on the maximum depth of fluid penetration

The depth of fluid penetration refers how far the fluid penetrates in terms of the number of threads. As the ultrasonic coverage of threads was described in section 4.2, threads 4 to 8 are within the range of the sensors. However, as seen before, fluids do not penetrate that far. It was thought that physical properties might have an effect, therefore a plot of surface tension and viscosity of fluid samples created as shown in Figure 5.38. The blue, yellow, red dots mean that the fluid reaches thread 6, 7 and 8 respectively. It is hard to see a clear relationship between the depth of fluid penetration and fluid viscosity. Most of the fluids penetrate up to thread 7, whilst only a few of them penetrate to thread 6 or 8.

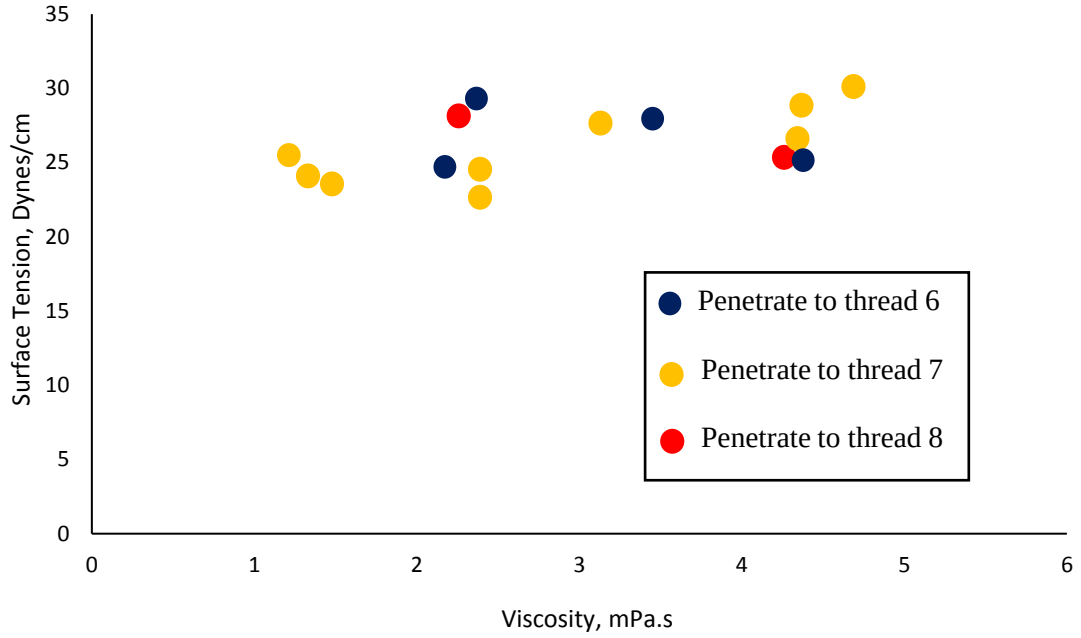

Figure 5.38 Effect of fluid properties on maximum depth of thread penetration

Chemical composition of the fluid might have an effect on the fluid penetration process. For instance, the presence of long chain molecules. At this moment, as listed in table 5.1, the chemical composition is only provided for some of the fluids. Further investigation is not within the scope of this thesis, but for future work, it will be useful to have a full knowledge of the chemical composition and explore its effect on penetration performance.

5.6 Conclusions

- Fluid penetration time is an important performance indicator of the penetrants. The ultrasonic instrumentation developed for the purpose of this study proved was capable of measuring penetration time of a range of fluids with different physical properties. The total time of fluid penetration varied from 20 s to 90 s for the fastest and slowest samples.
- The two possible fluid mechanisms were discussed. It was suggested that the directly downwards fluid flow from one thread to the next one could be the main penetration mechanism. However, it is also possible that as the spiral revolution of fluid flow occurs, secondary fluid flow paths from the loose side to the tight side of each thread take place. Other observations were the presence of bubbles in the threads, fluid leakage from one thread to another one. Residual oil films in the thread were also detected.
- This study was carried out considering ideal conditions (clean bolt and nut specimens), to establish an ultrasonic technique that can measure fluid samples with a range of viscosities in a threaded contact. Therefore, in a corroded and seized threaded contact, the penetration mechanisms will be affected. This technique has the potential to study fluid penetration in such conditions.
- Commercial penetrant products are mostly slow, although WD-40 Specialist Penetrant Product (UK Sample) and 3 In One Penetrant were seen to perform the best. Results prove that WD-40 Specialist Penetrant is an improvement to the typical WD-40 (UK Sample), as expected. In addition, it also outperforms PB Blaster Penetrating Catalyst by being around two times faster and confirmed the data available from the nail climb test.
- Different VOC content of WD-40, between 10% and 67% were studied. Although there was some slight increase in the penetration speed with an increase in volatility, but no significant change in performance was observed.
- A number of pure solvents were tested. This group has some of the less viscous fluid samples, hence their fast penetration speed. However, it is important to note that these solvents are designed to be an element of a penetrant product package, and therefore may not have good lubrication properties. The lubrication performance is studied in Chapter 7.

- Effect of fluid properties on penetration performance has been explored and it was found that viscosity had a more dominant effect on the penetration performance; penetration speed increased as viscosity decreases.
- The findings also suggests that maximum number of threads penetrated by fluids is different for some of the fluids. Most of the fluid penetrate to thread 7, with some penetrating to a further thread 8, whilst only a few of them penetrated only to thread 6. Effect of physical properties were considered, however, no clear relationship was found. Effect of chemical composition is not known at the moment, however, this is an area which requires further investigation.
- Flow velocity analysis was carried out in the loose tight regions. For the loose region, the general trend suggests an overall decrease in velocity as fluid penetrates to later threads. However, for the tight region, some fluctuations in velocity such as an increase in penetration speed at thread 5 was observed, which could be because of the change of gap size at thread contact resulting from different loadings.

6

Analytical Modelling

In this chapter, fluid penetration into threaded fasteners is studied from a theoretical point of view. To do this, an equation is derived, which is essentially the Washburn equation but with a slight difference due to the geometry of the channel.

6.1 Introduction

The penetration of fluids into capillaries by capillary forces has been of great significance in a wide range of applications. Some of the initial works concerning the principles of fluid penetration in capillary tubes was carried out in the early years of the 20th century (Cameron et al. 1906; Washburn, 1921; Rideal, 1921). The main achievement of those contributions was the derivation of the Washburn equation for laminar fluid penetration in horizontal capillary tubes (Washburn, 1921). Since then, capillary penetration in tube has been extensively researched (Fisher and Lark, 1979; Ichikawa and Satoda, 1993). The result of these studies show that Washburn equation is appropriate for the interpretation of capillary penetration rates for most systems of practical interest. One particular area of interest has been capillary rise into porous media (Lago et al., 2001).

In space technology, capillary action has been used in a liquid propellant management system on board a space vehicle (Grove, 1986). Fluid penetration in the microfluidic system has also been an active area of interest, which has resulted in many technological advances especially in the field of biomedical research. For instance, the device used at home for pregnancy tests or the portable glucometer used for monitoring blood glucose levels are all based on the capillary action (Sackmann et al., 2014).

Fluid penetration into threaded fasteners is a relatively new area. The focus of this study is to develop a theoretical framework to model the fluid penetration process in the threaded contact based on the laminar fluid mechanics and capillary pressure. The input data into the model will be fluids properties as given in Chapter 5 (Table 5.1) and geometrical characteristics, which are all measured for the purpose of this work. This chapter begins with a study of the thread geometry and fluid paths. The equation for the model will then be derived based on Washburn equation to give the penetration time.

6.2 Geometrical characteristics of a threaded fastener system

Geometrical characteristics of the threads are significant when considering the capillary flow in threaded fasteners. The helical geometry is explored in order to find the length of any possible micro channels. Figure 6.1 shows an unwrapped single helical rotation of a thread.

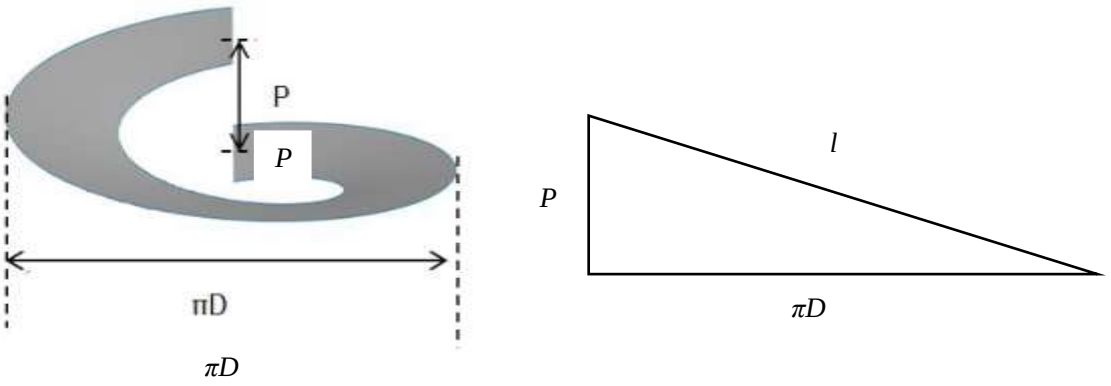

Figure 6.1 Geometrical characteristics of a single thread

The path length of the thread is given by:

$$l = \sqrt{(\pi D)^2 + P^2} \tag{6.1}$$

where D is the thread diameter and P is the pitch.

If more than one thread is being considered, equation (6.1) needs to be multiplied by n (number of threads).

$$l = n\sqrt{(\pi D)^2 + P^2} \tag{6.2}$$

6.3 Flow paths through threaded fastener

As described in Chapter 5 (section 5.3), it is assumed that two main fluid flow mechanisms occur in the threads. Figure 6.2 shows the loose and tight sides of the thread. As indicated, fluid flow in the loose region could also happen at the crest and root of the thread contact.

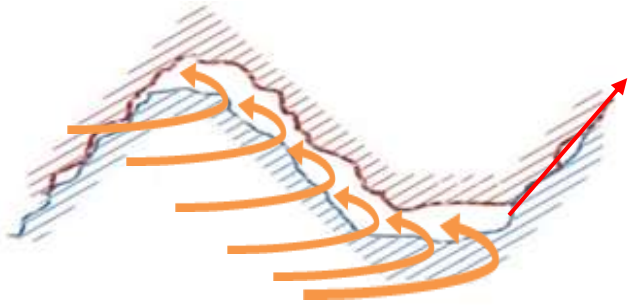

Figure 6.2 Fluid flow through a threaded fastener, orange and red arrows show fluid flow in the helical channel and tight thread contact respectively

6.4 Measurement of path dimensions

A total six samples, 3 bolts and 3 nuts were cleaned in the ultrasonic bath and dried. A Loctite glue was added between the bolt and nut threads to keep the threads fully engaged. After this, the bolt was tightened up to 40Nm. The prepared tightened samples were then sliced using a precision cutting tool. Figure 6.3 shows the cross section of the sample, magnified by the microscope. Threads 3 to 8 have been presented.

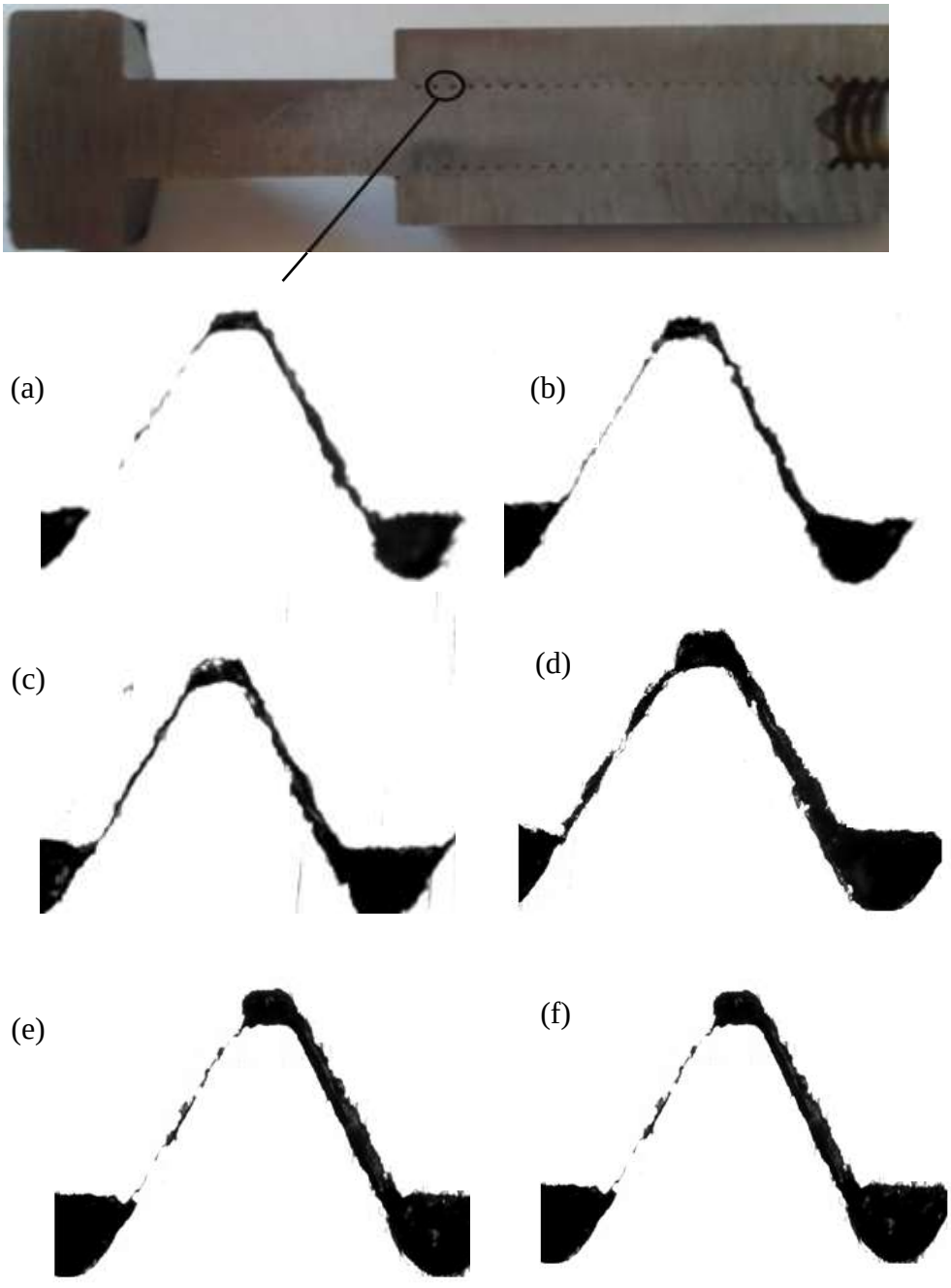

Figure 6.3 A cross section of threaded contact cut in half and images (a) to (f) show threads 3 to 8

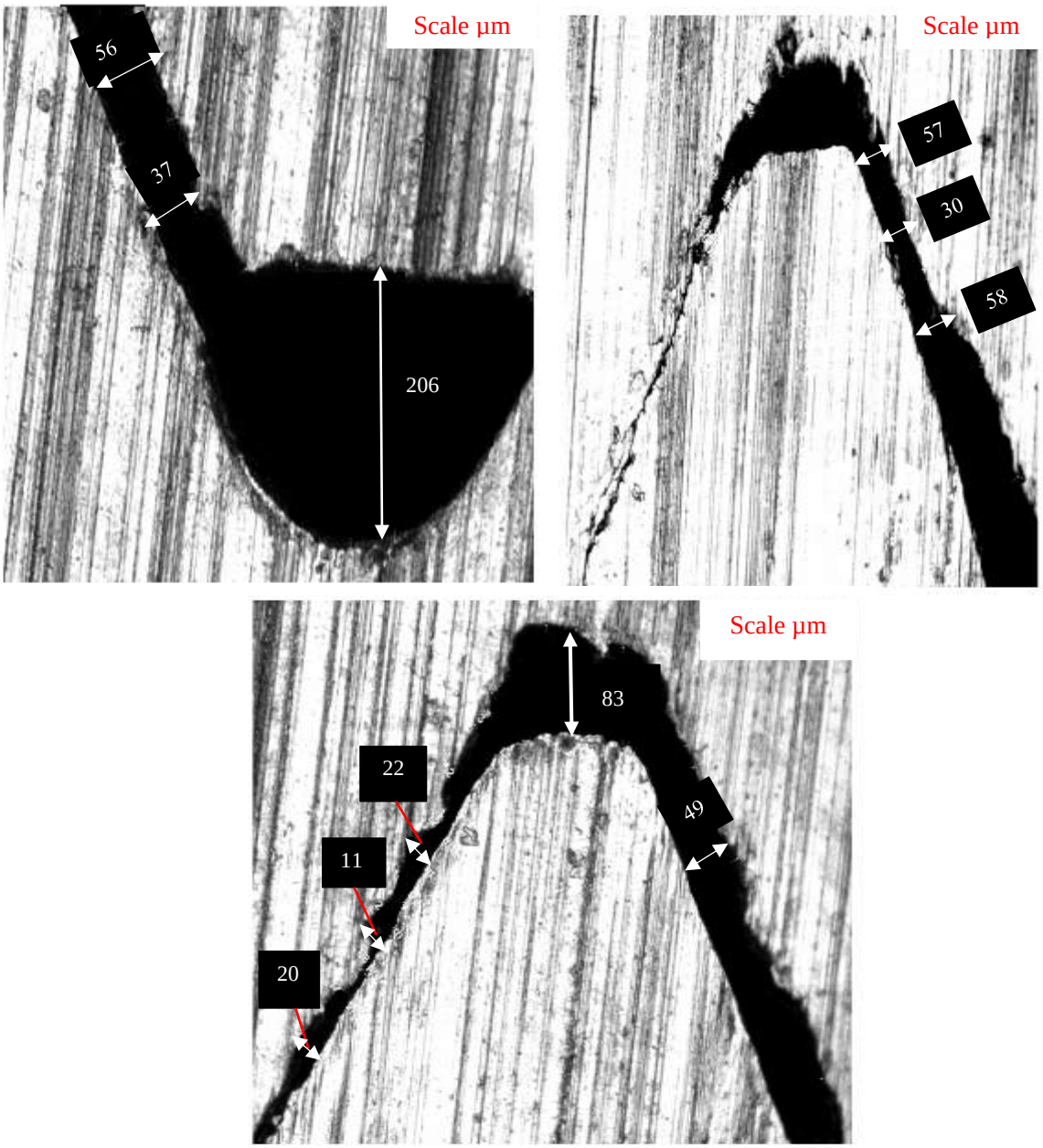

Figure 6.4 Measurement of the gap along the thread in the crest, root, loose and tight regions

In order to measure different regions of the threads, further magnification was done, as shown in Figure 6.4. As it can be seen, the gap varies across different regions of the thread, such as the crest, root, loose and the tight regions. Measurements were taken for each of threads and averaged (Table 6.1). The total average is then taken for all the regions. These numbers are used for inputs into the theoretical model.

Thread Region / Thread Number, n	Loose side, µm	Tight side, µm	Crest, µm	Root, µm
3	74	16	82	220
4	82	16	75	179
5	73	18	90	200
6	60	12	63	206
7	55	19	86	190
8	42	19	92	210
Average	68	17	81	200

Table 6.1 Dimensions of the different regions of the thread

6.5 Fluid flow between parallel plates

6.5.1 Fluid Mechanics

As the fluid flow penetrates between two parallel plates with a small distance *h*, there is an applied pressure difference that causes fluid motion between the two stationary surfaces. This is called Poiseuille flow.

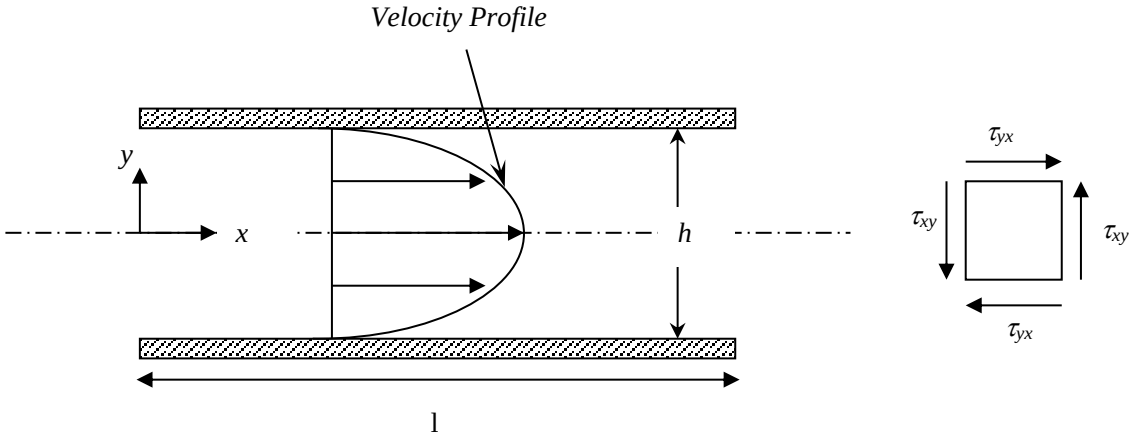

Figure 6.5 Velocity profile of fluid between two parallel plates

The following assumptions are made about the flow:

1. It is steady and Newtonian with constant fluid properties (density and viscosity).
2. 2-D problem (*xy* plane)
3. Laminar, and fully developed flow

4. $v \approx 0$ because the fluid flows between two parallel plates as the velocity does not change in the x direction. Therefore the velocity u is a function of only y, $u = u(y)$.
5. Pressure does not change in y direction. $\frac{\partial p}{\partial y} = 0$

And the governing equations are:

- 2-D Incompressible Continuity Equation: $\frac{\partial u}{\partial x} + \frac{\partial v}{\partial y} = 0$
- The Navier-Stokes Equation: $\rho \frac{D\vec{v}}{Dt} = \rho \vec{g} - \vec{\nabla} p + \mu \nabla^2 \vec{v}$
- Shear Stress (for xy plane): $\tau_{xy} = \tau_{yx} = \mu \left(\frac{\partial v}{\partial x} + \frac{\partial u}{\partial y} \right)$

The continuity equation becomes:

$$\frac{\partial u}{\partial x} + \cancel{\frac{\partial v}{\partial y}} = 0 \Rightarrow \frac{\partial u}{\partial x} = 0$$

The Navier-Stokes equation in ***y*** direction is not useful because $v \approx 0$.

Thus, the Navier-Stokes equation in ***x*** direction:

$$\rho \left(\cancel{\frac{\partial u}{\partial t}} + u \cancel{\frac{\partial u}{\partial x}} + v \cancel{\frac{\partial u}{\partial y}} \right) = \cancel{\rho g_x} - \frac{\partial p}{\partial x} + \mu \left(\cancel{\frac{\partial^2 u}{\partial x^2}} + \frac{\partial^2 u}{\partial y^2} \right)$$

Therefore:

$$0 = -\frac{\partial p}{\partial x} + \mu \frac{\partial^2 u}{\partial y^2} \tag{6.3}$$

The pressure gradient between the inlet and exit is assumed to be linear:

$$-\frac{\partial p}{\partial x} = \lim_{\Delta x \to 0} \frac{\Delta P}{\Delta x} \approx -\frac{P_2 - P_1}{l} = \frac{P_1 - P_2}{l} \tag{6.4}$$

Equation (6.4) is integrated twice to give an expression for velocity. Considering no-slip at the wall, the velocity profile after integration is obtained as:

$$u_x = \frac{1}{2\mu}(-\frac{\partial p}{\partial x})(\frac{h^2}{4} - y^2) \tag{6.5}$$

Integration of the velocity profile gives an expression for the volumetric flow rate per unit width of the system. Observing that the differential flow rate through an element of depth *dy*, which is $u_x dy$:

$$q = \int_0^q dq = \int_{-\frac{h}{2}}^{\frac{h}{2}} u_x dy = \int_{-\frac{h}{2}}^{\frac{h}{2}} \frac{1}{2\mu}(-\frac{\partial p}{\partial x})(\frac{h^2}{4} - y^2)dy = \frac{h^3}{12\mu}(-\frac{\partial p}{\partial x}) \tag{6.6}$$

The mean velocity is total flow rate per unit depth:

$$u_{m_x} = \frac{q}{h} = \frac{h^2}{12\mu}(-\frac{\partial p}{\partial x}) \tag{6.7}$$

Equation (6.7) can be rearranged as (6.8). This is the basis of the Washburn equation (Washburn 1921).

$$\frac{dl}{dt} = \frac{h^2}{12\mu}(-\frac{\partial p}{\partial x}) \tag{6.8}$$

6.5.2 Surface tension and capillarity

When exploring a bulk liquid at the molecular level, a combination of attractive and repulsive forces act on the molecules. The interaction of molecules together will lead to a reduction in the potential energy, hence stabilising the system. The result of this is cohesion between the liquid molecules and adhesion between the liquid and the solid surface in contact. However, the location of the molecules dictate the amount of potential energy. Molecules at the surface are limited in the number of neighbouring molecules compared to the ones inside (Figure 6.6), therefore they have a higher potential energy. This explains the surface tension, which is basically the interface potential energy divided by the interface area (J/m^2). This can be interpreted as force per unit length (N/m).

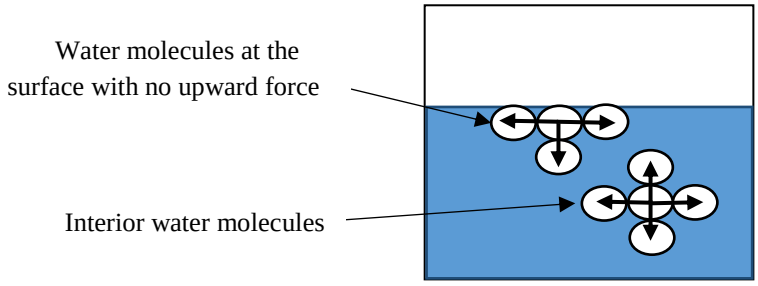

Figure 6.6 Molecules at the surface and inside of water

When a liquid makes contact with a solid surface, there are two main interacting forces. One is adhesion of liquid with solid and air and the other one is cohesion of the liquid. As these forces are balanced a contact line is formed, which is practically where the liquid meets the surface. The angle formed is the contact angle θ (Figure 6.7). This can change based on the wettability of the fluid sample. For perfect wetting $\theta = 0°$, high wettability $0° < \theta < 90°$, low wettability $90° < \theta < 180°$ and perfect non-wetting $\theta = 180°$.

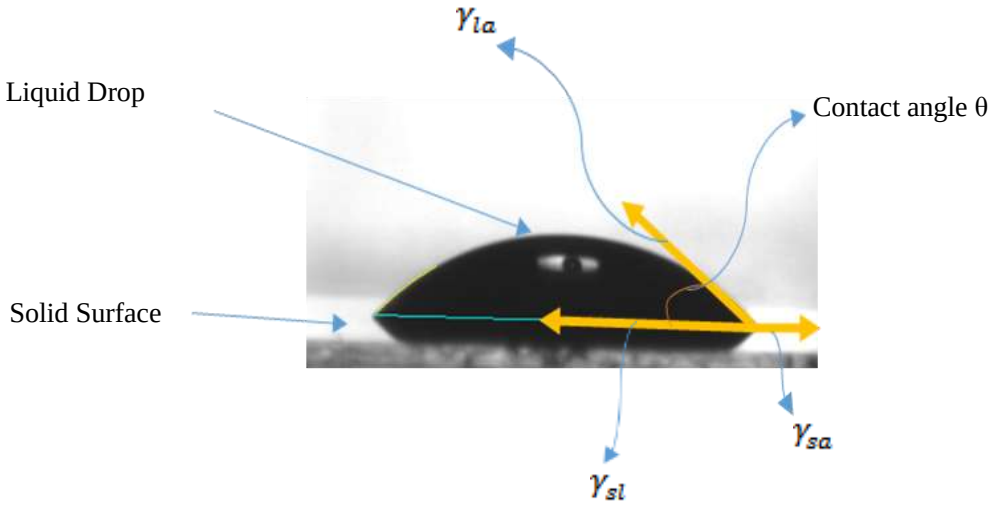

Figure 6.7 Contact angle of a liquid drop on a solid surface

There are three main forces per unit length acting on the liquid/solid/air interface. These are surface tension at liquid-air interface γ_{la}, surface tension at solid-liquid interface γ_{sl} and surface tension at solid-air interface γ_{sa}. Young's equation (Young, 1805) describes the relationship between these forces as:

$$\gamma_{sa} = \gamma_{sl} + \gamma_{la} cos\theta \tag{6.9}$$

6.5.2 Capillary pressure and fluid flow time in a micro channel

To derive the capillary pressure in a micro channel, the surface energy needs to be considered. The total surface energy consists of four parts. First is the area with no liquid, which is $(A_T - A_X)$ multiplied by γ_{sa}. The second part is the wetting area A_X multiplied by γ_{sl}. The third part is the surface energy E_0 stored in the filling reservoir. But E_0 is negligible because the amount of fluid that fills the micro channel capillary is very small. The last part (meniscus front) is not taken into account due to the small area.

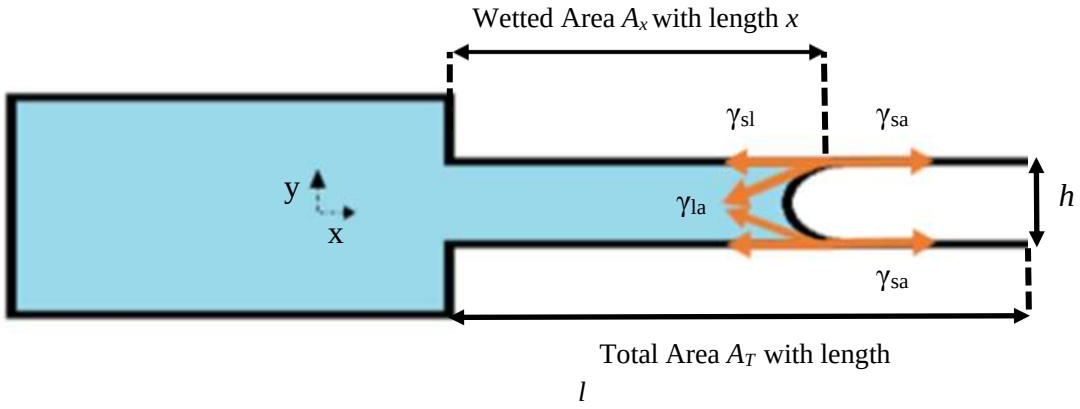

Figure 6.8 Configuration of a microchannel

Therefore, the total energy of the capillary channel is given by:

$$E_s = E_0 + [(A_T - A_X)\gamma_{sa} + A_X\gamma_{sl}] \tag{6.10}$$

Assuming that the cross-section of the capillary channel in Figure 6.8 is rectangular with a width of *w* and height of *h*. A_T denotes the total area with the length of *l* and A_x denotes wetting area with the length of *x*, the total energy can be re-arranged as:

$$E_s = E_0 + 2(h + w)[l\gamma_{sa} - x(\gamma_{sa} - \gamma_{sl})] \tag{6.11}$$

Taking the derivative of this equation will give the capillary force applied on the fluid in the x direction.

$$F_s = -\frac{dE_s}{dx} = 2(h + w)(\gamma_{sa} - \gamma_{sl}) = \Delta p_{la} wh \tag{6.12}$$

where it is assumed that the channel height *h* is considerably smaller than channel width *w*:

$$\Delta p_{la} = \frac{2(h+w)(\gamma_{sa}-\gamma_{sl})}{wh} \approx \frac{2(\gamma_{sa}-\gamma_{sl})}{h} \tag{6.13}$$

Equation (6.13) can be written as the Laplace Pressure Drop equation (Laplace 1806),

$$\Delta p_{la} = \frac{2(\gamma_{sa}-\gamma_{sl})}{h} = \frac{2\gamma_{la}cos\theta}{h} \tag{6.14}$$

In order to find the fluid flow time, knowing that $\frac{\partial p}{\partial x} = \frac{p_2-p_1}{l}$

and substituting Δp gives:

$$\frac{\partial p}{\partial x} = \frac{2\gamma cos\theta}{hl} \tag{6.15}$$

Equation (6.8) can be rearranged as:

$$\frac{dl}{dt} = \frac{h^2}{12\mu}\left(-\frac{2\gamma cos\theta}{hl}\right) = -\frac{h\gamma cos\theta}{6\mu l} \tag{6.16}$$

Integrating equation (6.16) determines the fluid flow time in the micro channel:

$$\int_0^l ldl = \int_0^t \frac{h\gamma cos\theta}{6\mu} dt \tag{6.17}$$

$$t = \frac{3\mu l^2}{h\gamma cos\theta} \tag{6.18}$$

Equation (6.18) is the equation for fluid flow between parallel plates under the capillary forces. This derived equation is essentially the Washburn equation (Section 2.4.2) but with a slight difference due to the geometry of the channel. For the Washburn equation, fluid flow is considered in a cylindrical capillary tube, whereas in here it is a rectangular one. Therefore, there is a mathematical difference of a factor of $\frac{3}{2}$.

6.6 Application to the threaded fastener geometry

The geometry of a typical threaded contact was characterised in section 6.2. The Washburn equation (6.18) derived previously is here applied to a threaded fastener system. Both fluid flow mechanisms discussed in section 5.3 are modelled.

6.6.1 Directly downwards fluid flow

Total penetration time in the loose and tight region is calculated based on the downward direction of fluid flow from one thread to the next one. Therefore, the time of fluid

penetration in both the loose and tight side is found and added together to give the total penetration time in one thread:

$$t_{total} = \frac{3\mu}{\gamma cos\theta}\left[\frac{l_l^2}{h_{loose}} + \frac{l_t^2}{h_{tight}}\right] \quad (6.19)$$

where l_l and l_t refer to the length of fluid penetration in the loose and tight region. h_{loose} and h_{tight} are the gap size for the loose and tight sides of the thread.

6.6.2 Spiral fluid flow

For the purpose of calculation as discussed in Section 5.3, the equation is obtained in two steps by modelling flow in the helical channel (loose, crest and root regions) followed by flow in the tight region.

The length of the helical channel was obtained in equation (6.2), which is substituted in equation (6.18). Hence, time of fluid penetration in the helical spacing of the threaded fasteners is found as:

$$t_{l1} = \frac{3\mu((\pi D)^2+P^2)n^2}{h_{loose}\gamma cos\theta} \quad (6.20)$$

$$t_{l2} = \frac{3\mu((\pi D)^2+P^2)n^2}{h_{crest}\gamma cos\theta} \quad (6.21)$$

$$t_{l3} = \frac{3\mu((\pi D)^2+P^2)n^2}{h_{root}\gamma cos\theta} \quad (6.22)$$

Different regions of the thread used in the above calculations are labelled in Figure 6.9.

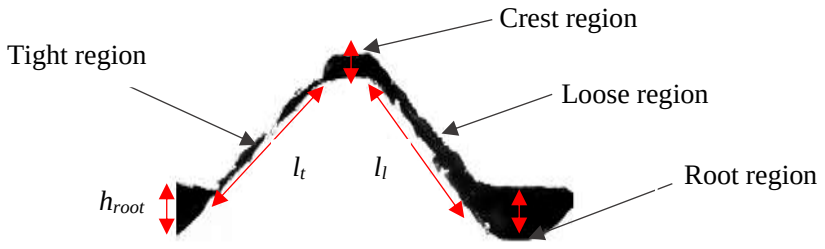

Figure 6.9 Thread regions shown

The fluid flow time into the tight region is given as:

$$t_t = \frac{3\mu {l_t}^2}{h_{tight}\gamma cos\theta} \quad (6.23)$$

As the fluid fills in the helical channel of each thread, it could start to find other routes into the tight region. To model the whole penetration process discussed, the penetration time obtained for both the helical channel and the tight region are added together to give the total penetration time:

$$t_{total} = \frac{t_{l1}+t_{l2}+t_{l3}}{3} + t_t \tag{6.24}$$

$$t_{total} = \frac{3\mu}{\gamma cos\theta}\left[\frac{\left((\pi D)^2+P^2\right)n^2}{3}\left(\frac{1}{h_{loose}}+\frac{1}{h_{crest}}+\frac{1}{h_{root}}\right)+\left(\frac{x^2}{4h_{tight}}\right)\right] \tag{6.25}$$

Equation (6.25) was used to generate penetration map with a range of viscosities (1-100 mPa.s) and surface tension (1-100 Dynes/cm) data. The justification for this is that the fluid properties will fall into the mentioned categories. Furthermore, effects of the penetration length is studied by considering the data for multiple consecutive threads.

Figure (6.10a) to (6.10c) show 3 penetration maps, with different colour maps and intensities indicating different penetration times. It can be observed that fluid penetration takes longer for higher values of viscosity and lower values of surface tension. Moreover, it is clear that for further threads down the bolt, i.e., Thread Number 3, the increase in penetration length results in a greater penetration time for the same combination of viscosity and surface tension.

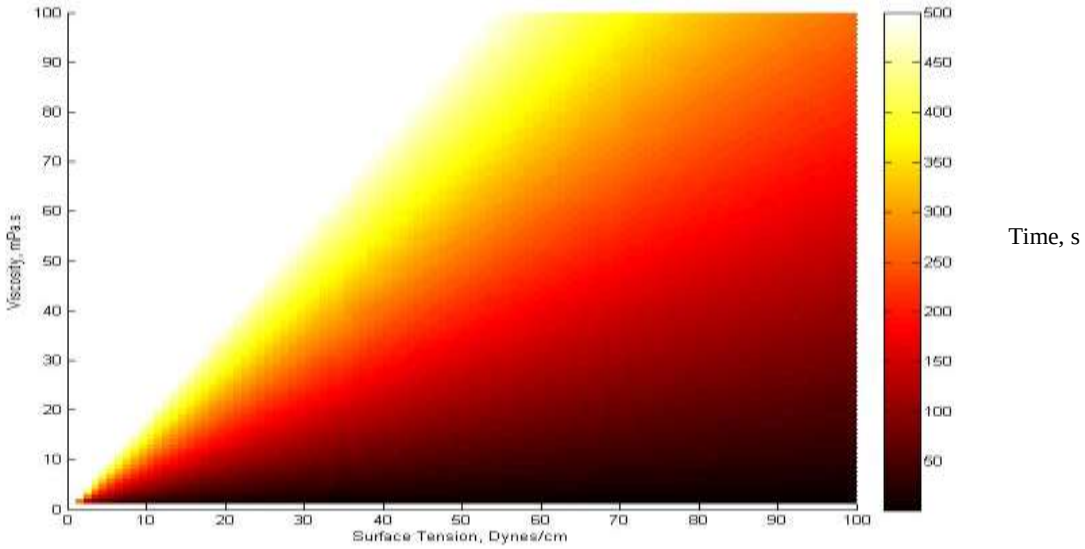

Figure 6.10(a) Penetration map for thread 1

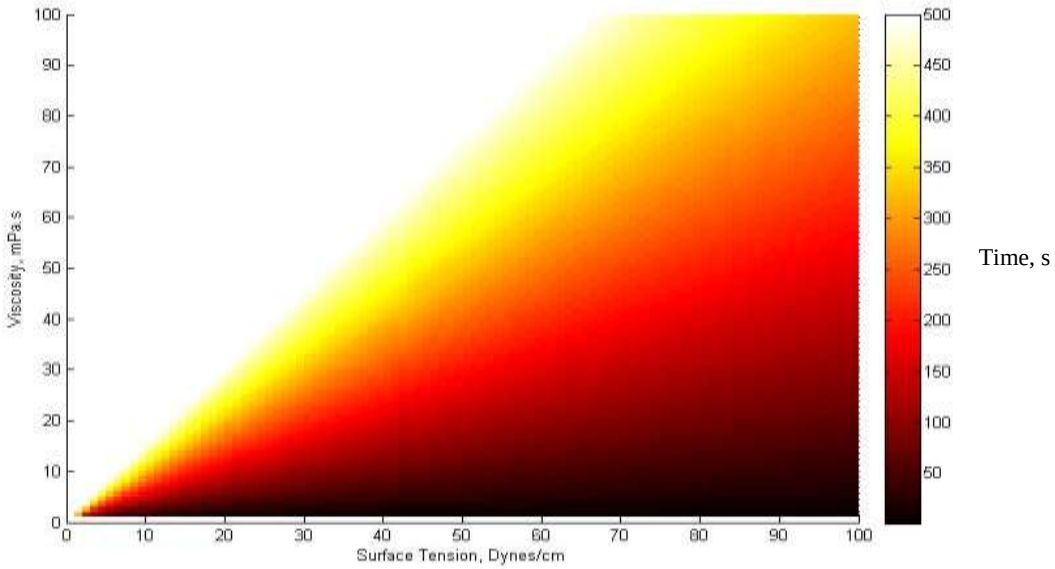

Figure 6.10(b) Penetration map for thread 2

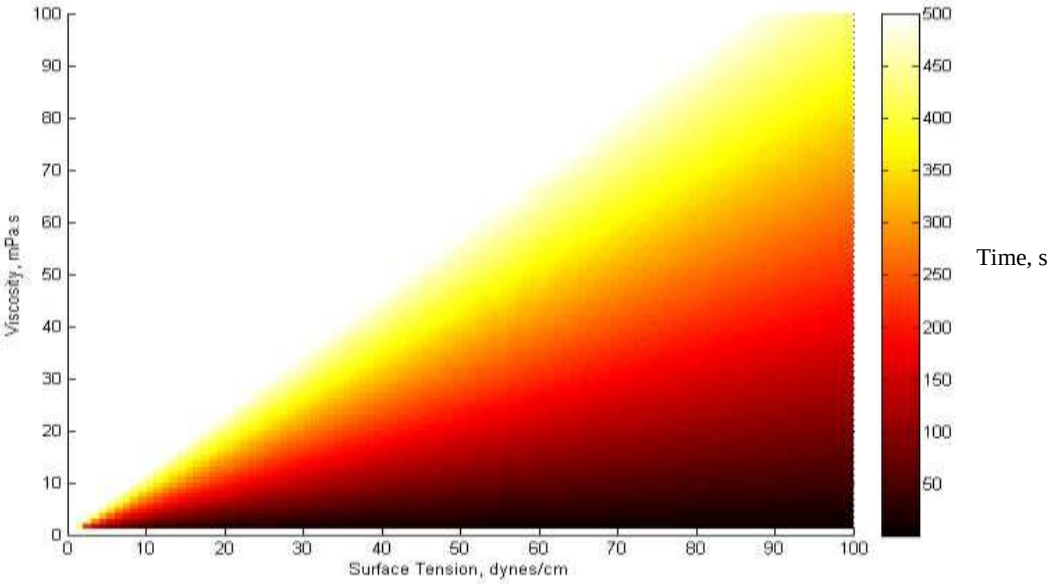

Figure 6.10(c) Penetration map for thread 3

6.7 Penetration time across thread regions

6.7.1 Directly downwards fluid flow

As fluid progresses into each thread, the penetration time taken in the loose and tight regions of the thread is different. Based on equation (6.19) and using the average values

of gap size for both the loose and tight regions of the thread (Table 6.1), 20% and 80% of total penetration time in each thread is spent in the loose and tight sides respectively.

6.7.2 Spiral fluid flow

As described in Chapter 5, this fluid penetration path is assumed to consist of two main fluid paths and the penetration time taken to get to each thread's helical channel and tight side are different. In addition to this, the overall penetration time increases from one thread to the next. However, as the time taken for the fluid to get from the helical channel to the tight side is the same, the main parameter that changes is the average time of penetration in the loose, crest and root of the thread contact. Based on equation (6.25), the penetration time in the helical channel for the first 6 threads are listed as below:

Thread 1 $$t_{helical} = \left[\frac{\mu((\pi D)^2+P^2)}{\gamma cos\theta}\left(\frac{1}{h_{loose}}+\frac{1}{h_{crest}}+\frac{1}{h_{root}}\right)\right]$$

Thread 2 $$t_{helical} = \left[\frac{4\mu((\pi D)^2+P^2)}{\gamma cos\theta}\left(\frac{1}{h_{loose}}+\frac{1}{h_{crest}}+\frac{1}{h_{root}}\right)\right]$$

Thread 3 $$t_{helical} = \left[\frac{9((\pi D)^2+P^2)}{\gamma cos\theta}\left(\frac{1}{h_{loose}}+\frac{1}{h_{crest}}+\frac{1}{h_{root}}\right)\right]$$

Thread 4 $$t_{helical} = \left[\frac{16\mu((\pi D)^2+P^2)}{\gamma cos\theta}\left(\frac{1}{h_{loose}}+\frac{1}{h_{crest}}+\frac{1}{h_{root}}\right)\right]$$

Thread 5 $$t_{helical} = \left[\frac{25\mu((\pi D)^2+P^2)}{\gamma cos\theta}\left(\frac{1}{h_{loose}}+\frac{1}{h_{crest}}+\frac{1}{h_{root}}\right)\right]$$

Thread 6 $$t_{helical} = \left[\frac{36\mu((\pi D)^2+P^2)}{\gamma cos\theta}\left(\frac{1}{h_{loose}}+\frac{1}{h_{crest}}+\frac{1}{h_{root}}\right)\right]$$

Figure (6.11) shows the first 6 threads. For the first thread, fluid penetration time into the tight region is reasonable. However, as the fluid progresses, it is clear that fluid penetration in the helical channel starts to take more time. Equation (6.23) for the tight region remains the same, hence, the penetration time in the helical channel increases from thread to thread.

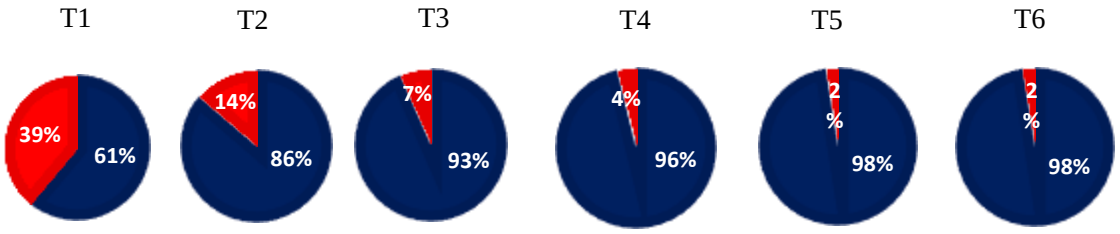

Figure 6.11 Percentage of the total penetration time in the helical channel (blue) and tight channel (red) for threads 1 to 6.

Threads 4, 5 and 6, which are the first three threads important from the experimental work point of view. The dominance of fluid penetration time in the helical channel can be clearly observed. One point to note is that fluid properties do not have any effect on this ratio.

6.8 Effect of bolt geometry on penetration time

6.8.1 Directly downwards fluid flow

By inspection of equation (6.19), fluid properties can be grouped into a single parameter called the Fluid Penetration Coefficient (FPC). Penetration coefficient has been used previously by (Schwiebert et al., 1996) to define the penetration power of fluids.

$$\text{FPC} = \frac{\gamma cos\theta}{3\mu} \tag{6.26}$$

The geometrical terms are grouped into a geometrical factor, G. where:

$$G = \left[\frac{l_l^2}{h_{loose}} + \frac{l_t^2}{h_{tight}}\right] \tag{6.27}$$

Thus, total penetration time can be arranged as $t = \frac{G}{FPC}$.

In this section, the geometrical effect is considered by varying the gap size, *h*, at the loose and tight sides of the thread contact. A fluid sample was chosen (WD-40 UK) and the penetration time against the threads was plotted with the average data, as listed in table 6.1, for the gap size in different regions of the thread contact (Figure 6.12). As shown by Figure 6.12, the reference line is the yellow one, and the other two lines were calculated by considering a 10µm decrease in the gap size at each region, whilst keeping the rest of values constant.

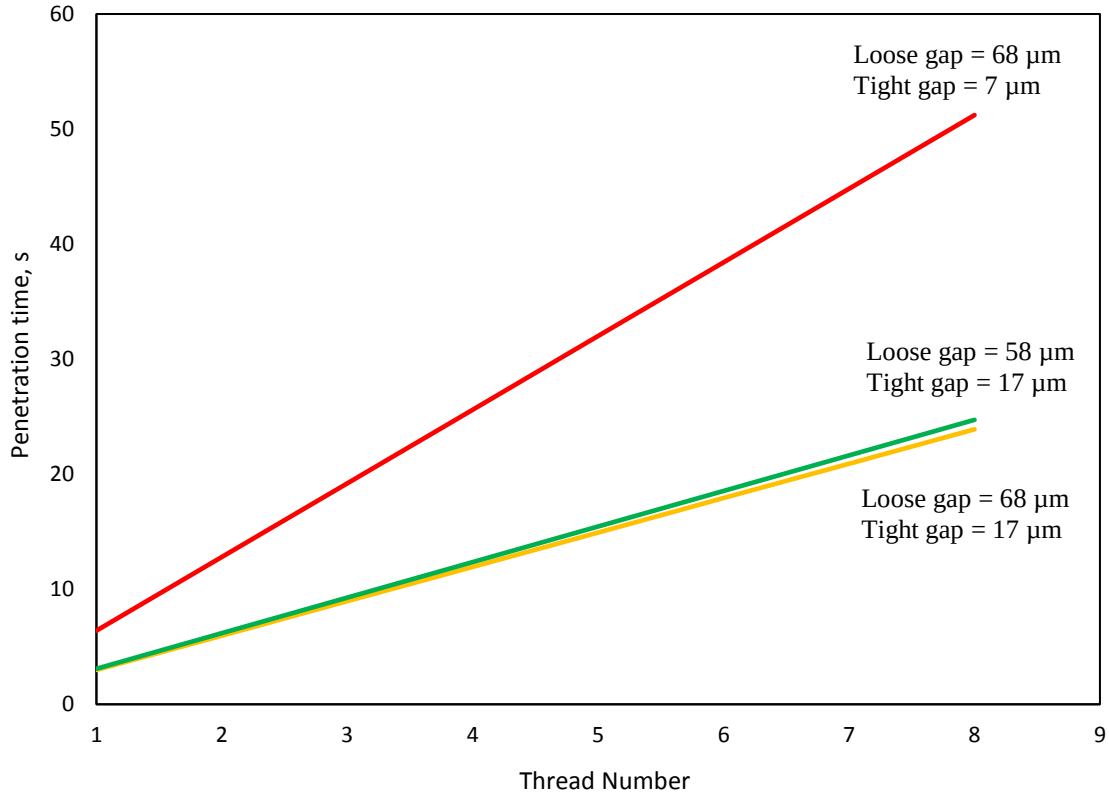

Figure 6.12 Effect of the gap size, h, on the penetration time

6.8.2 Spiral fluid flow

In a similar approach to previous section, equation (6.25) is inspected and the geometrical terms are grouped into a geometrical factors:

$$G = \left[\frac{\left((\pi D)^2+P^2\right)n^2}{3}\left(\frac{1}{h_{loose}}+\frac{1}{h_{crest}}+\frac{1}{h_{root}}\right)+\left(\frac{x^2}{4h_{tight}}\right)\right] \quad (6.28)$$

The geometrical effect is considered by varying the gap size, *h*, at the crest, loose side, tight side and the root of the thread contact. A fluid sample was chosen (WD-40 UK) and the penetration time against the threads was plotted with the average data, as listed in table 6.1, for the gap size in the four different regions of the thread contact (Figure 6.13). As shown by Figure 6.13, the reference line is the yellow one, and the rest were calculated by considering a 10µm decrease in the gap size at each region, whilst keeping the rest of values constant.

As it can be observed, the gap size at the crest and loose side have the most effect especially on the later threads, whilst the tight and root regions are less sensitive.

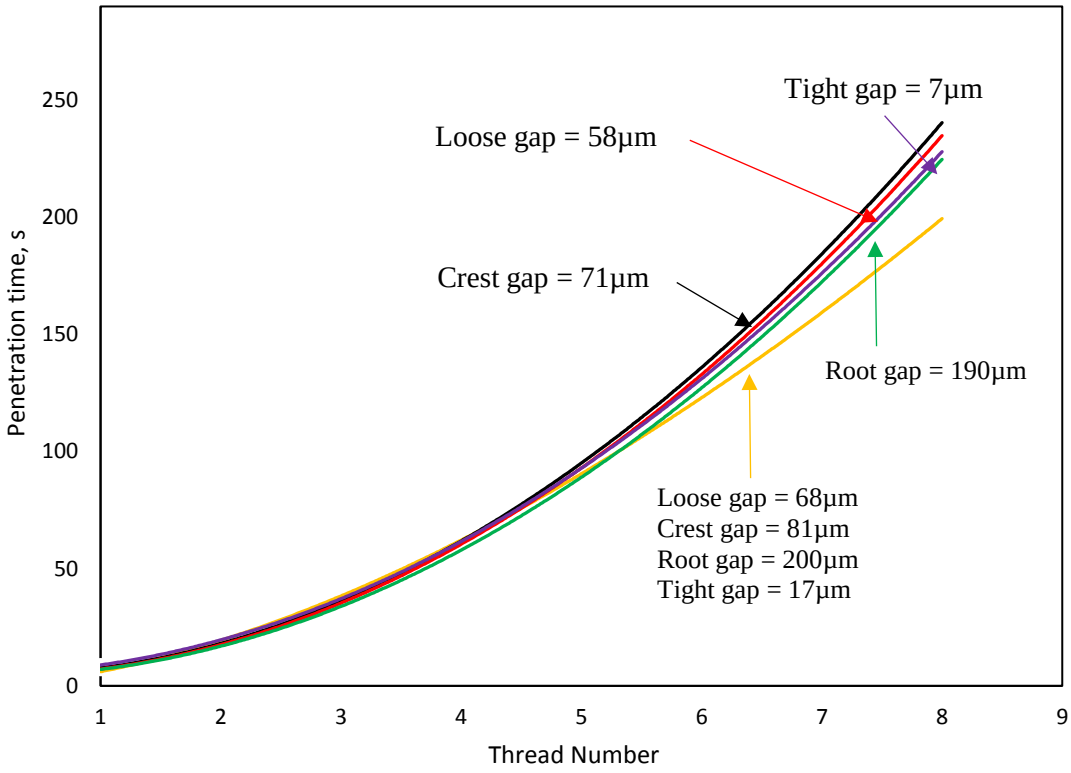

Figure 6.13 Effect of the gap size, h, on the penetration time

6.9 Comparison of model with experimental data

In this section, the data obtained from the theoretical modelling of the fluid flow is compared with the experimental data. The comparison and analysis of the data includes both possibilities of fluid flow mechanism in the threads.

6.9.1 Directly downwards fluid flow

The mechanism of this fluid was discussed previously and the equation for it was given in section 6.8.1. Equation (6.19) gives the time taken in one thread, therefore as the fluid progresses in the contact, the equation needs to be multiplied by the number of threads the fluid has penetrated into.

The first comparison made here involves the experimental penetration time data obtained from all the sensors for PB Blaster fluid (Figure 4.19) and the theoretical model of the same fluid. Both data sets are shown in Figure 6.14.

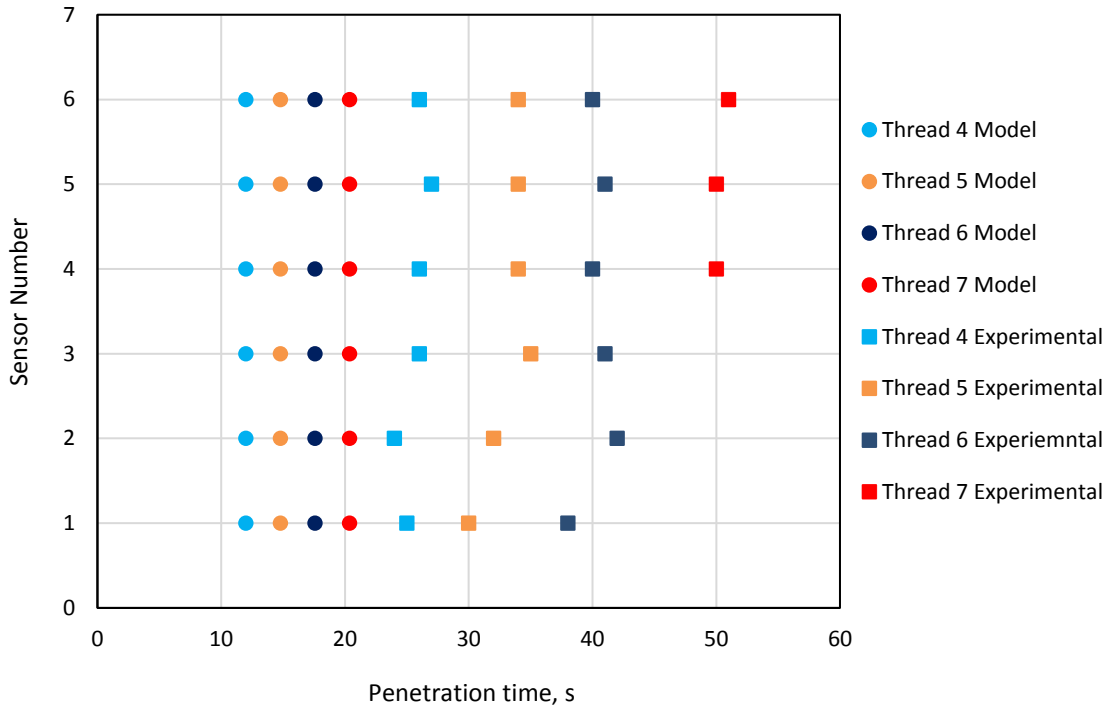

Figure 6.14 Comparison of the theoretical model with the experimental data

As it can be observed in Figure 6.14, both sets of data show more or less a similar trend indicating a simultaneous penetration of fluid flow into the locations monitored by all the six sensors. However, the results from the theoretical model show a shorter penetration time compared to the experimental data.

This could be due to variation in the surface roughness at the contact which affect the gap size, hence slowing down the fluid flow. In addition, there might be other fluid flow mechanisms existing at the same time, as it is difficult to assume a certain fluid penetration mechanism occur all the time.

Another way to compare the theoretical model with the experimental data is to plot the FPC of each fluid against their penetration time. This is shown for all the samples in Figure 6.15. The threads considered are only the ones which were detected by the ultrasound waves.

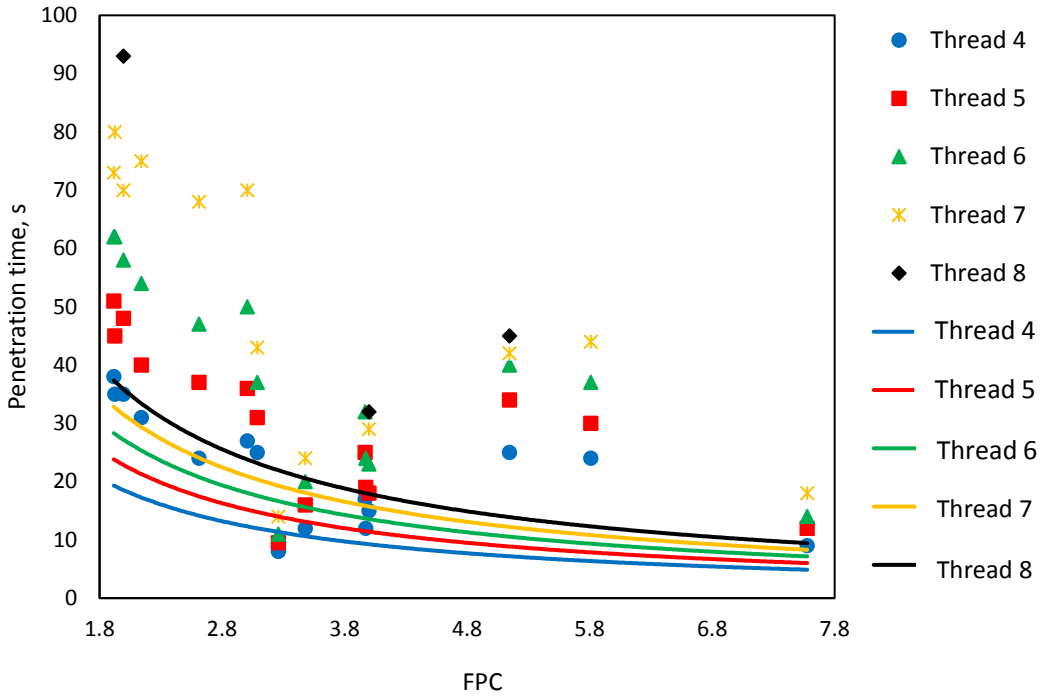

Figure 6.15 Comparison of the theoretical model (solid lines) with the experimental data

6.9.2 Spiral fluid flow

Similar to previous section, the experimental penetration time data obtained from all the sensors for PB Blaster fluid (Figure 4.19) is compared with the theoretical model for spiral fluid flow mechanism and presented in Figure 6.16.

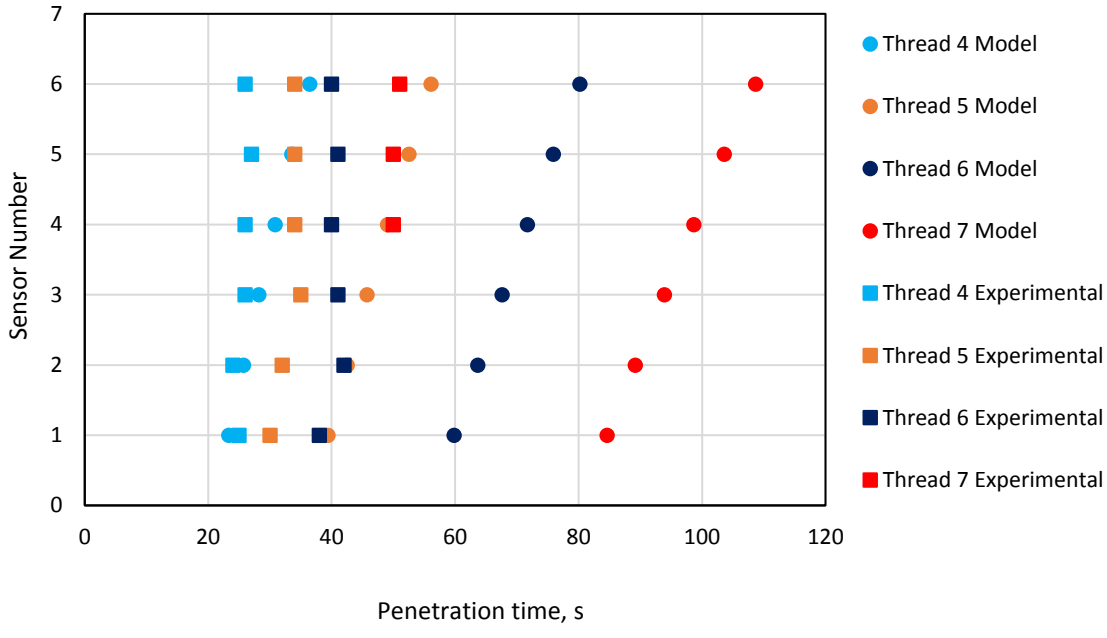

Figure 6.16 Comparison of the theoretical model with the experimental data

As it can be observed, the results of penetration time obtained from the theoretical model is longer than the experimental ones especially for further threads.

To compare the theoretical model with the experimental data for all the samples, the FPC of each of the fluids is plotted against their penetration time, as shown in Figure 6.17.

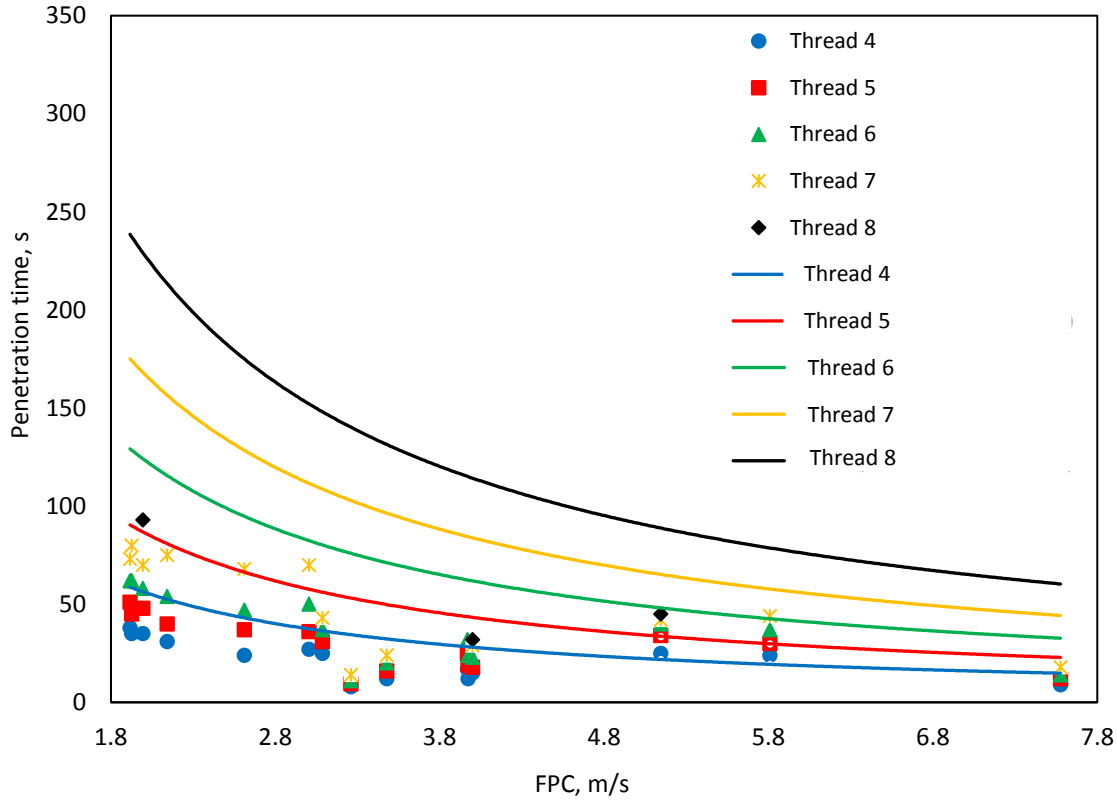

Figure 6.17 Comparison of the theoretical mode (solid lines) with the experimental data

As it can be seen, the theoretical trend shows that fluids with higher FPC are faster than the ones with the lower FPC. And the experimental data appear to agree with this trend to some extent especially for threads 4, 5 and 6. However, for fluids with FPC above 4 this is not the case. The reason why fluids with the FPC of more than 4 does not follow the trend could be due to flow separation effects, which is not considered in the model

The theoretical model shows a slower penetration time when compared to the experimental data. For threads 4 and 5, it appears that there is a better agreement, however, for further threads, this not the case. There are several reasons, which could explain this:

Inlet fluid velocity

The mechanism of fluid entry into threads was discussed in chapter 4. The fluid sample was injected into the fastener via the injection port using a pipette. This would imply that the initial velocity could be higher than zero and the model assumption, which considers the initial velocity to be zero i.e. reservoir might not be true. Therefore, the velocity of the flow in the following threads could also be affected as a result.

Complexity of fluid flow in threads

There are multiple fluid penetration routes but the most common route was modelled. This route considers the helical channel of the threads to be filled before fluid penetration into the ultrasound detectable tight region occurs. However, it is possible that there are additional flow paths, which may help with a faster rate of fluid penetration into the contacts. For instance, fluid penetration into the tight region might occur at the same time as the helical channel is being filled up, or certain locations of the thread may be filled faster than others. It was explained in Chapter 5, that surface roughness and the local geometry could contribute towards different rates of fluid penetration.

Tolerances and surface roughness

Fluid flow takes place in the channels created by the bolt tolerances. In an ideal situation, these channels are parallel surfaces, however, this is not the case and in practice there will be irregularities in the geometry, which will result in the contraction of the fluid. This in turn will increase the speed of the fluid flow. This is one of the limitations of the model since the surfaces are assumed to be parallel. Effect of surface roughness on fluid flow in micro channel have been researched (Silva et al., 2008; Mahrous et al., 2011; Kuhnert et al., 2008). However, modelling of flow in rough walled channels is beyond the scope of this work. In addition to this, considering the microscale dimensions of the channels, changes in the surface roughness influences the geometry of the channels, which again violates the assumption that the two contact surfaces are parallel with each other.

6.10 Conclusions

In this chapter, an analytical model for fluid penetration into threaded fasteners was developed. The model was based on the laminar fluid mechanics, considering fluid flow

between parallel flat plates. Equation for fluid flow under capillary forces in micro channels of the threaded contact was derived, which is essentially the Washburn equation, but with a slight difference due to the geometry of the channel in this study as the fluid is considered to flow between two parallel surfaces.

This equation was then applied to fluid flow in the capillary channels created in a threaded fasteners system and the data obtained from the theoretical model was compared with the ones collected from the ultrasonic technique.

- The effect of bolt geometry was studied by firstly measuring the size of the gap at the threaded contacts. The main thread regions identified was the "loose", "tight", crest and root. It was shown that the gap varies across each of those regions. The size of the gaps were subjected to a 10μm decrease to explore the sensitivity of penetration time to minor changes. It was found that it was from thread 6 onwards, when a notable decrease could be observed.
- The relationship between the fluid properties (FPC) and penetration time was explored. It was observed that for higher values of viscosity and lower values of surface tension, the fluid penetration process takes longer. However, it is important to note that viscous forces are more dominant.
- The proportion of total fluid penetration in the helical and tight channel was investigated. For the first three initial threads, the penetration time is reasonable, although a clear decrease was observed from thread 1 to thread 3. But from thread 4, the fluid penetration in the tight region is around 2% of the total time of penetration.
- Two assumed fluid flow mechanisms were modelled and compared with the experimental data. For the directly downwards fluid flow, the experimentally measured penetration time was longer than the ones calculated from the model. However, for the spiral fluid flow, it was the vice-versa especially for the later threads. It is suggested that a combination of both fluid mechanisms could occur in the contact.
- Although the model provides a starting framework for the problem of fluid penetration in threaded fasteners, it has some limitations. For instance, geometrical irregularities, surface roughness or the multi-phase effects were not considered in this study.

7

Torque Measurement to Study the Lubricating Behaviour of Penetrants

Chapter 6 covered the measurement of oil penetration into a threaded contact. This chapter will investigate the lubrication of threaded contact by first measuring torque and tension force in a fastener and then deducing the bolt thread friction. Measurements were carried out before, during and after fluid penetration to find a relationship between the penetration time of the fluids, torque and coefficient of friction.

7.1 Introduction

The loosening process of a lubricated bolt involves two steps, fluid penetration and then lubrication once the fluid has penetrated. Effectiveness of the oil penetrants has been investigated both from an experimental and a theoretical point of view. However, neither of these studies explored the lubrication behaviour once the fluid has penetrated into the contact. In addition, modelling of penetrant behaviour is also limited to how the fluid advances under capillary forces in a threaded contact, and thus cannot suggest anything regarding the lubrication performance.

A literature survey of friction and lubrication in fasteners was carried out in Chapter 2. The focus of the studies was mainly on the effect of lubrication on torque, tension, coefficient of friction in threads and under head bearing ((Sakai, 1978),(Nassar et al., 2005), (Zoe et al., 2007), (Nassar et al., 2007)). In addition to this, the effect of coatings or zinc plated materials on the torque was investigated.

However, what is not explored in the studies above, is the change in the torque and friction coefficient of friction as a fluid penetrates in a threaded contact. The benefit of this work is to understand the rate of lubrication provided by each of the fluid samples tested.

To achieve this, an experimental set up has been prepared to measure the torque and tension force. A mathematical formula was then used (Motosh, 1976) to work out the bolt thread friction. Five commercial penetrant products, listed in Chapter 5, have been tested. The main series of tests involve measuring the loosening torque as fluid penetrates in the contact with the knowledge of penetration time obtained previously. In addition to this, a dry condition has been considered and also a control test involving all the specimens fully lubricated before conducting the torque tests.

7.2 Experimental approach

Figure 7.1 shows the experimental apparatus. The bolt was held in place by a collet and ball bearing. The nut collet was then fixed in place by 6 locating studs as labelled on Figure 7.1 and then tightened up. The load cell was placed in the housing provided.

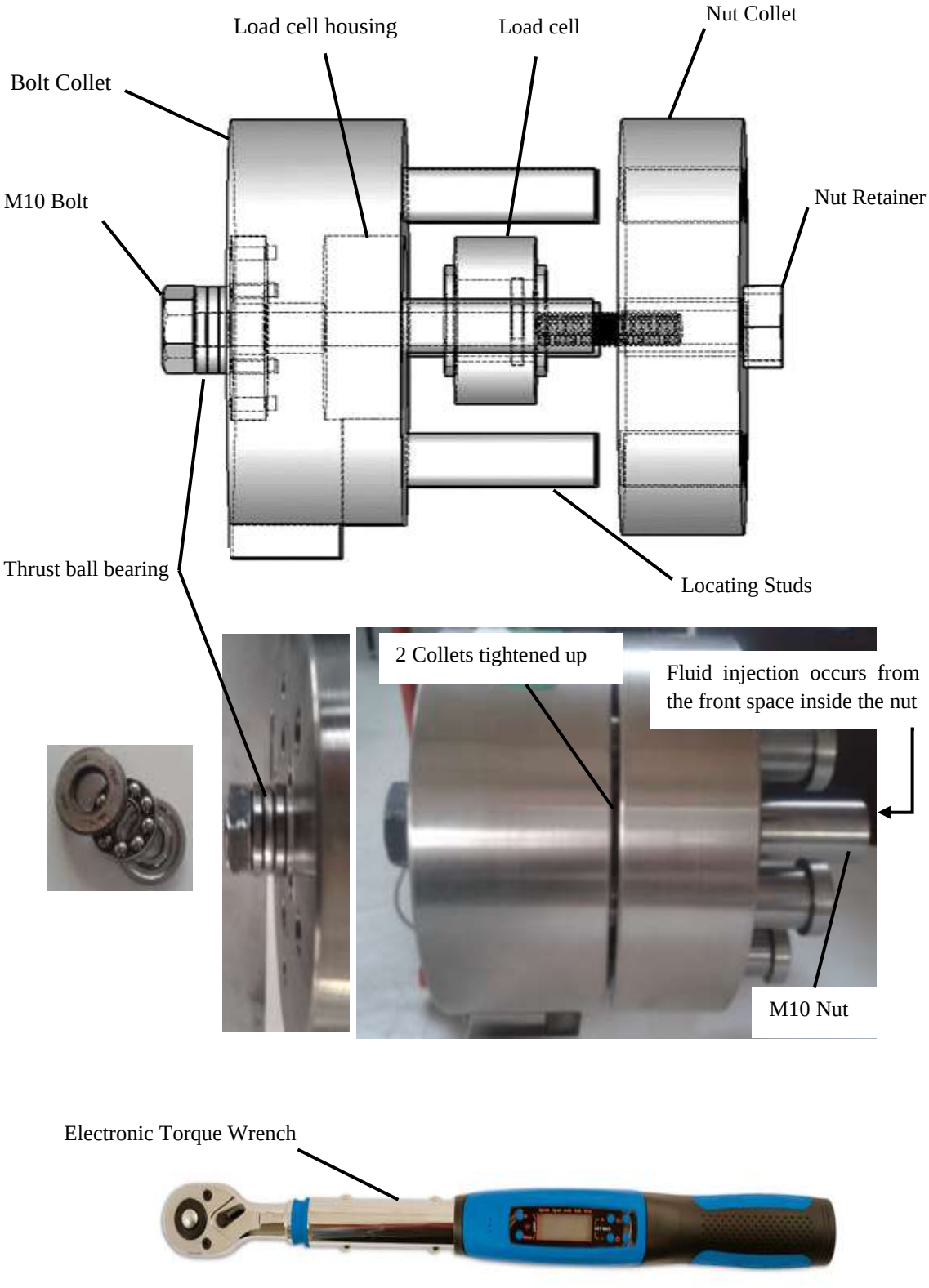

Figure 7.1 Schematic of the rig and apparatus for measuring torque and tension force

Parts of the rig and other experimental apparatus are described as below:

Bolt and Nut Specimens

M10 bolt and nut specimens were machined using the same approach described in Chapter 4 to ensure the thread geometry was as consistent as possible. The bolt, however, had to be larger so it could go through the rig. As shown in Figure 7.2, a hexagonal nut retainer on the rig can accommodate the nut specimens. In this way the nut specimen was fixed in position and when bolt was tightened up or released, the nut would not rotate.

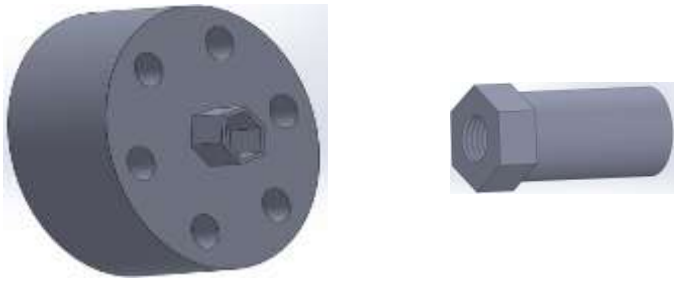

Figure 7.2 M10 Nut Specimen and the nut retainer

Thrust bearing

As shown in Figure 7.1, a thrust bearing was placed under the bolt head. This was used to support an axial force and minimise the under head friction.

Load cell

Figure 7.3 shows a schematic of the data logging process for measurement of tension force. As the bolt was tightened up, a tension force was generated which stretches the bolt, and the reaction force compressed the bolt and nut collets of the test rig. The load cell was connected to an amplifier powered by a 15 Vdc supply, which gives an analogue output of 0 V to 5 V. The scaling is 0 V=0 kN and 5 V =120 kN. The data was then logged using the NI DAQ controlled by the LabVIEW programme on the PC.

Electronic Torque wrench

An electronic torque wrench was used for tightening and releasing the bolt. The required torque value for tightening was set to ensure no excessive tightening occurs. The torque wrench was calibrated by the manufacturer and the accuracy given as $\pm 2\%$.

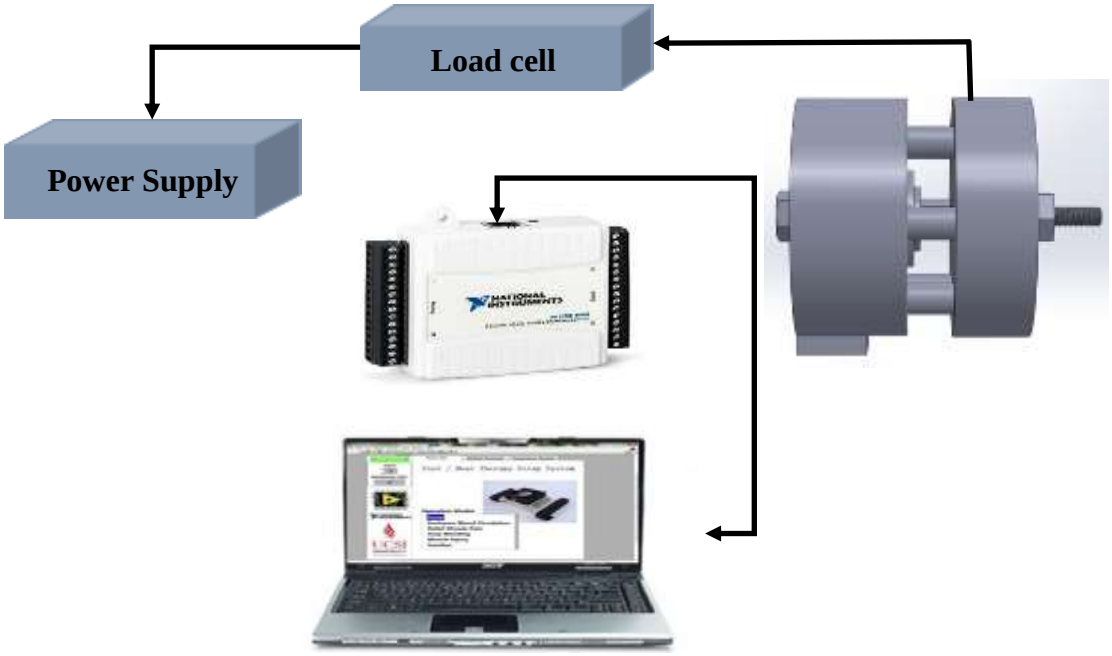

Figure 7.3 Schematics showing the hardware and the data logging process for measuring tension force

7.3 Experimental procedure

- **Specimen cleaning**: Bolt and nut samples were cleaned in acetone in an ultrasonic bath and fully dried. This was to ensure any residual oil film, wear debris or any other contaminations were removed before taking any measurements.

- **Tightening torque:** The tightening torque was required to be determined because, firstly it is to avoid excessive load as this can potentially damage the bolt threads, and secondly insufficient torque results in a poor clamping force. The torque-tension relationship, which is commonly used in engineering practice (Bickford, 1977), is given as:

  $$T = KDF \tag{7.1}$$

  This equation is also referred to as the short form equation, where T is the tightening torque, K is the dimensionless nut factor, D is the nominal diameter of the bolt and F is the fastener tension. For M10 bolt, a series of tests were carried out to measure tension force variation with applied torque. Figure 7.4 shows the relationship between torque and tension.

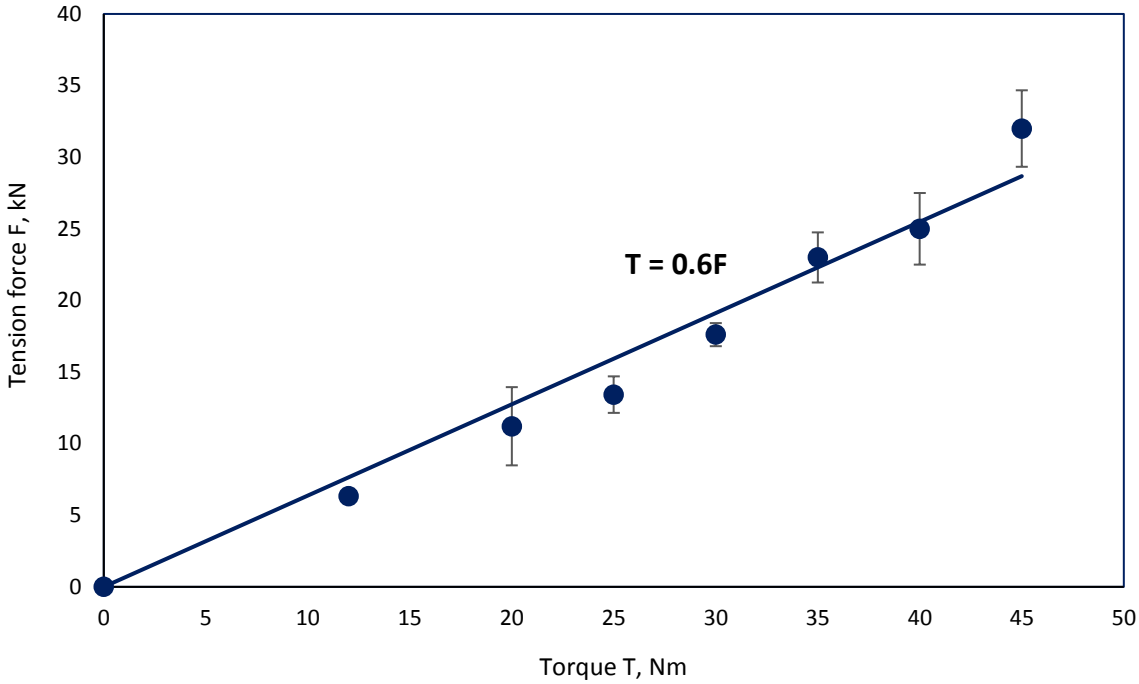

Figure 7.4 Torque tension relationship found experimentally for M10 bolt grade 8.8

Each of the data points is an average value from three measurements, and the torque-tension relationship is shown on the line of best fit (Figure 7.4), where *T* is torque, and *F* is the tension force. The slope of the line consists of the nominal dimeter *D* and the nut factor *K*. Given that *D* is 10mm, *K* is calculated to be 0.18.

For the class 8.8 bolt used in dry conditions (Technical Reference Guide, 2005) *K* is 0.20, but the suggested value is just an estimation. Nevertheless, the value found experimentally is close. Using the maximum suggested tension force given in the guidelines for fasteners (Technical Reference Guide, 2005), which is 25.225 kN, the maximum recommended torque was calculated to be 45 Nm, which was used in the testing programme. The bolt was tightened and untightened prior to each test to calculate the coefficient of friction when no fluid was present.

- **Fluid injection into threads.**

  After tightening the fastener, fluid was injected into the bolt using the space available in front of the nut, as the last few threads were not engaged. There were a total of 11 threads which were engaged and the fluid entered from thread 11.

- **Choice of Fluid samples**

  The testing samples were five commercial penetrant products (Table 5.1), which have lubricant present in them, and therefore can be tested to investigate their lubricating properties.

- **Measurement of loosening torque**

  As each of the fluid samples penetrated, the bolt was released at different times for each test. Some of the releasing times were decided based on the penetration time of the fluid into the threads that was identified in Chapter 5. For each of the samples, there were also several tests, which were carried out outside the normal range of penetration time measured by ultrasound. The last series of tests were measured at 300s, when penetration was assumed to have been completed.

7.4 Results and discussion

7.4.1 Measurement of loosening torque before fluid penetration

Figure 7.5 shows both the tightening and loosening torque obtained at different tension forces. As it can be observed, that the loosening torque is smaller than the tightening torque. As a bolt is tightened up, almost 90% of the input torque is used to overcome the friction forces at the threads and the bolt under head and the remaining of it is used to produce a tension force, extending the bolt. However, during the loosening process, the thread extension torque will help with the loosening process, hence the loosening torque is lower than the tightening torque.

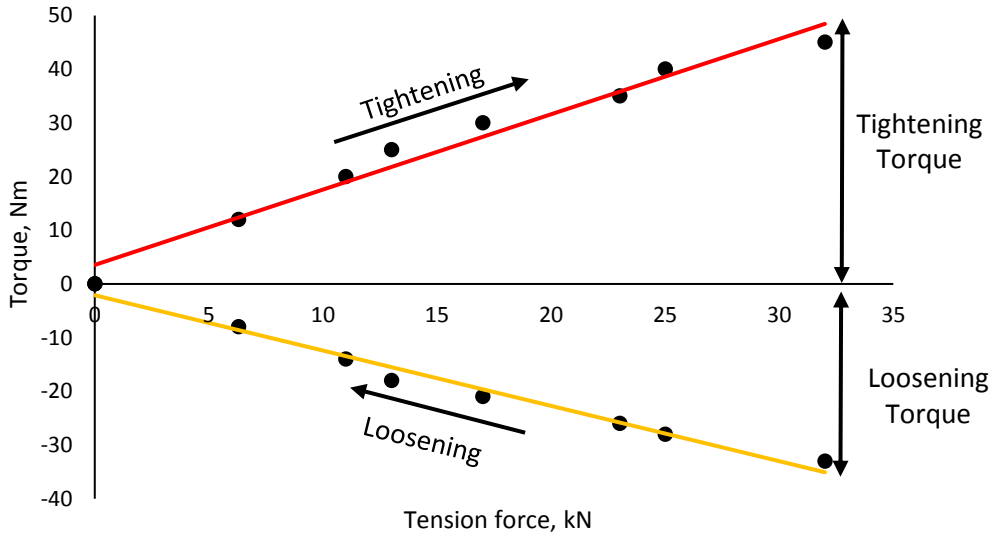

Figure 7.5 Tightening and loosening torque at different tension forces

According to Motosh (1976), the tightening torque is given by:

$$T_t = F\left[\frac{\mu_t r_t}{cos\beta} + \frac{p}{2\pi} + r_b\mu_b\right] \tag{7.2}$$

where T_t is the input tightening torque, F is the tension force, p is the thread pitch, μ_t is the coefficient of friction between internal and external threads, μ_b is the coefficient of friction at the under head bearing, r_t is the effective contact radius between threads, r_b is the effective bearing radius of the bearing contact under the bolt head and β is half of the thread profile angle. The loosening torque is given as:

$$T_l = F\left[\frac{\mu_t r_t}{cos\beta} - \frac{p}{2\pi} + r_b\mu_b\right] \tag{7.3}$$

Therefore:

$$T_t - T_l = F\left[\frac{p}{\pi}\right] \tag{7.4}$$

Using equation (7.4), tension force can be calculated from pairs of tightening and loosening torque values. This data can then be plotted against the tension force data obtained from the load cell. Figure 7.6 shows a reasonable agreement between both sets of data when compared with the exact data, i.e., measured from the load cell.

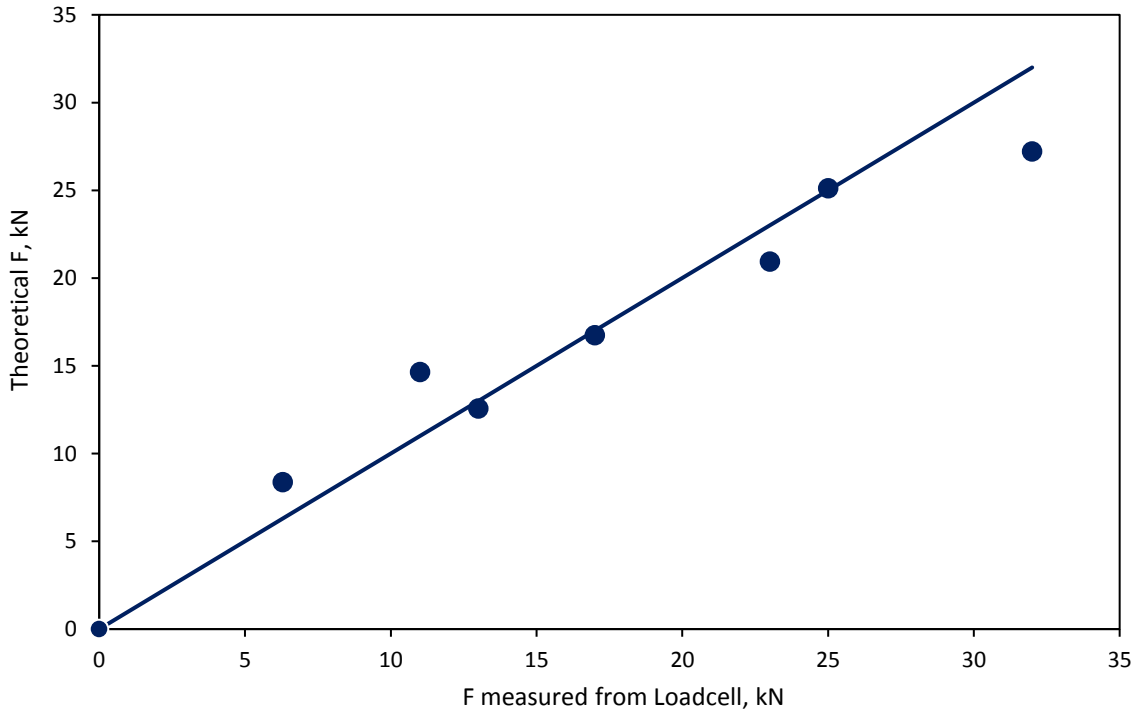

Figure 7.6 Comparison of measured data with data obtained from equation 7.4

7.4.2 Loosening torque and fluid penetration

Figure 7.7 shows the change in the loosening torque as the fluid penetrates into the threaded contact.

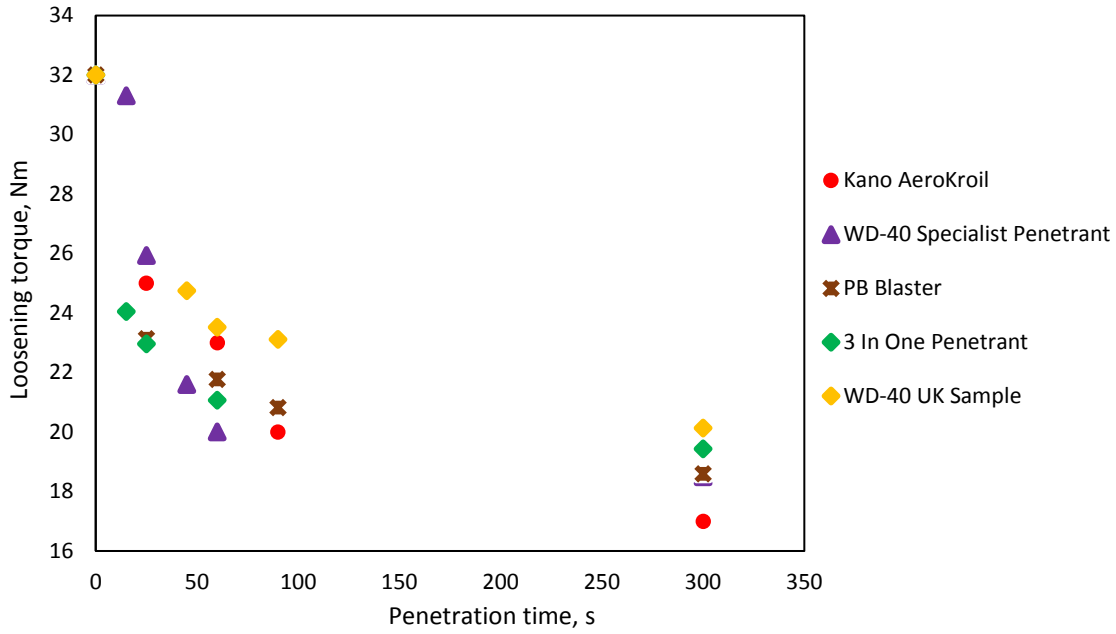

Figure 7.7 Loosening torque vs fluid penetration time

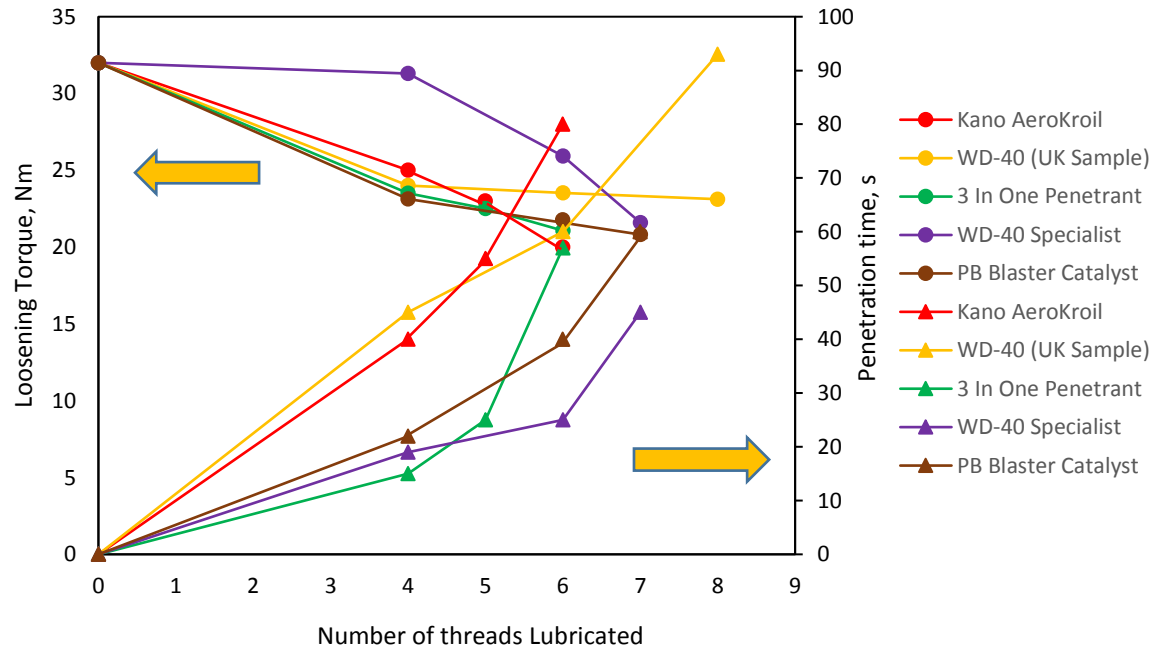

Figure 7.8 Loosening torque and penetration time against the number of threads lubricated (Based on ultrasound data)

According to the trend observed in Figure 7.7, within the first 45s, the reduction in the loosening torque is significant for all the fluid samples. This is due to the fact that during this time, the fluid has already lubricated most of the threads. Figure 7.8 shows the number of threads lubricated against the ultrasonically measured penetration time (Chapter 5) and loosening torque.

Within the first 100 s, the fluid penetration was expected to be complete for all the samples according to the experimental penetration time data, implying that the maximum length in terms of threads was reached, hence why most of the tests were carried out in this time frame. Examining the trend in Figure 7.7, between 100 s and 300 s, it appears that the reduction in the loosening torque is small, which supports the observation that most of the fluid penetration had already taken place.

At 300 s, a notable observation is the fact that Kano AeroKroil appears to show better lubrication properties than other fluids, however, during the initial 45s of fluid penetration, WD-40 Specialist demonstrates to have the best rate of lubrication.

7.4.3 Loosening torque after fluid penetration

Figure 7.9 shows the loosening torque at 300s after initiation of fluid penetration. A clear difference between the dry and lubricated contacts can be observed. For the fluid samples tested, although some slight increase in the amount of torque required to remove the bolt can be observed from Kano AeroKroil to WD-40(UK Sample), no major difference can be noticed between the different samples.

Overall, it can be seen that whilst a fluid such as WD-40 Specialist facilitates the removal of the bolt in a shorter time, Kano AeroKroil provides slightly better lubrication when it has fully penetrated. To explore the lubrication behaviour further, the coefficient of friction at the threads is investigated in the next section.

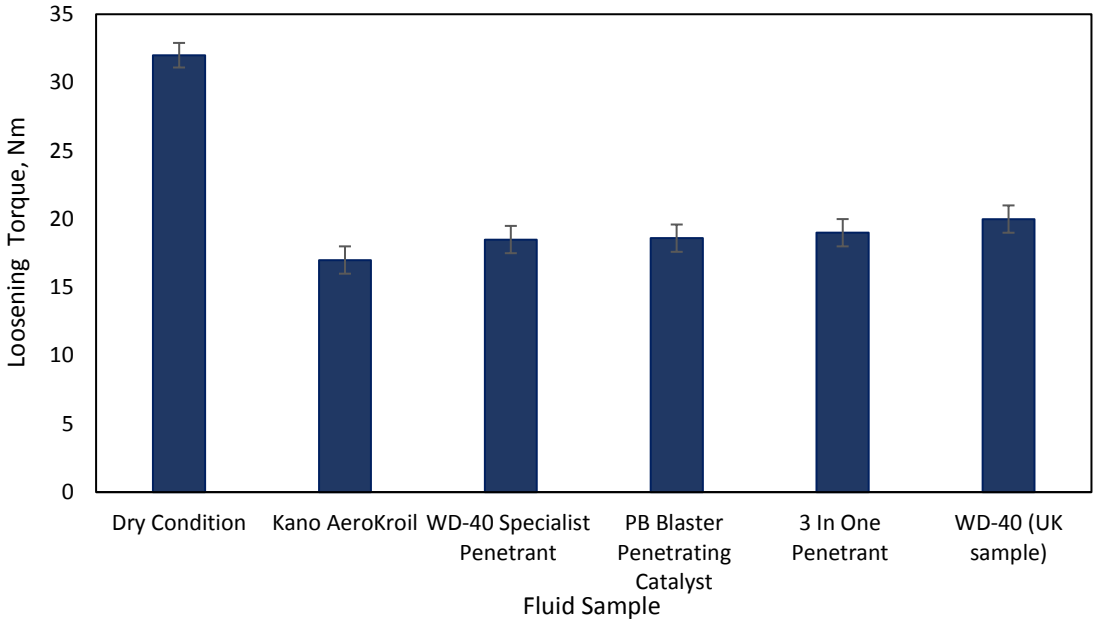

Figure 7.9 Loosening torque after complete fluid penetration (300s)

7.4.4 Coefficient of friction

The coefficient of friction can be obtained using equations (7.3) and (7.4) for both the tightening and loosening process. However, the main two data inputs are the total torque and tension force, since the thrust bearing, as described in section 7.2, is used to minimise the friction under the bolt head, it is assumed that the bearing torque is zero.

So equations (7.3) and (7.4) simplify to:

$$T_t = F\left(\frac{\mu_t r_t}{cos\beta} + \frac{p}{2\pi}\right) \tag{7.5}$$

$$T_l = F\left(\frac{\mu_t r_t}{cos\beta} - \frac{p}{2\pi}\right) \tag{7.6}$$

Control test

The coefficient of friction was determined for the dry case and a fully lubricated case, where a bolt was dipped in a beaker of each penetrant. Figure 7.10 shows the tightening and loosening torque. Figure 7.11 show the resulting coefficient of friction.

The fluids tested show only slightly different lubrication performance. This is shown both by the difference in the tightening and loosening torque.

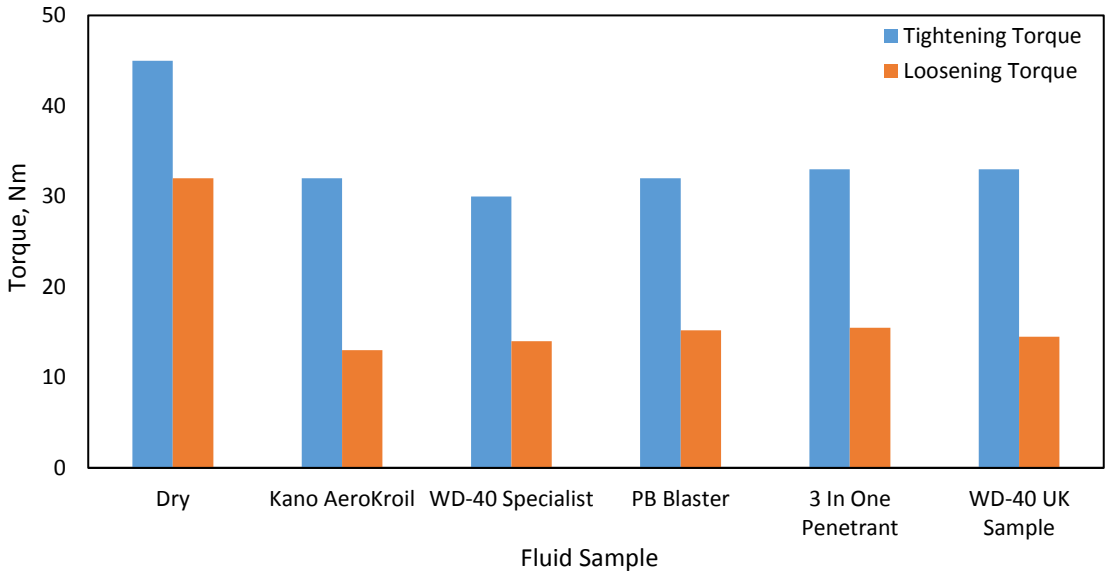

Figure 7.10 Loosening and tightening torque when the threads are fully lubricated

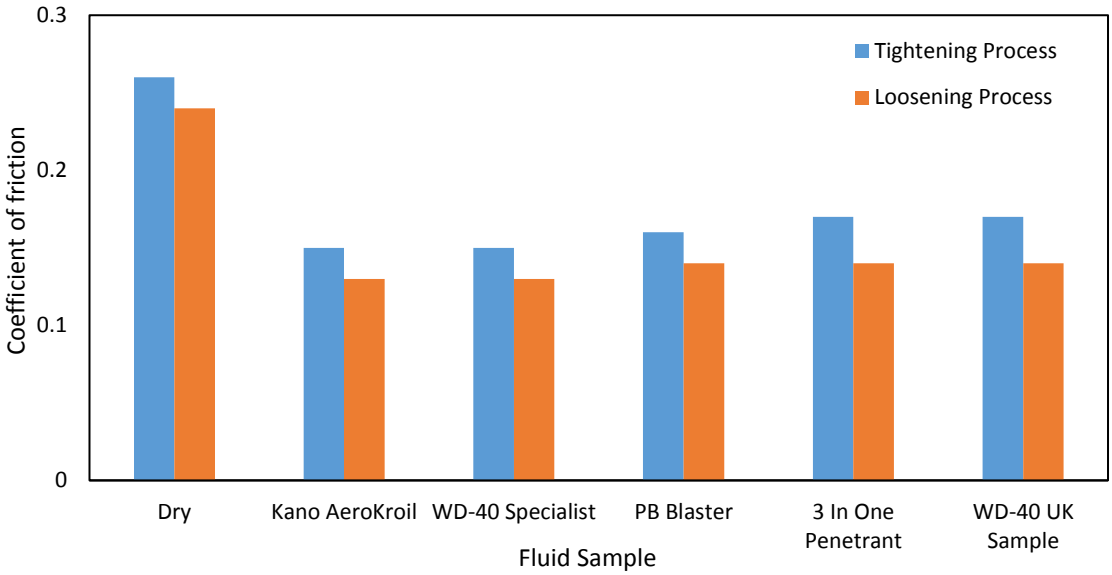

Figure 7.11 Coefficient of friction when the threads are fully lubricated

It can be seen that coefficient of friction for both the tightening and loosening process in the dry condition is 0.26 and 0.24 respectively and this data agrees reasonably with the coefficient of friction data available for steel threads in the dry conditions (Maryland Metrics, 2011).

With regards to the lubricated conditions, the coefficient of friction obtained is within 0.13 to 0.14. This is in close agreement with the data available from literature (Zoe et al., 2007), when using low viscosity oil at the boundary lubricated condition, which is within a range of 0.11 to 0.17 for the oiled threads. But it is important to note that the samples

used in the tests are not oils, and they only make up some of the penetrant, hence the lubrication properties may not be similar to mineral oils. These control tests provides some understanding of how the penetrants may perform, but the coefficient of friction might be different when measured during or after fluid penetration.

Coefficient of friction before and after fluid penetration

Figure 7.12 shows the coefficient of friction as the fluid penetrates in the threaded contact. This data was deduced from the data of Figure 7.7 using equation 7.6. One important observation is the value of coefficient of friction after 300s for the fluid samples, which lies between 0.17 and 0.18. Comparing these data with the ones obtained from the control tests, it is clear that the coefficient of friction obtained during the fully lubricated conditions is slightly lower by 0.03. This could imply that fluid penetration does not fully lubricate the contact, or indeed it may not penetrate deep enough in terms of the number of threads.

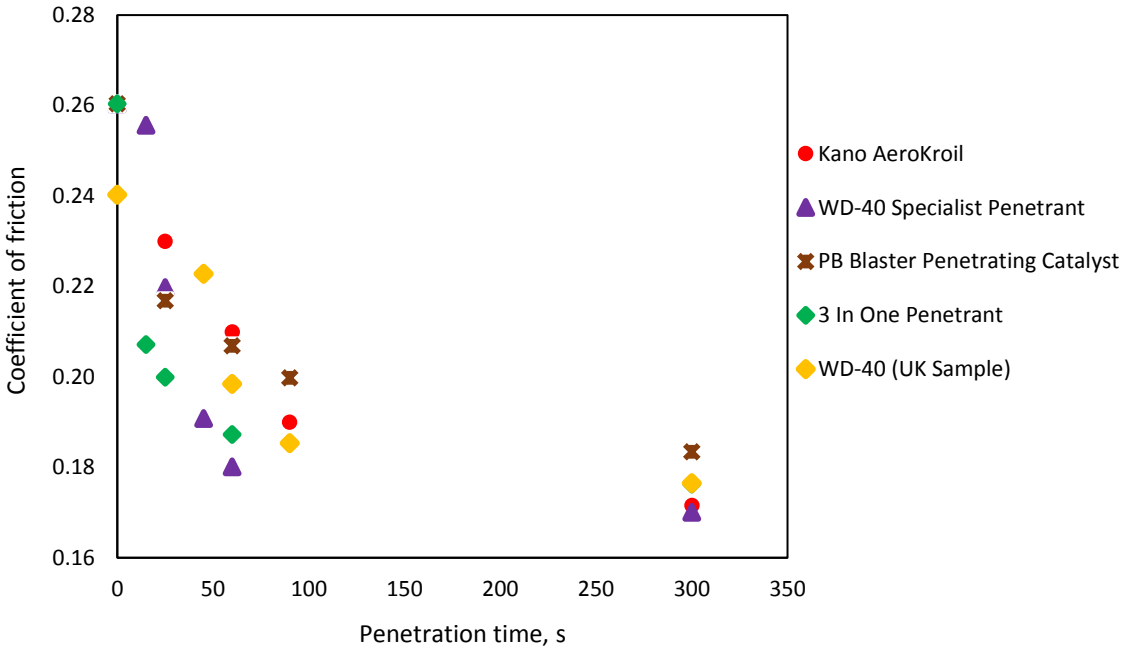

Figure 7.12 Coefficient of friction against the time of fluid penetration into threads

7.5 Modelling the lubrication behaviour

In the previous section, the coefficient of frictions were determined as the fluid penetrated into the threaded contact. Considering that lubrication changes over time, there are three main conditions at the threaded contact:

a) A fully dry contact, where no fluid is present
b) A partially lubricated contact, when one or more threads are lubricated, but the rest are dry.
c) A fully lubricated contact, when all threads are assumed to be lubricated.

The coefficient of friction for conditions (a) and (c) were found by the control tests in section 7.3.4. But for the second condition, the combined effect of the dry and lubricated conditions needs to be modelled. Figure 7.13 shows a threaded contact, as one thread is filled with a penetrant. An unwrapped version of the contact is shown as well.

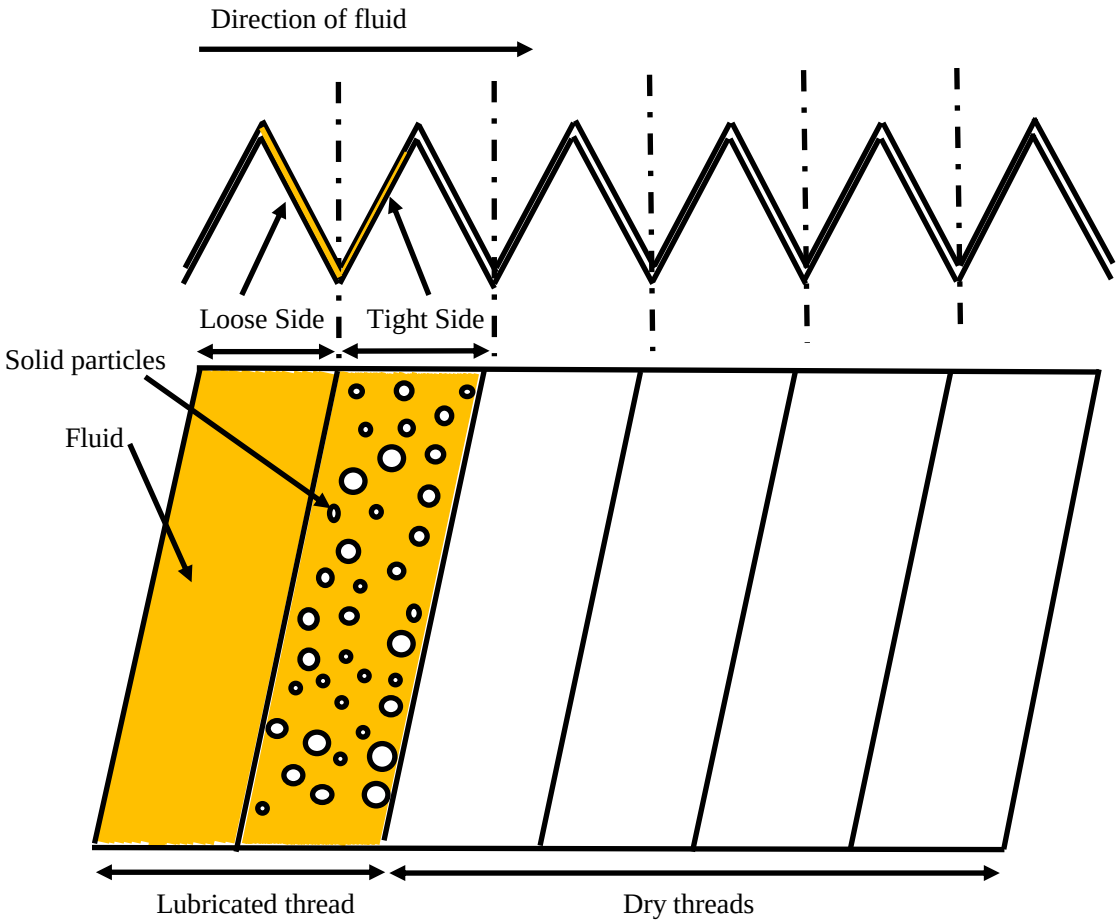

Figure 7.13 Schematic of the threaded contact, the lubricated and dry length

The unwrapped section represents the length of all threads in the loose and tight regions. When penetrant fills up the first thread, a proportion of the total length is lubricated. This means the coefficient of friction at this thread will be different to the rest of threads in a threaded contact. In order to find the combined coefficient of friction for the whole system as fluid penetrates, the following approach is taken:

Total friction of the system

The total coefficient of friction in the system can be found by finding friction force at each thread, whether they are dry or lubricated. There are a total of 11 engaged threads in the contact, *F* is the total friction for all the threads.

$$F = \sum_{i=1}^{11} F_i \tag{7.7}$$

where *F* is given in terms of coefficient of friction, μ_i and the normal reaction force R_i at each thread *i*:

$$F = \sum_{i=1}^{11} \mu_i R_i \tag{7.8}$$

When fluid penetrates into thread p and lubricates it, the total coefficient of friction consists of the lubricated threads μ_{wet}, and the dry threads μ_{dry} as given by equation (7.9):

$$F = \sum_{i=1}^{p} \mu_{wet} R_i + \sum_{i=p}^{11} \mu_{dry} R_i \tag{7.9}$$

To find the total friction, μ_{Lub} and μ_{Dry} are the ones obtained previously from the control tests in section 7.3.4, which are 0.14 and 0.24 respectively. But the normal reaction force varies as it is a component of the axial load acting on the thread. Figure 7.14 show the axial load and the normal reaction force acting on a V threaded contact.

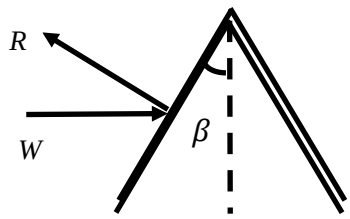

Figure 7.14 Schematic of the reaction force and axial load on a V threaded contact

For the angle shown in Figure 7.14, $\beta = 30^{\circ}$, therefore the normal reaction force is:

$$R = \frac{W}{cos30^{\circ}} \tag{7.10}$$

where *W* is the axial load, which is distributed over the engaged threads. There has been several studies on the load distribution in a threaded contact (See Chapter 2) and they all confirm that the first few of the engaged threads take most of the load. According to table 2.1, the experimentally measured axial load of 32 kN is distributed over 11 threads as shown in Table 7.1.

Thread Number	*Axial Load W (kN)*
1	9.92
2	6.40
3	4.80
4	3.50
5	2.56
6	1.92
7	1.28
8	0.96
9	0.64
10	0.32
11	0.32

Table 7.1 Load distribution across the 11 engaged threads

These load values are used in a calculation to determine the friction force at each thread. As the total friction force and the total normal reaction force is known, the total coefficient of friction of the system, μ_t, can be found:

$$\mu_t = \frac{\sum_{i=1}^{p} \mu_{wet} R_i + \sum_{i=p}^{11} \mu_{dry} R_i}{\sum_{i}^{11} R_i} \tag{7.11}$$

Fitting of experimental data with μ_t

The experimental data for the coefficient of friction obtained from the loosening torque data are plotted against the penetration time and the number of threads lubricated, as shown in Figure 7.15.

The data obtained from the model are then plotted against the coefficient of friction calculated from the loosening torque measurement, which is shown in Figure 7.16. The reason that the dataset at thread 11 is encircled is due to the fact that fluid penetration is expected to be completed within the first 100 s, which would be up to 8 threads according to the ultrasound data obtained in Chapter 5. Therefore, at 300 s, assuming that the fluid penetrates as far as thread 11 then all the threads are lubricated.

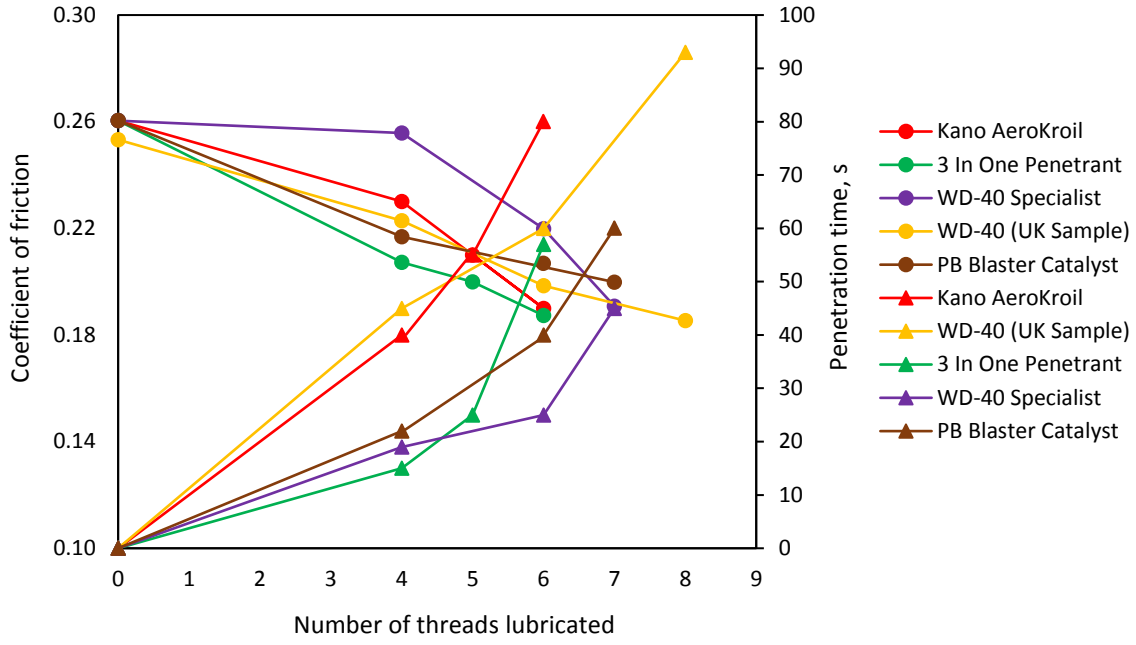

Figure 7.15 Coefficient of friction and penetration time against the number of threads lubricated (Based on ultrasound data threads identification) deduced from Figure 7.8

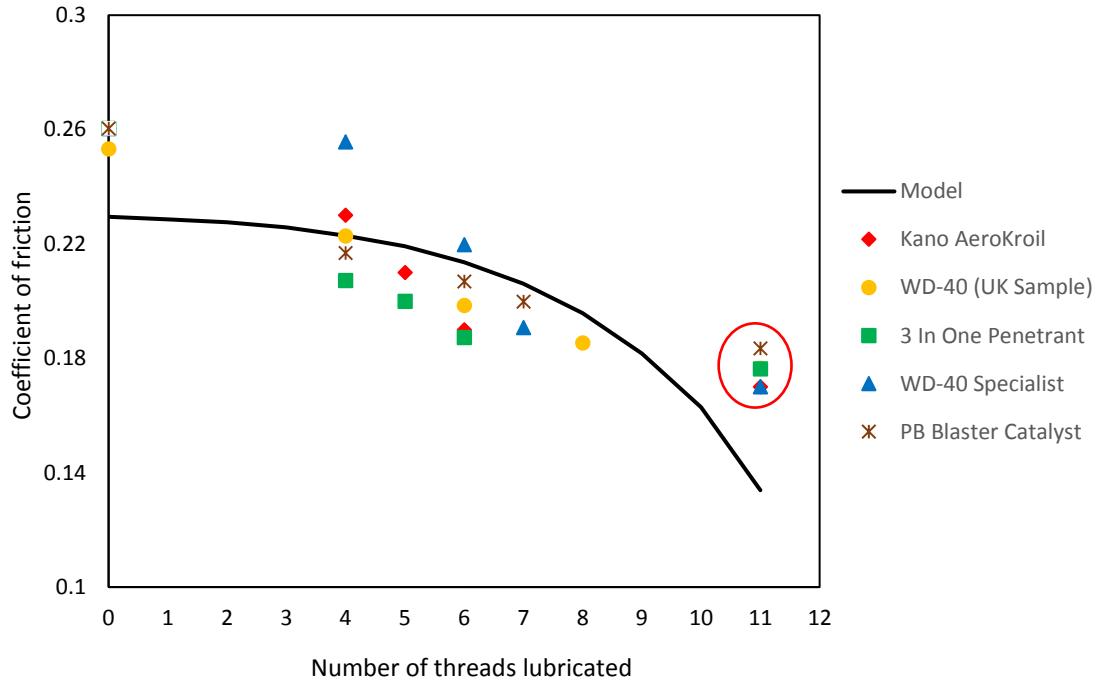

Figure 7.16 Comparison of coefficient of friction between the model (equation 7.11) and Coefficient of friction obtained from the loosening torque data

In terms of the trend, both the model and data from the fluid samples reasonably agree with each other, with only WD-40 Specialist fluid being slightly different. WD-40 Specialist is clearly a fast penetrant and despite providing a good rate of lubrication, the

coefficient of friction in the initial threads is slightly higher. One reason for this could be due to the fluid sample being a suspension, dependent on the second phase materials responsible for providing better lubrication. Therefore, the fluid is faster in terms of reaching the contact, but it may take more time to lubricate the contact.

7.6 Conclusions

- In this study, the lubrication behaviour of five commercial penetrant samples in a fastener was investigated. An experimental set-up was used to measure the loosening and tightening torque by an electronic torque wrench, as well as a load cell to measure the tension force. The torque-tension relationship for both tightening and loosening torque in the dry condition was established, which confirmed the literature findings (Eccles, 2014) that less torque is required to loosen a fastener.
- The loosening torque was also measured as a function of the penetration time of the fluids between 0s to 300s. It was found that the loosening torque for all the fluid samples decreased mainly within the first 100s of the tests. At 300s, there was no noticeable change in the loosening torque between the different samples. Furthermore, the relationship between the number of threads lubricated and loosening torque was shown. Within the first 100s, different samples lubricated from 6 to 8 threads depending on their penetration depth.
- Coefficient of friction at the bolt threads was found from a mathematical formula modelling the loosening process (Eccles, 2014) using the loosening torque and tension force, as the input data. It was found that the coefficient of friction in the dry condition was from 0.24 to 0.26 and decreased to values from 0.17 to 0.18 after the fluid penetration was complete.
- The lubrication behaviour was modelled, by considering the whole length of the threaded contacts (11 threads) as dry and lubricated segments. The coefficient of friction found by the model compared with the coefficient of friction from the loosening torque and a close agreement was observed for most of the fluids.

8

Conclusions and Recommendations

8.1 Introduction

Oil penetrants such as WD-40 are commonly used in tackling the problem of seizure in bolted joints. A penetrant product performs at its best, when it gets to the threaded contact in the shortest time and reduce the friction. WD-40 Research and Development team first raised some questions regarding a direct method to assess fluid penetration in threads. This led to some initial work at the University of Sheffield (Vail, 2013), where an in-situ measurement concept based on ultrasound principles was developed and penetration time of a few fluids were measured. However, this tool did not measure the lower viscosity fluids.

Therefore the primary motivation of further investigation was to get the ultrasonic technique functional for fluids with a range of viscosities. However, other research questions were also raised:

- What are the factors that affect fluid penetration inside a threaded contact? Is it possible to model the process?
- How about the lubrication performance? Is there a way to measure this when a penetrant reaches the threaded contact?

The work discussed in this thesis met the research objectives and answered the questions above, although some limitations were faced. In this chapter, both the contributions and limitations are considered and future research avenues are recommended.

8.2 Conclusions

8.2.1 Measurement of fluid penetration in threaded fasteners

A non-invasive ultrasonic technique was refined and demonstrated that it was possible to measure fluid penetration for a range of physical and chemical properties. This technique utilised the principles of ultrasonic reflectometry and detected the presence of penetrant as it flowed inside a threaded contact.

Fluids tested, fell into three categories of commercial products, solvents and WD-40 penetrant samples with different amount of Volatile Organic Compound (VOC). The measured total penetration time varied from 20s to 90s for the fastest and slowest samples respectively. Commercial penetrant products are mostly slow, WD-40 Specialist

Penetrant and 3 In One Penetrant were seen to penetrate more effectively than the rest of commercial products. WD-40 Specialist outperformed PB Blaster Penetrating Catalyst by being around two times faster, which agreed with the data available from the nail climb test. Investigation of pure solvents showed that they generally have a shorter penetration time, which is due to their low viscosity. Furthermore, the effect of VOC content on the penetration performance of WD-40 penetrant was studied and it was found that an increase in VOC from 10% to 67% reduced the total penetration time by 10s.

Effect of viscosity on penetration performance was explored and it was found that it had a dominant effect on the penetration performance; fluid penetration velocity increases as viscosity decreases. Analysis on fluid flow velocity was carried out and it was suggested that variation of load distribution in threads had an effect. For instance, it was observed that there was an increase in fluid velocity at thread 5 for most of the fluid samples. It was explained that a sudden change of load from a higher load to a lower load may have resulted in an increase in the gap at the thread contact, hence causing an increase in fluid penetration velocity. Nevertheless, the overall trend was a decrease in fluid velocity as fluid penetrated along the threads and the Reynolds number for all the samples was found to be less than 1, suggesting a laminar creeping flow.

Moreover, mechanism of fluid flow penetration was discussed. It was explained that fluid flow may get delayed when reaching certain locations of a thread and it was reasoned that variation in surface roughness profile could cause this complication. There were also some anomalies in measurements which resulted in recording some observations. One of these was the presence of bubbles, which could form due to several reasons such as air trapped in threads, surface roughness, and geometrical irregularities. However, further work is recommended to prove this phenomena (Section 8.3).

Furthermore, it was observed that at some instances fluid may leak from one thread to the next one. Based on the SEM images of the bolt specimen, it was explained that absence of materials at bolt thread crest possibly due to adhesive wear may have caused this fluid phenomena. Further tests with a new bolt specimen rectified this. Another interesting phenomena was the occasional presence of residual oil films in the threaded contact, which affected the ultrasound response slightly. It was discussed that poor cleaning of specimens caused this. This issue was resolved when specimens was carefully cleaned.

There were other complications in fluid flow such as the depth of penetration. Majority of the samples reached thread 7, some of them only penetrated to thread 6, but some others penetrated further to thread 8. The effect of viscosity and surface tension on depth of fluid penetration was investigated, however, no relationship was found. Chemical composition might have an effect, but it remains unknown as more information about the composition is required before this issue can be explored further.

To conclude, although complex fluid penetration mechanisms exist in a threaded fastener, the ultrasonic technique developed in this work can measure the penetration time with improved measurement sensitivity and repeatability for a variety of fluid samples with a range of viscosities and surface tension.

8.2.2 Analytical modelling of fluid penetration process

The focus of this work was to model the fluid flow process in the fasteners. Principles of laminar fluid mechanics for fluid flow between parallel plates was applied and pressure gradient was defined by the Laplace-pressure drop equation to derive an equation which related the penetration time to fluid properties and geometrical characteristics of the threaded contact. The data from the analytical model was then compared with the experimental data using the ultrasonic technique.

To study the effect of the geometrical characteristic of the contact, the gap size at different regions of the threaded contact such as the root, crest and the loose and tight sides were measured. It was shown that the gap varies at each of these regions. The penetration time was found to be sensitive to a 10μm decrease in gap size from thread 6 onwards.

Moreover, penetration time across different thread regions was investigated by studying different fluid flow paths. It was found that for thread 4 onwards, the fluid penetration time in the tight region is around 2% of the total time of penetration.

Surface tension and viscosity were grouped into a single parameter called the Fluid Penetration Coefficient (FPC). The effect of FPC on penetration time obtained from the model was studied and it was found that for higher values of viscosity and lower values of surface tension, the fluid penetration process takes longer.

Data obtained from the theoretical model and ultrasonic technique were compared and their trend agreed to some extent for threads 4, 5 and 6. However, this was true for fluids with FPC lower than 4. In addition, the penetration time obtained from the model was

found to be longer than the measured ultrasonic data. Several factors such as the inlet fluid velocity, complexity of fluid flow in threads, tolerances and surface roughness may cause the difference.

To summarize, although the model has some limitations such as not considering the multiphase effects or other factors explained above, it still provides an understanding of the fluid penetration process in threaded fasteners and can be a starting framework for further research.

8.2.3 Measurement of direct torque to study the lubricating behaviour

The purpose of this study was to investigate the lubrication performance of commercial penetrants. An experimental approach was used to measure the loosening torque at different stages of fluid penetration process. The tension force was also measured using a load cell.

In the first part of study, a torque-tension relationship was found experimentally for both tightening and loosening process in dry condition. It was shown that loosening torque is less than tightening torque. The tension force was then found theoretically using measured tightening and loosening torque values and compared with the data obtained from the load cell, which showed good agreement between both data sets.

In the second part of study, effect of lubrication was investigated by measuring loosening toque at certain penetration times between 0s to 300s. The timing of the tests were based on the measured penetration time obtained from the ultrasonic technique. Using this information, it was possible to find the number of threads lubricated.

The experimental results indicated that the loosening torque for all the fluid samples decreased mainly within the first 100s of the tests. It was found that different products exhibited a different rate of lubrication and WD-40 Specialist Penetrant performed the best compared to the rest of samples. At 300s, when fluid penetration was assumed to have been completed, the difference in the loosening torque values was negligible.

In the third part of the study, the coefficient of friction at the bolt and nut thread were deduced from the measured loosening torque and tension force. The coefficient of friction in the dry condition was 0.24 to 0.26 and after complete fluid penetration was 0.17 to 0.18.

In the final part of this work, the lubrication behaviour was modelled, by considering the whole length of the threaded contacts (11 threads) as dry and lubricated segments. The coefficient of friction found by the model was compared with the coefficient of friction from the loosening torque and a close agreement was observed for most of the fluids.

To conclude, the lubricating behaviour of commercial penetrants was studied and the results of this work can be used to improve the lubrication performance of penetrating products.

8.3 Future work

There are a few avenues of research which can be explored. Some of them are summarized in the section:

- Measuring fluid penetration time with rusted specimens

  In the study carried out in this thesis, bolt and nut specimens were not rusted and they were cleaned in acetone before each test. It would be useful to investigate how effective the penetrants are when they are applied to a rusted condition. To do this, rust can be produced onto the specimens to a consistent level and then another series of penetration tests are carried out.

- Study of anomalies in penetration measurements

  Presence of bubbles was thought to be one of the factors that affect the fluid penetration process. To investigate this, it would be beneficial to make some bolt and nut specimens out of Perspex and observe the fluid motion as it penetrates through a transparent threaded contact. It is suggested to dye the fluid samples and use a high speed camera to record the process.

- Investigating the effect of surface roughness on fluid penetration

  In Chapter 5, the SEM images of the bolt threads showed that roughness changes as expected. To investigate the effect of surface roughness, it is suggested that some experiments are run on a pair of parallel plates with different degree of roughness, matching the ones expected in the threaded contact. The idea is to inject some fluid

from the centre of one plate into the contact and measure how the fluid spreads in-situ by means of multiple ultrasonic sensors.

- Analytical modelling of the fluid penetration process

In order to develop the model further, issue of surface roughness and bubble formation in the threaded contact needs to be considered. In addition, the multi-phase effects of the fluid should be taken into account.

- Studying different mixture of solvents, lubricating oils and additives

Penetration time of some of the solvents used in penetrating oil products were measured in Chapter 5. It will be useful to study the effects of them as they are mixed with the base oils at different ratios. A solvent and base oil mixture can then be tested for penetration and lubrication performance inside a threaded contact applying the techniques developed in this thesis.

The effect of additives can be investigated in the same style. Some of the common additives used in a penetrating oil are micro dispersants, which consist of solid and liquid particles such as graphite polytetrafluoroethylene (PTFE), graphite, and molybdenum disulfide or boron nitride. Some of the products used in this work have 2^{nd} phase materials and in order to have a better understanding of their contribution to lubrication, it is suggested to firstly measure the lubricating behaviour of a penetrant without the additives. And then study the effects of additives by adding them to the penetrant and carry out the measurements again.

References

Astridge, D.G. & Longfield, M.D., 1967. Capacitance measurements and oil film thickness in a large-radius disc and ring machine. *Proceedings of the Institution of Mechanical Engineers*, 182(314), pp. 89–96.

Ballerini, Li X & Shen, W., 2011. Flow control concepts for thread-based microfluidic devices. *Biomicrofluidics, 5(1),* pp. 1-11

Baulch, J, 2011. What factors should be considered for stainless steel fasteners in bolted flanged connections*?* Available at: http://www.pumpsandsystems.com/topics/seals/gaskets/fsa-sealing-sense-december-2011. [Accessed: 10 September 2016]

Bickford, J.H., 1977. An introduction to the design and analysis of bolted joints. 3rd ed, Marcel Dekker, New York.

Bickford, J.H. & Nassar, A.S. 1998. Handbook of bolts and bolted joints. Marcel Dekker, New York

British tools & fasteners - BSW thread profile (no date) Available at: https://www.britishfasteners.com/threads/bsw.html (Accessed: 30 August 2016).

Brunskill, H.P., 2013. The real-time characterisation of dry machine element contacts using ultrasonic reflectometry. PhD thesis, University of Sheffield.

Bosanquet, C. H., 1923. On the flow of liquids into capillary tubes. *The London, Edinburgh, and Dublin Philosophical Magazine and Journal of Science*, 45:267, pp. 525-531.

Bowden, F.P., 1944. The physics of rubbing surfaces. *J. Proc. R. Soc. New South Wales, 78,* pp. 187-195.

Bowden, F.P. & Tabor, D., 1964. The Friction and Lubrication of Solids: Part 2, Oxford (in English)

Dang-vu, T., 2005. Characterization of porous materials by capillary rise method. *Physicochemical Problems of Mineral Processing*, 39, pp. 47–65.

Den Hartog, J.P., 1929. *The mechanics of plate rotors for turbo-generators. Trans ASME, J. Appl. Mech,* 51, pp. 1-10.

Drinkwater, B. W. , Dwyer-Joyce, R. , Cawley, P., 1996. The interaction of ultrasound with a partially contacting solid-solid interface in the low frequency regime. *In Review of Progress in Quantitative Nondestructive Evaluation*, Vol. 15 (Plenum Press, New York), pp. 1229-1236

Dwyer-Joyce, R. S., Drinkwater, B. W., Quinn, A. M., 2001. The use of ultrasound in the investigation of rough surface interfaces. *ASME Journal of Tribology*, 123, pp. 8-16.

Dwyer-Joyce, R. S., Drinkwater, B.W., Donohoe, C.J., 2003. The measurement of lubricant-film thickness using ultrasound. *Proceedings of the Royal Society Series A: Mathematical Physical and Engineering Sciences,* 459(2032), pp. 957-976.

Dwyer-joyce, R.S., Harper, P. & Drinkwater, B.W., 2004. A method for the measurement of hydrodynamic oil films using ultrasonic reflection. *Tribology Letters*, 17(2), pp. 337–348.

Dwyer-Joyce, R.S., Reddyhoff, T. & Zhu, J., 2011. Ultrasonic measurement for film thickness and solid Contact in elastohydrodynamic lubrication. *Journal of Tribology*, 133 (3). pp. 1-11

Eames, A. 2012. The history of the bolt. Available at: http://www.nord-lock.com/bolted/the-history-of-the-bolt/. [Accessed 1 September 2016].

Eccles, W., 2010. Tribological aspects of the self-loosening of threaded fasteners. PhD thesis. University of Central Lancashire

Eccles, B., 2011. Bolt Science. Retrieved from Self-Loosening of Threaded Fasteners: Available at: http://www.boltscience.com/pages/self-loosening-of-threadedfasteners.pdf [Accessed: 30 May 2018]

Eccles, W., 2014. A new approach to the checking of the tightness of bolted connections. *LUBMAT 2014 – Lubrication, Maintenance and Tribotechnology*, pp. 1-9.

Eccles, W., (no date). Historical background on screw threads. Available at: http://www.boltscience.com/pages/screw2.htm [Accessed: 30 August 2016].

El-Sisi, S.I. & Shawki, G.S. a., 1960. Measurement of Oil-Film Thickness Between Disks by Electrical Conductivity. *Journal of Basic Engineering*, 82(1), pp.12.

Fastener + Fixing Magazine, 2015. Fastener Industry News. Available at: http://www.fastenerandfixing.com/news/global-fastener-demand-to-reach-us-93-8-billion-in-2018. [Accessed: 25 June 2016]

Fisher. L. R & Lark. P. D., 1979. An experimental study of the Washburn equation for liquid flow in very fine capillaries. *Journal of Colloid and Interface Science*. 69, pp. 486-92.

Friction, Wear and Lubrication Glossary, 1969. Organisation for Economic Co-operation and Development, Paris.

Good, R.J., 1973. The rate of penetration of a fluid into a porous body initially devoid of adsorbed material (1, 2). *Journal of Colloid And Interface Science*, 42(3), pp. 473–477.

Ghosh, P., 2014. Shape of the Interfaces. Lecture notes, Department of Chemical Engineering, IIT Guwahati India.

Grewal, a. S. & Sabbaghian, M., 1997. Load distribution between threads in threaded connections. *Journal of Pressure Vessel Technology*, 119(1), pp. 91.

Greenslade, J., 1995. How to Stop Thread Galling on Stainless Fasteners. *Am. Fasten. J.*, p. 7.

Hemmati Vand, E., Oskouei, R. H., Chakherlou, T. N., 2008. An experimental method for measuring clamping force in bolted connections and effect of bolt threads lubrication on its value. *World Academy of Science, Engineering and Technology*, vol. 46, pp. 457- 460.

Hertzberg, R.W., 1989. Deformation and Fracture Mechanics of Engineering Materials, 3rd edition. New York: Wiley

Ibbotson, A.B. & Talbot, F.J., 1877. Improvement in forming threads on screw bolts and nuts. *U.S. Patent 191,968.*

Ichikawa N. I. & Satoda Y. S., 1994. Interface dynamics of capillary flow in a tube under negligible gravity condition. *Journal of Colloid and Interface Science*. 162, pp. 350-355.

Jensen, M. K., 2002. Bubbles in microchannels. Master thesis. Denmark: Technical University of Denmark.

Jiang, Y., Chang, J., Lee, C., and Xu, B., 2001. An experimental study of the torque-tension relationship for bolted joints. *International Journal of Materials and Product Technology*, Vol.16, pp. 417-429.

Juvinall, R. C. & Marshak, K. M., 2000. Fundementals of machine component design, 3rd edition.

Kenny, B. & Patterson, E.A., 1989. The distribution of load and stress in the threads of fasteners – A review. *Journal of the Mechanical Behavior of Materials*, Volume 2, Issue 1-2, pp. 87-106

Laplace, P.S, 1806. Mechanique Celeste, suppl.10th vol.

Lochovsky, C., Yasotharan, S., Gunther, A., 2012. Bubbles no more: in-plane trapping and removal of bubbles in microfluidic devices, *Lab Chip*, 12(3), pp. 595–601

Letelier, M. F. S., Leutheusser. H.J., Rosas, C.Z., 1979. Refined mathematical analysis of the capillary penetration problem. *Journal of Colloid and Interface Science*, 72, pp. 465-470.

Ling, F.F. & Saibel, E.E., 1957. Thermal Aspect of Galling of Dry Metallic Surfaces in Sliding Contact, *Wear 1*, pp. 80–91.

Mahrous, A., Mahmoud, S., Al-dadah, R.K., 2011. Numerical investigation of laminar flow in micro-tubes with designed surface roughness. *3rd Micro and Nano Flows Conference Thessaloniki, Greece, 22-24 August 2011.*

Marshall, M.B., Lewis, R. & Dwyer-Joyce, R.S., 2006. Characterisation of contact pressure distribution in bolted joints. *Strain,* 42, pp. 31-43.

Marshall, M.B., Lewis, R., Howard, T. & Brunskill, H., 2011. Ultrasonic measurement of self-loosening in bolted joints. *Proceedings of the Institution of Mechanical Engineers, Part C: Journal of Mechanical Engineering Science*, 226, no. 7, pp. 1869-1884.

Mills, R.S., Avan, E.Y. & Dwyer-joyce, R.S., 2013. Piezoelectric sensors to monitor lubricant film thickness at piston - cylinder contacts in a fired engine. *Proceedings of the Institution of Mechanical Engineers, Part J*: *Journal of Engineering Tribology*, 227 (2), pp. 100-111.

Miller, D. L., 1983. Determination of Load Distribution in a Threaded Connection," *Mechanism and Machine Theory,* 18, No. 6, pp. 421-430.

Motosh, N., 1976. Development of Design Charts for Bolts Preloaded up to the Plastic Range.

Journal of Engineering for Industry, 98(3), pp. 849-851.

Nassar, S. A., Barber, G. C., and Zuo, D., 2004. Bearing Friction Torque in Bolted Joints. *STLE Tribology Transaction,* 48, pp. 1-7.

Nassar, S.A., El-Khiamy, H., Barber, G.C., Zou, Q. & Sun, T.S., 2005. An Experimental Study of Bearing and Thread Friction in Fasteners. *Journal of Tribology*, 127(2), pp. 263-272

Nassar, S.A., 2007. Effect of Tightening Speed on the Torque-Tension and Wear Pattern in Bolted Connections. *Journal of Pressure Vessel Technology*, 129(3), p 426.

NDT Resource Centre. Radiated fields of ultrasonic transducers. Available at: https://www.ndeed.org/EducationResources/CommunityCollege/Ultrasonics/EquipmentTrans/radiatedfields.htm (Accessed: 20 August 2016).

NDT Resource Centre. Mode conversion. Available at:

https://www.ndeed.org/EducationResources/CommunityCollege/Ultrasonics/Physics/modeconversion.htm (Accessed: 20 May 2018)

Pilli, S., Bhunia, P., Yan, S., LeBlanc, R.J., Tyagi, R.D., 2011. Ultrasonic pretreament of sludge: a review. *Ultrasonics Sonochemistry,* 18, pp. 1-18.

Pau, M. & Baldi, A., 2007. Application of an Ultrasonic Technique to Assess Contact Performance of Bolted Joints. *Journal of Pressure Vessel Technology*, 129, pp. 175-185.

Review of the Wear and Galling Characteristics of Stainless Steels, 1978. American Iron and Steel Institute, Designers Handbook Series.

Reddyhoff, T. & Harper, P., 2008. A New Approach for the Measurement of Film Thickness in Liquid Face Seals. *Tribology Transactions*, 51:2, pp. 140-149.

Rideal. E. R., 1922. On the flow of liquids under capillary pressure. *The London, Edinburgh, and Dublin Philosophical Magazine and Journal of Science,* 44:264, pp. 1152-1159.

Roberge, P.R., 1999. Handbook of Corrosion Engineering. McGraw-Hill.

Sachs, K. and D. G. Evans, 1973. The Relaxation of Bolts at High Temperatures. *Proceedings of the Institution of Mechanical Engineers*, pp. 59-67

Sakai, T., 1978. The friction coefficient of fasteners. *Bulletin of the JSME*, 21, pp. 333-340.

Sauer, J.A, Lemmon, D.C., Lynn, E.K., 1950. Bolts: How to prevent their loosening. Machine Design, 22, pp. 133-139.

Schwiebert, M. K. S. & Leong, W. H., 1996. Underfill flow as viscous flow between parallel plates driven by capillary action. *IEEE Transactions on Components Packaging and Manufacturing Technology Part C*, 19(2), pp. 8-13

Shih, R., 2014. Principles and Practice: An Integrated Approach to Engineering Graphics and AutoCAD2015. pp. 11-2.

Silva, G., 2008. Effect of wall roughness on fluid flow inside a microchannel. 14th Int Symp on Applications of Laser Techniques to Fluid Mechanics, Lisbon, Portugal

Sopwith, G., 1948. The Distribution of Load in Screw Threads. *Proceedings of the Institution of Mechanical Engineers*, 159, pp. 373-383

Stephen, J. T., Marshall, M.B., Lewis, R., 2014. An investigtation into contact pressure distribution in bolted joints. *Proceedings of the Institution of Mechanical Engineers, Part C: Journal of Mechanical Engineering Science,* Vol 228, Issue 18, pp. 3405-3418.

Summers, G.V., 2011. Galling of Stainless Steel Fasteners. Available at: http://www.pencomsf.com/wpcontent/uploads/2012/08/TB_GALLING.pdf_. [Accessed: 31 August 2016].

Tattersall, A, G. (1973). The ultrasonic pulse-echo technique as applied to adhesion testing. *Journal of Physics D: Applied Physics,* 6(7), p. 819.

Technical Reference Guide, 2005. Rev. 9. [pdf] . Available at https://www.fastenal.com/content/documents/FastenalTechnicalReferenceGuide.pdf [Accessed: 31 August 2016].

Thomas, T. R., and Sayles, R.S., 1977. Stiffness of Machine Tool Joints: a Random-process Approach. *Trans. ASME: Journal of Engineering for Industry*, 99, p. 918.

Vail, J.R., Mills, R.S., Stephen, J.T., Marshall, M.B., Dwyer-Joyce, R.S., 2013. An ultrasonic method for measuring of fluid penetration rate into threaded contacts. *Tribology International*, 67, pp. 21-26.

Wang, W., Marshek, K.M., 1995. Determination of the load distribution in a threaded connector having dissimilar materials and varying thread stiffness. *Journal of Engineering for Industry*, 117, pp. 1-8.

Washburn, E. W., 1921. The Dynamics of Capillary flow. *Physical Review*, 17, pp. 273-283.

Williams, J.A., 1994. Engineering Tribology, Oxford University Press, Oxford.

Young, T., 1805. An essay on the cohesion of fluids. *Philosophical Transaction of the Royal Society of London*, 95, pp. 65-87.

Zhang, Jie, Drinkwater, B. W., Dwyer-Joyce, R.S., 2006. Acoustic measurement of lubricant film thickness distribution in ball bearing. *Journal of the Acoustical Society of America*, 119(2), pp. 863–871.

Zou, Q., Sun, T.S., Nassar, S.A., Barber, G.C. & Gumul, A.K., 2010. Effect of Lubrication on Friction and Torque- Tension Relationship in Threaded Fasteners. *Tribology Transactions*, 50, pp. 127–136.

.

Appendix

Dynamic Viscosity Measurement

For viscosity measurements, a vibrational viscometer as used as shown in Figure 1. The viscometer has two sensor plates that are placed in the fluid sample, and viscosity is measured by detecting the electric current required to resonate the two sensor plates at constant frequency of 30Hz and amplitude of less than 1mm. The measurements were carried out at room temperature (20° c).

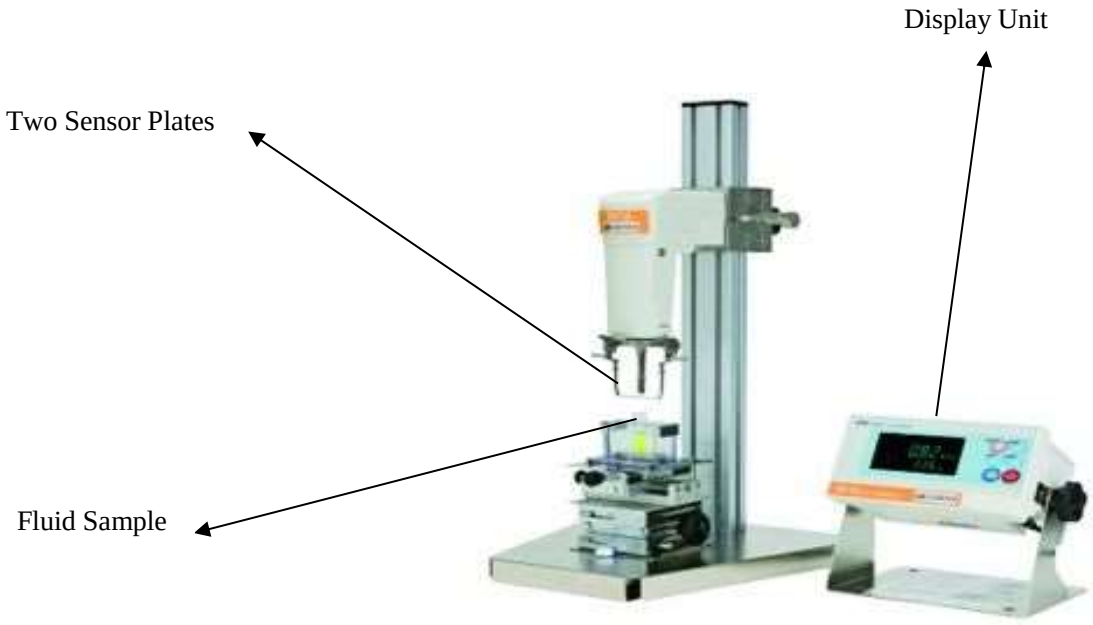

Figure 1. Vibrational Viscometer

Surface tension measurement

Surface tension is measured using an optical tensiometer (Figure 2a). The apparatus consists of a syringe, camera and a stage for placing a solid substrate in the case of contact angle measurement. For direct surface tension measurement especially for fluids with low surface tension, the most accurate way to do it is by pendant drop method.

In this method, syringe was filled with the fluid sample. The syringe driver allowed controlled pumping of the fluid so that a droplet can form and hang from the needle. The camera capture the image of the droplet as shown in Figure 2b. The surface tension of the

fluid was then found by the software automatically. The software is programmed to fit the geometrical shape of the drop into the Young-Laplace equation, relating interfacial surface tension to drop shape. Prior to taking any measurement, the apparatus was calibrated using water with its known surface tension.

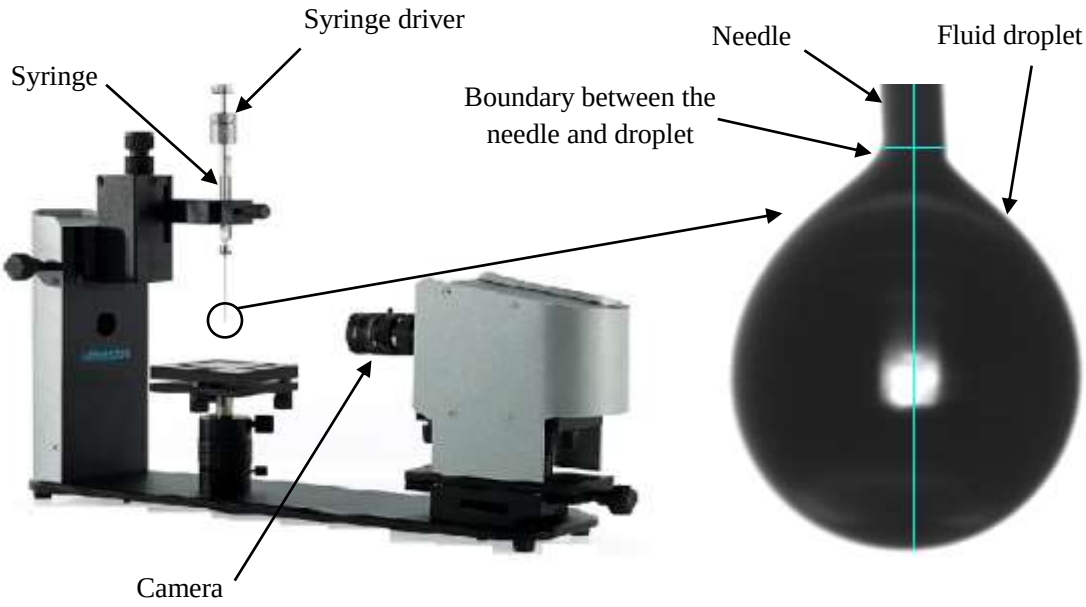

Figure 2(a) Optical tensiometer (b) Captured image of the fluid droplet

Density measurement

To measure density, the mass and volume of the fluid sample is measured. This can be done by using a measuring cylinder and a scale. The mass of a dry measuring cylinder was recorded, and then 20ml of a sample fluid was added. Once the mass of the fluid was determined, the density was found.

The viscosity, surface tension and density of the fluid samples were given in Table 1 of Chapter 5.